MSU
LIBRARIES

RETURNING MATERIALS:
Place in book drop to remove this checkout from your record. FINES will be charged if book is returned after the date stamped below.

LIGHT-ACTIVATED ELECTROCHEMICAL REACTIONS ON CHLORO-GALLIUM PHTHALOCYANINE-MODIFIED ELECTRODE SURFACES

By

Clovis Alan Linkous

A DISSERTATION

Submitted to
Michigan State University
in partial fulfillment of the requirements
for the degree of

DOCTOR OF PHILOSOPHY

Department of Chemistry

1983

87-0635

ABSTRACT

LIGHT-ACTIVATED ELECTROCHEMICAL REACTIONS ON CHLORO-GALLIUM PHTHALOCYANINE-MODIFIED ELECTRODE SURFACES

By

Clovis Alan Linkous

Phthalocyanines have been considered for use as chemical surface modifiers of electrodes, due to their chemical and thermal stability and catalytic properties. They have also been considered for use in optical energy conversion devices, due to their strong absorption in the red region of the visible spectrum. Thus phthalocyanines are ideal candidates for use in photoelectrochemical cells.

Chloro-gallium phthalocyanine, GaPc-Cl, had distinguished itself among other metal phthalocyanine derivatives as having a large photocurrent response for the electrolysis of hydroquinone. This thesis details efforts to make a more complete voltammetric characterization of GaPc-Cl thin film electrodes. Photocurrent was measured as a function of voltage, light intensity and wavelength, redox species and its concentration, film thickness, and substrate material. Conventional visible and near-infrared spectrophotometry, scanning electron microscopy, and X-ray photoelectron spectroscopy were also used to characterize the film electrodes.

Enroute to interpreting voltammetric results of electrolysis with GaPc-Cl film electrodes, it was found that

two types of voltammetric response could be obtained on gold, depending on pretreatment. The more reversible response to hydroquinone was attributed to a clean gold surface while another, less active surface could be obtained by the adsorption or one or more uncharacterized solution species. The passivating effect of trace electrolyte impurities on electrode activity through time, especially on rotating disk electrodes, was noted. On substrates such as silver and brass, coating with nonporous films of GaPc-Cl enabled electrolysis of redox species well past the anodic decomposition limit of the substrates themselves.

The unique voltammetric behavior of GaPc-Cl electrodes was attributed to a combination of enhanced photoconductivity and nonporosity of the films. Both factors are related to the ability to grow 0.3 μm sized grains in close proximity to each other. It is suggested that the ability to form highly ordered crystals is related to the tendency of some Group III metal trihalides to crystallize in a four coordinate, instead of a six coordinate geometry.

ACKNOWLEDGMENTS

The author wishes to acknowledge the help of his dear wife, Li-Ching, in the preparation of this thesis, his little boy, Henry, who helped him rise and shine every morning, and his academic advisor, Dr. Neal R. Armstrong, who kept after him to write this thesis and get a job.

TABLE OF CONTENTS

LIST OF TABLES

LIST OF FIGURES

1. INTRODUCTION

1.1 Photoelectrochemical Cells

Ever since Becquerel (1) observed an enhanced rate of electrolysis upon irradiation of a Hg electrode, it has been known that electrochemical reactions could be hastened by the absorption of light energy by the electrode. This effect received little more than curious interest until the theory of semiconductor electrodes was developed (2), after which the photogeneration of electron/hole pairs became a diagnostic tool (3).

It was observed that these irradiated semiconductor electrodes had considerable oxidative power. The photo-oxidation of H_2O on n-TiO_2 (4) and n-SnO_2 (5) was reported. In 1972, Fujishima and Honda (6) reported the electrolysis of H_2O to O_2 on n-TiO_2 electrode when irradiated with ultraviolet light, with the simultaneous evolution of H_2 on a Pt electrode. This opened up a new field in which photoelectrochemical cells were studied as potential energy conversion devices.

In Figure 1.1, schematics demonstrating the two main types of energy conversion via photoelectrochemical cells are shown. A direct light to electrical energy conversion takes place in a liquid junction photovoltaic cell. In this

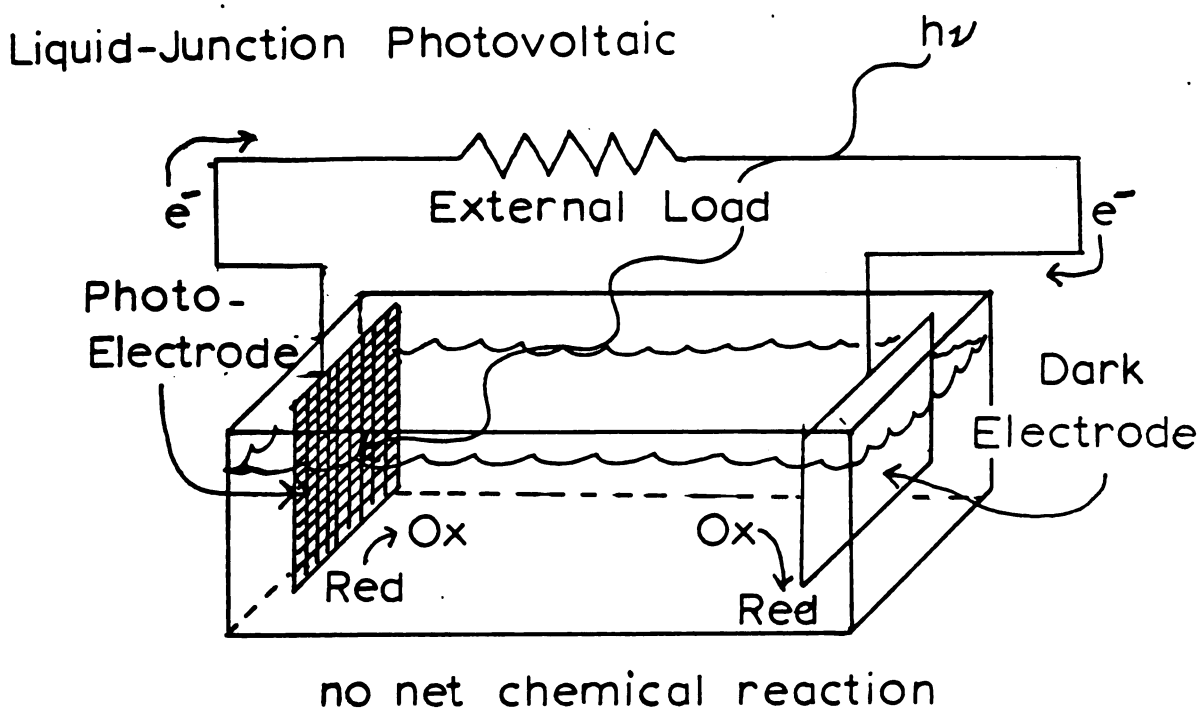

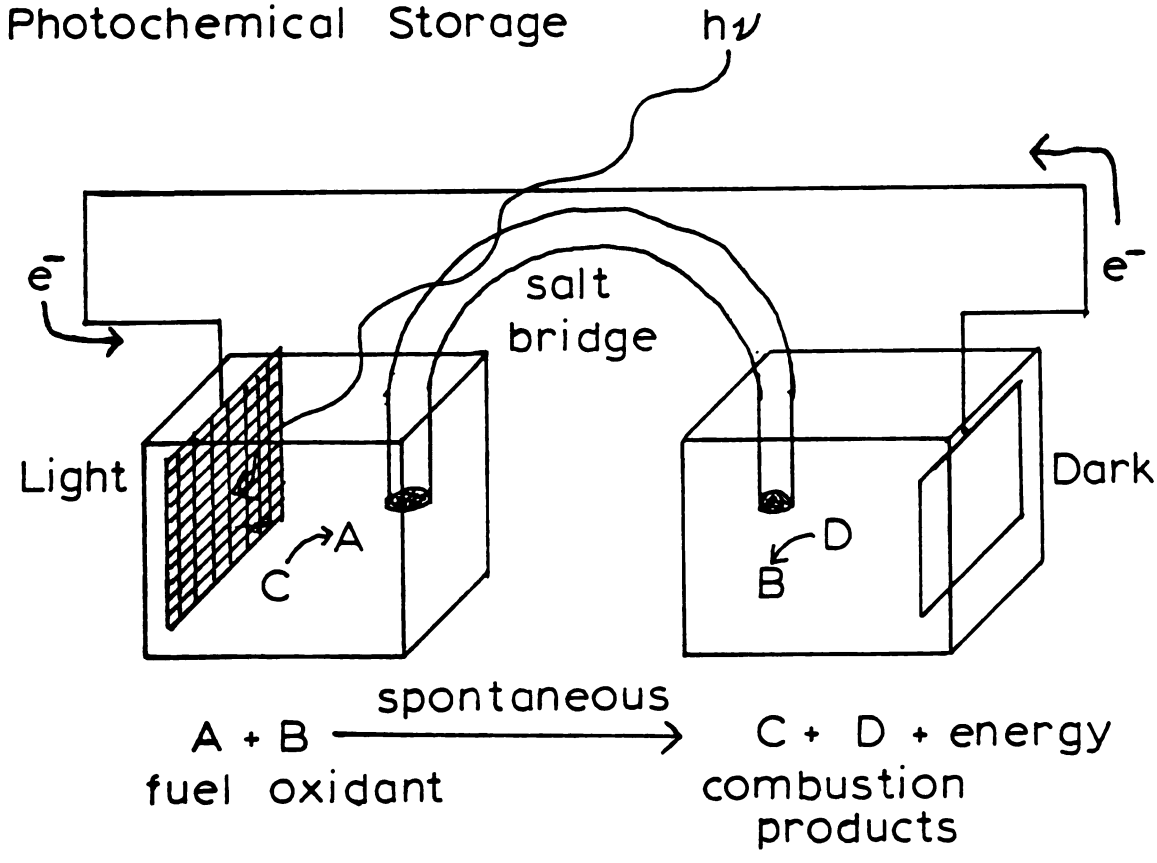

Figure 1.1: Energy-Converting Photoelectrochemical Cells

system, two electrodes, a photoelectrode and a dark electrode, are placed in an electrolyte containing a single redox couple and connected through an external load. Irradiation of the photoelectrode with light causes the conversion of one form of the redox couple to the other. The figure shows the conversion of the reduced form, Red, to the oxidized form, Ox, for example. A new concentration ratio of Ox to Red at the photoelectrode surface results, causing a photopotential to develop. A potential difference now exists between the photoelectrode and the dark electrode, and so a current will flow between them. The current generated is then used to operate an external device. The dark electrode, in order to maintain its potential, reduces Ox back to Red at the same rate as the reverse reaction is occurring at the photoelectrode. Thus liquid junction photovoltaic cells are closed electrochemical systems, where no net chemical change occurs, but light energy input results in electrical energy output.

The other type of photochemical energy conversion takes place where light energy is stored in energy-rich compounds via the electrochemical process. While any redox product that results in an increased free energy of reaction may be considered, the most common application is the production of a fuel such as H_2 or CH_3OH which can be stored for an indefinite period of time and then be either burned or electrochemically consumed for recovery of the stored light energy. In this system the electrodes are directly connected

so that the full free energy difference generated at the photoelectrode is delivered to the dark electrode. By using separate containers, electrolytes most suitable for their respective electrode reactions may be used, and the products may be separated conveniently and safely for later use.

A fundamental materials problem in photoelectrochemical cells is photocorrosion of the electrodes. One of the possible relaxation processes for a photogenerated charge carrier is dissolution of the electrode, or in aqueous solution, formation of a passivating oxide. As work progressed in the development of durable, stable photoelectrochemical cells, two trends emerged. One trend was to use a semiconductor of optimal bandgap, such as Si, CaS, or GaAs, and protect it from photocorrosion with the use of thin, conductive films (7-10), or surface bound (11) or solvated (12-16) redox species which could effectively compete with the surface corrosion reaction in the gain or loss of electrons. Another approach was to use electrode materials that possessed good intrinsic stability toward photocorrosion. Doped transition metal oxides such as n-$TiO_2$and n-SnO_2 were shown to be good candidates in this regard (4, 5, 17). However, the bandgaps for the two materials are greater than 3 electron volts. Thus the only part of the solar spectrum which could contribute to the photoelectrochemical reaction was in the ultraviolet, which only comprises about 10% of the total solar irradiance.

Thus in order to achieve a practical power conversion efficiency (light energy in/electrical energy out), generally taken to be about 10% (18), these electrodes need to be activated by, or sensitized toward, visible wavelength light. This process of activation is called spectral sensitization.

1.2. Spectral Sensitization

Spectral sensitization is the process in which a solid surface is made more chemically active by exposure to light of a given wavelength. This is achieved by the incorporation of some chromophore into the system in close proximity to the surface. The chromophore is chosen so that it absorbs photons corresponding to the wavelength range to which the surface is to be sensitized. It should also have good chemical and thermal stability, and a high quantum efficiency (electrons injected per photon absorbed) for that surface. For many applications, large highly conjugated organic molecules with high molar absorptivities in the visible region have proven useful as spectral sensitizers. Some of these compounds are frequently employed as dyestuffs in the clothing industry and elsewhere; hence the term dye sensitization has become synonymous with spectral sensitization.

Interest from the photographic and electrophotographic industries spurred efforts to understand the mechanism of charge transfer between semiconductor surfaces and dye

sensitizers. Dyestuffs such as rhodamine-B (19-29), rose bengal (18, 30-32), methylene blue (28-29, 33), and various cyanine dyes (25, 28, 34) were studied as sensitizers on materials such as CdS, TiO_2, SnO_2, and ZnO_2. The application of dye sensitization to photoelectrochemical cells was later advanced by Tributsch (35) and by Calvin (36).

Most of the early work on dye sensitization was done with the dye in solution. Due to the short lived electronic excited state lifetimes with respect to diffusion rates of molecular species in solution, only photon absorption within the first 10 Å of the electrode surface could be expected to contribute to the observed sensitized photocurrent. The use of adsorbed (34, 27-39) or covalently attached (26, 38, 40) dye molecules was an improvement over the dye solutions since a higher surface concentration of dye was in principle obtainable, and it was a much more economical use of the dye material.

In order to be an effectve sensitizer, it is desirable for the dye layer to absorb as much of the incident light as possible. The more sensitizer that is placed on a surface, the more photons can be absorbed per second. But most sensitizers are organic compounds, which, taken as a group, are considered to be electrical insulators. Increased film thickness causes increased film resistance, which can slow or eliminate an electrochemical reaction. Even though a greater portion of the incident photons are absorbed, an accompanying increased film resistance may drastically affect the quantum

efficiency for change transfer, which in turn affects the overall conversion efficiency. Therefore, film thickness should not be increased without regard to its effect on quantum efficiency. The trade-off between quantum efficiency and absorbance implies that for any given dye material there may be an optimum thickness above monolayer levels which maximizes the power conversion efficiency of a photoelectrochemical cell.

1.3. Chloro-Gallium Phthalocyanine as Dye Sensitizer

Chloro-gallium phthalocyanine, GaPc-Cl, possesses many of the attributes expected of successful dye sensitizers. GaPc-Cl absorbs strongly in the red region of the visible spectrum, so that it would be a good photoreceptor for solar radiation. The solid film absorbance of GaPc-Cl is broadened and red shifted with respect to its solution spectrum, so that as a film it can also collect some of the appreciable near infrared solar output.

The phthalocyanine family of compounds as a whole exhibits good chemical and thermal stability, making GaPc-Cl a potential candidate as a dye sensitizer in harsh environments or for long-term use. Our preliminary results (41) showed that GaPc-Cl was quite active on SnO_2 electrodes in the photoelectrolysis of H_2Q.

In this dissertation, the author will examine the ability of GaPc-Cl to serve as a dye sensitizer. To achieve

this goal, a kinetic analysis of H_2Q photoelectrolysis on GaPc-Cl was made. The dependence of photocurrent on factors such as dye film thickness, substrate, electrolyte concentration, and light intensity was obtained. Cyclic voltammetry and Tafel data gave additional mechanistic information. By comparison to other phthalocyanines, information regarding the specific catalytic action of GaPc-Cl was revealed. X-ray photoelectron experiments examined the porosity of GaPc-Cl films and the lability of the chloride counterion. In addition, thermodynamic information on GaPc-Cl was obtained in experiments involving the electrolysis of various quinones, photoaction spectra, and capacitance measurements. On the basis of these experiments and others mentioned above, conclusions on the means and ability of GaPc-Cl to act as a dye sensitizer will be made.

The author found that in order to understand the kinetics of photoelectrolysis on GaPc-Cl, the behavior of the supporting substrate must also be understood. In the case of gold, two distinct types of behavior toward H_2Q were observed. A number of experiments were performed in order to explain this observation, the results of which will be reported in this thesis.

2. BACKGROUND AND THEORY

2.1. Phthalocyanines

The first phthalocyanine identified as such was iron phthalocyanine (FePc) in 1928. Workers at the Grangemouth works of Scottish Dyes, Ltd., noticed a deep blue residue along a crack in a glass-lined iron kettle that had been used to prepare phthalimide. Supported by Imperial Chemical Industries, Professor R. P. Linstead of Oxford University began to investigate this apparently new compound. The first of over 30 articles by Linstead and coworkers on the phthalocyanines and related macrocycles appeared in the Journal of the Chemical Society in 1934 (42).

The compound was named phthalocyanine by Linstead, because of its color and its main structural component. The word cyanine comes from the Greek word "kyanos", which means "blue". Phthalo- comes from the Greek work for naptha, which contains napthalene. Oxidation by acid produces o-phthalic acid, from which phthalonitrile can be obtained. The phthalocyanine macrocycle can be split up into four phthalonitrile molecules plus two electrons.

The structure of a divalent metal phthalocyanine is shown in Figure 2.1 along with that of a similar metalloporphyrin. The phthalocyanines are structurally quite

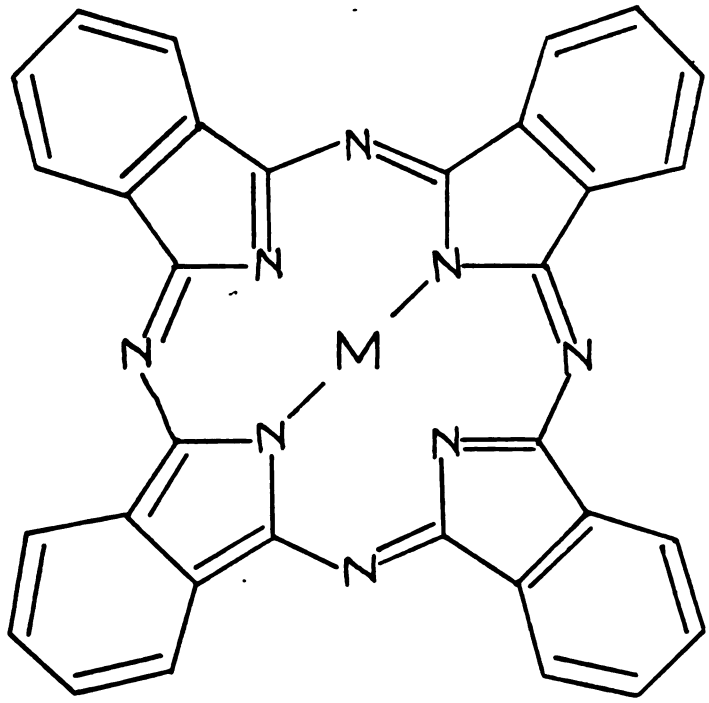

Metal Phthalocyanine

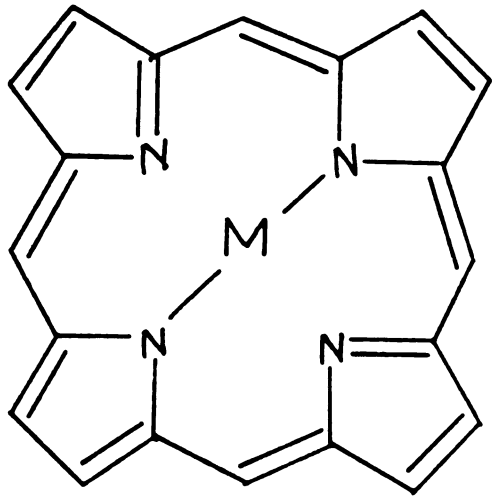

Metalloporphyrin

Figure 2.1: Structure of Divalent Metal Phthalocyanine and Metalloporphyrin

similar to the biologically important porphyrins, differing only in that the bridging moeity is nitrogen (-N=) rather than a methine (-CH=), and a benzene ring is fused to the base of each pyrrole ring. For this reason phthalocyanines have sometimes been referred to as tetrazabenzporphins in the literature.

The physical and chemical properties of porphyrins and phthalocyanines are similar as well. The optical absorption spectra are similar, although electronic transitions in phthalocyanines tend to be more intense and red shifted, due to its more extended π electron system (43).

Phthalocyanines have been used to simulate certain functions performed by porphyrins in nature. For example, iron porphyrin, or heme, is the prime consistuent of hemoglobin, the O_2 carrier in our blood stream; iron phthalocyanine (FePc) also has exceptional O_2 binding capability, and so has been used in artificial blood systems (44). Magnesium porphyrin is a main constituent of chlorophyll, and so magnesium phthalocyanine (MgPc) has been used to simulate the reaction center in photosynthesis (45).

In general, the phthalocyanines are characterized by high chemical and thermal stability, and high molecular absorptivity, especially in the red region of the visible spectrum. They are insoluble in water and most organic solvents, but do show slight solubility in concentrated sulfuric acid, chloronapthalene, and nitrogenous aromatics, such as pyridine, quinoline, and nitrobenzene. The planar

nature of the phthalocyanine macrocycle coupled with the coordination shell of most of the possible metal centers leaves both axial sites, above and below the macrocylic plane, available for coordination. As for molecular solids in general, phthalocyanines are considered insulators, but under various conditions of doping and preparation have demonstrated metallic behavior with near metallic conductivity (46-56). Thus, while phthalocyanines were first investigated for use in the dyestuff industry, they have also generated interest in numerous other unrelated industries as high temperature lubricants (57-59), adsorbants (60), organic synthetic catalysts (61-63), dielectrics (64), opto-electronic sensors (65-66), and photoconductors (67-68). Phthalocyanines were the first organic materials used as passive Q-switching elements in lasers (69). For those who have worked with phthalocyanines, their use in fire extinguishers (70) and hair dyes (71) may seem unsavory but have nevertheless been tried.

The phthalocyanines form a variety of crystalline phases (72-73). There is some disagreement as to the number and means of formation, but it seems certain there are at least three. The most common phases are designated α and β. The α phase is a metastable form, made by precipitation from solution, or sublimation onto a cool substrate. The β phase is the stablest form, made by heat treatment or sublimation onto a hot (200°C) substrate.

The third phase, called the x-phase, was developed by the Xerox Corporation (74). It consists of stacks of dimerized molecules, and thus shows a distinctive x-ray spectrum (hence the name "x"-phase) as well as optical absorption. The x-phase of demetallated phthalocyanine (H_2Pc) shows exceptional photoconductivity and has been used as a potential photoconductor in electrophotographic processes (75). The x-phase of copper phthalocyanine (CuPc) has also been formed (76), suggesting that other x-phase MPc's are possible.

Still another use for phthalocyanines was as a catalyst for certain electrodic reactions. Jasinski demonstrated that cobalt phthalocyanine served as a catalyst for oxygen reduction (77). As might be expected in light of its O_2 binding ability, FePc has also been extensively studied as an O_2 reduction catalyst (78-84).

Soon after the advent of dye sensitized semiconductor electrodes in photoelectrochemical solar cells, phthalocyanines were being employed to sensitize cell reactions. Of greatest interest were copper phthalocyanine, CuPc (40-41, 85-90), and the parent compound, demetallated phthalocyanine, H_2Pc (87, 91-95). Other phthalocyanines of interest in this regard were the cobalt (40, 86, 95), iron (87, 95), nickel (86, 92), magnesium (95), titanyl (95), vanadyl (95-96), and zinc (87, 92, 95) derivatives.

Armstrong (41) proposed to sensitize electrodes with multimolecular layers of phthalocyanines which had a tendency

toward aggregation or polymerization in the solid state. These included aluminum, gallium, and indium derivatives with fluoride, F^-, as a counterion (53-55). Also, stable dimers and trimers of silicon phthalocyanine, SiPc, as well as for germanium, were available for use (97-98). It was in testing these and other halide forms of the group III phthalocyanines that the photocatalytic abilities of GaPc-Cl became known.

2.2. Electrolysis of Quinones

The quinone family of compounds is perhaps the most thoroughly studied organic redox couple. A number of reviews on quinones and tabulations of redox potentials for various series of quinones have been made (99-104). One reason would be due to its biological importance (105, 106). In several cases, quinones function as intermediates in the biosynthesis of other secondary metabolites, such as the tetracyclines and aflatoxins. They are also important redox reagents in biological systems. The Q/H_2Q redox couple is one of the elements in the electron transport chain in photosynthesis and respiration. Ubiquinones are found in the respiratory apparatus of eucaryotic organisms, while menaquinones (vitamin K) are found in procaryotic organisms. Plastoquinones, major constituents in chloroplasts, the photosynthetic organelles found in green plants, may have a multiple role as electron carrier, proton translocator, and mediator of directional flow of hydrogen (107). Other uses of quinones are in pigments and drugs.

Most quinone electrochemistry has been done in organic, aprotic media. One reason is solubility, but another is that quinones have long been thought to interact very weakly with the electrode and its products in such media, yielding uncomplicated results for kinetic analysis (108). In most aprotic solvents, quinones are reduced in two one-electron reversible steps.

Some electrochemical studies on the simpler quinones have been done in aqueous solution. Most have been done on the simplest quinone, benzoquinone. The most important reaction is the two proton, two electron reduction of benzoquinone to its corresponding hydroquinone:

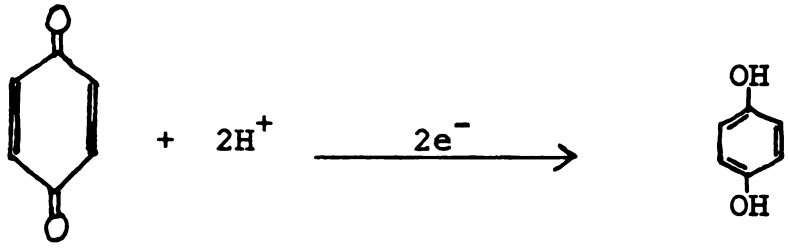

A diagram showing the possible sequences of chemical and electron transfer steps in quinone reduction is shown in Figure 2.2. All the available permutations have been recommended at one time or another. The first study of quinone electrolysis in aqueous electrolyte occurred just after the turn of the century (109). Much later, Vetter (110) studied the pH dependence of the reaction on a Pt electrode. He found evidence for two different, simultaneous reactions occurring between pH 0.2 to 7.2. One mechanism would predominate over the other, depending on pH, with the transition occurring around pH 5 to 6.

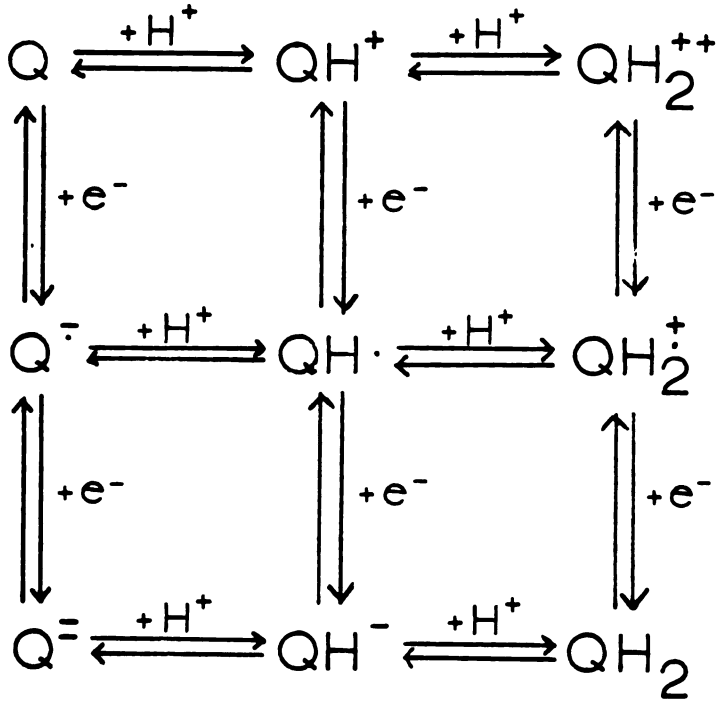

Figure 2.2: Possible Mechanisms of Quinone Electrolysis

Below pH 5, the reaction sequence

$$Q \xrightarrow{H^+} QH^+ \xrightarrow{e^-} QH\cdot \xrightarrow{H^+} QH_2^+ \xrightarrow{e^-} QH_2$$

would predominate, while above pH 6,

$$Q \xrightarrow{e^-} Q^- \xrightarrow{H^+} QH\cdot \xrightarrow{e^-} QH^- \xrightarrow{H^+} QH_2$$

would predominate. The two mechanisms could be presented as CECE and ECEC types, respectively, where each C stands for a chemical step (protonation) and each E stands for an electron transfer step. Vetter later found the same transition for duroquinone (2,3,4,6-tetramethylbenzoquinone) in methanol/water solution between pH 3.1 to 6.6 (111).

Parsons (112) studied the oxidation of various quinones on a dropping mercury electrode. He used the method described by Koutecky for obtaining kinetic parametics from current-voltage data, and in turn used then to calculate the free energy profiles for various possible reaction mechanisms. On that basis, he concluded that Vetter's proposed mechanism of higher pH was correct. However, at low pH consecutive two one-electron transfer steps after protonation (CEEC) would be the most probable mechanism, since that pathway has the lowest free energy of activation. There was, however, a significant disagreement between theoretical transfer coefficients based on this mechanism and those found experimentally. One reason given for disagreement in mechanism at low pH was that Vetter's work was done on Pt, which has a greater tendency to adsorb organic species than Hg. Thus the semiquinone

intermediate may be stabilized on Pt, allowing a CECE mechanism at low pH.

Bagotzkii and coworkers (113) studied the quinone reaction on a Pt electrode. They favored a CCEE mechanism in aqueous acid solution, and an EECC mechanism in aqueous basic solution, stressing the importance of adsorption of reactive intermediates.

Very recently Hubbard and Soriaga (114) completed a linear potential scan and potential step coulometric study of adsorption of organic species on Pt using thin layer electrodes. They found that hydroquinone spontaneously converts from a solvated reactive state to an unreactive adsorbed state. Once an adsorbed layer was present, however, electrolysis of any remaining solvated hydroquinone proceeded reversibly. The adsorbed species could be oxidized, but only irreversibly at high overpotential to unknown products.

Hubbard (115) had observed similar behavior before, when he studied the adsorption of alkenyl biphenols such as 2-allylhydroquinone on polycrystalline Pt. In that case, however, the inactivating adsorption was due to strong adsorption of the vinyl moiety, which left the hydroxyl groups outside of the double layer.

There are other possible mechanistic steps for quinone reduction not considered in Figure 3. The semiquinone radical $QH^{\cdot}$, formed by the acquisition of one proton and one electron, may disproportionate to form Q and H_2Q (116). Quinhydrone, a 1:1 molecular complex of benzoquinone and

hydroquinone, has been well characterized in the solid state (117, 118), but separates in solution. Some portion of the solvated quinhydrone remains undissociated, however (119).

2.3. Theory of Semiconductor Photoelectrochemistry

2.3.1. Band Theory Applied to Semiconductors

A single molecule possesses a set of discrete energy levels. If a large assembly of identical molecules are brought in proximity to one another, as in a crystalline lattice, so that outer orbitals overlap, a splitting of levels occurs. As the number of participating orbitals increases, the energy separation between the highest and lowest levels increases at an even slower rate. Thus, as the number of atoms increases, the energy separation between adjacent levels decreases. For a crystal the size of a cubic centimeter, for example, there would be on order of 10^{20} levels of equal energy mixing to form 10^{20} new orbitals, each with its own energy. If the highest and lowest levels were 1 eV apart, then the splitting between levels would be on order 10^{-20} ev, so that the set could be considered a continuum. Therefore, the range of energies covered by this continuum of levels is called a band. This effect is shown in Figure 2.3.1.

In general, adjacent molecules in a solid approach each other closely enough that the lowest unoccupied orbitals strongly overlap, and the highest occupied orbitals also

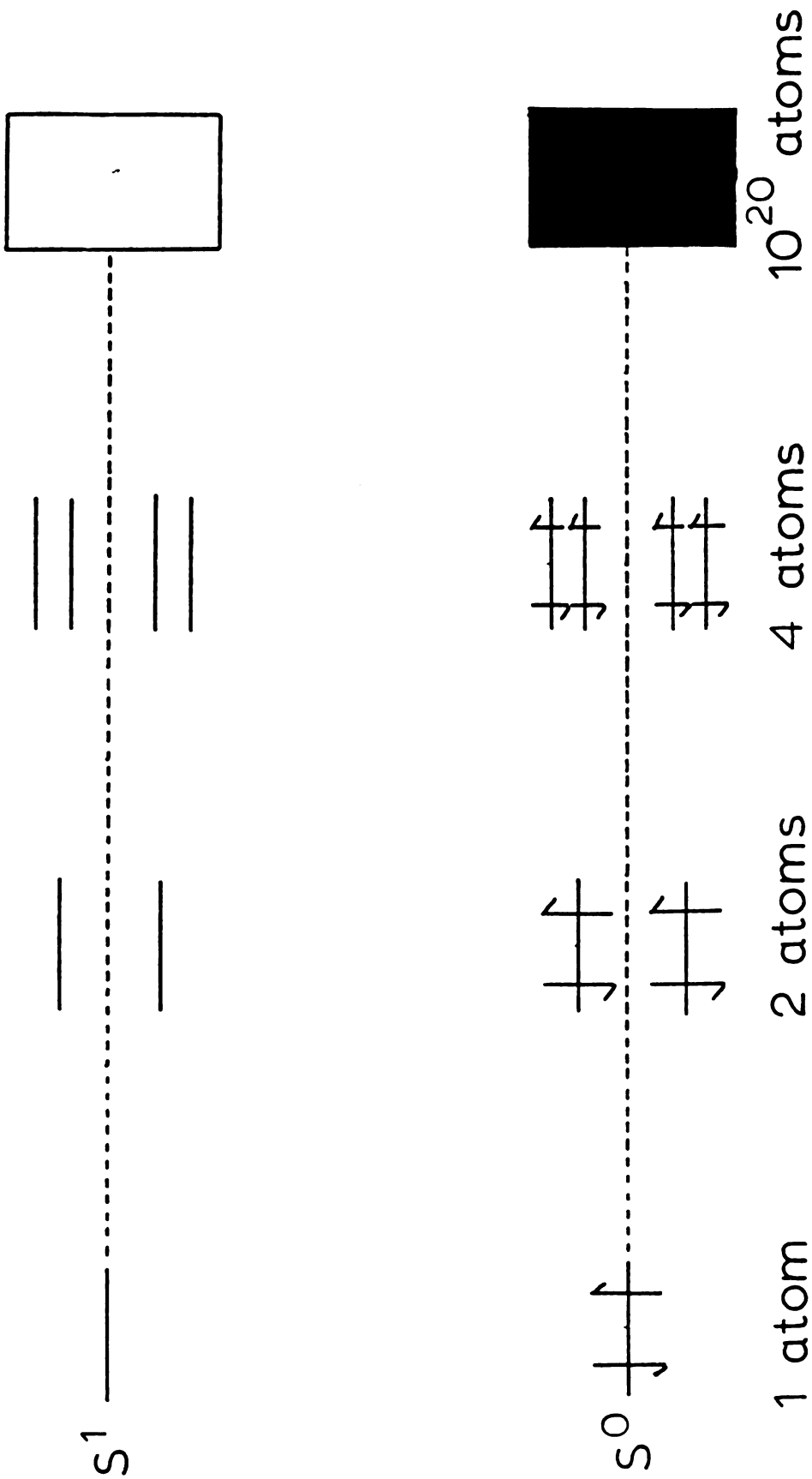

Figure 2.3.1: Band Formation in the Solid State

overlap but to a lesser extent. The core electron shells have little interaction with one another, so whether as a gas phase molecule or as part of a solid crystal, these levels show no band structure.

Our interest then lies in the energy bands formed by the lowest unoccupied and highest occupied orbitals. Their positions relative to one another on the energy scale is determined by the width of each band, which is determined in turn by interatomic distance and the original separation of the two orbitals on the isolated molecules. A diagram of semiconductor band structure, along with those of insulators and metals, is shown in Figure 5.

The band made from highest occupied orbitals employ valence shell electrons, so it is called the valence band. The valence electrons that comprise the valence band are most commonly bonding electrons, though in some cases they are nonbonding as in various semiconductor transition metal sulfides and selenides.

Thus we have a filled valence band with an empty band above it. The orbitals in this empty band extend in a periodic manner throughout the crystal. For semiconductors to be at all conducive, there must be some finite population of electrons in this upper band. Since the electrons in this band contribute to electrical conductivity, it is called the conduction band.

The energy difference between the upper edge of the valence band, E_{VB}, and the lower edge of the conduction band,

$E_{CB'}$ is called the band gap energy. This is the minimum energy that must be supplied to promote an electron to an excited state for "direct" semiconductors. Sub-band gap transitions may occur through interaction with quantized lattice vibrations called phonons. For materials such as GaAs, it is a negligible effect, yet for Si, the most widely known and utilized semiconductor, it is the predominant mechanism for putting electrons in the conduction band.

2.3.2. The Fermi Level and Electron Distribution

Electrons are fermions, particules with half integral spin, so that an assembly of them must obey Fermi-Dirac statistics. The expression that gives the energy distribution for an ensemble of fermions is

$$n(E) = \frac{1}{1 + \exp\left[-(E_f - E)/kT\right]}$$

where n is the probability that an energy level with an energy E will be filled, or populated, k is Boltzmann's constant, T is the absolute temperature, and E_F is the Fermi energy.

The Fermi energy is the chemical potential, μ, which is constant for each system of the grand canonical ensemble used to derive the Fermi-Dirac distribution. Rigorously speaking, the Fermi energy equals μ at the absolute zero of temperature, since E_F is temperature dependent. Therefore we will henceforth refer to E_F at any given temperature (and electrode potential) as the "Fermi level".

The Fermi level can be used as a yardstick to quickly determine whether a particular energy level in thermal equilibrium with the rest of a system is filled or not. Typical values for E_F vary from 1 to 5 ev, while kT at room temperature is $(1.38 \times 10^{-23}$ J/deg)(298 deg)$(6.24 \times 10^{18}$ ev/J) = 0.025 eV. Thus at room temperature and below, n(E) is a very sharp exponential around E_F. For energies greater than E_F, the exponential is much greater than unity, and n(E) is nearly zero. For energies less than E_F, the exponential is much less than unit, and n(E) is nearly one, or 100% probability of occupation. It is only within the first few hundredths of eV on either side of E_F that n(E) varies from the two probability extremes. Since electrons contributing to current and charge transfer will then most probably come from these levels we can think of E_F as the average energy of electrons in a solid.

2.3.3. Correlation Between Band Structure and Conductivity

The difference in conductivity between metals, semiconductors, and insulators can be explained by their difference in electronic structure, shown in Figure 2.3.2.

In a metal, the conduction and valence bands overlap. There is no band gap; instead, there is a continuum of energy levels about E_F so that the conduction levels can be easily populated at room temperature through thermal excitation, which at any given temperature is on order of kT. Therefore metal carrier densities are large, on order of 10^{22} to 10^{24} cm^{-3}.

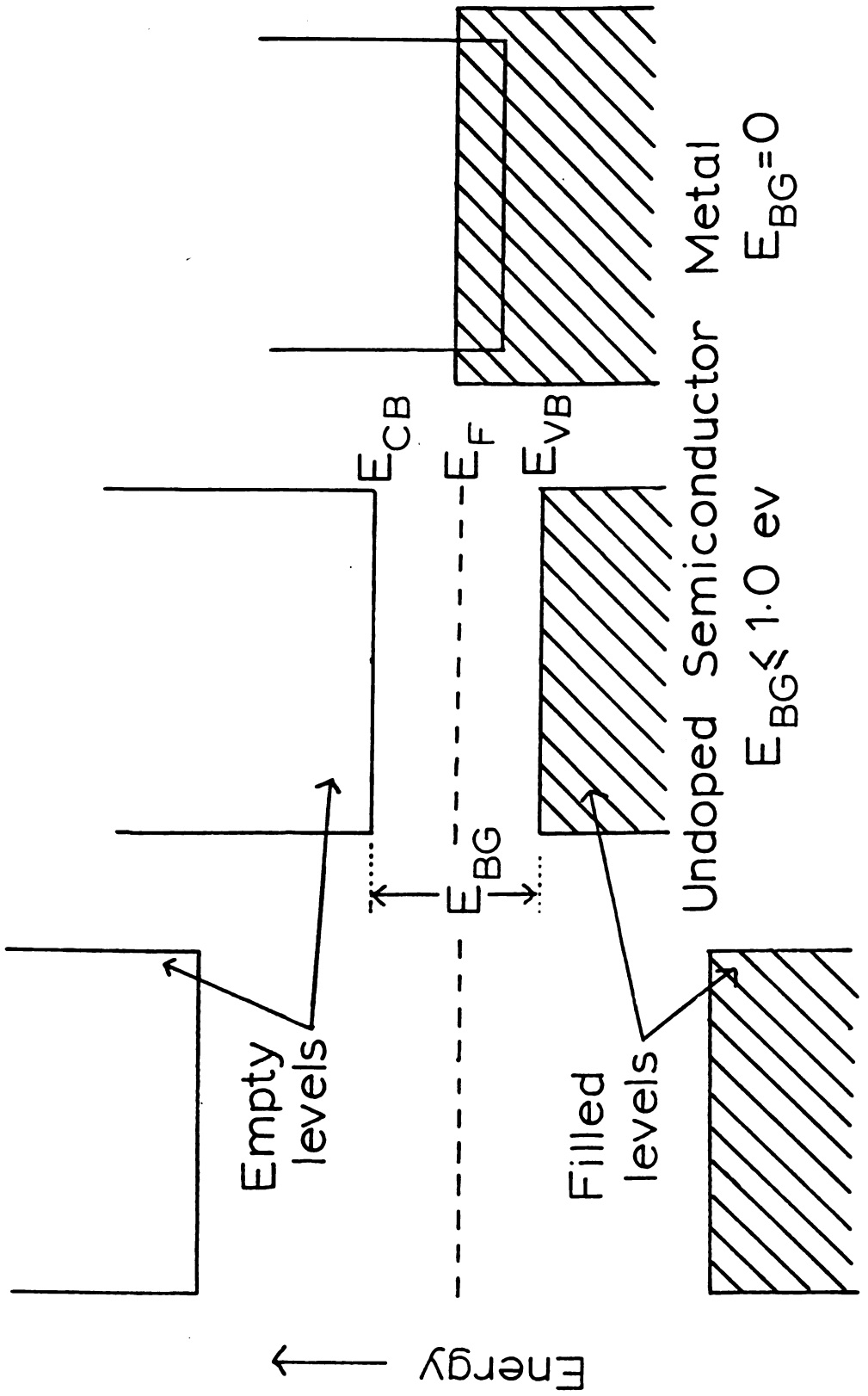

Figure 2.3.2: Energy Band Diagrams for Metals, Semiconductors, and Insulators

For insulators, the conduction and valence band are separated by a large band gap energy, generally defined as 1.0 eV or higher. From the Fermi-Dirac distribution, we know that if the band gap energy is greater than kT then the conduction band levels of insulators is then extremely small at room temperature. Thus insulators are poor conductors of electricity, with carrier densities of 10^{12} cm^{-3} and below.

For semiconductors, the conduction and valence bands are separated by 1.0 eV or less. Carrier densities for semiconductors are thus intermediate between semiconductors and metals, on order of 10^{14} to 10^{20} cm^{-3}.

2.3.4. Doping of Semiconductors

The conductivity of insulators and semiconductors can be greatly increased through doping. A dopant is typically an element whose valency is either one unit greater or less than the base material. If the dopant is electron rich, it is called a donor inpurity. When incorporated into the crystalline lattice, one of its valence shell electrons will not be able to form a bond with any of the nearest neighbor atoms. By careful choice of dopant, energy levels can be placed inside the band gap region near the conduction band edge. The energy separation between these donor levels and the conduction band can be small enough that thermal energies can promote electrons into the conduction band, increasing conductivity. Thus, conductivity can be varied over many orders of magnitude by varying the doping density. The upper

limit to this approach is reached where the dopant begins to damage the integrity and order of the lattice.

The same effect can be achieved with valence electron deficient, or acceptor impurities. These dopants are unable to use all the bonding electrons around them, and so an empty valence orbital exists on each dopant species. If this new empty dopant level lies just above the valence band, then electrons can be easily promoted into it. The dopant becomes a fixed negative ion, while the base atom that just lost an electron is positively charged. This region of net positive charge created by a vacated valence and usually bonding orbital is called a hole. This orbital may be filled by electron removal from another adjacent atom, which may in turn also be reduced by its neighbor. By this mechanism the hole may travel through the atomic lattice in the valence band, in much the same way as electrons travel in the conduction band.

The charge carrier population in undoped, or intrinsic, semiconductors is evenly divided between holes and electrons, since an electron promoted across the band gap simultaneously creates a hole. Doping increases the population of one type of charge carrier at the expense of the other. Semiconductors whose free electron population has been increased by donor impurities are called n-type, since negatively charged carriers are in the majority. When acceptor impurities increase the hole population, the semiconductor is p-type, for positively charged majority

carriers. Energy band diagrams for n-type and p-type semiconductors appear in Figure 2.3.3.

Another effect of doping a semiconductor is that it moves the semiconductor's Fermi level from its intrinsic value halfway between the conduction and valence band edges. Introduction of filled donor impurity levels above E_F will cause it to move at least as high as those filled levels. Introduction of empty acceptor impurity levels below E_F will cause E_F to drop at least as low as those empty levels. Thus, for n-type semiconductors E_F is near the conduction band edge, while for p-type semiconductors E_F is near the valence band edge.

2.3.5. Junction Formation between Semiconductor Phases

Whenever two phases possessing a common mobile species are placed in intimate contact with one another, that species will traverse the interface until its chemical potential is the same in both phases. For semiconductors the mobile species are electrons and holes, and the chemical potential for electrons in each isolated component is simply its Fermi level. Thus when two semiconductors are joined together electrons will traverse the interface until E_F has the same value across the junction. This situation could involve either two semiconductors of different elemental composition, or the same semiconductor with different doping type or density.

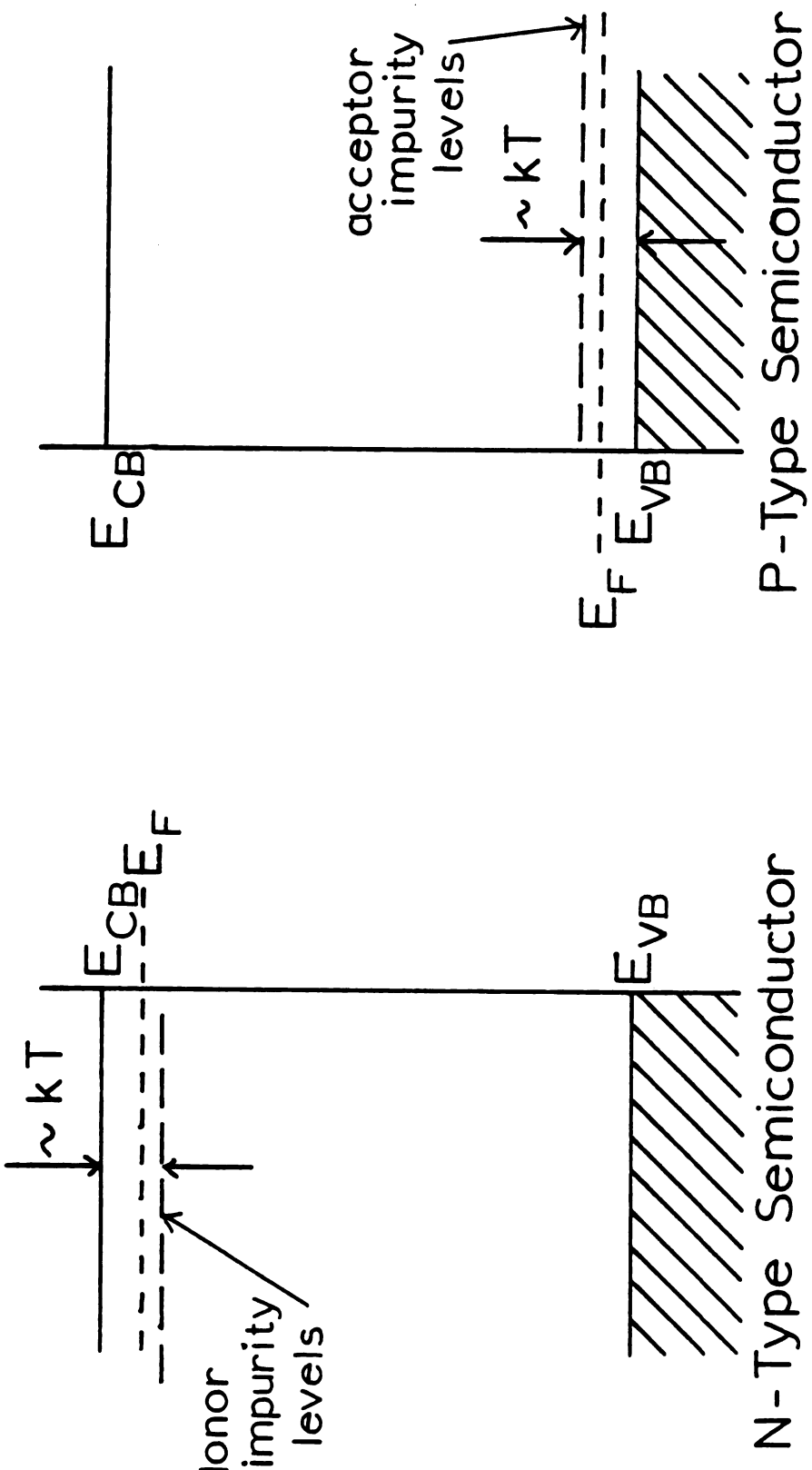

Figure 2.3.3: Energy Band Diagrams for n-Type and p-Type Semiconductors

Junction formation between two phases of the same semiconductor, one of which is doped n-type and the other p-type, is shown in Figure 2.3.4. As isolated components, the conduction and valence band edges are flat, and have the same potential energy as their counterparts in the other phase. The Fermi level is near the conduction and valence band edges according to the type of dopant.

When the two component phases are brought together, electrons traverse the interface until E_F is constant across the junction. The amount of charge transferred is just enough to build up an electropotential difference equal and opposite in sign to the original difference in Fermi levels. Thus on either side of the junction there exists a region of net positive or negative charge, depending on the direction of electron flow in reaching equilibrium. This region is the space charge layer.

At the junction between the two phases, E_F is the sum of two terms, the usual chemical term plus an electric field term, making E_F an electrochemical potential. The electric field term arises from any electric potential difference applied to a solid with respect to a reference potential. The expression for the Fermi level of electron in a solid is then

$$E_F = \mu + e\Delta\phi$$

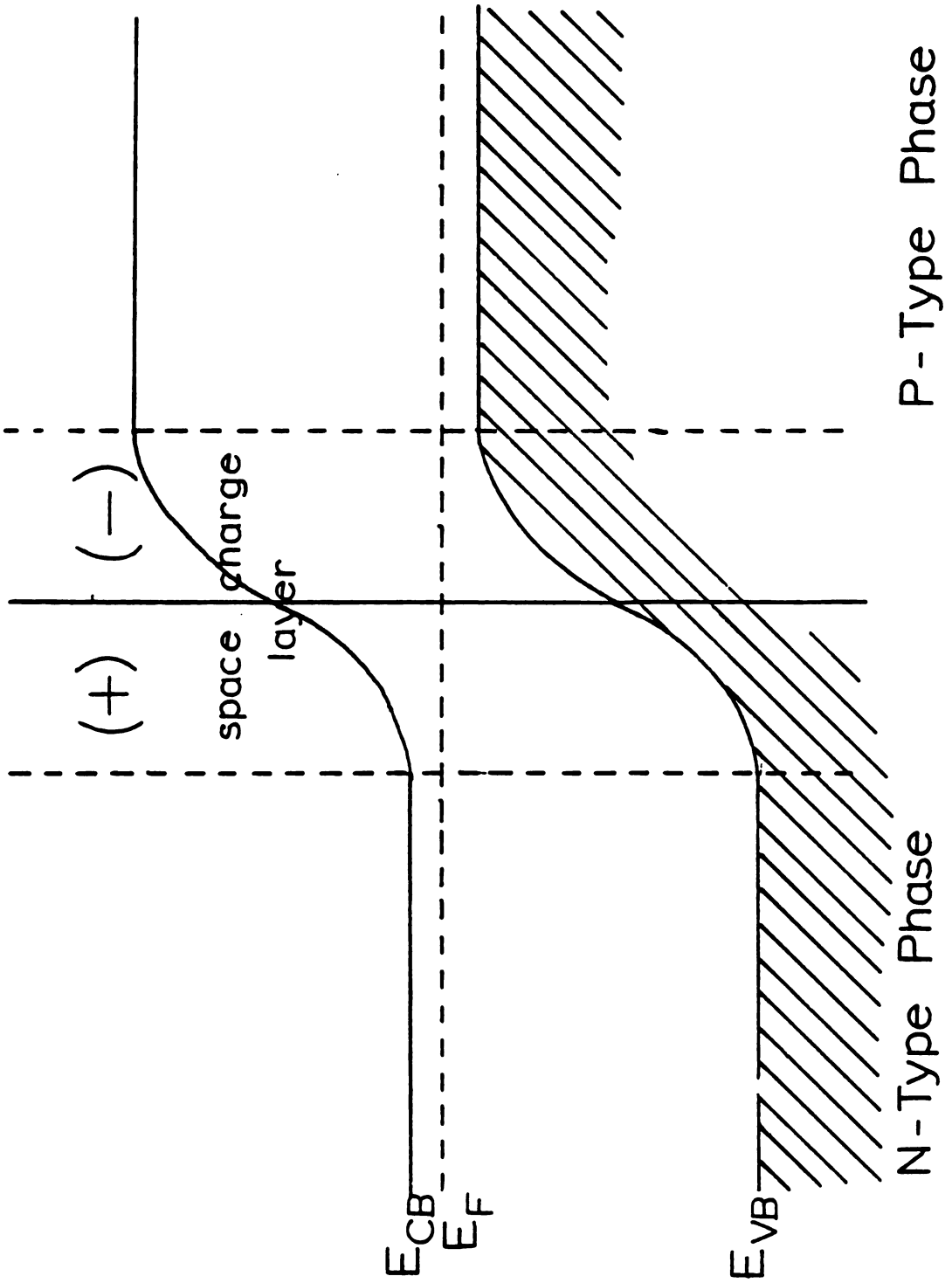

Figure 2.3.4: Phase Formation Between Semiconductors

where e is the fundamental electron charge and $\Delta\phi$ is the electric potential difference. Thus through the combined effects of a material's intrinsic μ and the potential applied to it, an energy level can be filled or emptied by adjustment of the Fermi level. This is a fundamental concept in modeling charge transfer at electrode/electrolyte interfaces.

One phenomenon resulting from semiconductor junction formation is rectification. A rectifying element is a device which allows current to flow more easily through it in one direction than another. Referring to Figure 2.3.5, barrier formation between the two semiconductor phases is a dynamic equilibrium, with a small population of electrons on the p-type side being attracted across the interface by the built-in internal field, and a large population of the n-type side having to move against the field to traverse the interface.

If one imposes an external bias on the junction such that the p-type material is made negative with respect to the n-type, the effect is to move the Fermi levels apart, even farther away from their original positions. This has the effect of increasing the amount of band bending or barrier height. Electron flow from the negative pole to the positive through the device is minute and somewhat indifferent to potential, since we have a situation where a low density of conduction band electrons in the p-type material flow with the internal field -- the probability for an electron to be

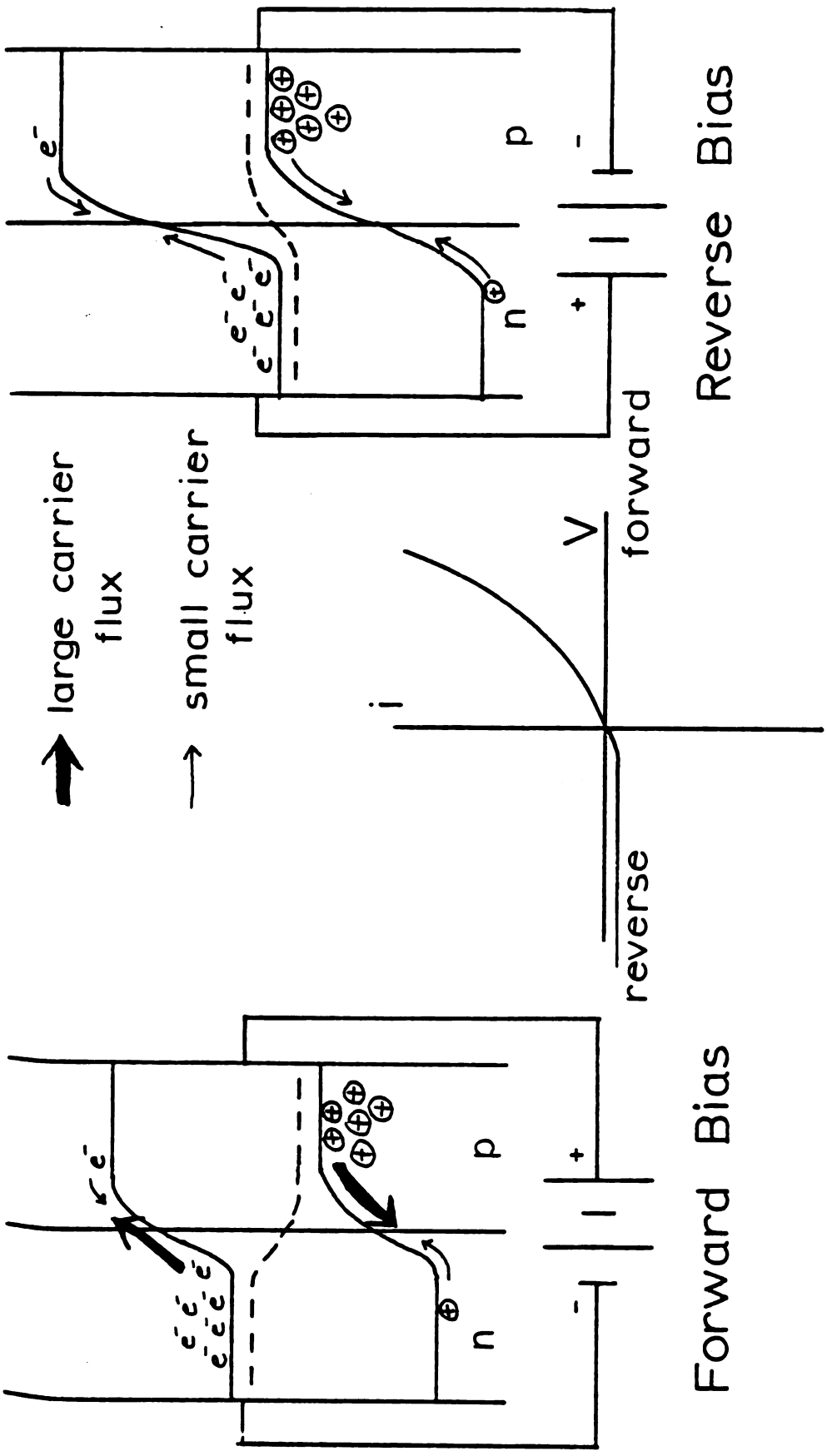

Figure 2.3.5: Rectification at a Semiconductor Junction

able to traverse the interface has not significantly changed from the equilibrium state. This arrangement of polarity is called reverse biasing.

In forward biasing, the p-type component is made positive with respect to the n-type component. Electron flow is now against the internal electric field, and so the current response will be strongly dependent of the potential controlled barrier height. The probability of an electron surmounting the barrier is an exponential function of potential, and so a small change in band bending will make a great difference in the current drawn through the device.

The characteristics of the space charge layer in terms of electron transport are determined by the sign and magnitude of the external bias and internal electric field. For the situation depicted in Figure 2.3.4, the space charge layer on either side of the junction has an increased minority carrier density and a decreased majority carrier density. Usually the new proportion of charge carriers is less than the bulk semiconductor carrier density, and so there is a depletion of charge at the junction. For this reason, the space charge layer is often known as the "depletion layer". This behavior is observed in a limited potential range when E_F is near the center of the band gap.

If the bias on the p-n junction were made increasingly reverse, a situation would be reached where the minority carrier density actually exceeds that of the majority carrier in the bulk. This state is known as "inversion".

If a large forward bias were imposed on the p-n junction, the bands across the space charge layer could be bent in a direction opposite to that of the equilibrium state. In this state the majority carrier density in the space charge layer is greater than its equilibrium value, while the minority carrier density is less. This is called "enrichment".

Thus there is a variety of situations obtainable regarding charge carrier proportion and density in the space charge layer. The depletion layer is of greatest importance for semiconductor photoelectrochemistry, because it typically exists at the moderate potentials (1-2 volts) imposed on the electrode for most electrochemical reactions.

2.3.6. Solid State Photovoltaic Effect

If a p-n junction such as the one depicted in Figure 2.3.4 were irradiated with light whose photon energy was greater than or equal to the band gap energy of the semiconductor, absorption may occur resulting in the creation of election/hole pairs. The photogenerated electron and hole are free to move independently of one another, so that if they are acted on by an electric field they will be pulled in opposite directions. Thus if photon absorption occurs within the space charge layer of a semiconductor p-n junction, the electron will be drawn by the internal electric field into the n-type component, while the hole will be drawn into the p-type component. This is shown in Figure 2.3.6.

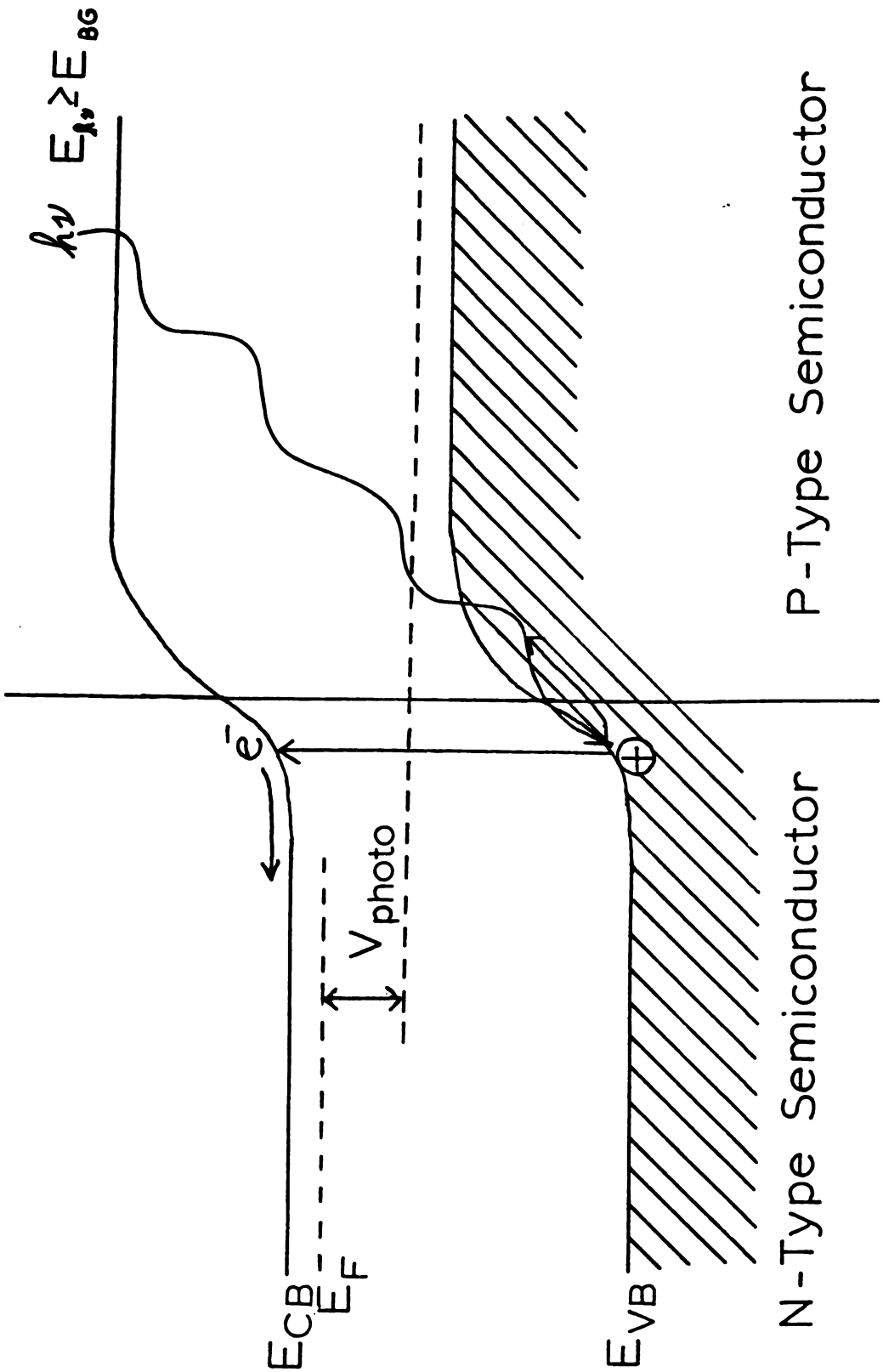

Figure 2.3.6: Photovoltaic Effect in the Solid State

This phenomenon is the basis of the photovoltaic effect. Under continuous irradiation, a new charge distribution will be built up at the junction, so that the electropotential no longer compensates for the difference in chemical potential between the two semiconductor components. The steady state difference in the Fermi levels on either side of the junction is the photopotential. This potential can serve as a power source to drive electrical devices.

The magnitude of the photopotential is determined by the intensity of light incident upon the junction. The upper limit of obtainable photopotential is the difference in E_F of the isolated components. As the photopotential increases, the amount of band bending decreases until at the theoretical limit the band bending has disappeared -- there is no longer an internal electric field to separate the electron/hole pair.

2.3.7. The Schottky Barrier

A Schottky barrier is the junction formed between a semiconductor and a metal. The energy band diagram for Schottky barrier formation between an n-type semiconductor and a metal is shown in Figure 2.3.7. The n-type semiconductor behaves just as it did in p-n junction formation. The behavior of the metal is modeled somewhat differently.

When metal and semiconductor are brought together, charge will traverse the interface just as before when both

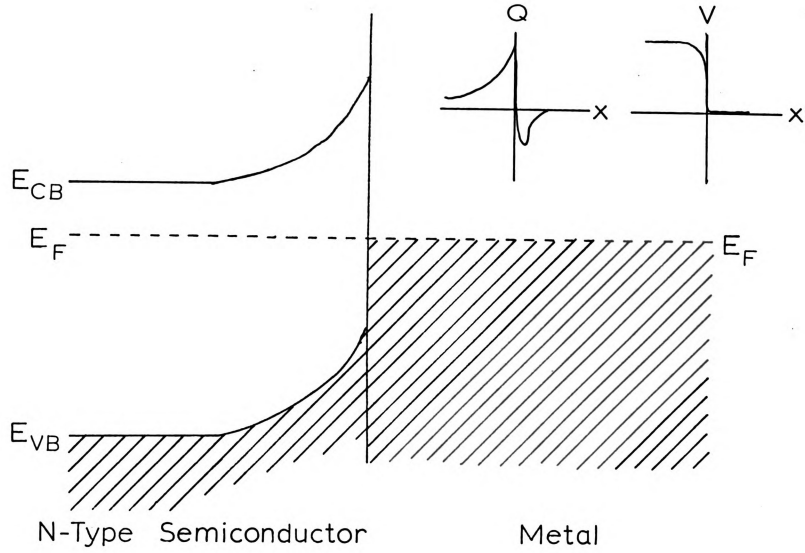

Figure 2.3.7: Schottky Barrier Formation

components were semiconductors, in accordance with the initial separation of their Fermi levels. Because the carrier density of the metal is so high, a space charge layer will not form, but rather, any net charge will accumulate at the interface within the first few atomic layers.

Rectification will occur analogously to the p-n junction. Forward biasing corresponds to making the metal positive with respect to an n-type semiconductor, or making it negative with respect to a p-type semiconductor. This assumes, of course, that a reasonable device is envisioned, where E_F of the metal is greater than that of the n-type semiconductor and less than that of the p-type semiconductor.

Since band bending and hence internal electric field formation still occur in the semiconductor side of the Schottky barrier, a photovoltaic effect is also possible. In practical device application the metal component is made very thin, so that incident light may pass through the metal phase and be absorbed within the semiconductor space charge layer. Once again, the maximum obtainable photopotential is determined by the original energy separation of the Fermi levels in the isolated components.

2.3.8. The Semiconductor/Electrolyte Interface

The theory of energy band level diagrams can, with some modification, be applied to the electrode/electrolyte

interface. In this section, the theory will be used to explain the kinetics and energetics of photoelectrochemical reactions occurring at semiconductor electrodes.

The semiconductor electrode will be treated as before, with valence and conduction bands separated by a band gap, and with a Fermi level giving the population distribution of electrons within it. To deal with the electrolyte, the concept of a thermodynamic redox level, E_{redox}, is introduced that corresponds to the electrochemical potential of the electrolyte. The position of E_{redox} can be determined from the Nernst equation:

$$E = E^{\circ} - \frac{RT}{nF} \ln \frac{[Red]}{[Ox]}$$

where E is the potential of an electrode in equilibrium with the electrolyte, E° is the standard redox potential of the electroactive species, R is the ideal gas constant, T is the temperature, n is the number of charge equivalents per mole transferred, F is Faraday's constant, and [Red] and [Ox] are the activities of the reduced and oxidized forms of the electroactive species, respectively.

E_{redox} is then simply the energy equivalent of the electrode potential, E:

$$E_{redox} = e \cdot E$$

where e is the electron charge and the other symbols have been previously defined. A convenient system of units is electron volts (eV), since an electrode potential of x volts results in an E_{redox} of x electron volts on the same energy scale.

Another problem involving convention arises when one attempts to place E_{redox} on the same energy scale as the semiconductor. Work functions (which for our purposes will be the same as the Fermi level) for solids are measured with respect to an electron an infinity, while E°'s for electrochemical reactions are given with respect to the normal hydrogen electrode (NHE). By measuring E_{redox} for the NHE on an absolute scale any E° in the electrochemical series can quickly be placed relative to semiconductor energy levels. The value of E_{redox} for the NHE on an absolute scale is approximated to be -4.5 eV (120).

When the solid semiconductor electrode is placed in contact with a liquid solution containing an electroactive species, charge will traverse the interface until the electrochemical potential is constant across the interface. In the energy band/level diagram of Figure 2.3.8, this is shown by the Fermi level of the semiconductor and E_{redox} of the electrolyte adjusting to the same value.

The energy level diagram much resembles that of the solid state Schottky barrier. In fact, the conductivity phenomena within the semiconductor component are the same in each case, so that equations derived originally for the

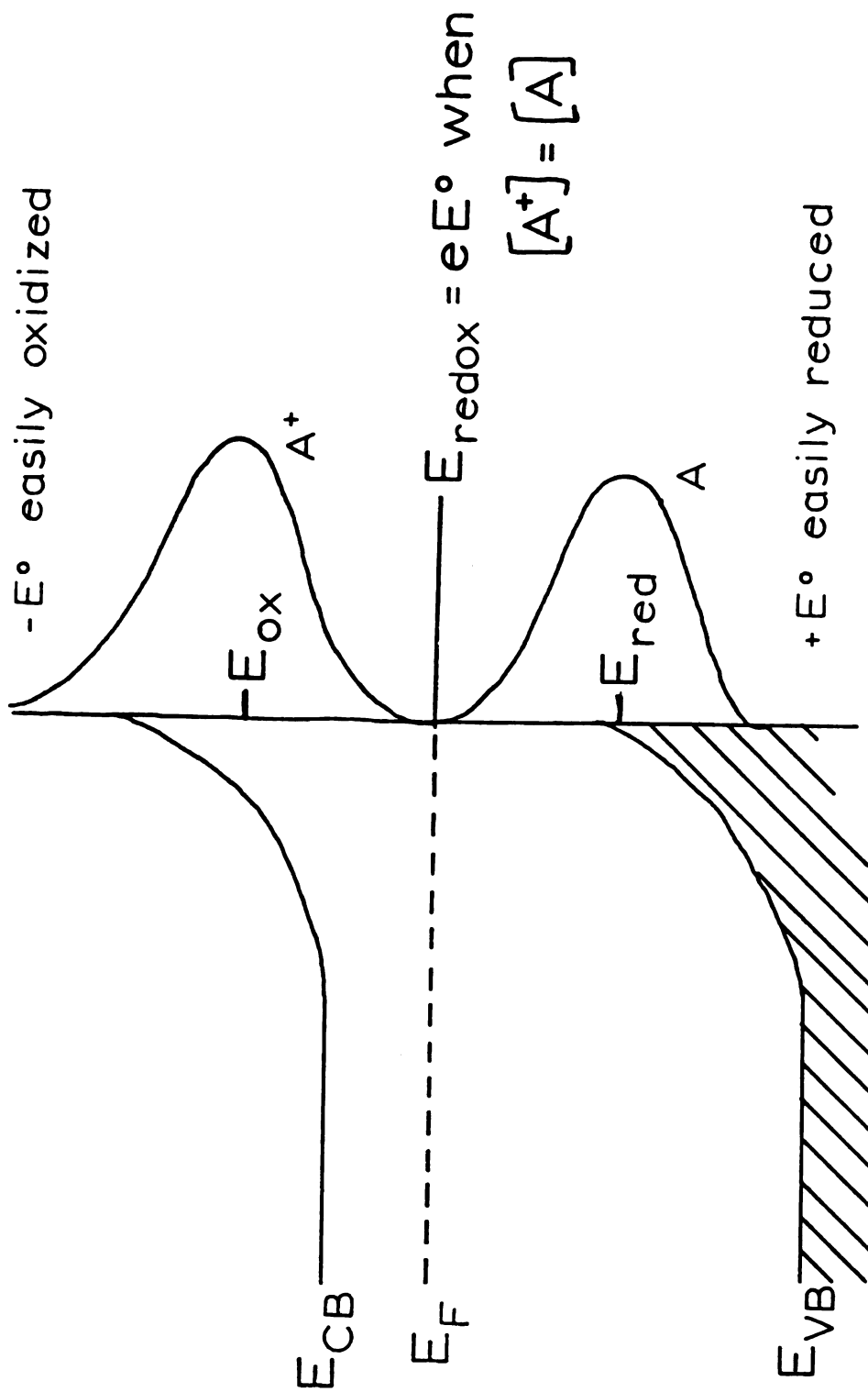

Figure 2.3.8: Energy Level Diagram of the Semiconductor/Electrolyte Interface

solid state case also apply to the semiconductor/electrolyte junction. One example is the Mott-Schottky relationship, which relates semiconductor capacitance to the potential applied to it (121).

The result of equilibration between E_F and E_{redox} is a build up of charge at the semiconductor/electrolyte interface. The semiconductor behaves just as in previous cases involving solid state junctions, forming a space charge layer at the interface. The charge distribution in the electrolyte is described by the Stern model, a synthesis of Helmholtz-Perrin, and Gouy-Chapman theories (122). Instead of electrons and holes, anions and cations become the charge carriers. Most of the net ionic charge congregates within the first few angstroms of the electrode, at what is called the outer Helmholtz plane. Beyond that distance, ion concentration decays exponentially into the bulk of the electrolyte, defining a micron-wide region of slight net ionic charge known as the diffuse layer.

The distribution of charge in electrode and electrolyte in turn determines the distribution of potential through the system. The total potential drop across the system can be divided into three parts: (1) the potential drop within the semiconductor itself; (2) the potential drop across the electrified interface to the outer Helmholtz plane; and (3) the potential drop across the diffuse layer. The third part is usually quite small compared to the other two, and is generally neglected in determining potential distribution.

The potential drop within the semiconductor is an inverse function of carrier density, so that lightly doped semiconductors can have a substantial potential drop within themselves. This is considered a voltage loss regarding electrochemical reaction, since a decreased potential drop across the electrified interface means a decreased electric field strength to drive the electrode reaction. In metals, which have high carrier densities, there is essentially no potential drop within the electrode itself, and so the external voltage is fully applied across the electrified interface. This is why in general greater overpotentials are required to drive electrochemical reactions at semiconductor electrodes than at metal electrodes.

2.3.9. Charge Transfer at Semiconductor Electrodes

To complete the energy level diagram for some redox couple, A/A^+, the energy of the orbital being filled or vacated during charge transfer is marked on the vertical axis. If the redox couple existed as free particles in the gas phase, we could simply mark a single point on the energy axis for the orbital involved in charge transfer. But since redox couples are solvated and commonly charged, there exists a solvent molecule polarization around the redox species which affects the outer orbital energies. The solvent polarization energy fluctuates around some equilibrium value, so that the orbital energy of the redox couple also fluctuates and must be expressed as a distribution. This effect is

depicted as a Gaussian curve whose maximum corresponds to the equilibrium orbital energy and whose baseline is the vertical energyscale at the electrified interface.

Since the charge on the oxidized and reduced forms of the redox couple differ by one or more fundamental unit charges, the equilibrium polarization of each will also differ, and so each will have its own distribution curve, one for A, and one for A^+. This is shown in Figure 2.3.8.

The fluctuating energy level concept is important in explaining rates of electron transfer at semiconductor electrodes. The Marcus theory of electron transfer (123) assumes that electron transfer occurs between orbitals of equal energy. Therefore, for an oxidation reaction, the electroactive species must have a filled level adjacent to an empty semiconductor level, while for reduction the electroactive species level must be empty and the semiconductor level filled.

In a metal electrode, there is a continuum of energy levels, so that by altering the electrode potential (raising and lowering the Fermi level) one can make empty or filled levels available for oxidation or reduction, respectively, of an electroactive species. In a semiconductor electrode, however, there is a band gap region where no levels are available to be filled or emptied. Thus there can exist situations where the electrode is biased at a potential where electrolysis is thermodynamically possible but cannot occur because there are no levels available in the electrode for charge transfer.

For highly doped semiconductors such situations can be overcome by electron tunnelling. Under conditions of high carrier density and high overpotential, the space charge layer is very thin, and the band edges are steeply bent. This results in a potential barrier on order of a few Angstroms thick, through which electrons may tunnel. This type of behavior has been observed on highly doped SnO_2 electrodes (124-126).

The redox level is determined by the relative concentrations of oxidized and reduced forms of the redox couple and its E°. The orbital energy level is determined by the electronic structure of the electroactive species, subjected to solvent polarization. When the concentrations of A and A^+ are equal, a convenient situation exists where the redox level lies midway between the probability maxima of the two distribution curves. The redox level at that point equals E°; therefore, E° of a redox couple can be used as a measure of where its orbital energy lies with respect to those of the electrode. This situation is shown in Figure 2.3.8.

2.3.10. The Irradiated Semiconductor/Electrolyte Interface

When the semiconductor electrode/electrolyte interface is irradiated with light whose photon energy is equal to or greater than the band gap energy of the semiconductor, absorption will occur within the semiconductor resulting in

the creation of electron-hole pairs. For photon absorption within the space charge layer, the electron-hold pair is separated by the internal electric field.

One of the newly created free charge carriers will migrate to the interface, where it can react with an electroactive species in the electrolyte. For oxidation, the electrode "injects" a hole into the electroactive species or equivalently, the electroactive species "captures" the hole from the electrode. For reduction, the electrode captures an electron from the electroactive species, or the electroactive species injects an electron into the electrode.

The case for photooxidation on an n-type semiconductor is shown in Figure 2.3.9. The energy level distribution curves have been approximated by the E° of the redox couple, A/A^{+}. In order for photooxidation to occur, the electric field in the space charge layer must be directed so that holes, and not electrons, migrate to the surface. This situation will hold if E_F is lowered from its intrinsic value, so that the band edges curve upward as they approach the surface. Under conditions of external potential control, photooxidation then only occurs when the electrode potential is held positive of the flat band potential, E_{FB}, that potential where the band edges are flat from semiconductor bulk to surface. To expand the available range of potentials for which photooxidation can be observed, n-type materials should be used which have large, negative, flat band potentials.

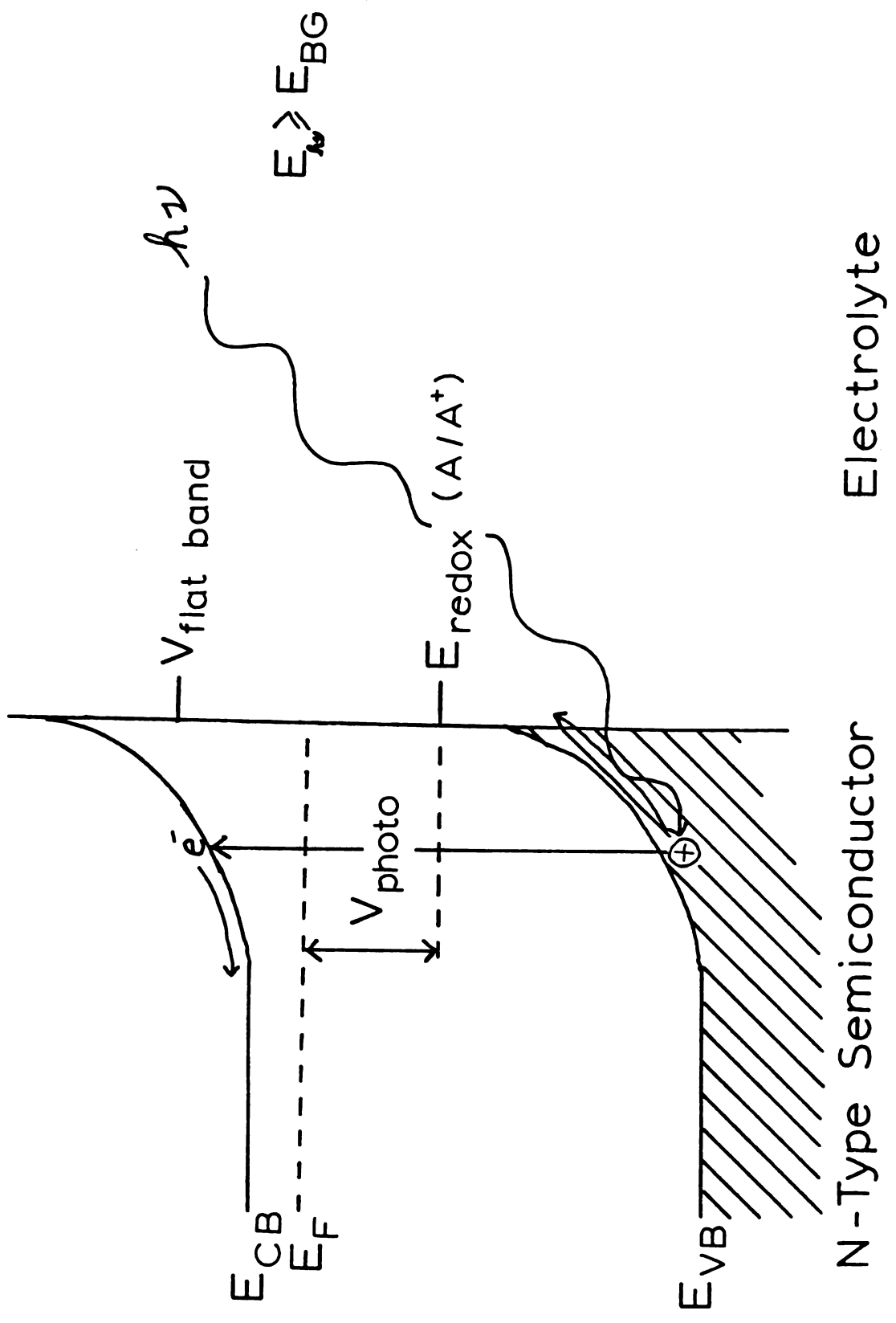

Figure 2.3.9: The Irradiated Semiconductor/Electrolyte Interface

In order to observe photooxidation at a semiconductor electrode not under external potential control, as in an energy converting photoelectrochemical cell (Figure 1a), E_{redox} must lie below, or positive of E_F of the semiconductor before junction formation; otherwise, the electrode upon immersion in the electrolyte would come to rest at a potential negative of E_{FB} and the photogenerated holes would migrate away from the electrode surface.

Just as in the case of solid state semiconductor junctions, a photovoltaic effect is possible. Under continuous irradiation, a new charge distribution results, moving E_F from its original position. The difference between E_F in the light and in the dark is the photopotential. The maximum obtainable from a given semiconductor and redox couple combination is the difference between E_{redox} of the redox couple and E_{FB} of the electrode. This value can be directly observed as the amount of band bending in the dark.

Thus far only photooxidation has been discussed. For photoreduction a p-type semiconductor would be employed and band edges would bend downwards as they approach the surface so that electrons would migrate to the interface. While for photooxidation photopotentials negative with respect to the dark occur (since E_F moves in a negative direction), photoreduction creates positive photopotentials. To model this situation a Fermi level for holes must be employed, which moves in a positive direction as light intensity is increased. The E_F for holes is then used to determine

positive photopotentials. Thus any semiconductor under irradiation has two Fermi levels, one for electrons and one for holes. Some theorists have tried to avoid this situation by calling these Fermi levels under irradiation "quasi-Fermi levels" (127) or "Imrefs" (128).

2.3.11. Dye Sensitization of Semiconductor Electrodes

As was discussed before in the introduction, light whose photon energy is less thann the band gap energy of the semiconductor will not contribute to the creation of a photocurrent. The electrode can be sensitized to sub-band gap radiation by adsorbing or otherwise confining to the surface a molecular species, such as an organic dye, which absorbs that wavelength range.

The function of a dye molecule on a semiconductor electrode surface can be represented in an energy level diagram (129) by two levels, as shown in Figure 2.3.10. One level represents the ground state redox level of the dye, and the other is the excited state redox level, denoted by an asterisk. The two redox levels are separated by an energy corresponding to some electronic transition of that dye species, typically a singlet π to π^* transition. Continuing with oxidation as the example, absorption of a quantum of radiation by the dye promotes an electron to a higher level adjacent the conduction band of the semiconductor. The dye can now inject the electron into the electrode, where it is

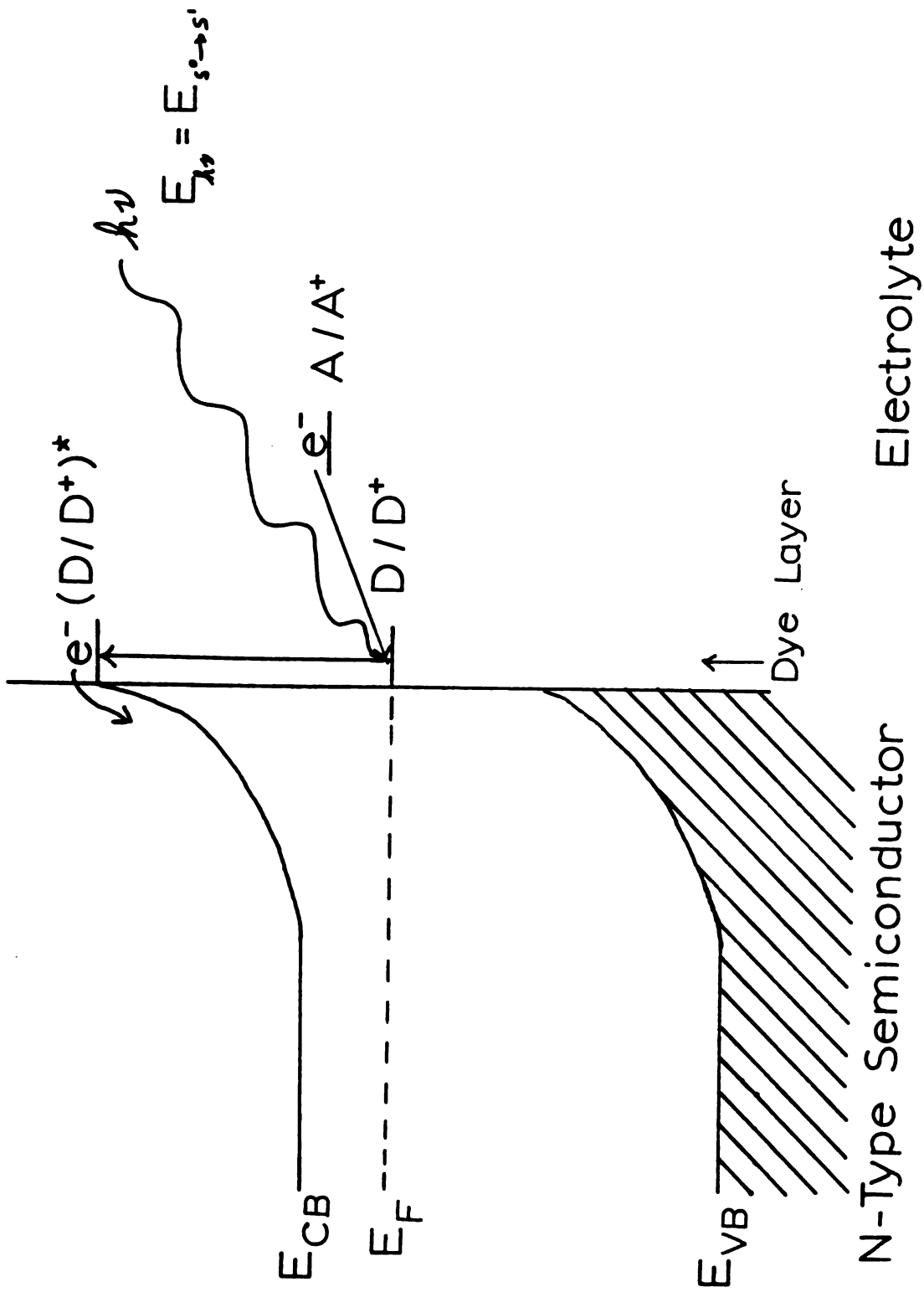

Figure 2.3.10: Dye Sensitization on Semiconductor Electrodes

drawn into the semiconductor bulk by the internal electric field.

The dye returns to the ground state as an oxidized species. If the semiconductor and sensitizing dye have been properly matched, so that the ground state redox level of the dye is well above the valence band edge, the semiconductor will be unable to reduce the dye. Thus under continuous radiation one would observe a quickly decaying photocurrent as the dye layer becomes completely oxidized. In order to maintain a photocurrent, a redox species capable of reducing the oxidized form of the dye must be present in the electrolyte. Thus any observed photopotential would be equal to the difference between E_F in the semiconductor and E_{redox} of the solvated redox species.

2.4 Examples of Spectral Sensitization

While this thesis mainly considers the electrode/ electrolyte interface under irradiation, the physical model employed finds application in technologies not usually associated with electrochemistry. In the next several sections, a number of important, light-activated, surface processes will be described, in which the problems described previously for photoelectrolysis and spectral sensitization are met again.

2.4.1. Photography

The chemistry and physics of photography has been reviewed by many authors (130-133). A schematic of the photographic process is shown in Figure 2.4.1.

Photographic film consists of a layer of photosensitive material, the emulsion, spread over a glass or paper substrate. The photographic emulsion consists of a photosensitive salt dispersed in a binder. The photosensitive salt is a silver halide. Usually mixtures of AgCl and AgBr or AgBr and AgI are used, depending on the photoresponse desired. The binder is usually gelatin derived from animal hides.

To make photographic film, an ammonium salt of one of the halides is mixed with $AgNO_3$ in a gelatin layer, producing the silver halide precipitate. In a process called ripening, the pH, concentration, and temperature conditions are held to values which cause the silver halide crystal to coalesce and recrystallize to form the desired grain size.

Upon the absorption of light a chemical reaction occurs on surface of the grain where Ag ion is reduced to its neutral state. Subsequent photon absorption by the grain causes more elemental Ag to form. The newly produced Ag, called photolytic silver, tends to concentrate at points on the surface of the grain called development centers. These centers are thought to be due to surface features on the grain known as sensitivity specks. These specks in turn are

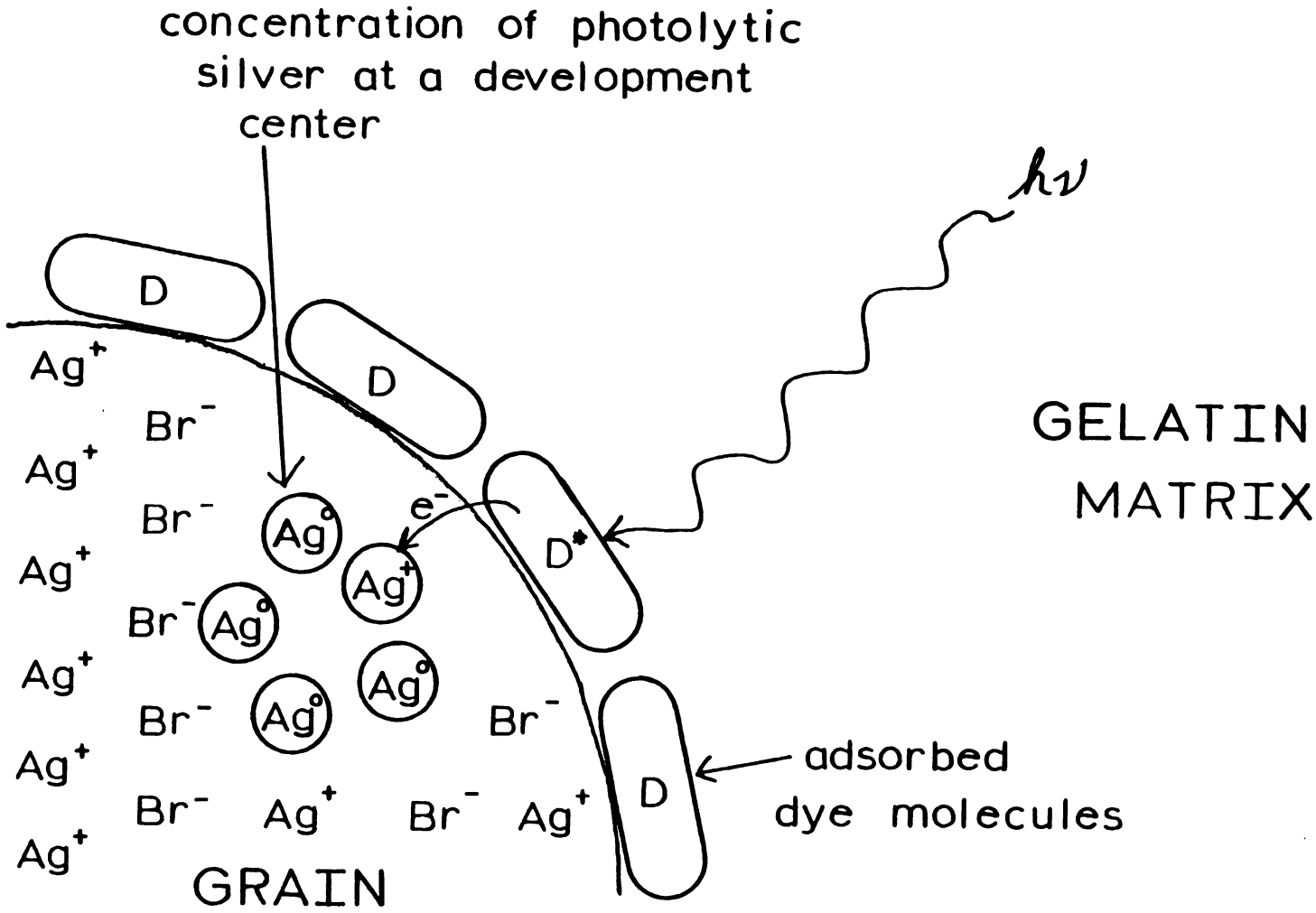

Figure 2.4.1: Latent Image Formation in Photography

the result of reaction of silver ion with trace sulfur, unintentionally included in the surrounding gelatin binder to form Ag_2S. The photographic industry had progressed to an advanced stage before the physics and chemistry of the photographic process was understood. Each grain, having undergone some degree of photochemical change, where silver halide is reduced to elemental silver, has formed a "latent image".

These sensitivity specks are very important, for the development process involves reducing to neutral silver only those AgX grains which have been exposed to light. The developing solution, usually an alkaline solution of certain amino or hydroxy derivatives of benzene, must act as a selective reducing agent. Attempts have been made to correlate developing action and standard redox potential, $E°$; a rigid correlation has yet to be found. It is thought that the sensitivity specks act as autocatalytic reagents for silver halide reduction. At least 200 silver metal atoms must have aggregated at a grain surface before reduction will occur, thus setting a lower limit to the amount of light required to form a latent image. The catalytic nature of the sensitivity speck may simply be in providing a neutralized area on the grain surface, which normally is covered by a negatively charged sheath of bromide ions, so that the developer reducing agent may approach to interact chemically with the grain.

While photographic film is still manufactured basically in the way just described, it was observed early on that using silver halide crystals possessed a limitation in that they were responsive to only a small portion of the visible range of wavelengths. AgCl is sensitive only to the ultraviolet and extreme violet; AgBr, pale yellow in color, is sensitive into the blue; and AgI, even more yellow in color, possesses an absorbance maximum at 423 nm but is not as photoconductive as the others. The highly colored objects in the greens, yellows, oranges, and reds would be contrasted on film only to the extent of variation of their absorbance in the blue and ultraviolet.

The first instance of dye sensitization occurred in 1873 when Vogel observed that his photographs were responsive to green light after he had included a green dye in the emulsion as an anti-halation agent (134). While many dyestuffs have been tested as a potential photographic sensitizer, most were eventually eliminated from consideration due to poor efficiency of sensitization, poor chemical stability, side reaction with emulsifier, and desensitization of other parts of the spectrum. Today, cyanine and related dyes are used to exclusion of all others in the photographic industry. By incorporating them into the emulsion so that they adsorb to the silver halide grains the entire visible spectrum may contribut to formation of the latent image.

One concept that bears introduction at this point is supersensitization. A supersensitizer is any substance which

improves the response of some spectral sensitizer, even though it may not have any sensitizing action of its own. It may not even be colored. The first supersensitization occurred when Bloch and Renwick (135) observed an increase in the red photoresponse of pinacyanol in the presence of the yellow dye auramine, itself a weak blue sensitizer.

Some have used supersensitization to describe the regeneration of a dye layer at a semiconductor electrode by a solvated redox species (24). Indeed, the presence of the electroactive species improves the spectral response of the dye sensitizer under continuous radiation. However, the author believes this to be an improper use of the term. Supersensitizers in the photographic industry are dyes which when mixed in small proportion with another dye serve to increase or shift the intensity of absorption, or enhance adsorption to the grain surface (136). In the photoelectrochemical situation, the redox couple does nothing to augment the fundamental spectral sensitizing ability of the dye. Furthermore, sensitizer/supersensitizer combinations involve specific interactions -- most dye combinations are desensitizing. On the other hand, the oxidized dye on the semiconductor electrode can use any redox couple whose E° is negative enough and has reasonably fast kinetics for charge transfer.

2.4.2. Electrophotography

In 1938 Mr. Chester Carlson successfully demonstrated a duplicating process based upon the idea of using photoconductor controlled electrostatic forces to form a latent image. He named the process electrophotography, but it was later to be named Xerography. Electrophotography has gone on to include any photography that uses electric processes to produce images. The two best known electrophotographic methods are Xerography and Electrofax (137). As an example, the xerographic process is described below and in Figure 2.4.2.

A photoconductive surface, typically a selenium alloy, is deposited onto a rotary drum, and given a positive electrical charge. A document or other object is illuminated, and its reflected image is focused onto the photoconductive surface. Areas on the surface which receive photons become neutral, while areas corresponding to darkened areas of the object remain charged. Negatively charged powder (graphite) is then spread over the surface. The powder adheres only to the charged image areas. A piece of paper is placed over the surface and given a positive charge. The powder image is electrostatically transferred to the paper and is fused into it by heat. The drum is then cleaned by a brush, so that the process may be repeated.

The heart of any electrophotographic process is in how the latent image is formed. Originally the surface was

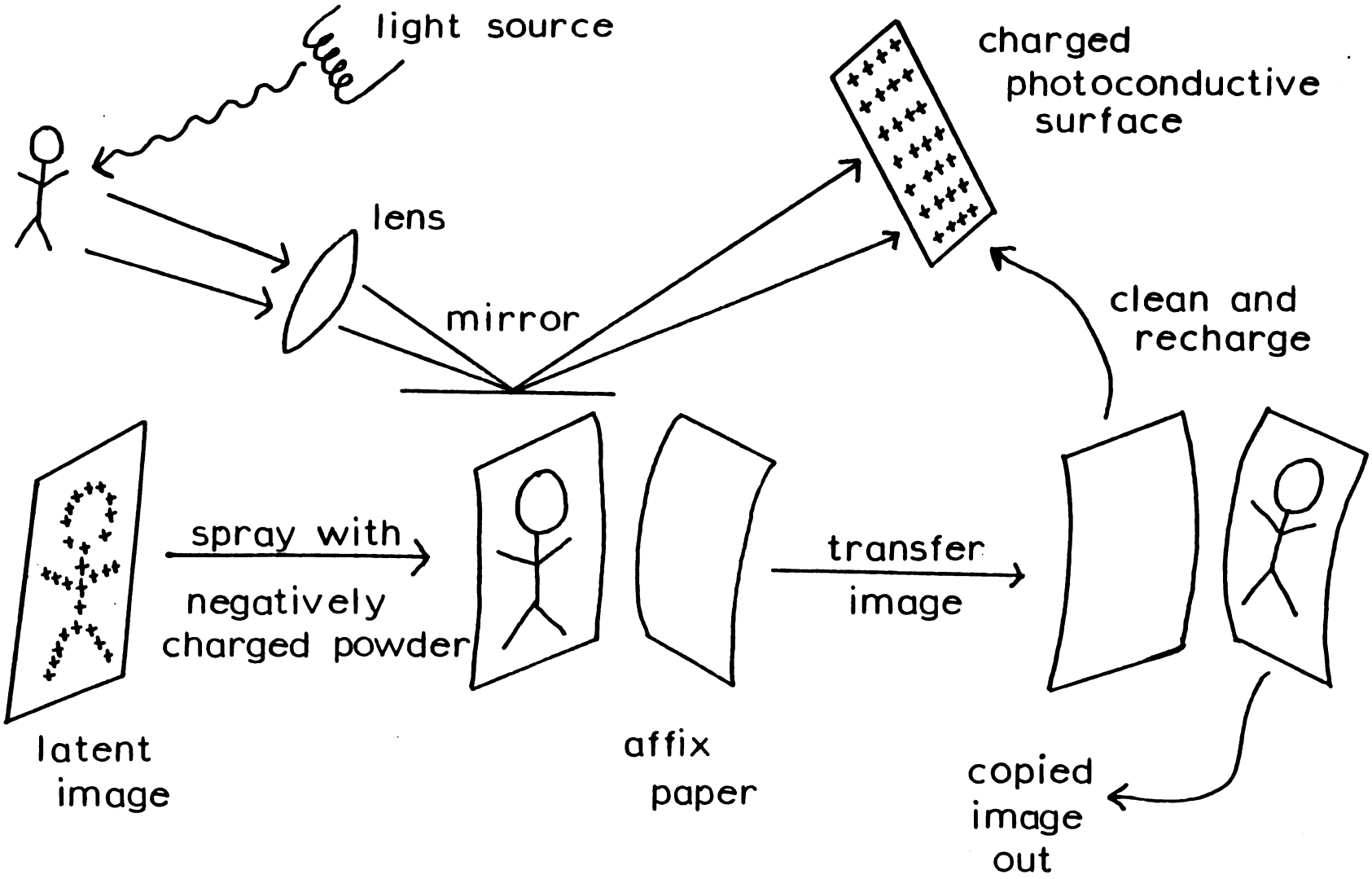

Figure 2.4.2: The Xerographic Process

charged by exposure to a corona discharge of an adsorbing gas, such as O_2 or N_2. Since then, development of electret materials has enabled charging by a temporarily applied high voltage.

An electret is a substance upon which an electric polarization can be induced that does not decay after removal of the stimulus. This effect has been observed for many insulators and semiconductors, some of which were inorganic while others were organic and whose morphologies varied from single crystal to polycrystalline to amorphous. Depending on the stimulus employed, electrets have been classified as thermo-, photo-, electro-, and radioelectrets. The principles of operation appear to be the same once the stimulus is applied. Using concepts that were elucidated in the chapter on electron transfer at semiconductor electrodes, an electret possesses an electronic band structure such that its electrical conductivity is negligible. Upon application of the stimulus free charge carriers are created which can then be acted on by an external electric field. Free electrons will be attracted in one direction, while the holes will be drawn in the opposite direction.

An electret possessed deep traps, localized levels well inside the band gap region; furthermore, it must not have shallow traps, levels that lie near the conduction or valence band edges. Many of the free carriers are trapped in these deep traps, creating a nonhomogeneous distribution of trapped electrons and holes. When the stimulus is removed, the

filled traps, having a very low probability of emptying via thermal excitation at room temperature, remain filled, and so the polarization is preserved.

Our interest is in the photoelectrets, substances which are charged or discharged via irradiation. In the xerographic process, irradiation discharges all areas of the surface except that of the image -- this is a positive image. One also has the option of applying the electric field during irradiation, thus charging the irradiated areas and creating a negative image, in analogy to positive and negative film in regular photography.

The wavelengths of light which will activate the electrophotographic process are once again determined by the absorption spectrum of the photoconductive surface. Some materials, such as ZnO, otherwise behave well but have no sensitivity toward visible light. Young and Frieg (138) first demonstrated dye sensitization of photoelectrets by depositing eosin, erytheosin, and rose Bengal on ZnO. Since then, numerous photoconductive materials, including some phthalocyanines (75, 139) have been employed.

2.4.3. Photosynthesis

Photosynthesis is the process performed by most plants that converts sunlight into chemical energy. The chemical equation expressing the overall reaction is

$$6\ CO_2 + 6\ H_2O \xrightarrow[Chl]{h\nu} C_6H_{12}O_6 + 6\ O_2$$

where hν refers to light input and Chl stands for chlorophyll, the substance that absorbs it.

Earth's plant life uses only 0.1 percent of the total annual solar irradiance, yet even that small fraction means 3×10^{21} Joules of fixed photosynthetic energy. That figure is nearly an order of magnitude larger than mankind's entire annual energy consumption (140).

The immediate products of photosynthesis are adenosine triphosphate, ATP, and nicotinamide adenine dinucleotide, NADPH, which are the standard energy currency of cells. These are used in turn to synthesize carbohydrates, fatty acids, and amino acids. The photosynthetic apparatus is contained in subcellular organelles called chloroplasts. In the higher plants, chloroplasts are discs or flat ellipsoids 3 to 10 μ across, and 1½ μ thick. Contained within the continuous outer membrane of the chloroplast is a somewhat granular, proteinaceous matrix, called the stroma, in which the internal membranes are embedded. Using the nomenclature of Menke (141) and Weier (142), these small membranous sac-like discs, called thylakoids, stack upon one another to form grana. An average chloroplast may contain about 1000 thylakoids, each about 5000 Å in diameter. The lamellar array of membranes is unusul in cellular systems, and so early on it was throught to function as a partition between oxidizing and reducing powers (143).

Within each thylakoid are on the order of 10^4 - 10^5 pigment molecules. These molecules act as the photoreceptors in the chloroplast. The main pigment photoreceptor is chlorophyll, whose absorbance spectrum is responsible for giving plants their green color. Its absorbance maxima in vivo lie at 430 nm and between 670 to 700 nm (144). The very structurally similar chlorophyll b absorbs at 470 and 650 nm.

Besides the chlorophylls, there are other secondary pigments present. The carotenoids, 40-carbon linear structures made from 8 isoprene units, consist of the all hydrocarbon carotenes and oxygen-containing xanthophylls. They generally absorb with three bands in the 400 to 550 nm region, and so are red, orange, or yellow in color. These colors can be observed in deciduous leaves in the fall season when colder temperature effect the decomposition of the predominant chlorophyll. The carotenes serve a protective role, keeping light and oxygen from breaking down the surrounding photoreceptor system. The xanthophylls act as true photoreceptors, transferring their absorbed quanta to neighboring chlorophyll a molecules.

Abundant in the blue green algae and the red algae are the phycobilins, absorbing from 570 to 650 nm. They are open chain tetrapyrroles, and appear to replace chlorophyll b in some of its functions.

Assuming a typical pigment band width of about 50 nm (145), the photosynthetic system of pigments does a good job

of using the available solar output. The short wavelength limit is set by ozone and other simple molecules at 300 nm, while water sets the upper limit at 970 and 1150 nm. Thus the 400 to 700 nm active range covered by the photosynthetic system well utilizes the remaining spectral window.

The pigment molecules organize themselves into photosynthetic units (PSU's). In the higher plants, some 200 to 400 chlorophyll molecules form a network of antennae photoreceptors, which direct their absorbed quanta via energy transfer to a reaction center, a specialized chlorophyll a molecule. Whether the entire assemblage of pigment molecules in a thylakoid form a continuous matrix in which the reaction centers are embedded in a statistical manner so that the photoexcitation energy can migrate to whatever center is open (lake model), or there are separate units, each with its own reaction center and antennae system (puddle model), is still not resolved.

The mechanism of photosynthesis is thought to be divided into two separate photochemical reactions coupled in series, photosystems I and II (PSI and II). To illustrate the progression electron flow through the system Hill and Bendall developed the "Z-scheme" (146).

In Figure 2.4.3, a simplified Z-scheme is shown where the various cytochrome and quinone proton and electron transfer agents are left out, in order to emphasize the overall reaction and the redox interpretation that may be applied.

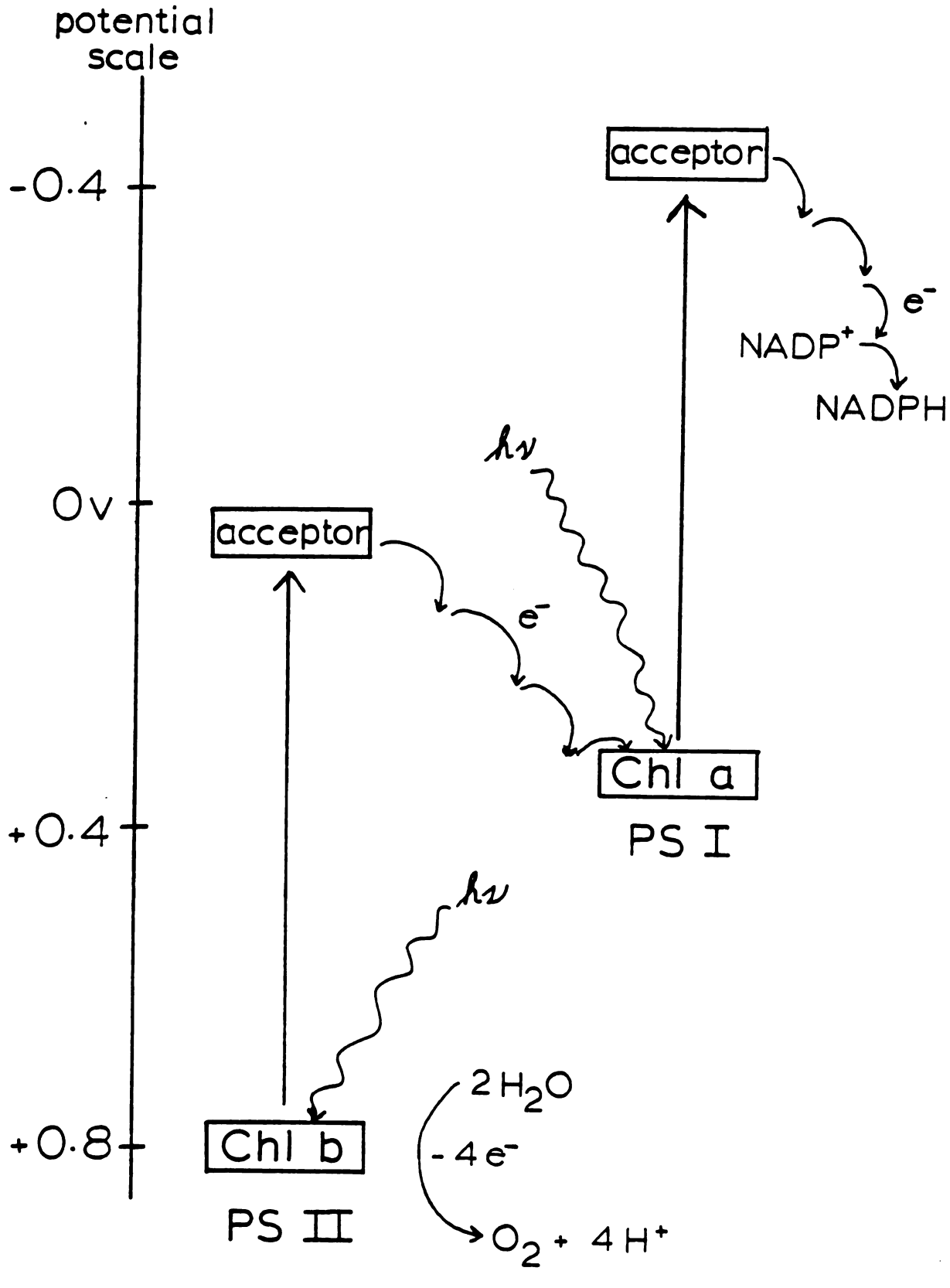

Figure 2.4.3: A Simplified Z-Scheme for Photosynthesis

Photoexcitation in photosystem II (PSII) creates an excited state with enough reducing power to produce ATP and reduce the oxidized reaction center in photosystem I. The result is an oxidized reaction center in PSII whose formal potential, or E°', at neutral pH is large and positive enough to oxidize water to oxygen. Photoexcitation in PSI results in a species with enough reducing power to reduce $NADP^+$, which has a large negative E°'.

In summary, the photosynthetic process is one where chlorophyll reaction centers are able to use the entire visible spectrum to drive a reaction whose products have formal potentials differing by 1.2 volts. Thus there is a prodigious driving force for the back reaction. The reaction of NADPH and O_2 is prevented, however, because they are produced on opposite sides of the thylakoid membrane. This is shown in Figure 2.4.4. The thylakoid membrane could be thought of as a semiconductor photoelectrode, with an oppositely directed flow of positive and negative charge carriers through it.

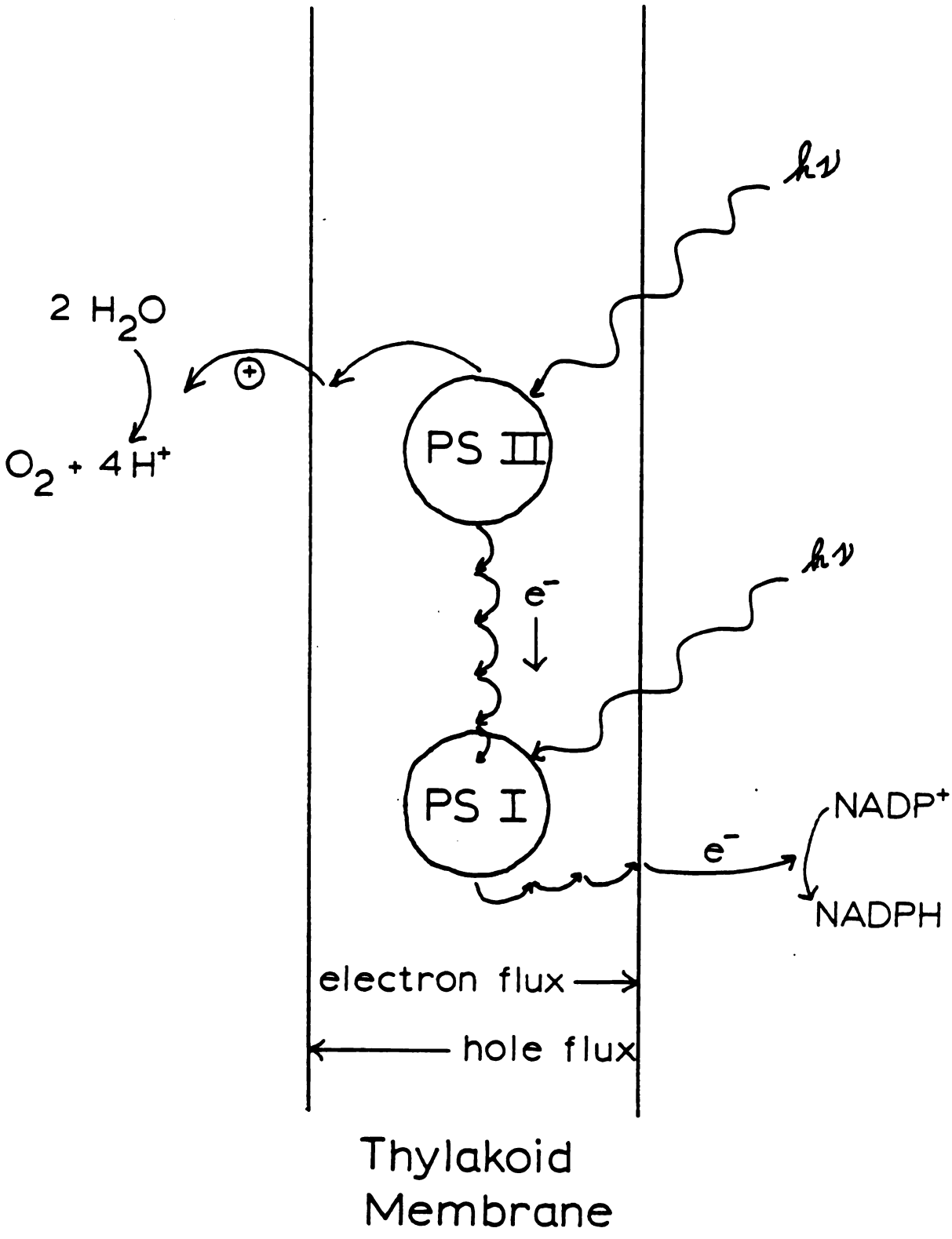

Figure 2.4.4: The Photosynthetic Membrane Acting as a Photoelectrode

3. EXPERIMENTAL

3.1. Photoelectrochemical Equipment and Materials

3.1.1. Voltammetric Apparatus

Electrode potentials were controlled by means of a potentiostat of conventional design constructed in the laboratory. A circuit diagram combining the elements of potentiostat, current to voltage conversion, and ring electrode modules is shown in Figure 3.1. A commercially available PAR 174A polarographic analyzer was also occasionally used. The working electrode potential was monitored on a Keithley 178 digital multimeter. Voltammograms were recorded on a Houston 2000 XY recorder

3.1.2. Optical Apparatus

The main light source used for photoelectrolysis was a 450 W Xenon arc lamp (Oriel Corporation). For most experiments it was desirable to use only the visible and near infrared output of the xenon lamp, and so a set of highpass and bandpass filters (Oriel) was used to cut out the other parts of its spectral output. The most common filter combination was a water filter to cut out most of the infrared and a longpass 0.47 μm filter which cuts out all of the ultraviolet. This gave a polychromatic beam energy of about 100 mW/cm^2. Intensity dependence measurements were

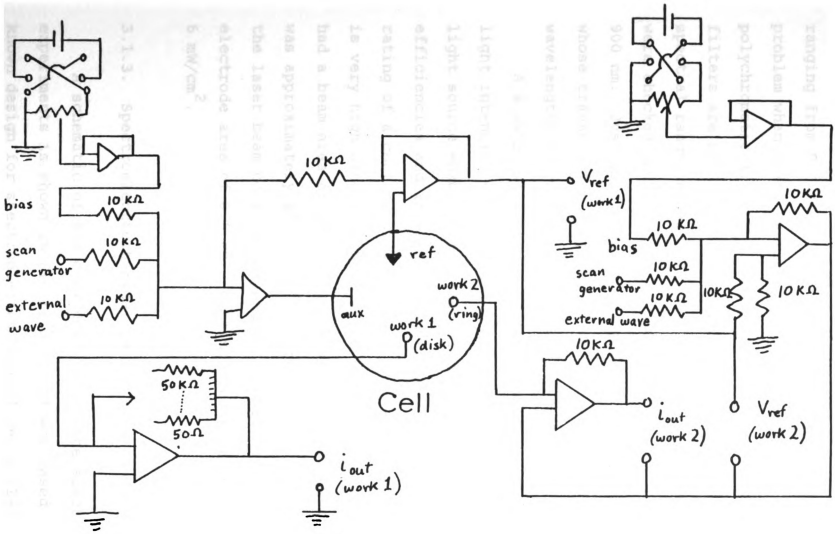

Figure 3.1: Circuit Diagram for a Four-Electrode System

accomplished with a set of neutral density filters (Oriel) ranging from 0.1 to 2.0 in optical density. A potential problem when using neutral density filters with a polychromatic light source such as the xenon lamp is that the filters are not truly neutral throughout the source's spectral range, especially in the infrared. These filters were checked and found to be neutral at least from 350 to 900 nm. Just as a precaution, a lowpass infrared filter whose transmission drops to 2% at 900 nm and longer wavelengths was used in the intensity dependence work.

A 4 mW He-Ne laser (Hughes Aircraft) was used for the light intensity experiments. The monochromatic (632.8 nm) light source enables accurate calculation of quantum efficiencies and intensity reductions. Even though the power rating of a continuous wave laser is low, its power density is very high since the beam width is so small. This laser had a beam area of about 0.01 cm so that its power density was approximately 400 mW/cm^2. With the use of a convex lens, the laser beam could be expanded to cover the normal electrode area of 0.6 cm^2, cutting the laser power density to 6 mW/cm^2.

3.1.3. Spectroelectrochemical Cell

A schematic of the cell used in all the electrochemical experiments is shown in Figure 3.2. It was based on a well known design for spectroelectrochemical cells (147), but with the following constraints:

Figure 3.2: Spectroelectrochemical Cell

a. exit port
b. reference electrode input
c. auxiliary electrode input
d. entry port
e. screw hole
f. electrolyte reservoir in optical path
g. electrical contact recess
h. O-ring recess
i. screws
j. front masking/fastening plate
k. window
l. O-ring
m. cell body
n. O-ring
p. electrode
q. rear masking/fastening plate
r. hex nuts

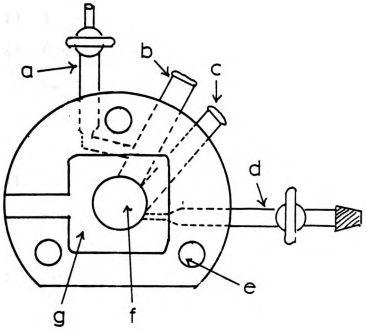
a
b
c
d
e
f
g

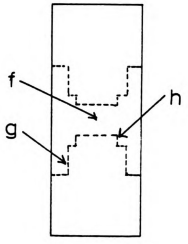
f
g
h

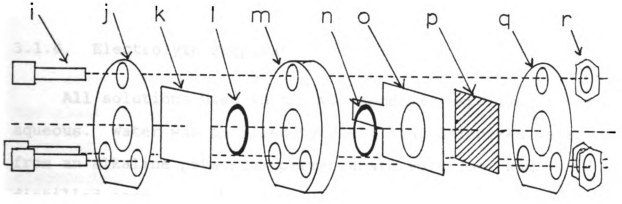
i
j
k
l
m
n
o
p
q
r

(1) 1 cm optical path length.

(2) Compatibility with the Shimadzu spectrophotometer cell compartment. The sample beam center-to-wall distance is one inch, setting an upper limit to the width of one side of the cell.

(3) The cell is adaptable to a vacuum degassing system, where the electrolyte is degassed in an auxiliary vessel and then flushed into the evacuated cell.

(4) The cell must accommodate three electrodes; a 1/2 to 1 inch square optically transparent working electrode, with an electroactive area 3/8 inch across; an Ag/AgCl reference electrode; and a coiled Pt wire as an auxiliary electrode. Although not necessary, this cell was made with the capability of holding two OTE's or other planar electrodes, one at either end of the optical path.

3.1.4. Electrolyte Preparation

All solutions used in the voltammetric experiments were aqueous. Water was purified by distilling deionized water from an alkaline potassium permanganate solution, and distilled once again before collecting in a Nalgene storage vessel.

All salts used in supporting electrolytes were ACS reagent grade and used without further purification. Low pH solutions of sulfuric acid were made by diluting the concentrated acid, which was obtained from J. T. Baker.

The origin and purification of the various redox couples are described below:

-- Hydroquinone: obtained from Kodak and recrystallized from water.

-- Catechol: obtained 99% pure from Aldrich, recrystallized from ethanol.

-- Benzoquinone: obtained practical grade from MCB and purified by sublimation at low heat from a gas burner under ambient atmosphere.

-- 1,4-napthoquinone-2-sulfonate: obtained from Kodak and recrystallized from water.

-- 9,10-anthraquinone-2-sulfonate: obtained practical grade from Eastman and recrystallized from an ethanol/water solution.

-- Potassium Ferro/Ferricyanide: analytical reagent grade, obtained from Mallinckrodt and used without further purification.

Solutions were purged of O_2 before use, unless O_2 was the electroactive species of interest. Solutions used in rotating disk experiments were purged by bubbling electrochemistry grade (99.95% pure) N_2 through them for at least a half an hour before use.

Solutions used in the spectroelectrochemical cell were deoxygenated via a vacuum degassing technique, where the electrolyte was alternately degassed and then flooded with purified N_2.

The N_2 gas line was made similar to the design recommended by Sawyer and Roberts (148), where an O_2 removal catalyst is placed between two molecular sieve chambers. The catalyst was originally Cu filings or mesh heated to 300°C, but the surface area/volume ratio was too small, so that the catalyst quickly darkened and had to be frequently regenerated by passing H_2 over it. A better catalyst was R3-11, made by BASF and obtained from Chemical Dynamics Corp. It consisted of finely divided Cu, stabilized on a pellet support. In its oxidized state the pellets appeared green, while in its active reduced form they are black. While the catalyst can be used at room temperature, it was found that its O_2-absorbing capacity was not great enough to change the color of the pellets. By heating the catalyst to 150°C, its absorbing capacity was increased and it could act as its own colorimetric indicator.

A specially designed glass vessel used to degass the solutions and transfer them to the spectroelectrochemical cell is shown in Figure 3.3. The vessel consisted of a spherical bulb with a sealed, curved tube in one side to admit and remove gasses, and a 12/18 outer joint on the other side. A thin, curved tube attached to a 12/18 inner joint mated into the outer joint of the main vessel, so that the tube could be pointed upwards while the solution was being degassed, and then rotated downwards to transfer the purged solution. A 10/18 outer joint on the end of the transfer tube enabled a tight seal with the spectroelectrochemical cell.

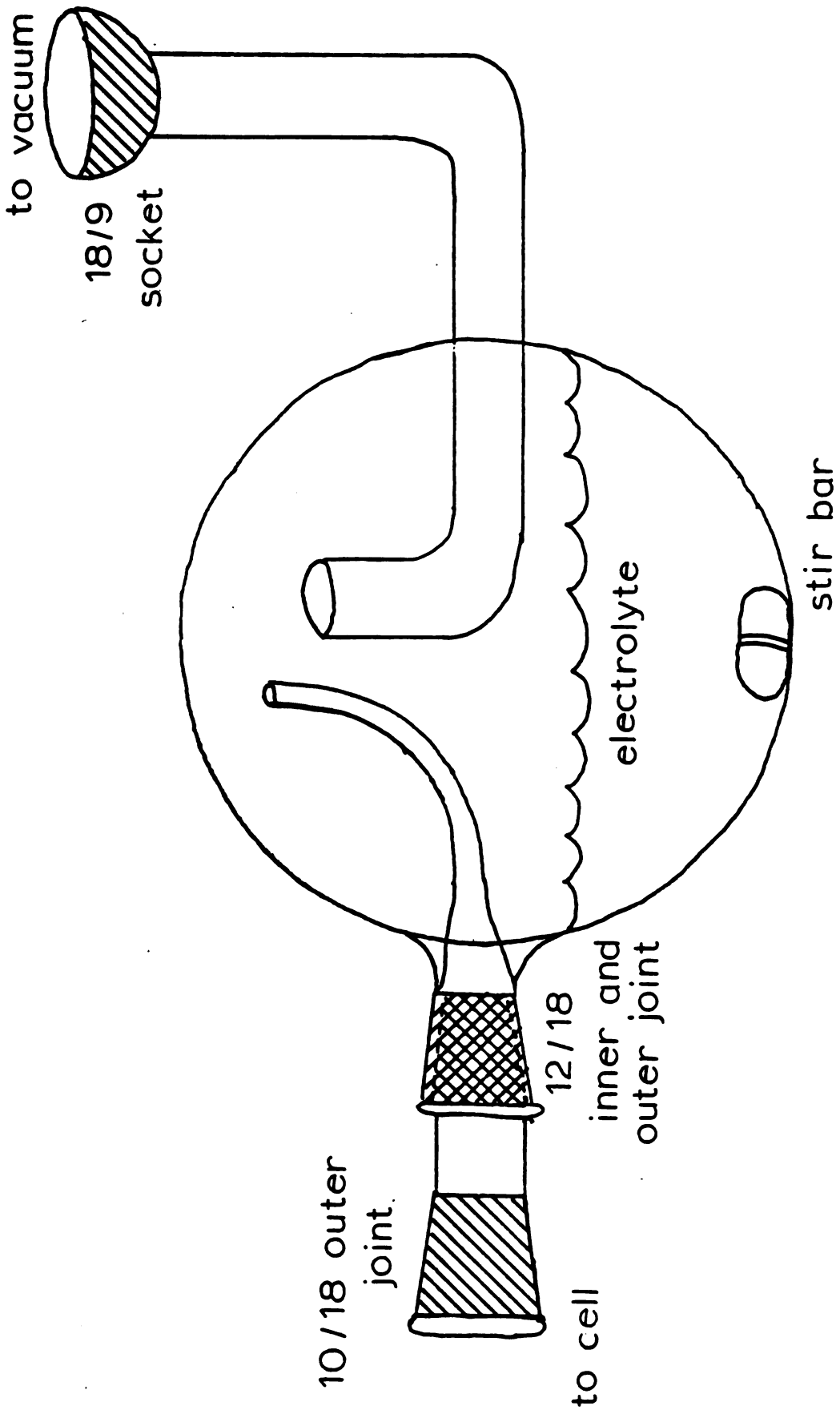

Figure 3.3: Degassing Bulb

The vacuum pump was protected by a trap cooled with either liquid N_2 or dry ice/isopropanol. Inspection of the trap after degassing a solution would reveal perhaps a milliliter of condensed solvent. Thus the degassing system did introduce some error concerning electrolyte concentration. This technique may be inadvisable for experiments where very accurately known concentrations are required, but for the experiments described here the error was of no consequence.

3.1.5. Electrode Preparation

The phthalocyanine electrodes used in all the voltammetric experiments consisted of a phthalocyanine film vacuum sublimed onto a conductive substrate. Since the difference between voltammetric results with phthalocyanine electrodes in this thesis and other reports in the literature may well be due to the film preparation, it will be described in some detail.

3.1.5.1. Substrate Preparation

Gold, silver, brass, and n-SnO_2 were used as substrate materials. Au substrates were cut from Intrex films obtained from the Sierracin Corporation. They consisted of a vapor-deposited thin (300 Å) metal film on a transparent polyester sheet, forming a metallized plastic which was utilized as an optically transparent electrode, or MPOTE (149). Intrex films consisting of thicker metal depositions on both sides of the polymer backing were occasionally used, when conditions

did not require OTE's. Au and Ag electrodes of this type were available. Their electrochemical performance was the same as the thinner Au Intrex, except that their resistance to anodic stripping was higher. The Intrex substrates were ultrasonicated 15 minutes each in ethanol and water and let dry before use.

The brass substrates were cut from a sheet (0.010 inch) and polished with increasingly fine abrasives, finishing with 50,000 mesh diamond dust. They were then ultrasonicated successively in CH_2Cl_2 and in ethanol before use.

N-SnO_2 was obtained as a 5000 Å thick film on glass plate from Pittsburg Glass. Roughly 3/4 inch square electrodes were cut and ultrasonicated in ethanol and water before use. Mott-Schottky measurements indicated a carrier density on order of 10^{19} - 10^{20} cm^{-3}, indicative of a heavily doped semiconductor.

3.1.5.2. Film Deposition Procedure

Several mg of purified phthalocyanine powder are spread evenly across the base of the sublimation vessel. A sketch of the sublimation apparatus is shown in Figure 3.4. An aluminum masking plate upon which the electrode substrates lay is supported by three indents in the walls of the vessel, two inches above the base. The 50 mm inner diameter of the vessel allows for film deposition on three 1/2 to 3/4 inch square substrates at a time. The vessel is closed and placed

Figure 3.4: Sublimation Apparatus

a. masking plate

b. indent supports

c. electrode substrates

d. thermometer

e. inner/outer 40/50 glass joint

f. to vacuum train

g. glass wool packing

h. heating mantle

i. phthalocyanine powder

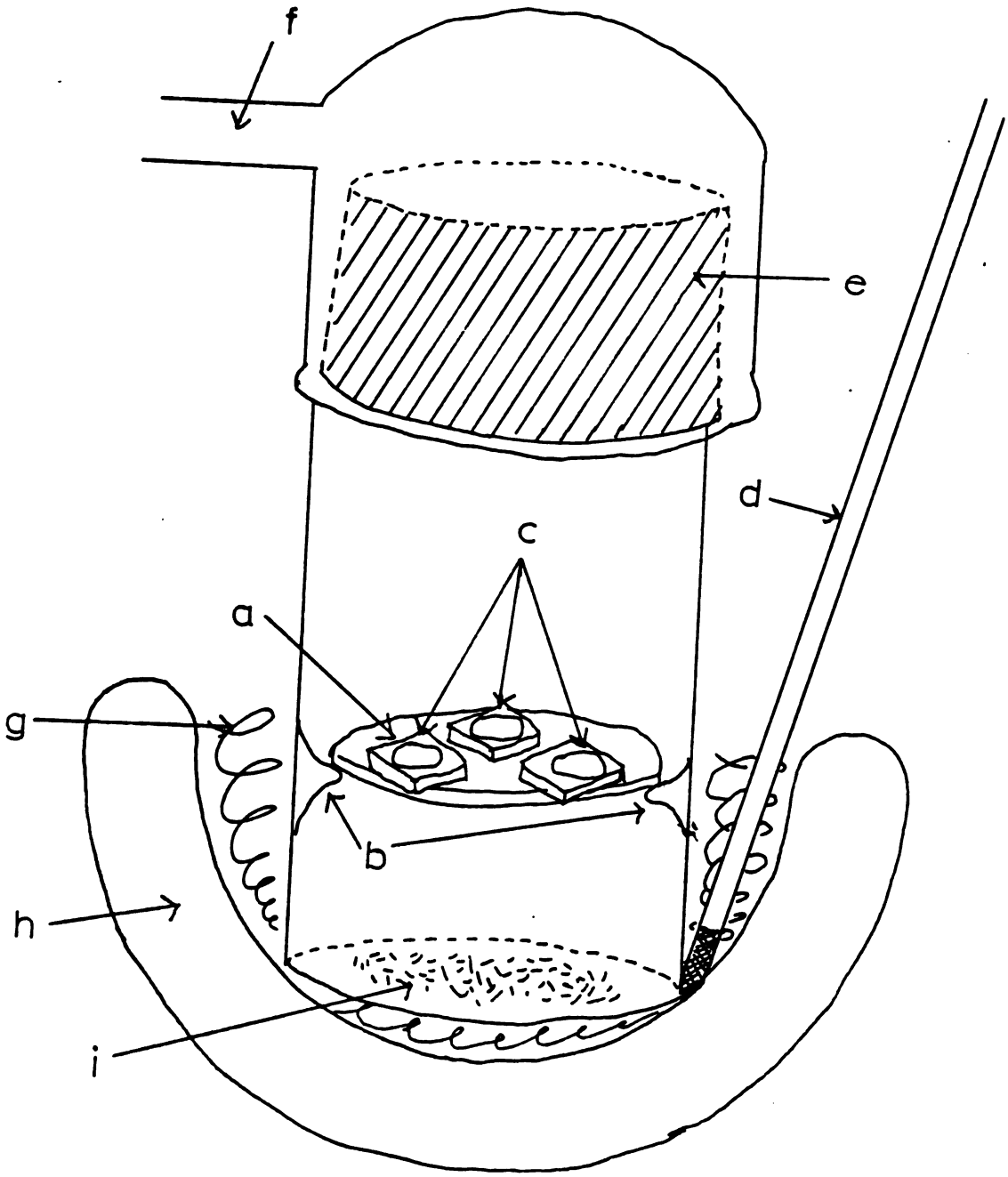
f
e
d
c
a
g
b
h
i

in a 500 ml heating mantle (Glas-Col). Glass wool is packed around the vessel, filling the volume of the mantle. A 360°C thermometer is then inserted through the glass wool packing as near the base of the vessel as possible.

The sublimation vessel is evacuated down to the 10^{-6} to 10^{-5} torr level. A variable transformer is used to apply from 55 to 60 volts to the heating mantle. In that voltage range the temperature will increase typically at 10°C per minute until a steady state is approached around 300°C. While some sublimation is occurring as low as 200°C, the rate only becomes appreciable near the steady state. Some heat is unavoidably transferred to the electrode substrates through the walls of the vessel and the masking plate during the course of deposition.

While the deposition rate is nonuniform through the course of each sublimation trial, a mean rate for the final ten minutes of sublimation can be estimated on order of tens of Angstroms per minute, which is much less than other rates reported in and calculated from the literature (10, 89, 91).

When the deposition is completed, the sublimation vessel is immediately removed from the heating mantle and the vacuum line is allowed to cool, still evacuated, under ambient conditions. The vessel is not allowed to completely cool to room temperature before opening however, for the silicone lubricant-sealed 50/60 mm ground glass joint joining the upper and lower pieces of the sublimation apparatus can become too stiff to take apart without special tools. The

slightly warm vessel is then opened and the film electrodes are ready for use.

3.1.5.3. Film Thickness Determination

While solution spectra of GaPc-Cl always gave the same absorbance maxima, those in the solid phase were less reliable. The λ_{max} for GaPc-Cl films varied between 760 and 810 nm from one sublimation trial to the next. Thus relative film thicknesses could not be directly measured to a high degree of accuracy. However, it was possible to obtain the number of moles of GaPc-Cl contained in the film to within ± 2% by dissolving the film off a substrate with a measured volume of pyridine or other suitable solvent and comparing the peak absorbance values to prepared standards.

Since there was not sufficient evidence to prove that the films were of single crystal quality, crystallographic data for phthalocyanines in the literature were not used to calculate film thicknesses. Instead, an "equivalent monolayer" was defined as an array of phthalocyanine molecules lying side by side, flat on the substrate surface. It was calculated that each phthalocyanine macrocycle would occupy about 150 $\mathring{A}^2$ surface area. By calculating the number of equivalent monolayers comprising a film, a good molecular picture of the film could be developed, against which voltammetric results could be compared.

3.2. Phthalocyanine Synthesis and Purification

3.2.1. Introduction

Eight phthalocyanines in addition to GaPc-Cl were tested in order that the function of various parts of the GaPc-Cl macrocycle in the photoelectrolysis of H_2Q could be differentiated. These additional derivatives were demetallated phthalocyanine, H_2Pc; the cobalt, iron, and copper derivatives, CoPc, FePc, and CuPc, respectively; vanadyl phthalocyanine, VOPc; the chloroaluminum derivative, AlPc-Cl; and the fluoro-gallium and iodo-gallium derivatives, GaPc-F and GaPc-I.

FePc and CoPc were chosen because they are generally considered the most catalytically active of all the phthalocyanines. CuPc was chosen because it is the most common, mainly due to its use in the clothing industry, but also because it has frequently been used in dye sensitization experiments (40, 41, 95-90). VOPc was chosen because it has been found to possess unusual spectral and photoconductive properties (150). H_2Pc was chosen because it has been a common electrode sensitizer (87, 91-95), but also because the effect of no metal center at all can be observed. AlPc-Cl was chosen so that the effect of varying the metal center within the same group of the periodic table while at the same time keeping the same counterion could be observed. Finally, GaPc-F and GaPc-I were chosen to observe any counterion effect.

3.2.2. Purification of Commercial Phthalocyanines

Of the nine total Pc derivatives, five were purchased from Eastman Organic Chemicals. The five derivatives were CoPc, FePc, CuPc, VOPc, and AlPc-Cl. They were generally quite impure, and so extensive work-up was required. The purification typically consisted of solvation in concentrated sulfuric acid, followed by precipitation by dilution with distilled water. The precipitate was collected by centrifugation or filtration, and then washed or refluxed in ethanol. Finally, a fractional sublimation was performed where only the sublimate on the lower portion of a vertical receptacle was collected.

For most of the phthalocyanines to be purified, the subliming impurities were so much more volatile than the desired product that a single sublimation trial was sufficient to achieve separation. For a few of the Pc derivatives, however, especially CoPc, a dark green, ethanol soluble impurity was only slightly more volatile than the phthalocyanines, so that a second sublimation was required.

In order to be certain that there would be no counterion exchange, the concentrated acid step was omitted for AlPc-Cl.

H_2Pc was also purchased from Eastman, but was found to be hopelessly impure. A sample from the J. T. Baker Company of much higher purity was obtained courtesy of Dr. Quintus Fernando at the University of Arizona. It was purified according to the procedure previously mentioned.

A few mg of GaPc-F were obtained from Ronald Nohr, who prepared it while working under Dr. Malcolm Kenney at Case Western Reserve. Due to the fact that it was in such a small quantity and had already been purified by sublimation, it was used without further purification.

GaPc-Cl and GaPc-I were synthesized in this laboratory. Their preparation is described in the following section.

3.2.3. Synthesis of GaPc-Cl and GaPc-I

These procedures are partly an adaptation of the method used by Busch (151) to prepare tetrasulfonated phthalocyanines. Practical grade phthalonitrile was purchased from Eastman Organic Chemicals and recrystallized from benzene. Reagent grade benzene (Fischer Scientific) and nitrobenzene (Mallinckrodt) were distilled and stored over molecular sieves until use. The anhydrous gallium trichloride and triiodide, $GaCl_3$ and GaI_3, were purchased in 1 g ampules from Alfa Products. $GaCl_3$ appeared as clear white crystals, and was listed at 99.999% metals basis. GaI_3 appeared as a yellowish powder with a few black specks, and was listed at a 99.5% metals basis. Both were used without further purification.

Several $GaCl_3$ ampules were opened under a dry argon atmosphere and solvated in benzene along with a stoichiometric amount (4 moles per mole $GaCl_3$) of phthalonitrile. The solution was put into an additional funnel and added dropwise

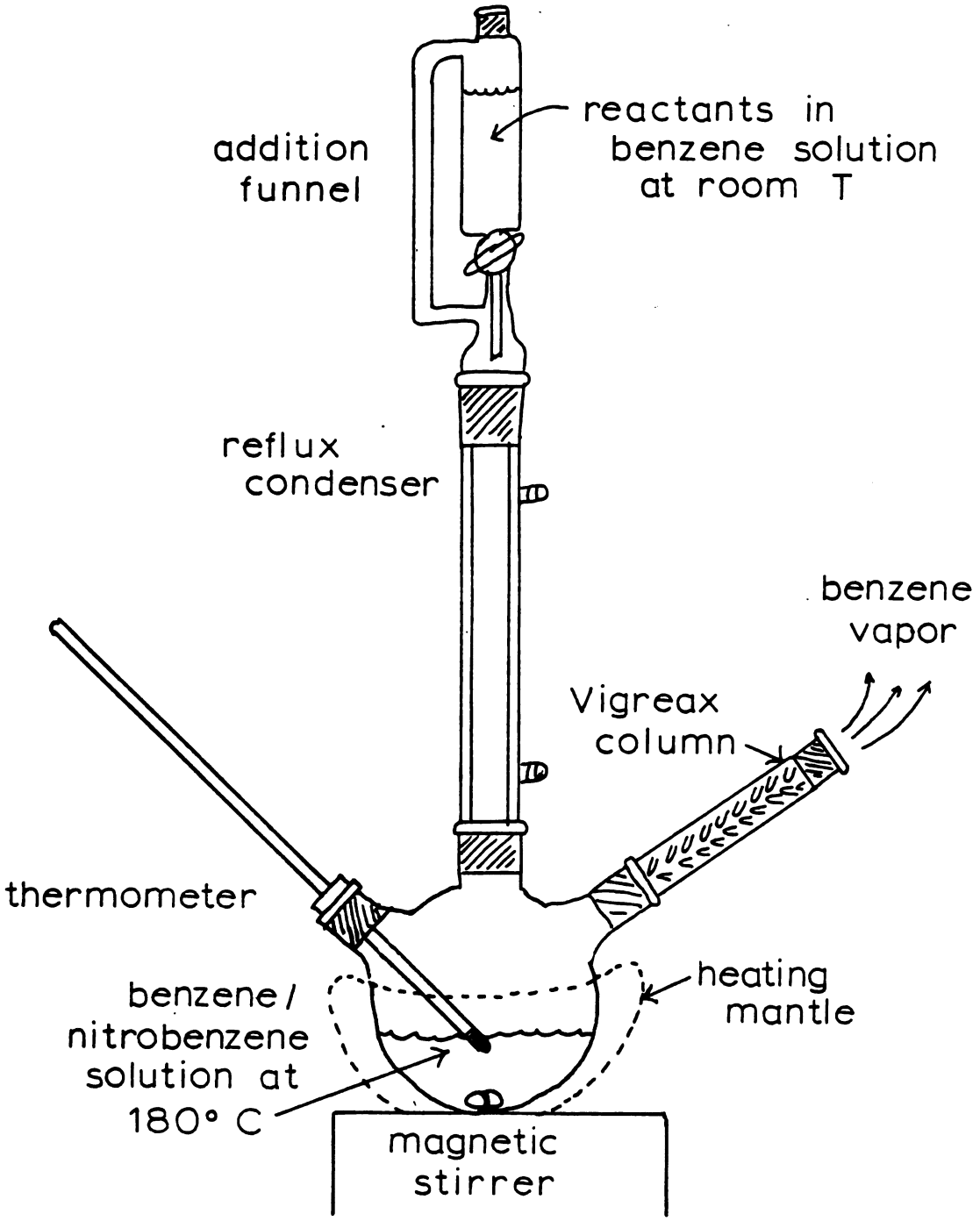

Figure 3.5: Apparatus for Synthesis of GaPc-Cl

to about 30 ml of the nitrobenzene, which had been preheated to 180°C. The drop time was kept slower than one every few seconds; otherwise, the reaction temperature could not be maintained. A sketch of the synthetic apparatus is shown in Figure 3.5.

A 3 neck round bottom flask was used as a reaction vessel. Heat was provided by a properly sized heating mantle. A water-cooled reflux column separated the addition funnel from the reaction vessel; otherwise, benzene vapor would rise through the side arm of the addition funnel and condense into the main chamber of the funnel, diluting the reactants and prolonging reaction time. Since the reaction temperature was much higher than the boiling point of benzene (80.1°C), benzene vapor was continuously boiling off and needed to be vented. A Vigreaux column was installed which allowed benzene vapor to escape without loss of any other reaction component. A condenser could be installed if it was desired to examine the exiting vapor.

The yellow nitrobenzene solution gradually darkened, turning green and finally deep purple as the reaction progressed. The reaction mixture was heated and stirred for an hour after the last of the benzene solution had been added. After the reaction mixture had cooled, it was filtered and washed, first with benzene to remove unreacted $GaCl_3$ and phthalonitrile, and then with ethanol to remove various byproducts.

The final purification step involved a fractional sublimation, utilizing a vessel quite similar to the one used to sublime electrode films except that there were no indents on the inner walls. A four inch section of a glass tube whose outer diameter was slightly less than in inner diameter of the sublimation vessel could be inserted to receive most of the subliming material and then removed for easy collection of the purified phthalocyanine layer.

The synthesis of GaPc-I was slightly different from that of GaPc-Cl. Instead of mixing the reactants in benzene at room temperature for addition to the reaction chamber, it was decided to heat the nitrobenzene with the metal halide already in it, so that the reactants would be separated until the proper reaction conditions were achieved.

When the yellow orange nitrobenzene solution was heated over 100°C, a purple vapor came off, characteristic of elemental iodine. The solution turned a similar color. Dark needlelike crystals began forming on the sides of the vessel. As the benzene solution was added, the iodine vapor began to flow out through the Vigreaux column. Varying the length of the distillation column failed to separate benzene and iodine components. The exiting vapor was collected as a purple solution and found to have an absorbance maximum at 500 nm, which was found to be characteristic of iodine in benzene by testing a solution made from shelf reagents.

At the conclusion of the reaction, the crude product appeared as a black sludge, indicative of a large proportion

of side products. Working-up as described for GaPc-Cl, however, sufficient GaPc-I was purified for experimentation.

It appears that premixing of the reagents is the preferred method of reaction. There is nothing about the physical properties of $GaCl_3$ to suggest it would behave any differently than GaI_3. Both exist as diborane-like dimers in aromatic solutions (152). $GaCl_3$ undoubtedly gives off Cl_2 as well, but it does not come off as a highly colored solution. The fate of the GaI_3 dimers after I_2 is given off is unknown. Phthalonitrile will also form side products when heated below 180°C. Thus the reactants are more apt to form side products with themselves than with the other reactant.

A possible compromise procedure would be to add the two reactants dropwise from separate vessels. This would require more complicated apparatus, but would allow for separation of reactants at room temperature until combination at the reaction temperature.

3.3. Experimental Techniques

3.3.1. Voltammetric

3.3.1.1. Steady State Current Measurements

Data for number of voltammetric experiments were obtained by applying a constant potential to an electrode and measuring the resultant steady state current. This method was used in the photocurrent dependence on concentration and intensity experiments and in the Tafel plot experiments.

Care was taken to poise the electrodes at potentials within the activation control region, so that diffusion and convection played no role in determining the resultant current.

All electrode potentials mentioned in this dissertation will be with respect to the silver/silver chloride (Ag/AgCl) reference electrode, which is 0.222 v positive of the normal hydrogen electrode.

3.3.1.2. Cyclic Voltammetry

Cyclic voltammetry is a voltammetric technique where current from an electrode is measured while its potential is varied at a constant rate. After covering a desired voltage range, the direction of voltage scan is immediately reversed, so that the electrode potential is returned to its initial potential, completing the cycle. The shape and position of the voltammetric curve can yield much information about an electrochemical reaction.

The voltammograms are plotted with current on the vertical axis and voltage or electrode potential on the horizontal axis. The voltammograms in this thesis will be presented in the American sign convention, where the positive or oxidative potentials increase to the left and negative or reductive potentials increase to the right. Positive or anodic currents will increase in the downward direction while negative or cathodic currents increase upward.

A voltammogram for a reversible one electron transfer is shown in Figure 3.6. Reversible in this sense means that the rate of charge transfer is much faster than the rate of diffusion, so that a quasi-equilibrium proportion of Ox and Red exists at the electrode surface. A coulometric analysis, one where the voltammetric curve is integrated with respect to time, would yield a net transferred charge of zero.

Terms commonly used in the description of voltammetric curves are the peak potentials, anodic and cathodic ($V_{p,a}$ and $V_{p,c}$), peak currents ($i_{p,a}$ and $i_{p,c}$), onset potentials (V_{onset}), and half-wave potential ($E_{½}$). These terms are marked in Figure 3.6. The onset potential observed is sometimes dependent on the current sensitivity used in observing the wave, as in the slow exponential growth of an irreversible wave, while in other cases it can be pinpointed, as in the onset of photocurrent when a semiconductor electrode is swept past the flat band potential.

The theory of cyclic voltammetry has been worked out by Nicholson and Shain (153). The theoretical voltammogram is derived from a complicated boundary value problem involving the Nernst equation, and Fick's Laws of Diffusion. Nicholson later wrote papers describing how kinetic data can be obtained from cyclic voltammetric curves using methods such as anodic to cathodic peak separation as a function of scan rate (154).

Qualitatively, the two types of rate control possible at the electrified interface are shown by different parts of the

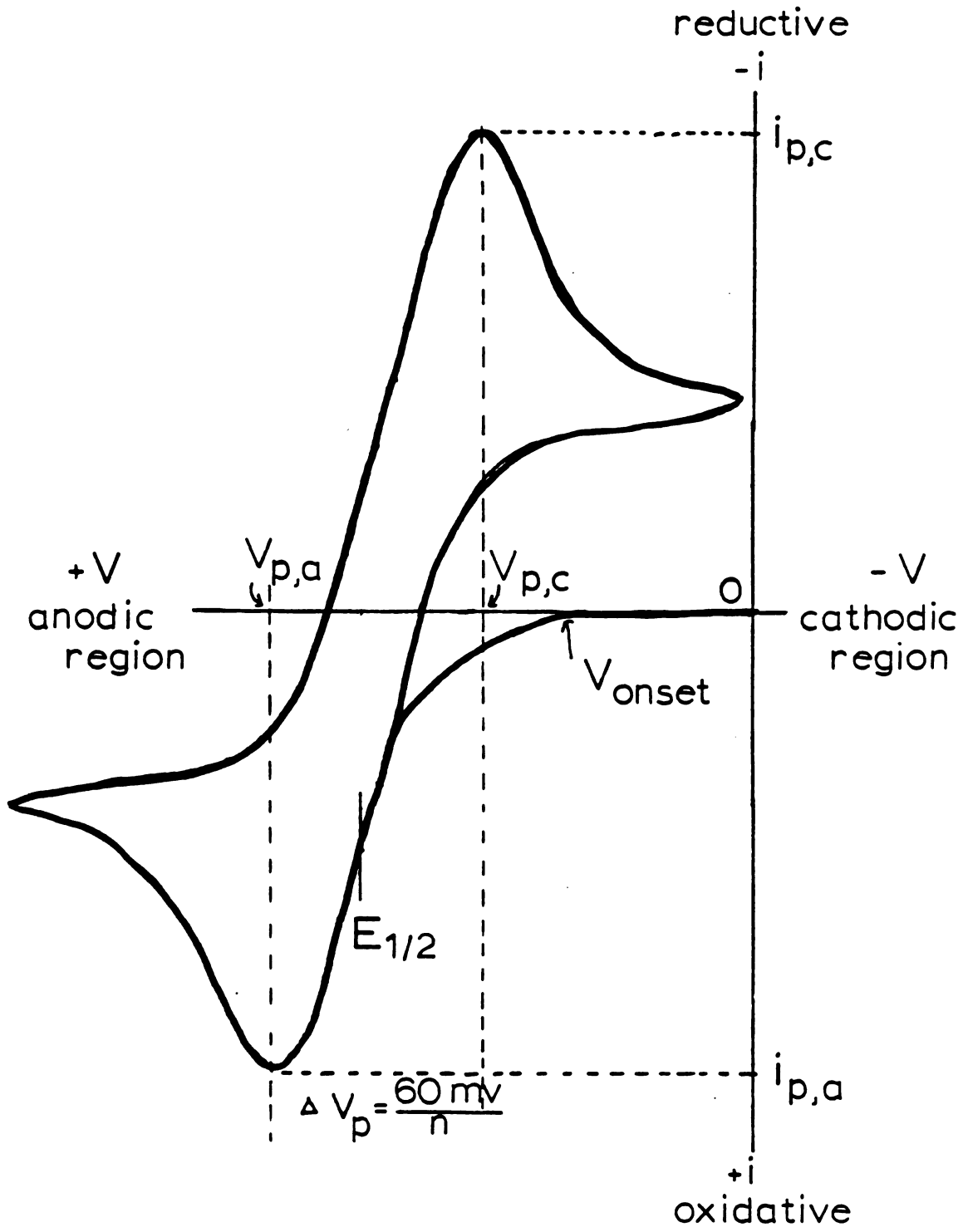

Figure 3.6: Terminology and Shape of a Reversible Cyclic Voltammogram

voltammetric curve. At low overpotential, where the rate of charge transfer given by the Butler-Volmer equation is less than the rate of diffusion, the act of charge transfer across the electrode interface is rate determining. As a result, the voltammogram in that potential range resembles the kinetic equation at low η. This region is called the activation control region.

In the high overpotential region past the current maxima, the rate of charge transfer greatly exceeds the rate of mass transfer, and so the voltammetric curve decays at a $t^{-1/2}$ dependence, much like the Cottrell equation describing chronoamperometry (155). This region is mass transport controlled. At intermediate potentials, a gradual transition from activation to mass transport control occurs.

While few redox couples exhibit completely reversible behavior, it is useful to know what theoretical limits can be approached. The theory shows that the minimum peak to peak separation between oxidative and reductive waves is RT/nF, or at 298 K, $\frac{0.059V}{n}$. Thus, for a totally reversible one electron transfer reaction the difference between $V_{p,a}$ and $V_{p,c}$ will be 59 mV. Another useful correlation is the relationship between E° and voltammetric wave. It was found that the polarographic half wave potential $E_{1/2}$, occurs at a point 85.17% of the way up the curve. The standard redox potential can then be calculated from the equation

$$E_{1/2} = E^\circ + (RT/nF) \ln (D_R/D_O)^{1/2}$$

where D_R and D_O are the diffusion coefficients for the reduced and oxidized forms of the redox couple, respectively. The E° would also correspond approximately to the midpoint potential between $V_{p,a}$ and $V_{p,c}$.

When an external bias is imposed on an electrode, it is generally assumed that the entire voltage drop occurs across the electrified interface. Very often, however, this is not the case. Even after allowing for potential drop within the electrode, which is discussed elsewhere in this report, there can be potential losses within the electrolyte as well. Unless the electrolyte is of sufficient ionic strength, its impedance will be high and can interfere with the voltammetric results. Its effect on the shape of the cyclic voltammogram has been discussed by Nicholson (156).

Any electrolyte, no matter how concentrated, will have some finite resistance. So long as its impedance is small enough that it has negligible effect on the potential imposed across the electrified interface, there is no problem. If the solution impedance does affect the potential drop across the electrified interface, i.e., the solution impedance is comparable to the "faradaic impedance", it can be partially compensated for with a positive feedback loop in the electrode circuitry between the reference and working electrodes (157).

Uncompensated solution resistance can be minimized by designing the cell so that the reference and working electrodes are close together, by keeping the working

electrode surface area and currents small, and by using a high salt concentration in the supporting electrolyte. For the cyclic voltammograms in this thesis, the cell volume was only a few milliliters, so the reference and working electrodes were by necessity close together. Supporting electrolytes were always 0.1 molar, the working electrode area was about 0.6 cm, and the currents were on order of hundreds of microamperes or less. Since the cyclic voltammetric experiments were designed only for semi-quantitative data, the precautions mentioned previously to minimize solution resistance were deemed sufficient to avoid the need for electronic compensation.

3.3.1.3. Rotating Disc Voltammetry

In regular stationary electrode voltammetry, the rate of charge transfer is controlled by the electrode potential until mass transport limitation sets in. No matter how facile the electron exchange between electrode and electroactive species, the reaction can proceed no faster than the rate at which reactants can be delivered to the electrode surface. In rotating disc voltammetry, the rate of mass transport can be varied by changing the rotational velocity of the electrode. Thus one has an additional means of control over the kinetics of an electrode reaction.

The theory of rotating disc voltammetry was developed by Levich (158). The general expression for the voltammetric curve is

$$i = \frac{nFADC_o}{1.61\ D^{1/3}\ v^{1/6}\ \omega^{-1/2} + (\frac{D}{k})}$$

where C_o is the bulk concentration of electroactive species, A is the electrode area, v is the kinematic viscosity of the solution, ω is the rotation rate, k is the rate constant for charge transfer, and the other variables have their usual meaning.

At a given ω, all variables are fixed during a potential sweep of the electrode except for the exponential dependence of k. At low overpotential, k is quite small compared to D, so that the second term in the denominator of the equation above is much larger than the first. The expression for current can then be approximated as

$$i = nFAkC_o,$$

which is identical to the term in the Butler-Volmer equation for charge transfer in one direction.

By increasing the rotation rate of the electrode, reactants are brought to the electrode surface at a faster rate. Higher potentials are then required to reach mass transport limitation. This has the effect of extending the potential region over which Tafel data may be obtained.

At high overpotential, k becomes larger than D, so that the first term in the denominator of the general expression dominates. The resulting independent current is given by

$$i_L = 0.62\ nFAC_oD^{2/3}\ \nu^{-1/6}\ \omega^{1/2}$$

where i_L is the limiting current.

Thus another advantage over stationary electrode voltammetry is the shape of the voltammetric curve. While diffusion limited currents on planar stationary electrodes have a transitory character, decaying with a $t^{-1/2}$ depndence, rotating disc electrodes have a constant limiting current. The effect of rotation is to hold the diffusion layer thickness to a constant value, typically 0.01 mm, so that the concentration gradient within is fixed. The limiting current is directly proportional to the bulk concentration of the redox couple and the square root of the rotation rate. Kinetic data can then be obtained by plotting i_L versus $\omega^{1/2}$ and measuring the slope.

3.3.1.4. Tafel Plots

The equation for potential controlled charge transfer at the electrode interface is the Butler-Volmer equation:

$$i = i_o\ (\exp\ [(1-\alpha)\ \eta F/RT]\ -\ \exp\ [-\alpha\ \eta F/RT]).$$

i is the observed, or net current density; i_o is the exchange current density, or the equal and opposite current flowing in each direction at the standard equilibrium potential; α is the transfer coefficient; η is the

overpotential, or difference between the applied potential and the standard redox potential of the redox couple involved in charge transfer: $\eta = V_{applied} - E°$; F, R, and T have their usual meaning.

The equation contains two exponentials, one corresponding to oxidation, the other to reduction:

$$\text{oxidation:} \quad \exp\ [(1-\alpha)\ \eta F/RT]$$
$$\text{reduction:} \quad \exp\ [-\alpha\ \eta F/RT]$$

At very low overpotential, on the order of 0 to 100 millivolts, the two terms are comparable in magnitude. At high overpotential, diffusion begins to affect the current and the Butler-Volmer equation is no longer valid. In the intermediate overpotential region however, the equation holds with one exponential being much larger than the other.

Using oxidation, for example, a positive η in the range described above makes the oxidation exponential so much larger than the one for reduction that we can ignore the reduction term in the Butler-Volmer equation and simplify it to

$$i = i_o \exp\ [(1-\alpha)\ \eta F/RT]$$

Taking the natural logarithm of both sides, and rearranging terms,

$$\ln i = [\frac{(1-\alpha) F}{RT}] \eta + \ln i_o$$

A plot of ln i versus η in the upper range of potentials in the activation control region will then give a straight line whose slope is $\frac{(1-\alpha)F}{RT}$ (or $\frac{-\alpha F}{RT}$ for reductive currents) and whose intercept is ln i_o. Thus the kinetic parameters α and i_o can be derived from Tafel Plots.

Since in practice E° is not always known for a given redox couple and electrolyte, rather than plot ln i versus n it is plotted against $V_{applied}$. If ln i is plotted for both oxidation and reduction, the intersection point of the two extrapolated lines will have E° as the horizontal coordinate and ln i_o as the vertical coordinate. This is shown in Figure 3.7. This approach was particularly important for the electrochemical systems under illumination, since any photopotential generated would shift the apparent E° from its dark value.

3.3.1.5. Capacitance Measurements: Mott-Schottky Plots

Assuming a Boltzmann distribution of charge at the surface of a semiconductor under depletion layer conditions, Mott (121) derived an expression for the capacitance as a function of potential:

$$\frac{1}{C^2} = (\frac{8 \pi}{\varepsilon\ en_o}) (V - V_{FB} - \frac{kT}{q})$$

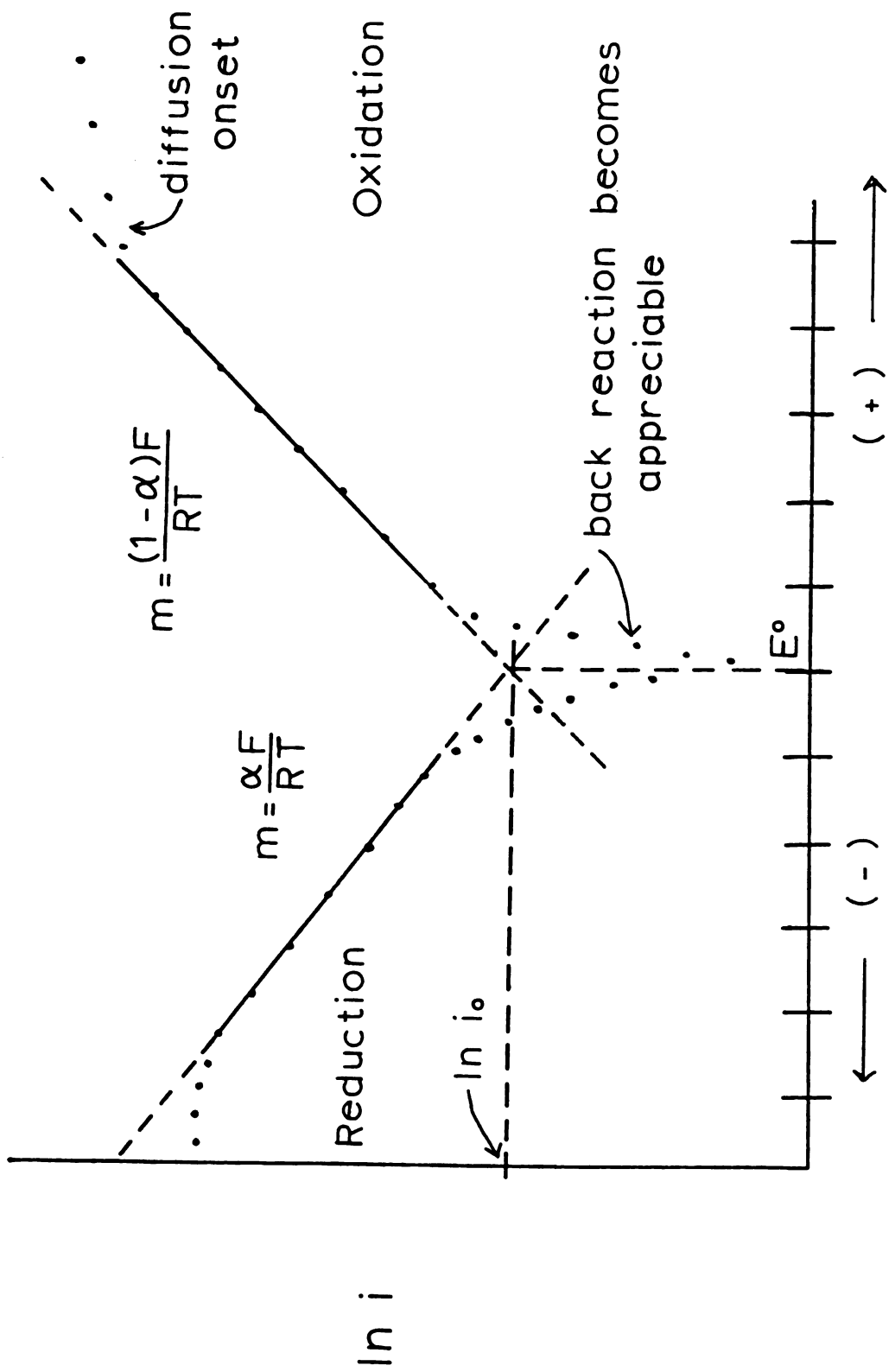

Figure 3.7: Kinetic Data from Tafel Plots

where C is the capacitance, ε is the dielectric constant of the semiconductor, e is the fundamental electron charge (in coulombs), n_o is the carrier density, V is the applied potential, and V_{FB} is the flat band potential. A plot of $1/C^2$ versus V will give a straight line, whose slope will contain η_D and whose intercept will contain V_{FB}.

The capacitance is measured via a modulation technique (144), where a small sine wave is imposed upon a constant bias and applied to the working electrode. A lock-in amplifier acts as a phase sensitive detector to measure the quadrature ($\pi/2$ out of phase) component of the observed current. This component will correspond to the purely capacitative current flowing in the electrode (145). By matching this result with dummy capacitors, the actual electrode capacity can be obtained.

The experimental apparatus is block diagrammed in Figure 3.8. The ac signal was supplied by a signal generator (Krohn-Hite 5200). The sine wave frequency was varied between 100 to 1000 Hz, and the peak to peak amplitude was 20 mV. A multi-channel oscilloscope (Tektronix 5441) was employed to monitor the input ac signal and the output current signal. A voltmeter with a two-way switch was used to alternately set the dc bias on the working electrode and measure the resultant lock-in output, which is proportional to the capacitance. The lock-in amplifier was an Ortec 9503. Measurements were taken in the dark and in the light, using the optical apparatus described previously.

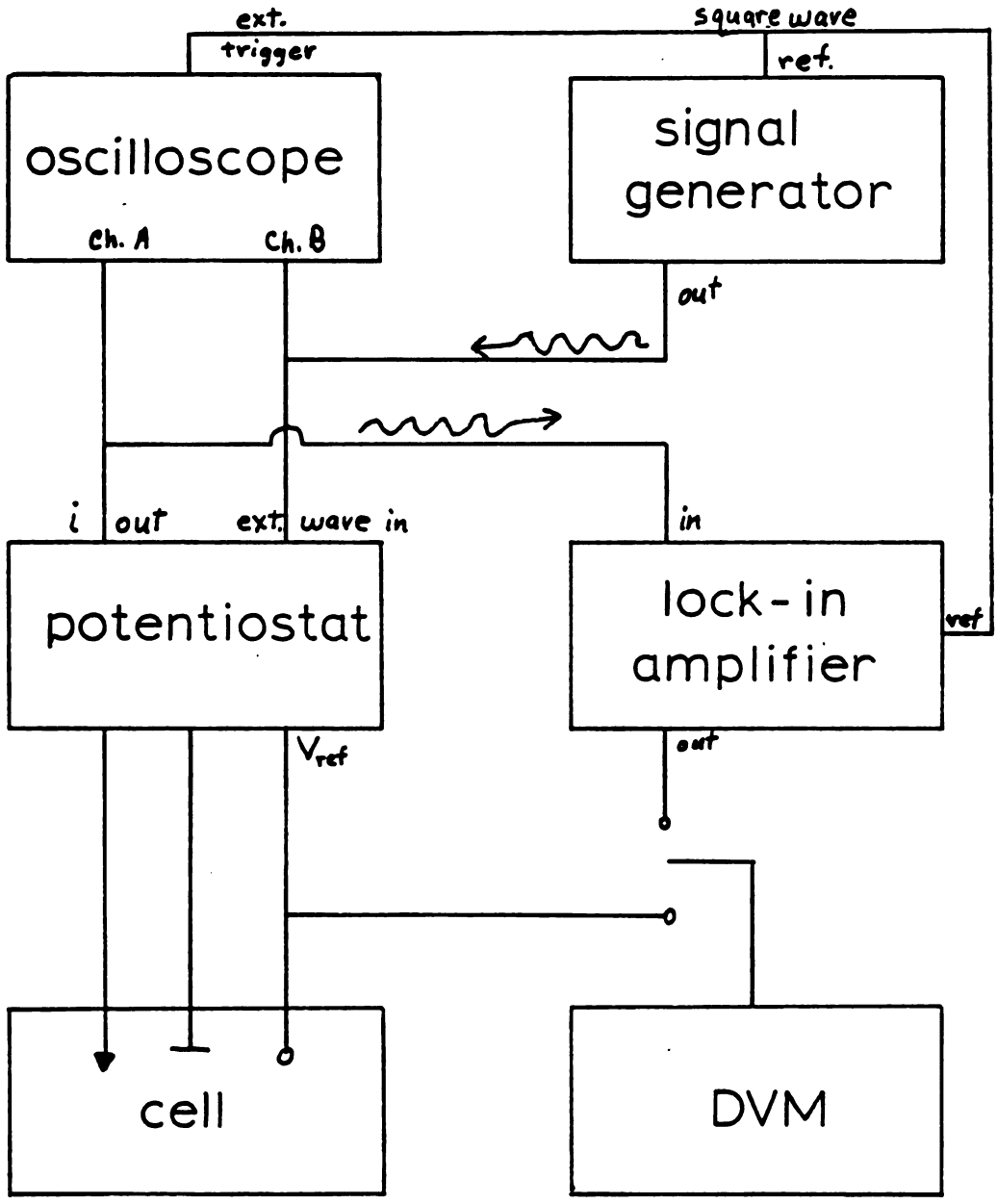

$$C = C_{std}\left(\frac{V_{lock\text{-}in}}{V_{std}}\right)$$

Figure 3.8: Block Diagram of Apparatus for Capacitance Measurements

3.3.1.6. Photoaction Spectra

Photoaction spectra were obtained with monochromatized light and a chopper/lock-in amplifier combination. A block diagram of the experimental set-up is shown in Figure 3.9. The working electrode potential was set by a potentiostat and monitored by a DVM. It was held at a potential where activation control was in effect, so that a steady state would rapidly be reached. The photocurrent output of the lock-in amplifier was fed into the vertical scale of an X-Y recorder. The horizontal wavelength axis was adjusted manually to plot the monochromator setting. The chopper (Princeton Applied Research) modulated the lamp intensity at 13 hertz. The monochromator was a Jobin-Yvon model with a range of 300 to 850 nm and a bandpass of 2 nm.

A photoaction spectrum could be converted to a quantum efficiency versus wavelength spectrum by measuring the photon flux out of the monochromator, and dividing the photocurrent accordingly. With the use of a photodiode (Hamamatsu) whose own response function was known and the absorbance and reflectance spectra of the film electrode, the desired conversion could be made.

3.3.2. Spectrophotometry

Optical absorption spectra of solutions and solid films were obtained on a Bausch and Lomb Shimadzu 210 UV spectrophotometer. It was equipped with tungsten and

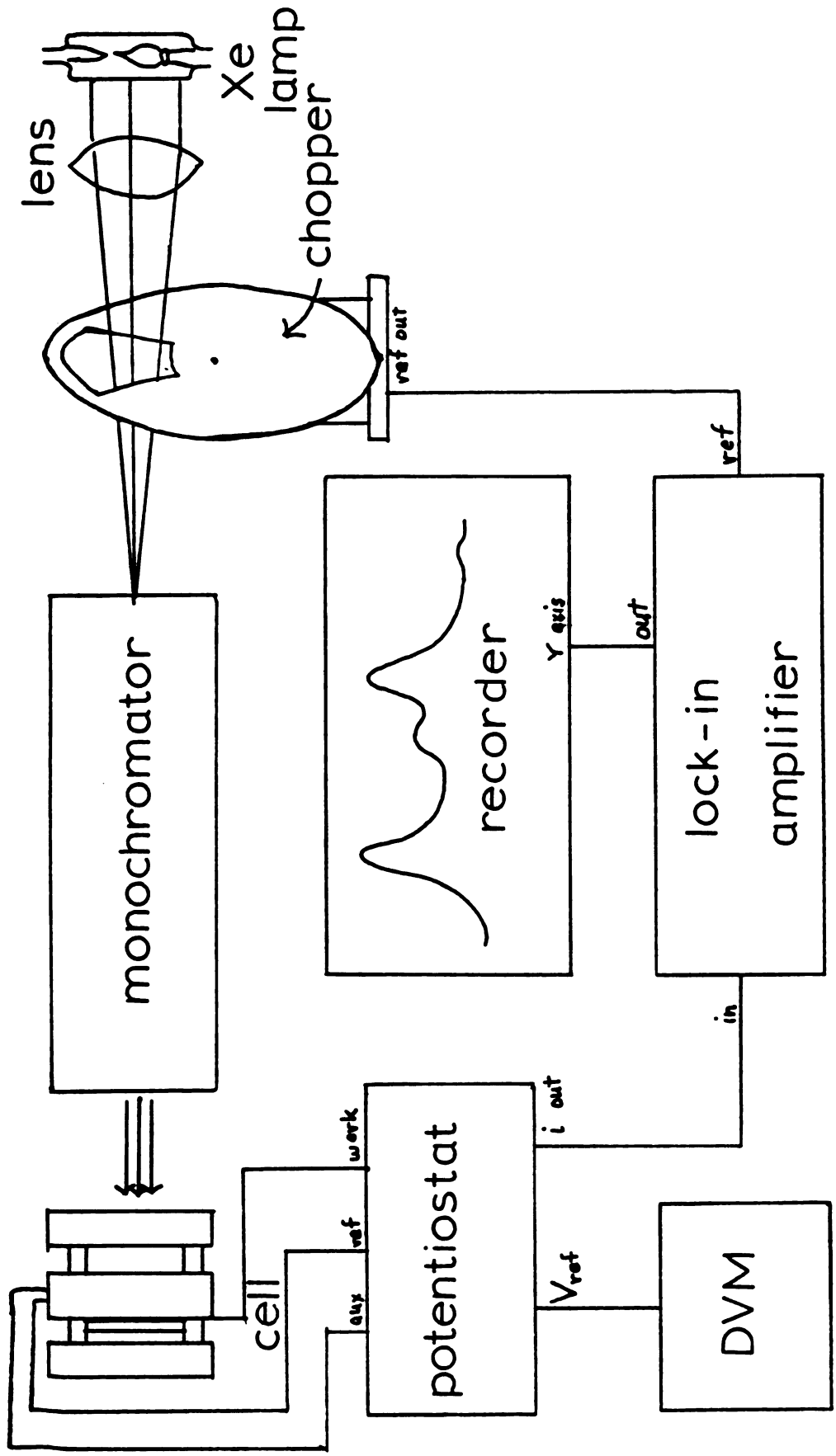

Figure 3.9: Diagram of Apparatus for Photoaction Spectra

deuterium (D_2) lamps, so that spectra from 190 to 900 nm could be taken. Spectra were recorded on a Houston 2000 recorder with a time base module which had been interfaced to the spectrophotometer.

Solution spectra were taken with conventional 1 cm square quartz cuvettes and cuvette holder. To obtain solid film spectra, precision-made masks each with a 3/8 inch diameter hole in it were attached to the front and back of the cuvette holder, for both sample and reference beams. The film OTE was then taped into place at the front of the mask cuvette holder assembly such that the circular phthalocyanine electroactive area was concentric about the mask hole. Thus any transmitted light in the sample beam must pass through the phthalocyanine film. The use of masks eliminated realignment problems associated with reproducing or comparing film spectra.

3.3.3. X-Ray Photoelectron Studies

X-ray Photoelectron Spectroscopy, XPS, is an analytical technique that gives atomic and molecular information about regions within the first 100 Å below the surface of a solid sample. A sample is irradiated by X-rays of known energy. These X-rays cause core level electrons to be ejected from individual atoms and leave the solid sample. These emitted secondary electrons are collected by an analyzer which measures emission intensity as a function of electron kinetic

energy. The binding energy of the core level can then be calculated, which is characteristic of that particular element. After accounting for matrix and instrument sensitivity, the signal amplitude may be used to quantitate the abundance of that element at the surface.

Subsequent to a core level electron emission, a number of relaxation processes may occur, one of which is the Auger transition. When a higher energy electron drops down to fill the recently vacated core level, it imparts its excess energy to another high energy electron which is then emitted from the sample. Since the cascade process occurs between quantized energy levels, the emitted Auger electron will possess an energy characteristic of the electronic structure of the element. These transitions can be observed along with direct photoelectron transitions in XPS spectra. The Ga Auger transition is one of the stronger intensity transitions observed for Ga, and is found at 191 ev on the binding energy scale when Mg-kα irradiation sources are used.

X-ray photoelectron spectra were taken with a GCA McPherson ESCA 36, using Mg-Kα radiation at 270 W. Typical operating vacuum was 5×10^{-6} Torr or less, maintained by a turbomolecular pump.

Samples were mounted on an 8-sample carousel. Each position on the carousel consisted of a spring-loaded support clip which pressed the sample outward against an immobile restraining edge of the carousel. This arrangement limited sample size to 1 inch by 3.8 inch, so that at least one side

of the electrodes had to be cropped before mounting. Samples were held to the support clip with double-stick adhesive tape (3M), and were grounded by making certain at least one edge of Au-Intrex substrate contacted the restraining edge.

Once sufficient vacuum had been obtained, the XPS data acquisition could be run by a PDP 8/e computer. After completion of all scans for a sample, the data were dumped onto a floppy disc (3M) for later manipulation. The data were plotted on a Tektronix interactive digital plotter, controlled by an LSI 11-23 computer. The LSI also did the curve fitting for quantitation of the various elements.

Two XPS experiments were performed. One was a porosity experiment designed to corroborate the results of the voltammetric porosity experiment. Two GaPc-Cl/Au electrodes, one of which was voltammetrically porous toward $Fe(CN)_6^{4-}$ in the dark, and another which was not, were scanned in the 84 to 100 ev binding energy range which covers the Au-4F transitions. The thicknesses of the GaPc-Cl films (> 500 Å) were much greater than the escape depth of an Au-4f electron emitted from the substrate, so that any Au signal must be due to pinholes or other imperfections in the phthalocyanine film.

The other XPS experiment concerned the lability of the chloride counterion on GaPc-Cl/Au electrodes, and the effect of various electrolyte components on the organometallic surface. The following samples were tested:

(1) GaPc-Cl/Au, soaked in 3 mM KOH for an hour. The intent was to see whether OH^- could replace Cl^- as a counterion.

(2) GaPc-Cl/Au, soaked in 50 mM H_2Q for over an hour. By comparing Cl and oxygen intensities the ability of the GaPc-Cl surface to adsorb or coordinate H_2Q may be observed.

(3) GaPc-Cl/Au, soaked in saturated KCl for over an hour. This sample would give the maximum possible loading for Cl^-.

(4) GaPc-Cl/Au, soaked in 0.1 M potassium hydrogen phthalate, KHP, for over an hour. This sample would determine whether the salt in the supporting electrolyte had any specific interaction with the electrode surface.

(5) GaPc-Cl/Au, having undergone two hours of continuous photoelectrolysis in 1 mM H_2Q and 0.1 M KHP. This electrode was part of a longevity experiment.

(6) GaPc-Cl/Au, an identical electrode to (5) without contact to any electrolyte, to be used as a control.

All samples, after their respective solution treatment, were rinsed with a continuous spray of triply distilled water for about 30 seconds and dried before mounting on the ESCA carousel.

For each sample, a full range scan from 0 to 1000 ev was made in two 500 ev windows. Then, some combination of the high resolution scans described below were made:

Element	Binding Energy (ev)
carbon	301 - 285
oxygen	545 - 529
nitrogen	415 - 399
chlorine and gallium (Auger)	211 - 187
gold	100 - 84
gallium (valence)	45 - 5

By weighting observed intensities to the instrumental response toward a gold standard, correlations in relative atomic abundance between samples could be made.

3.3.4. Scanning Electron Microscopy

Information on the porosity and crystalline morphology of the phthalocyanine films was obtaind with scanning electron microscopy, or SEM.

Due to the shorter wavelength characteristics of a 20 kV electron beam, sharp images up to 1000 time smaller than those obtainable with conventional light microscopy could be obtained.

To form the micrograph image, an electron probe spot is moved in a raster across the specimen. The emission current of back-scattered primaries and lower energy secondaries formed by ionization of specimen atoms is picked up by a detector and fed to a synchronous display tube, which generates a picture in the same way as in a television set.

The microscope instrument used was an ISI DS-130. Pictures were taken with Polaroid Type 55 positive/negative 4 x 5 land film. Electrodes were mounted via double stick tape onto regular EM studs and grounded to them at the edge with a carbon cement. The electrode samples were then sputter-coated with a 300 Å film of a Au-Pd alloy. This overlayer was necessary to prevent charging of the sample, which distorts the image and causes contrast problems. The Au-Pd film was sufficiently thin that it would not alter the appearance of any structure observed at the magnifications used (32,000X or less).

A problem commonly encountered in high magnification microscopy of insulating organic samples is beam damage. When higher magnifications are attempted, the electron beam is rastered over a smaller area. This increases the rate of sample heating in that area and the density of ionized species. Thus the sample itself sets a limit to the allowable magnification much below the resolving power of the instrument. Part of the procedure for obtaining good quality micrographs entailed stepping up the magnification to 10X the desired level, quickly adjusting the focus and astigmatism, and then stepping down. If more than a few seconds were spent at high magnification, beam damage would be observable as a darkened square patch in the middle of the image display. This problem was dealt with by carefully setting focus and astigmatism at high magnification at one area of the sample, deliberately damaging it, then moving to another

area, making a quick focus check, and taking the picture. This solution would not have been proper had the samples not possessed a homogeneous distribution of surface features, so that one area of the sample was as representative as another.

Another difficulty in obtaining quality micrographs is that a sample must have a reasonable amount of surface structure to focus on; otherwise, one cannot "find" the image on the display screen. This problem arose when comparisons of Au-MPOTE's with and without phthalocyanine films were made. The bare Au-MPOTE had no observable surface features below 10,000X, and so one had to depend on stray specks of dust to make an initial focus.

4. RESULTS

4.1. Electrolysis of H_2Q on Au Substrates

4.1.1. Variability of Voltammetric Behavior of H_2Q on Au

A thorough understanding of the behavior of GaPc-Cl thin film electrodes required some knowledge of the voltammetric response of the substrate upon which it was deposited. The sublimed GaPc-Cl layers were sometimes found to be porous, so that the recorded voltammetric wave would contain a component corresponding to electrolysis of the redox couple on the bare substrate. In order to know what part of the voltammetric wave was due to GaPc-Cl, an electrolysis on the unmodified substrate needed to be performed.

Also, it was necessary to know the substrate's activity toward a redox couple from the standpoint of catalysis. While there are applications such as photography where the chemical reaction must be indicative of the wavelength of incident light, there are photoelectrochemical applications such as batteries or fuel cells where a dye sensitizer is simply acting as a photocatalyst; its purpose is to use light to drive the reaction faster. The substrate's own electrocatalytic ability needs to be known in order to compare it to that of GaPc-Cl.

When the Au substrates were tested, it was obvious at first that at pH 4, the electrolysis of H_2Q on Au was poorly

reversible. Cyclic voltammograms typically showed peak to peak separations on order of 500 millivolts (mv) or more, as shown in Figure 4.1.1.(a). After numerous experiments, however, it became apparent that after certain pretreatments the electrolysis of H_2Q on Au could proceed much more quickly, as shown by the other voltammogram in Figure 4.1.1.(b).

It was desirable to know which of the voltammetric curves represented normal Au electrochemical response, since GaPc-Cl/Au electrodes were found to be photocatalytic with respect to the less reversible response, but passivating when compared to the more reversible response.

Also, it was of interest to see under what conditions the activated surface could be maintained. The Au substrates which had GaPc-Cl films sublimed onto them gave the less reversible response when used themselves as electrodes without additional pretreatment. If the activated Au surface could be generated and maintained while a GaPc-Cl film was being sublimed on it, a better contact between organic and metallic phases may be may be obtained, reducing ohmic overpotential losses.

In terms of modified and unmodified electrode performance and availability, Au was the most desirable substrate material. Thus, a lengthy set of experiments was undertaken in order to understand how H_2Q reacts on an Au surface.

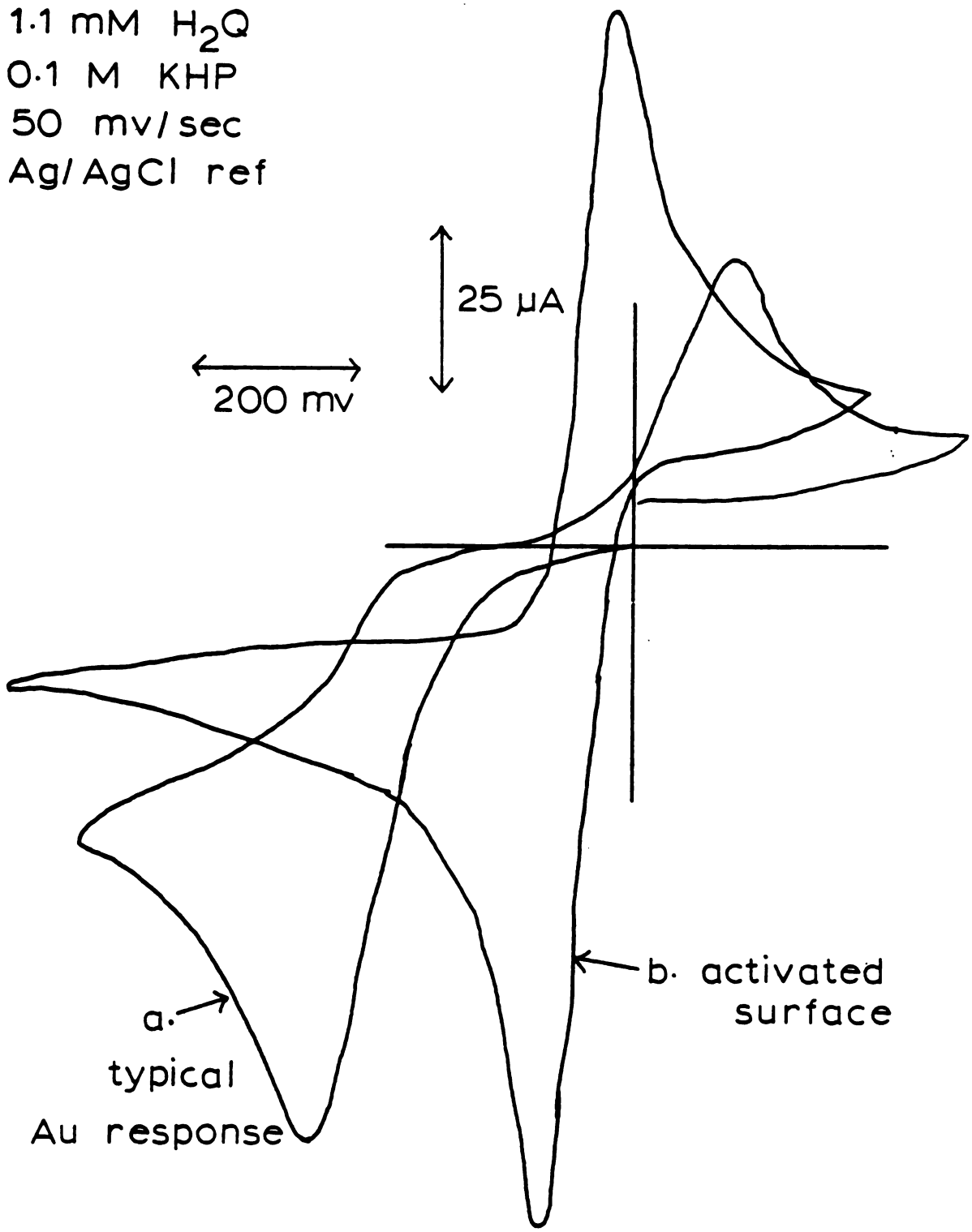

Figure 4.1.1: Two Types of Voltammetric Behavior of H_2Q on Au

4.1.2. Activation of the Au Surface Through Voltammetric Means

The easiest way to activate the Au surface was to poise the electrode at a large positive potential, near the aqueous solvent limit, for thirty seconds or more. This would usually result in a complete conversion of the less reversible, or inactivated, response to the more reversible, or activated, response.

In Figure 4.1.2., curve 1 is the cyclic voltammogram obtained when a plain Au-MPOTE, treated with ethanol and water as described in the Experimental chapter, was used to oxidize H_2Q. Curve 2 is the return sweep after poising the electrode in the far anodic region, from +1.2 to 1.5 volts. The symmetrical peak around +0.7 v is the desorption of gold oxide formed while the electrode was poised at the high positive potential. The H_2Q/Q redox couple now appears much more reversible, with a peak to separation of 135 mv.

A gradual transition from inactivated to activated behavior can be observed by continuously cycling the Au electrode out to the anodic solvent limit. In Figure 4.1.3., after an initial cycle to produce the inactivated waves was done, the electrode potential was swept out to +1.750 v and back five times. Each successive cycle produced an increased reversible wave and a diminished irreversible wave, until the irreversible waves had nearly disappeared. Also, a steady growth of the oxide desorption wave with successive anodic cycling was observed.

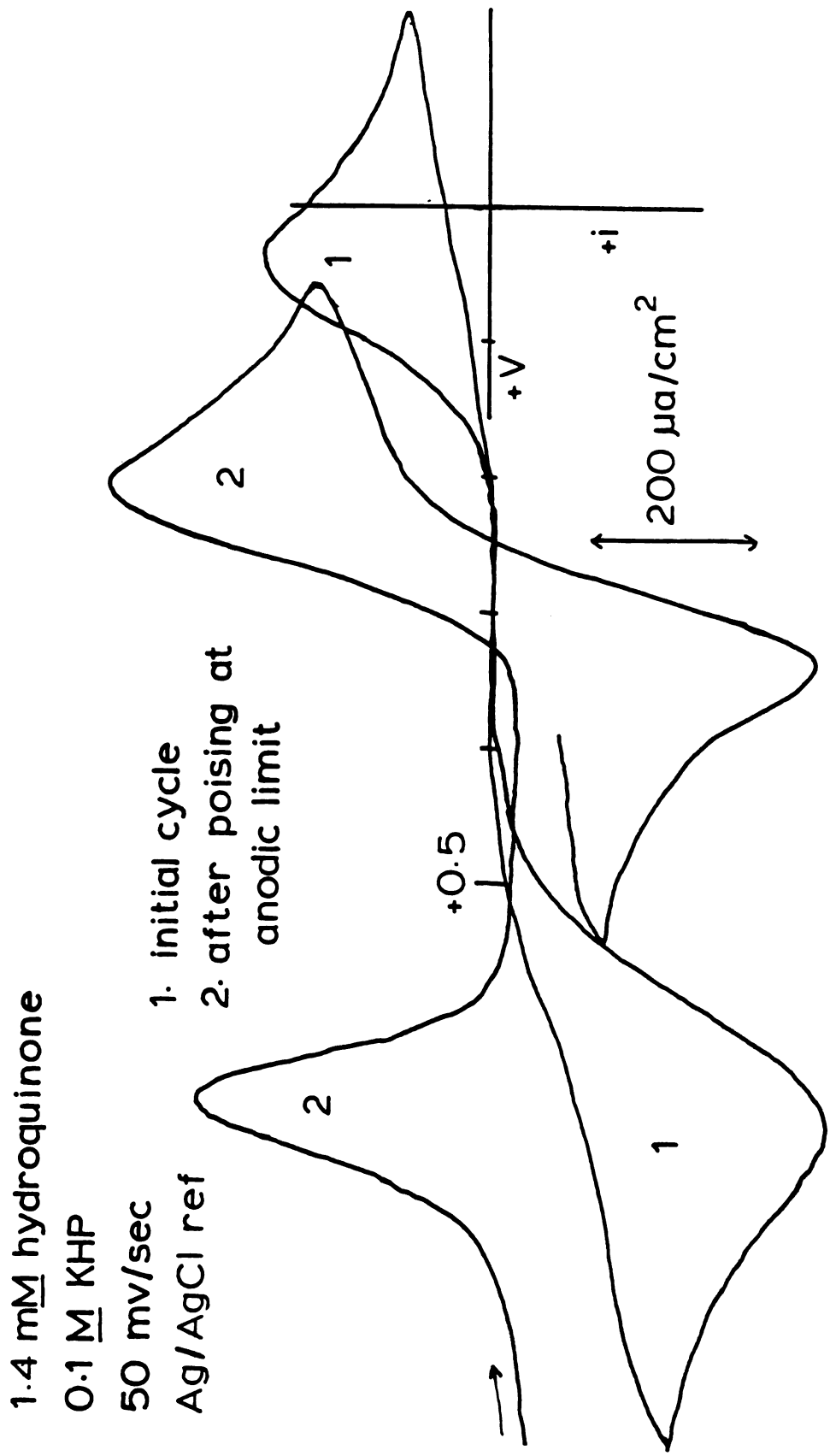

Figure 4.1.2: Activation of Au Surface toward H_2Q via Poising at Anodic Potential

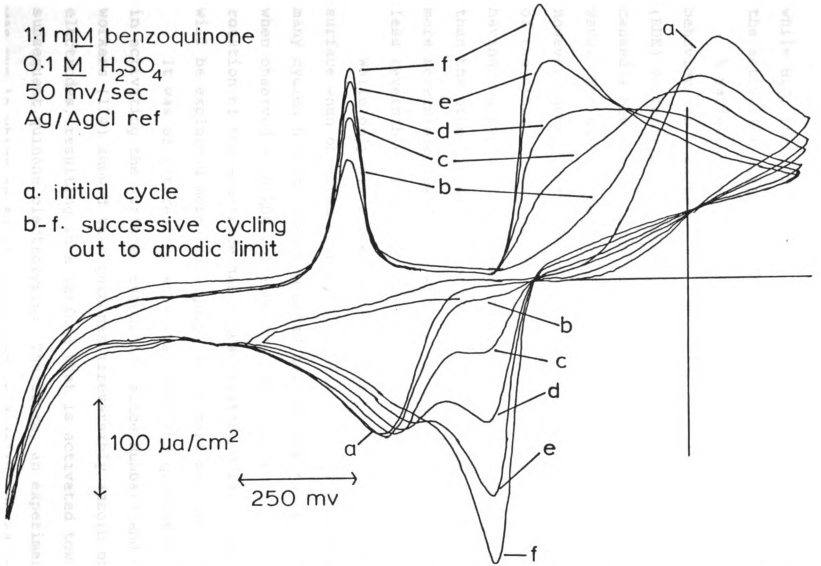

Figure 4.1.3: Activation of Au Surface toward BQ Through Continuous Anodic Cycling

The electroactive species in Figure 4.1.3. was benzoquinone, BQ, the oxidized form of the redox couple, while H_2Q, the reduced form, was used in Figure 4.1.2. Thus the activation effect is achieved with either BQ or H_2Q.

A variation between the two types of voltammetric behavior can also be observed by rotating disk electrode (RDE) voltammetry, as seen in Figure 4.1.4. Anodic cycling caused a new wave to grow on the low voltage side of the main wave. The sum of the two waves maintained a constant value, however, demonstrating that one wave increased at the expense of the other. Thus, the Au electrode can be thought of as having two types of surfaces, one more active toward H_2Q than the other. For the purposes of discussion, the surface more reversible toward H_2Q will be called "active" and the less reversible "inactive".

While only six cycles were required to activate the gold surface when observed with cyclic voltammetry, over twice as many cycles had not even converted half of the Au surface when observed with RDE voltammetry. The reason is that rotation of the electrode has a deactivating effect, which will be explained more thoroughly in the next section.

It was of interest to know what role the quinone played in activating the surface, especially since Hubbard and co-workers (114) showed that quinones irreversibly adsorb on Pt electrodes, resulting in a surface that is activated toward subsequent quinone electrolysis. Therefore, an experiment was run in which an Au electrode was anodically cycled in a

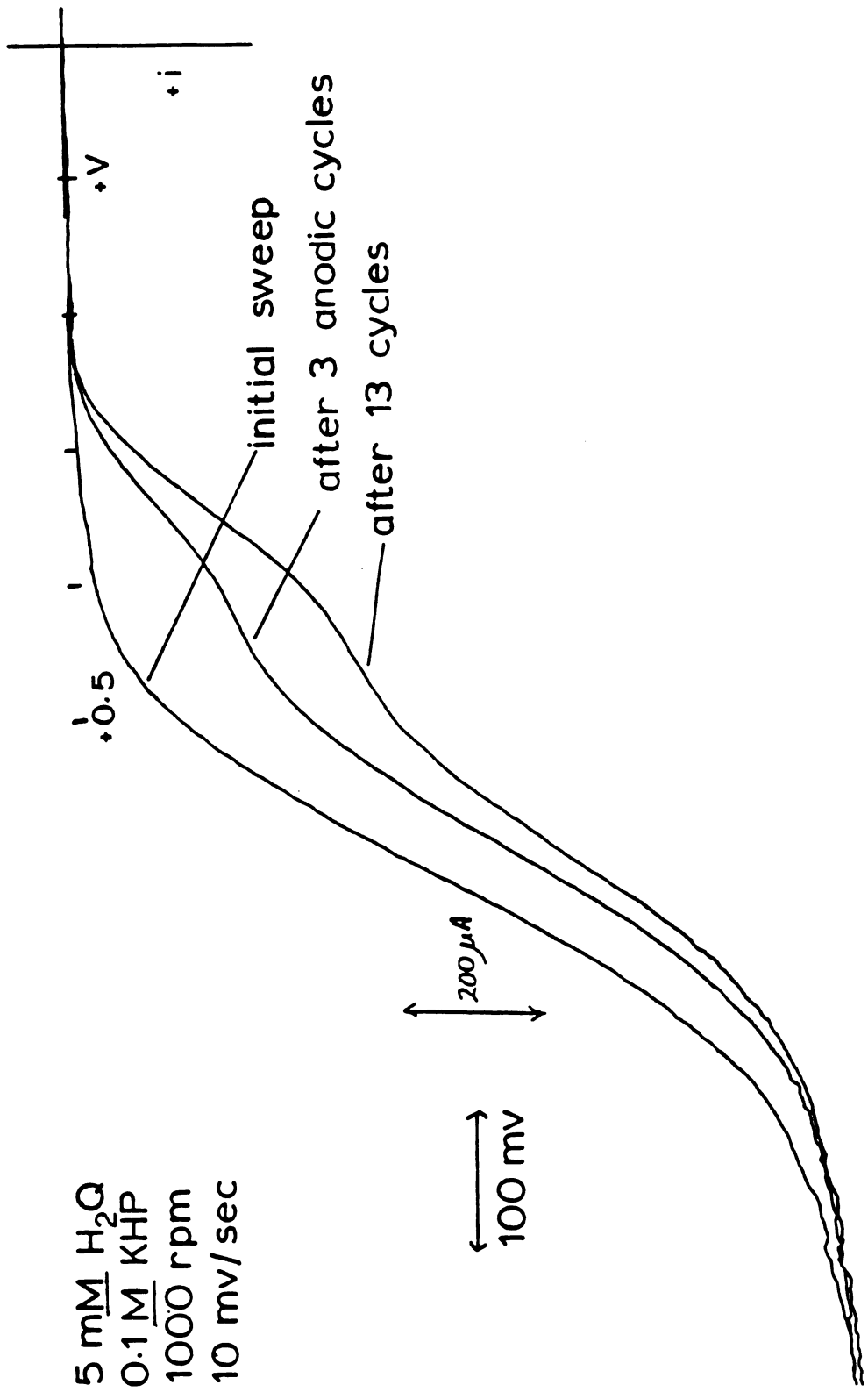

Figure 4.1.4: Growth of Active Au Surface via Anodic Cycling: RDE Voltammetry

blank electrolyte many times. An aliquot of H_2Q solution was then added and the electrolyte allowed to equilibrate for one minute. The initial cycle was then recorded. The result, shown in Figure 4.1.5., was that a reversible voltammogram was obtained; the Au surface had been converted to the active form in the absence of H_2Q.

Having established the ability of high anodic potential to activate the Au surface, the cathodic potential region was next examined. In Figure 4.1.6., the effect on H_2Q oxidation of poising the Au electrode at negative potentials is shown. An activation of the electrode surface toward H_2Q was observed. Since the solution was 1.3 mM in BQ, the anodic waves shown correspond to the electrogenerated products formed while the electrode was poised at negative potentials. In curves 2 and 3, the electrode was poised in the diffusion limiting region for BQ, so that equal amounts of H_2Q were formed over the same time period. Curve 1 is only the reverse sweep of the initial cycle on the inactive surface, so the amount of charge transferred was less than in the other two cases, as expected.

The effect of cathodically cycling a H_2Q solution is shown in Figure 4.1.7. After six cycles only a partial conversion of the inactive to the active surface had been achieved. After testing a number of Au electrodes, it was concluded as a general result that anodic cycling was more effective than cathodic cycling in activating the surface.

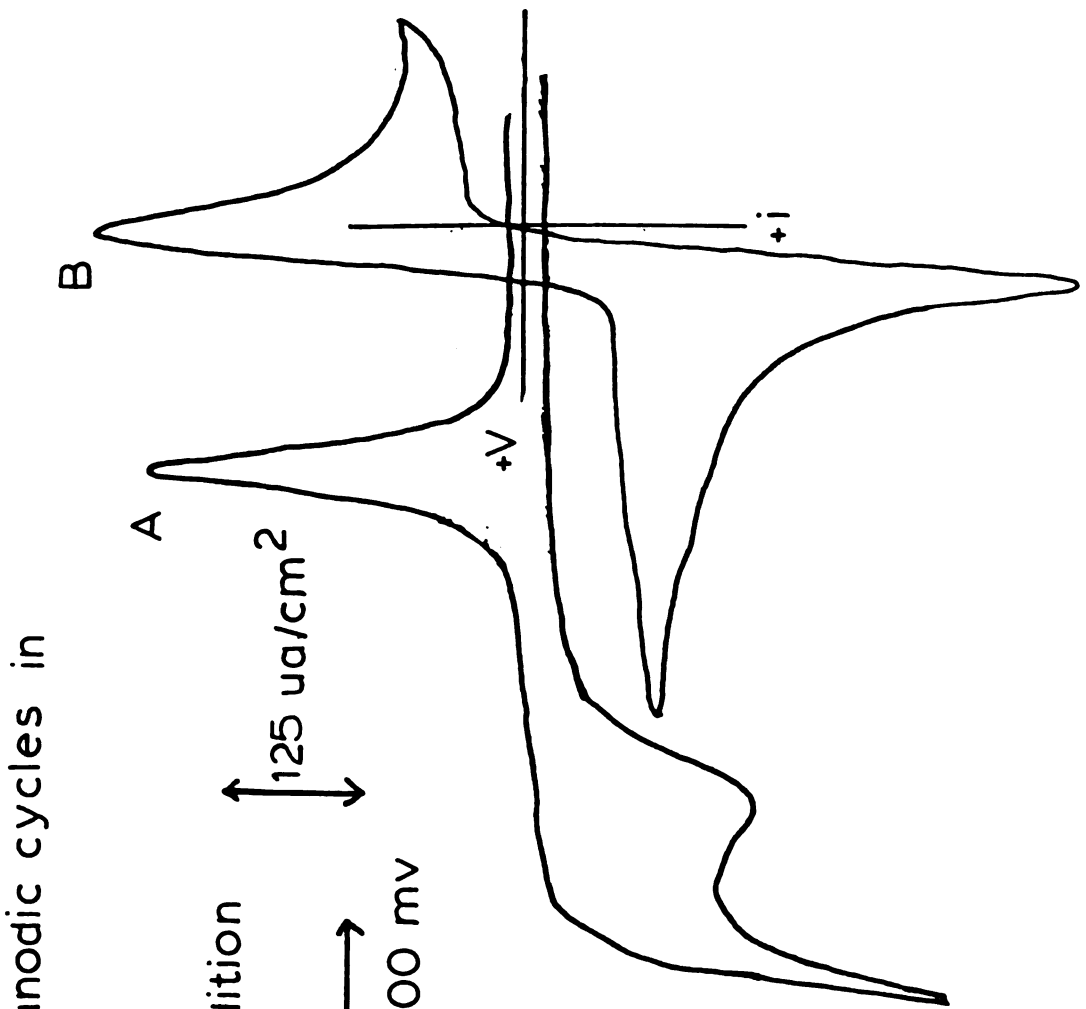

Figure 4.1.5: Au Activation in the Absence of H_2Q

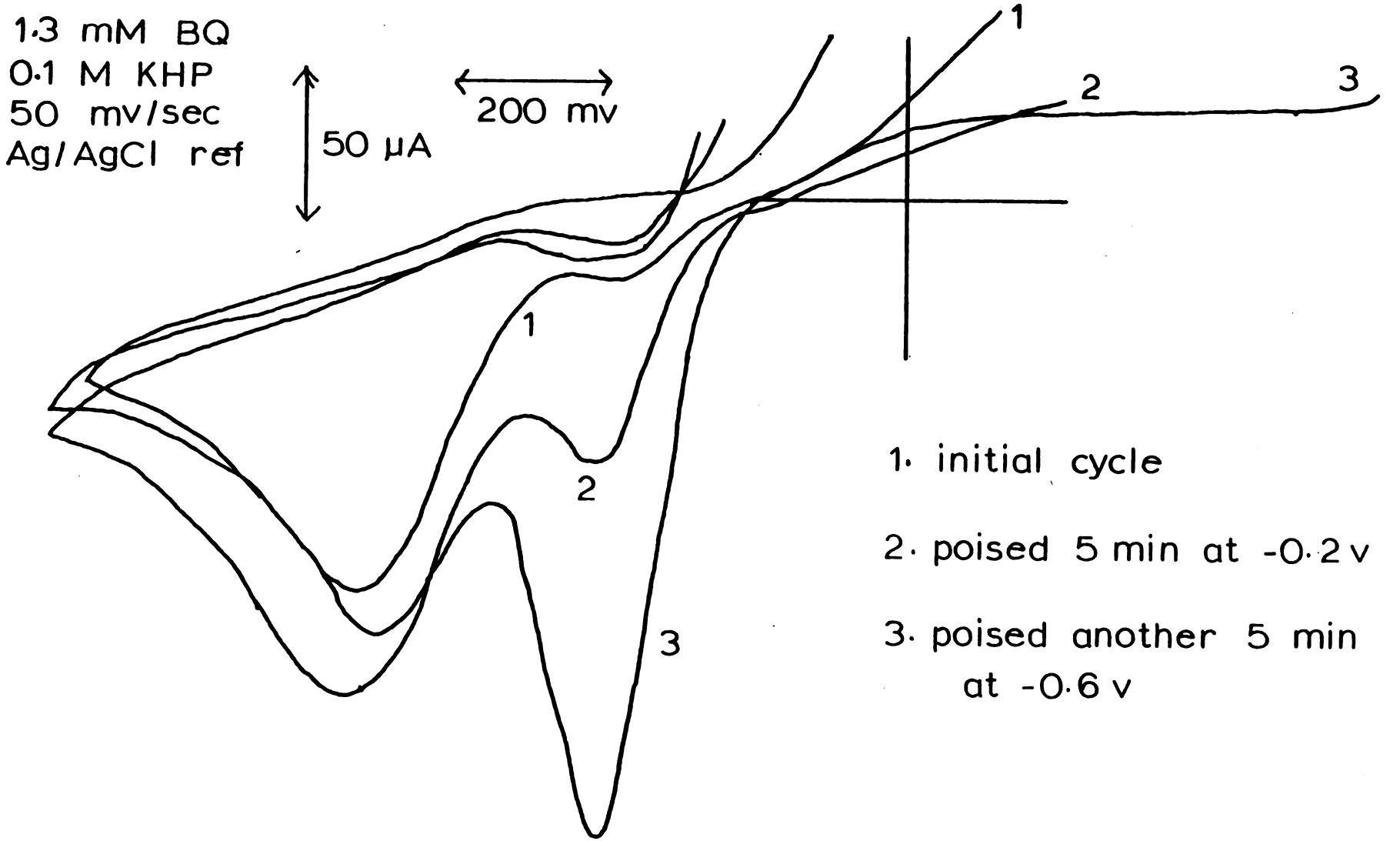

Figure 4.1.6: Au Activation by Poising in the Cathodic Region

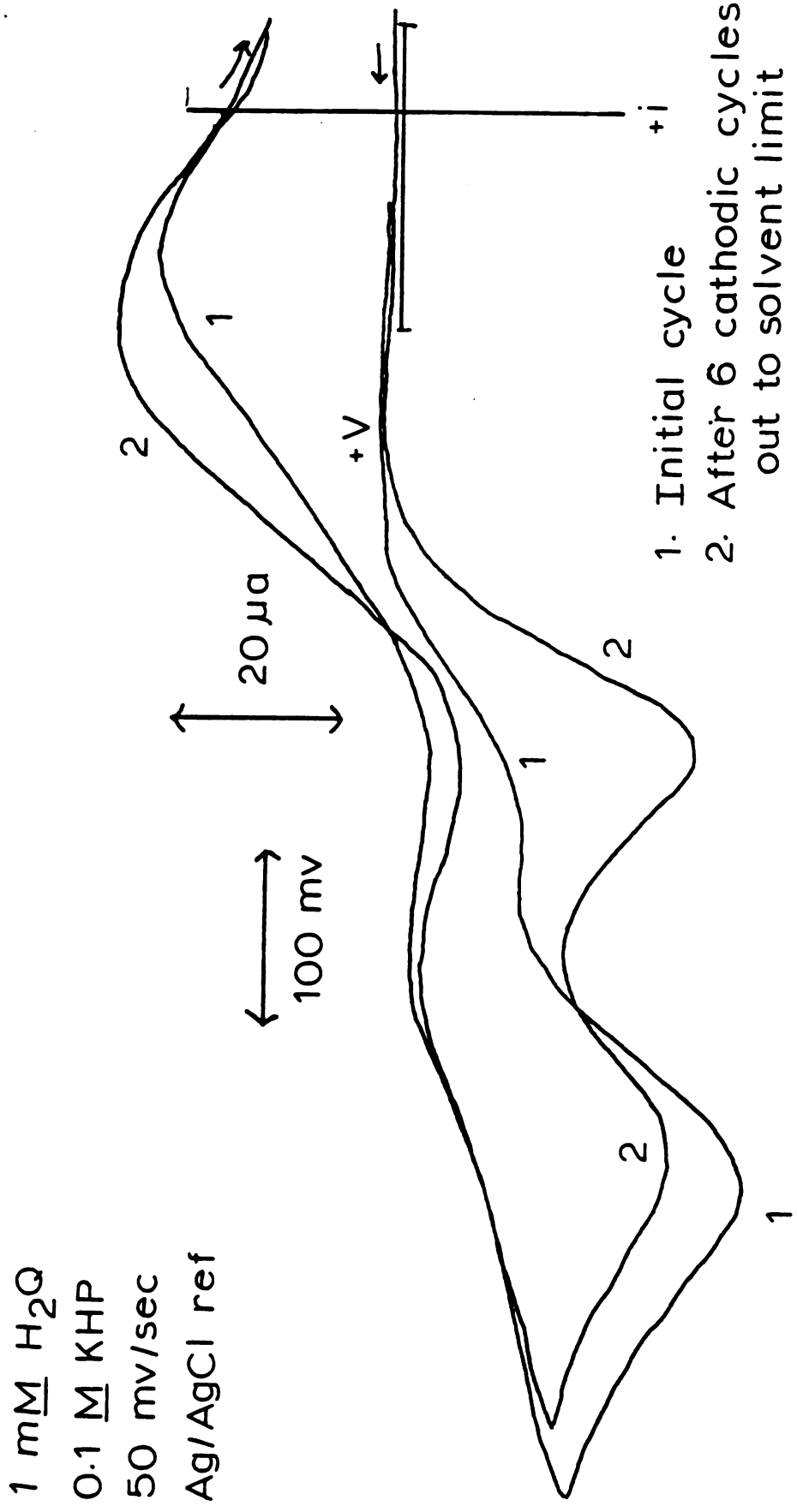

Figure 4.1.7: Au Activation by Cathodic Cycling

Another observation concerned the degree of activation of the Au surface to H_2Q relative to BQ. As in the previous figures, two distinct waves were observed for the oxidation of H_2Q, while for BQ there is some question as to whether one or two waves are present. Figure 4.1.3. clearly shows the growth of a reversible Q wave and the demise of the original one. An important difference between the two cases may be pH; the 0.1 M H_2SO_4 solution used for the voltammetry in Figure 4.1.3. had a thousand-fold greater concentration of hydronium ions available to protonate the reduced BQ than in the 0.1 M KHP used in Figure 4.1.7. The rate of protonation may determine whether the waves are distinguishable or not.

At this point it could be argued that the potential excursions are nothing more than cleaning steps, a well known procedure with noble metal electrodes (159). But close examination of the voltammograms shows that cycling produces irreversible changes on the electrode surface. In Figure 4.1.8., current traces for the formation of Au oxide in different electrolytes are shown. In H_2SO_4 and K_2SO_4 solutions, a new peak was observed under repetitive cycling, growing on the lower side of the broad oxidation wave associated with gold oxide formation. After the initial sweep, which gave a larger current near the onset of O_2 evolution, the size and shape of the waves remained roughly constant with each successive cycle. In contrast, an initial sweep in KHP electrolyte produced a wave far larger throughout the anodic range than any that would be

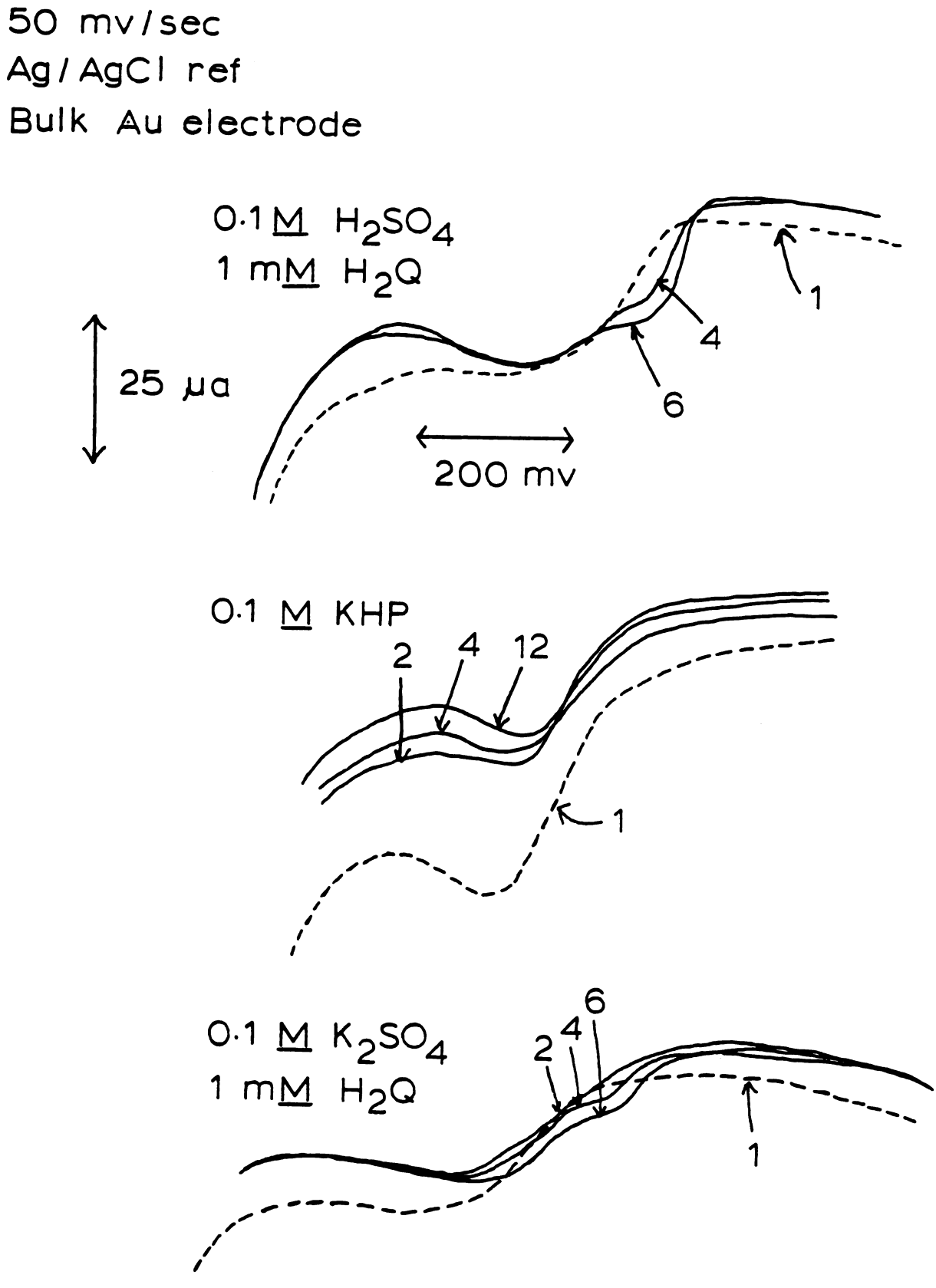

Figure 4.1.8: Electrochemical Formation of Gold Oxides in Various Electrolytes

subsequently observed. The following cycles appeared to be decreasing with each successive anodic sweep, but part of that effect was due to a moving baseline, which changed by 7 uA during the course of 12 cycles. Little or no growth of new oxide waves was observed in KHP electrolytes. While the set of curves for KHP shown here were taken in an electrolyte which did not contain H_2Q, the same behavior was observed for KHP solutions that did contain H_2Q.

4.1.3. Other Means of Activating or Deactivating the Au Surface

Several experiments were conducted in order to see how well the active Au surface, once created, could maintain itself. Figure 4.1.9. shows the result of an experiment where an Au electrode was activated by anodic cycling and then disconnected; allowing the electrode to equilibrate with the solution. The electrode was reconnected and cycled every few minutes to see if the kinetics had changed. A trend in which the electrode was slowly reverting back to its inactive surface was observed. After 38 minutes, $i_{p,a}$ for the active surface had decreased to 72% of its original value, and a small wave had appeared on the diffusion edge of the main peak. The main peak for reduction had only decreased to 90% of its original value, and a small prewave was observed growing apparently as a complement to the new wave on the anodic sweep.

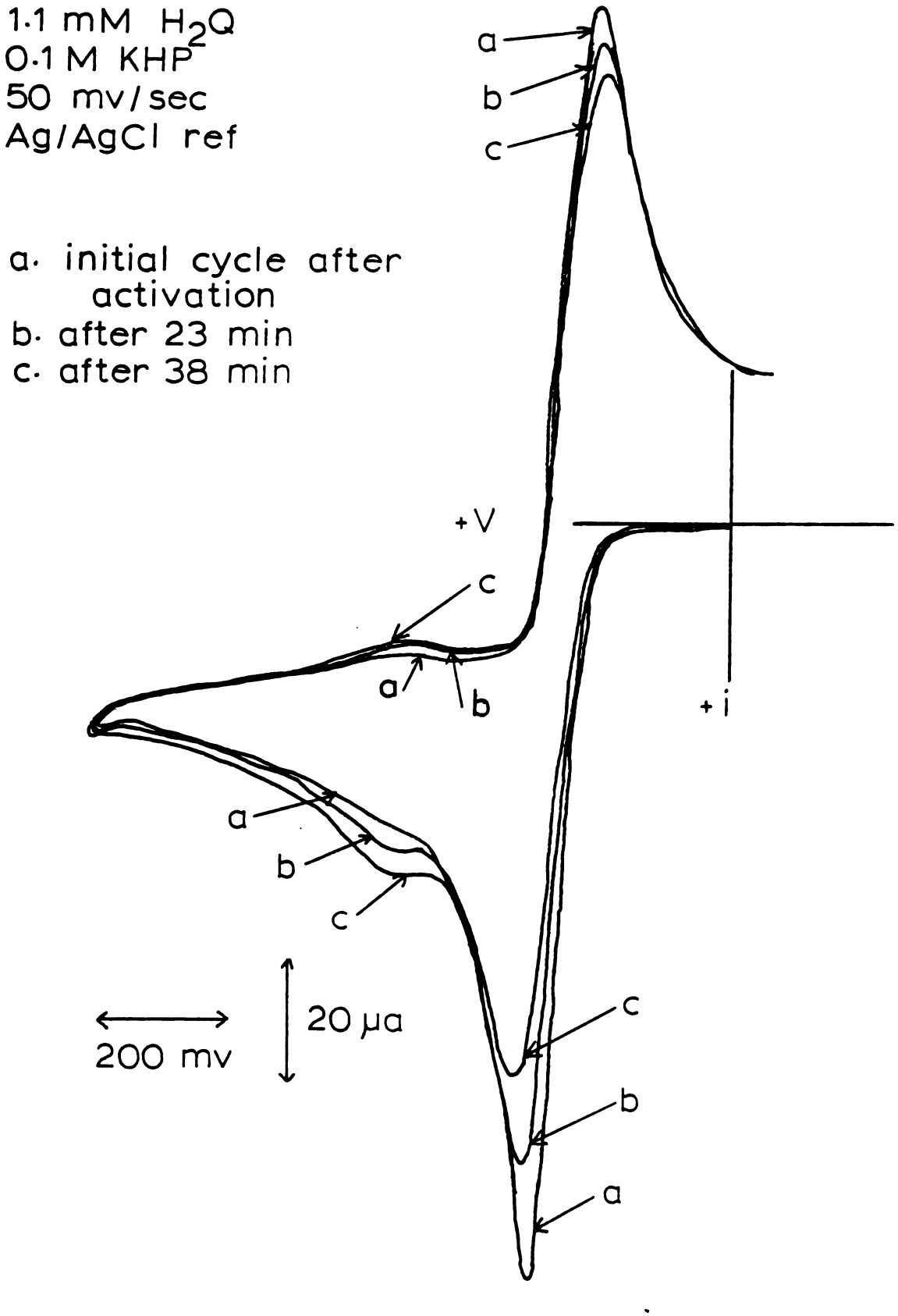

Figure 4.1.9: Effect of Letting Au Electrode Stand at Rest Potential

The deactivating process could be hastened by rotation of the electrode. Figure 4.1.10. shows that a complete conversion of active to inactive Au surface was achieved in 30 minutes, much faster than occurred when the electrode was allowed to stand in quiescent solution. Thus mass transport was shown to be a factor in the deactivation of the electrode. Some molecular species was being brought from solution to the electrode surface, where some unknown deactivating process would then occur.

To test the possibility that an impurity in the triply distilled water was the unknown molecular species, an Au electrode was immediately immersed in a thoroughly cleaned beaker containing about 100 ml triply distilled water, and rotated at 2000 rpm for 15 minutes. The resulting voltammogram showed a deactivation of the Au surface. Samples of the triply distilled water that came from the Nalgene storage vessel and directly from the freshly cleaned and rinsed glass still gave the same result. The result for the sample obtained directly from the still is shown in Figure 4.1.11.

Electrodes that were not pretreated were inactive, and they stayed that way as long as the electrode potential was kept between +1.0 v and -0.15 v. However, once an electrode had been activated and deactivated, reactivation could be achieved simply by cycling the electrode in the normal range for H_2Q. An Au electrode that had been activated by anodic cycling and then deactivated by rotation was repeatedly

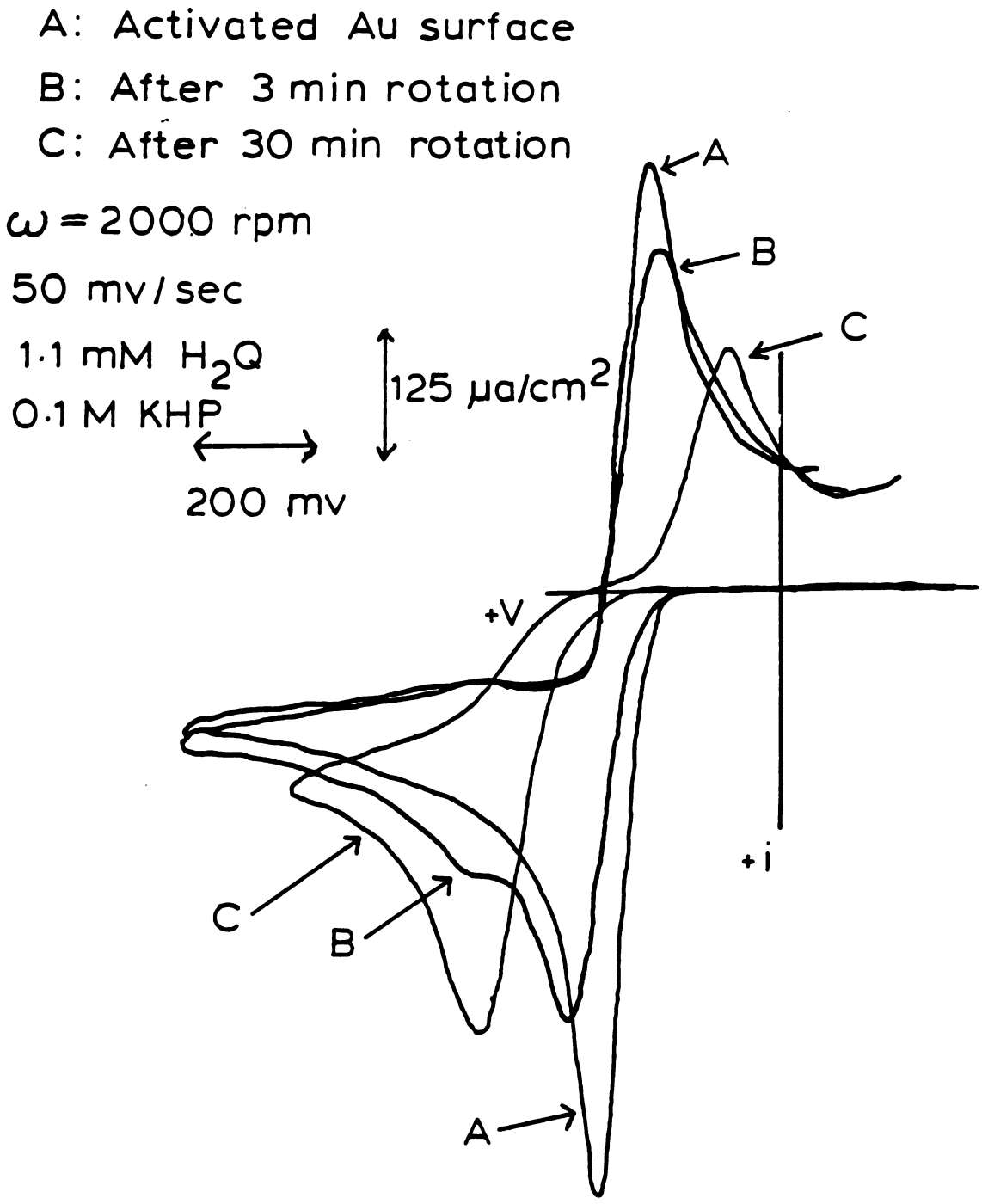

Figure 4.1.10: Effect of Rotation on Au Activity

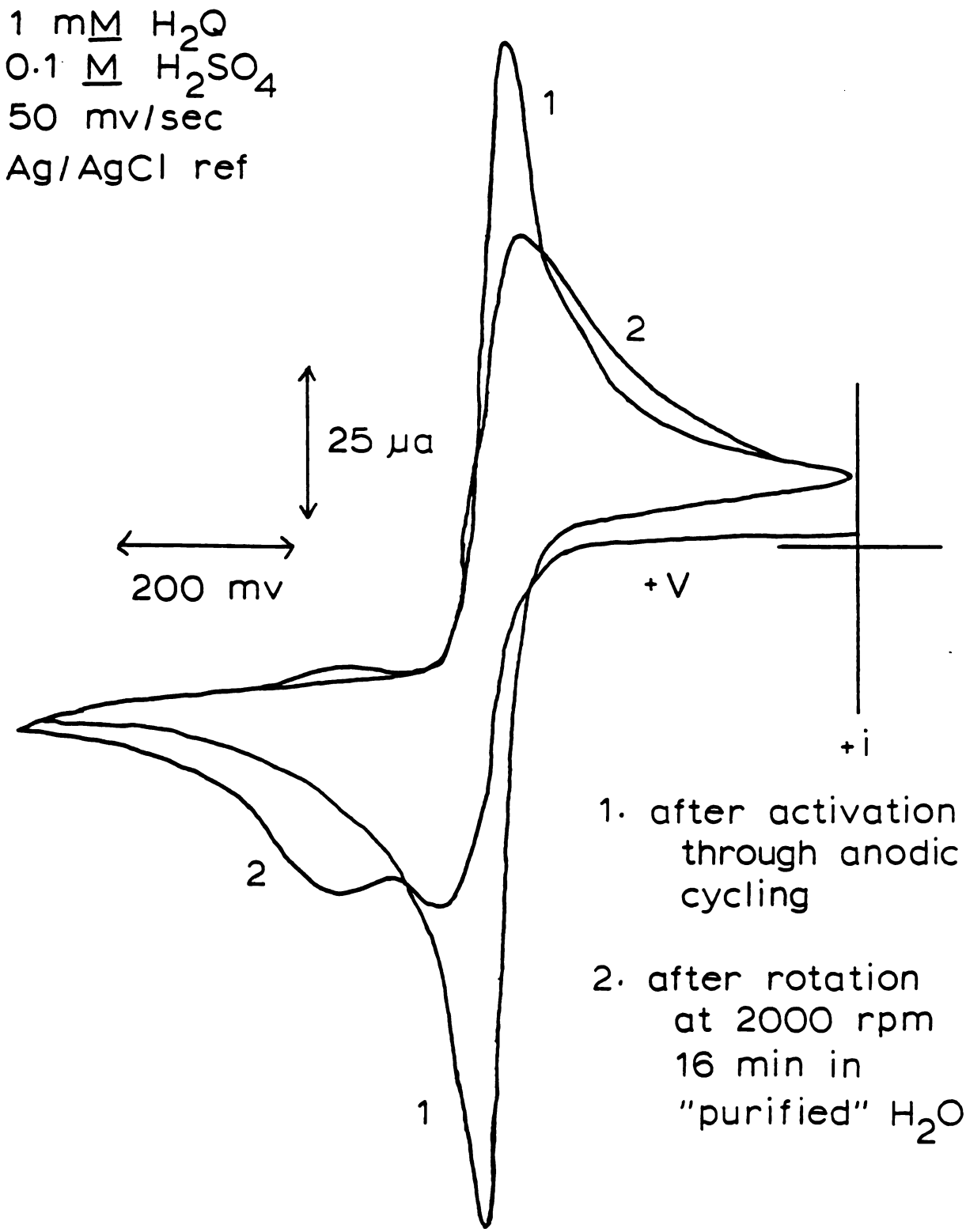

Figure 4.1.11: Deactivation of Au Surface by Exposure to "Purified" Water

cycled, with close attention paid to the time interval between successive cycles. The results are shown in Table 4.1. For time intervals of 5 minutes or less, the succeeding cyclic voltammogram had an increased reversible peak and a decreased irreversible peak compared to the previous one -- the active surface was being regenerated. For time intervals of 6 minutes or more, steady deactivation was observed. In the 5 to 6 minute time interval, successive voltammograms appeared about the same. Thus the activation which occurred during the 40 seconds required to make the voltammogram proceeded at least 8 times faster than the deactivation process.

The voltammograms used to complete Table 4.1 were scanned at 50 mv/sec. If the scan rate were slowed, the conversion from inactive to active surface could be observed during a single cycle. In Figure 4.1.12., cyclic voltammograms taken on the same deactivated Au electrode and electrolyte but at different scan rates are shown. At 10 mv/sec, the initial anodic sweep appeared just as it did at higher scan rates, but the reverse sweep gave an activated reduction wave that was nearly a third as large as the expected deactivated wave. Following immediately with a second anodic sweep, an activated oxidation wave was observed which had roughly the same magnitude as that for reduction. Thus a slow anodic sweep generated a prewave for the reduction, which in turn generated one for oxidation. The prewaves should not be thought of as comprising a new redox

TABLE 4.1.

Effect of Time Interval Between Cycles on Activation of Au Surface

Δt (min:sec)	Trend
0 (continuous)	R
1:15	R
1:35	R
2:25	R
2:56	R
4:39	R
5:45	~same
9:30	I
10:00	I
10:25	I

R: Second voltammogram appears more reversible than the previous one.

I: Second voltammogram appears less reversible than the previous one.

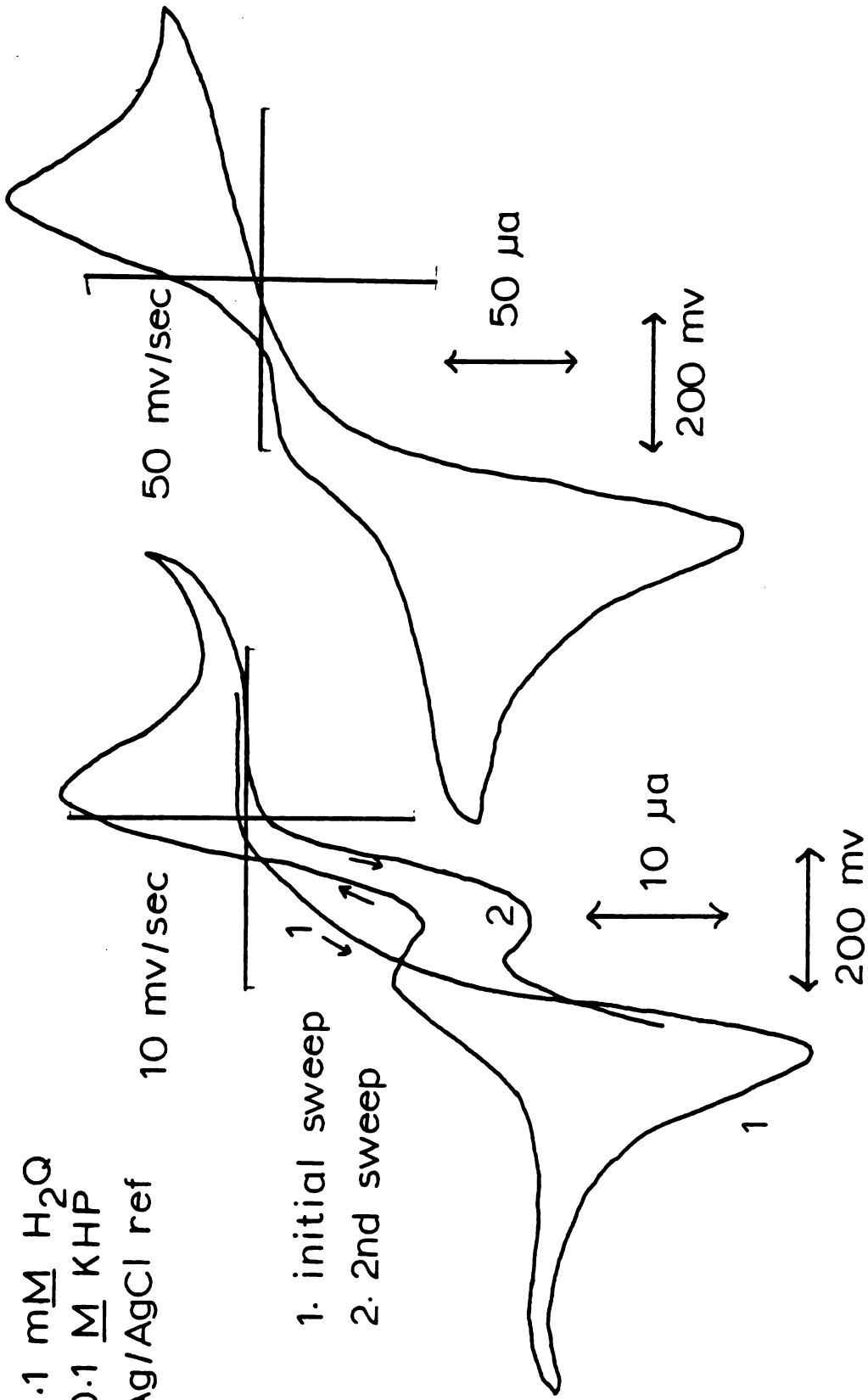

Figure 4.1.12: Effect of Slow Scan Rate on Deactivated Au Surface

species, however, since $V_{p,a}$ is negative of $V_{p,c}$ -- they could not possibly have the same E°.

Activation of the Au surface could also be accomplished by exposure to oxidizing acid. Au electrodes were soaked in acid for a given amount of time, rinsed briefly, placed in the electrolyte, and scanned. In Figure 4.1.13., the RDE voltammetric wave shows a prewave increasing in size as the exposure time to dilute chromic acid is increased. The position of the prewave is identical to the one observed after anodically cycling. Thus the effect toward H_2Q of oxidizing the Au surface chemically or electrochemically is the same.

Mechanical polishing also proved to be a fair method of activating the Au surface. As will be described in more detail later on in this section, K_2SO_4 solutions offered a degree of stability to the active state. This feature was utilized in examining the effect of polishing. An Au electrode whose initial cycle in K_2SO_4 indicated that more than half of the Au surface was already in the active state was used, as shown by the dashed curve in Figure 4.1.14. After some additional testing, which left the electrode nearly completely activated, it was placed in a KHP solution and deactivated by rotation. The electrode was then removed, rinsed briefly, returned to the K_2SO_4 electrolyte, and cycled. The result was that the inactive state of the Au surface was retained, as shown by the dotted trace in Figure 4.1.14. The electrode was again removed, polished briefly with alumina

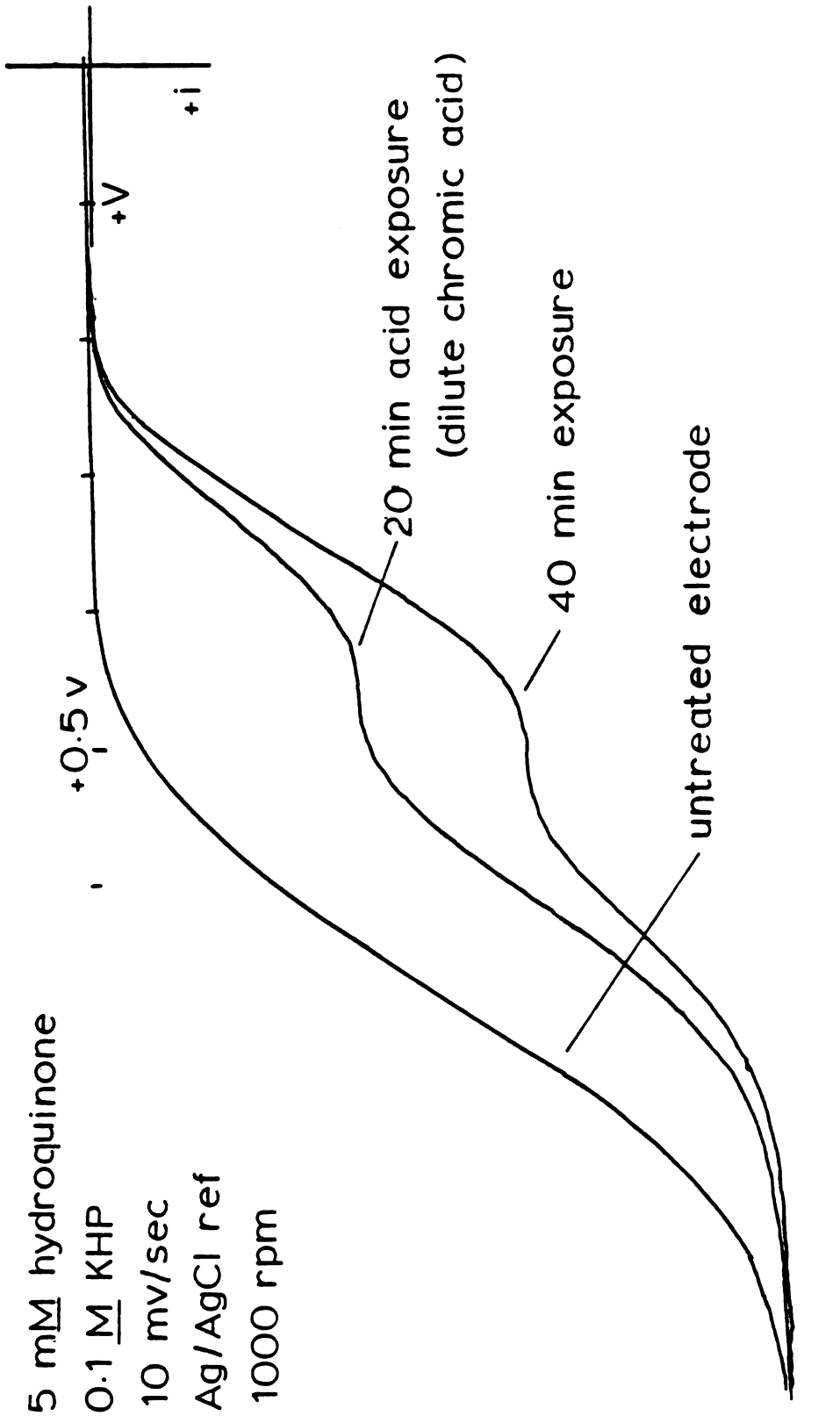

Figure 4.1.13: Activation of Au Surface by Oxidizing Acid:RDE Voltammetry

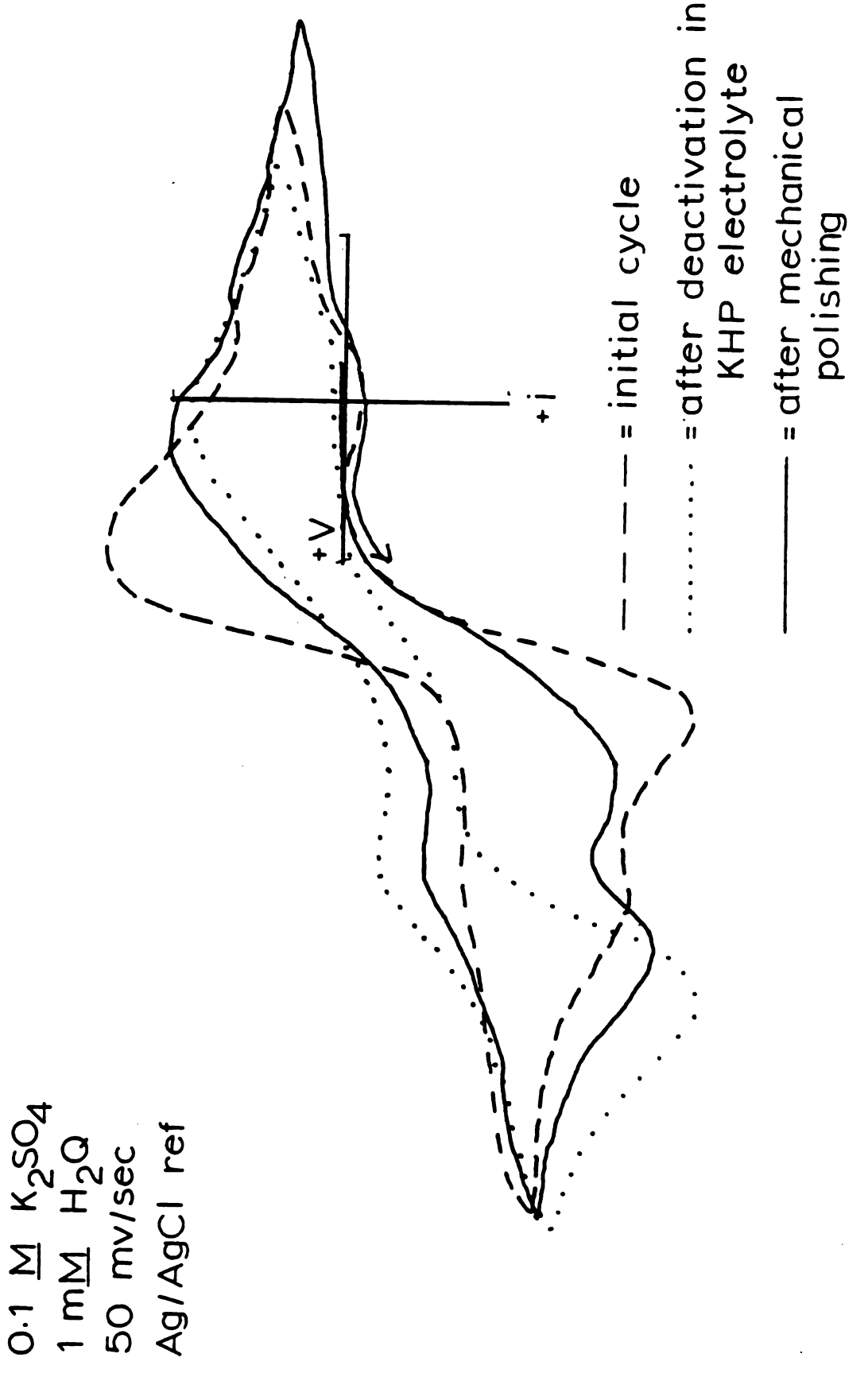

Figure 4.1.14: Activation of Au Surface by Mechanical Polishing

powder, rinsed, and retested. The result was a small but definite trend back to the active state, as shown by the solid trace in Figure 4.1.14. Thus it was found that deactivation in KHP produced a surface that was preserved upon removal from solution and was resistant to the action of K_2SO_4. Polishing could then remove the deactivating layer and restore the original activity.

The effect of O_2 on the electrolysis of H_2Q on Au is shown in Figure 4.1.15. No significant changes in Au activity toward H_2Q in the presence of O_2 were observed. The number of anodic cycles required to activate the Au surface seemed to increase, however. Anodic cycling also activated the reduction of O_2, as shown in Figure 4.1.15. by the solid wave in the cathodic region lying positive of the dashed wave.

The choice of supporting electrolyte also had an effect on the ease of activation or deactivation of the Au electrodes. A pH 4 phosphate buffer was prepared and showed identical behavior to KHP. Electrolytes prepared with K_2SO_4 and H_2SO_4, however, demonstrated an ability to resist deactivation through rotation. In Figure 4.1.16., cyclic voltammograms for H_2Q electrolysis in pH 7 K_2SO_4 and pH 1 H_2SO_4 solutions are shown. While the solid traces were taken after activation via anodic cycling, the initial cycles, like the dashed trace for K_2SO_4 in Figure 4.1.14., showed a mostly active Au surface for thoroughly cleaned and polished electrodes. The dotted traces were taken after a

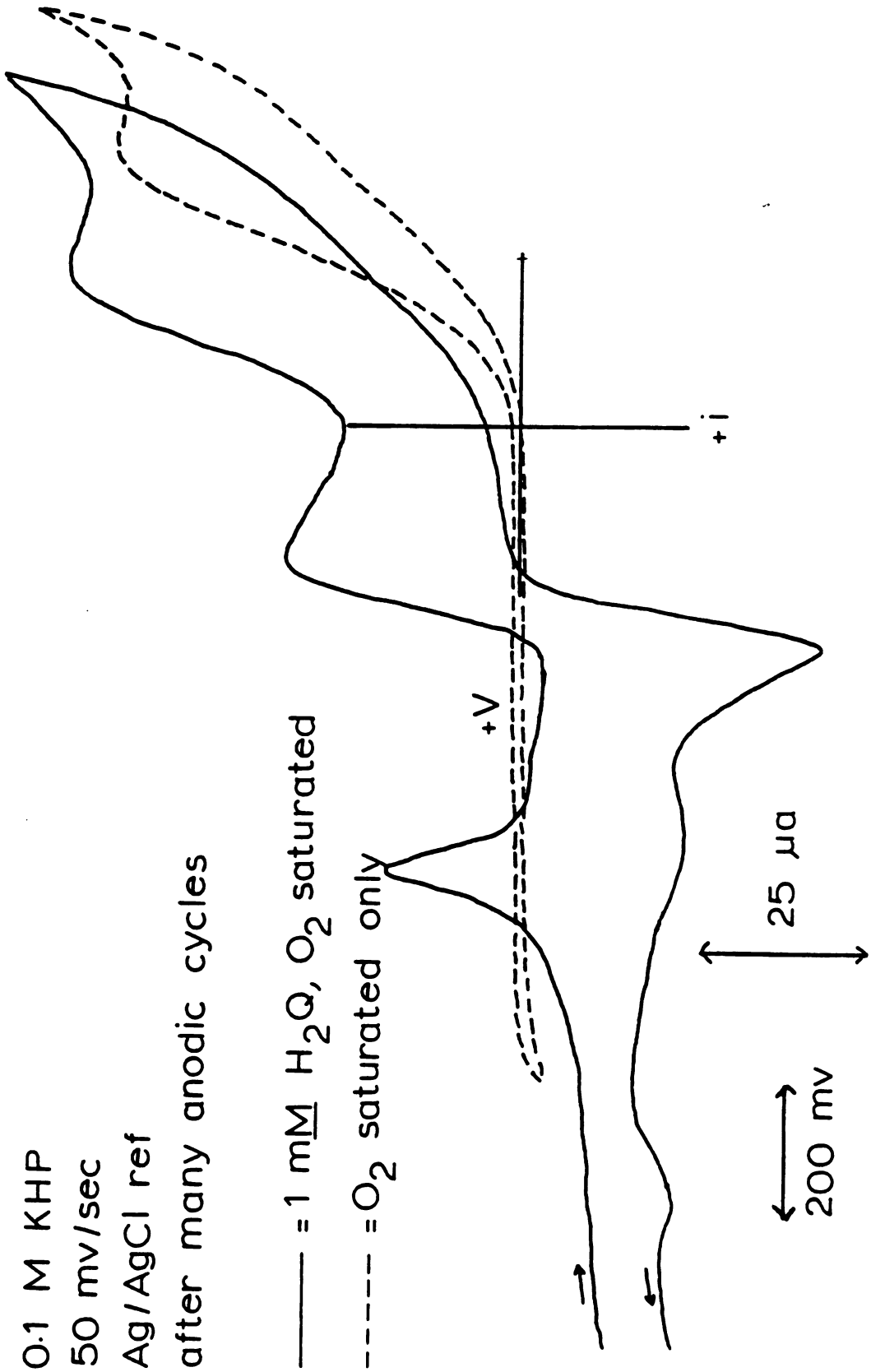

Figure 4.1.15: Effect of O_2 on Au Activation

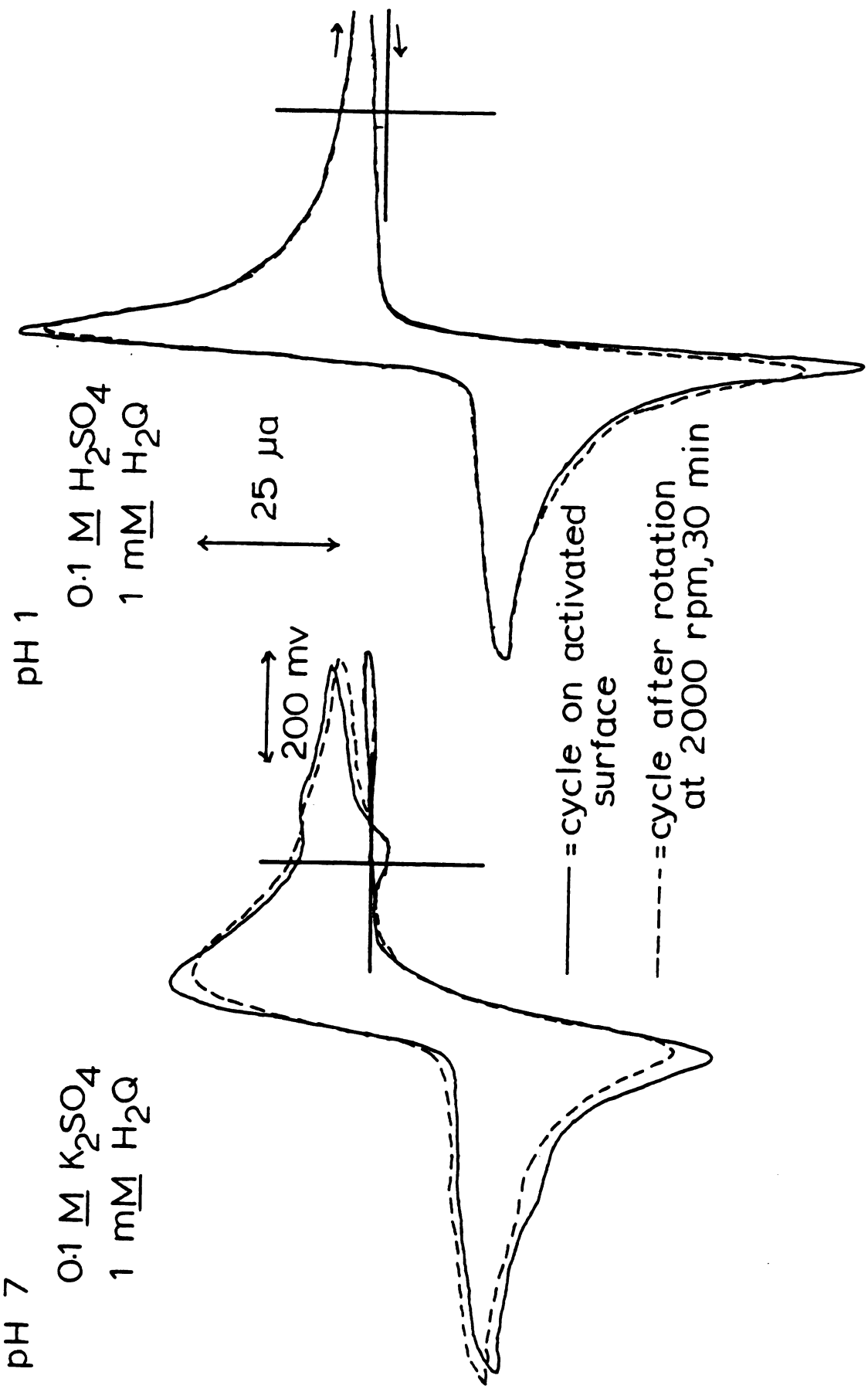

Figure 4.1.16: Rotation Effect in $SO_4^=$ Solution

rotational treatment that would have completely deactivated the electrodes in KHP -- the peak currents had only decreased by a few percent. Occasionally, a voltammogram taken after a few minutes' rotation would show an increase in activity. Since the solutions were prepared with the same water as that used in previous rotational deactivation experiments, the sulfate ion, $SO_4^{=}$, must be acting in some capacity to protect the active Au surface.

The effect of pH on H_2Q kinetics can also be seen in Figure 4.1.16. The current waves for the neutral case are shorter and broader than the acidic case, with a peak separation of 120 mv. The peak separation in the acidic case is only 50 mv. Peak separations as low as 36 mv were achieved, approaching the theoretical limit of simultaneous two electron transfer of 29.5 mv (156).

4.1.4. Unknown Redox Wave at Neutral pH

Close examination of the H_2Q voltammograms taken at neutral pH (Figures 4.1.14. and 4.1.16.) show small oxidation and reduction peaks in the cathodic region that are not observed in KHP electrolyte at pH 4 or H_2SO_4 electrolyte at pH 1. After repetitive anodic cycling to make the Au surface as active as possible, the two waves are clearly distinguishable as a reversible redox couple, as shown in Figure 4.1.17. The peak to peak separation of the waves was less than 60 mv, so that the kinetic process must either be a

Activated Au
1 m$\underline{M}$ H_2Q
0.1 $\underline{M}$ K_2SO_4

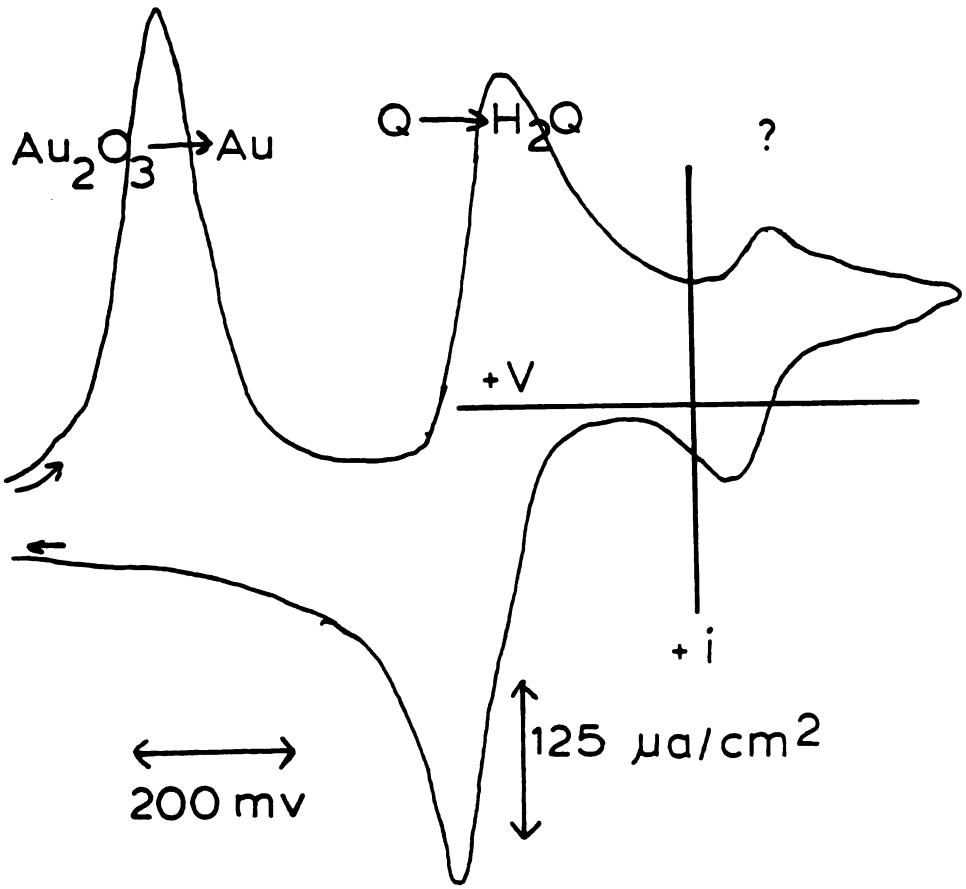

Figure 4.1.17: Full Range Cycle of H_2Q on Au at Neutral pH

two electron transfer or an adsorption reaction. The shape of the wavesdoes not appear to be symmetrical, thus arguing against an adsorption interaction with the electrode.

In order to identify the unknown redox couple, H_2Q was examined at the same pH, but in a different supporting electrolyte and electrode substrate. In Figure 4.1.18., the cyclic voltammogram for electrolysis of H_2Q in a KNO_3 electrolyte on a pyrolitic graphite electrode is shown. While the unknown redox process does not proceed as reversibly as on activated Au, its presence is nevertheless obvious. Thus the presence of the unknown redox couple is due to some form of H_2Q or Q which has electrochemical properties of its own, separate from the usual solvated, monomer quinone molecule. Figure 4.1.18. also shows that regular H_2Q electrolysis is required for the formation of the oxidized form of the unknown redox couple, which is in turn required to produce the reduced form. This is shown by the fact that an initial cathodic cycle gives neither positive nor negative signal. Thus BQ, or at least some oxidized form of H_2Q, is required for formation of the unknown species.

A study of the scan rate dependence of H_2Q electrolysis at neutral pH was undertaken in order to see if there was an equilibrium or interconversion between regular and unknown reduction waves. In Figure 4.1.19., two cycles are shown which reveal the overall trend: as scan rate increased, the size of the unknown wave relative to the main wave decreased.

Pyrolitic graphite
5 m$\underline{M}$ H_2Q
0·1 $\underline{M}$ KNO_3

1. initial cathodic sweep
2. after anodic cycle

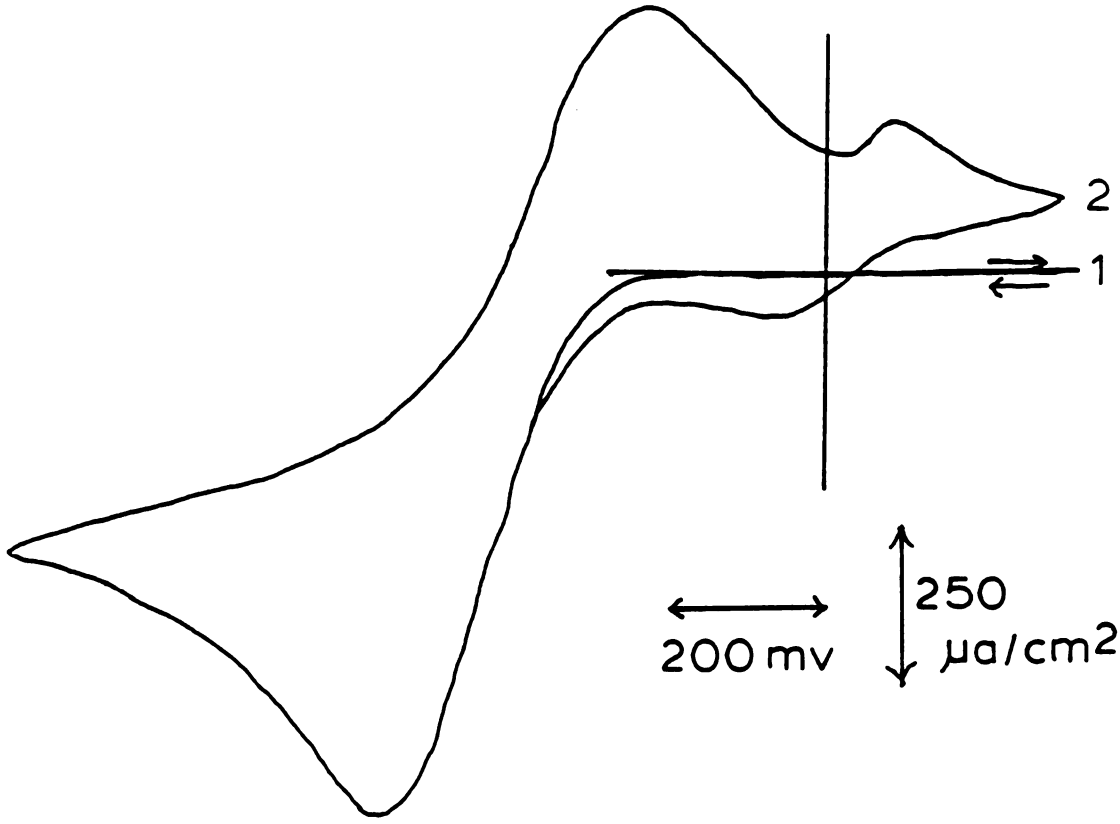

Figure 4.1.18: Electrolysis of H_2Q on Pyrolitic Graphite at Neutral pH

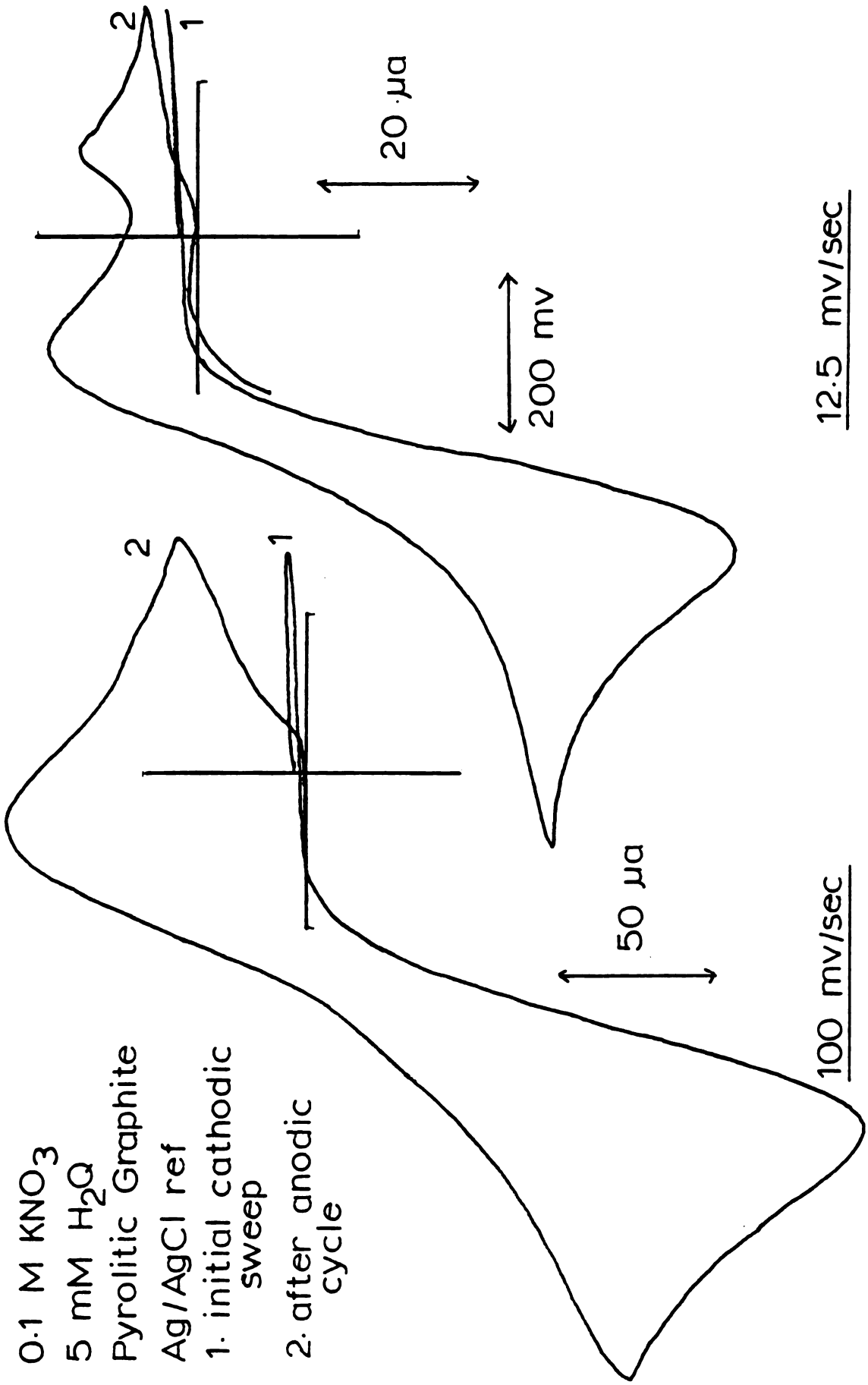

Figure 4.1.19: Scan Rate Dependence of H_2Q Electrolysis at Neutral pH

This suggested that a slow interconversion between normal and unknown reduction waves was occurring.

Another experiment involved poising the Au electrode past the main anodic wave for several minutes to build up a steady state concentration of the various products of electrolysis formed at that potential and below at the electrode surface, and then quickly scanning a cathodic sweep to observe what was present. The results are shown in Figure 4.1.20. The cathodic peak of the unknown redox couple was clearly resolved, even though in the cyclic voltammogram taken at that scan rate it was not observed. The unassigned wave is still quite small compared to the main one. The dotted lines simulate the diffusion limited current of the main wave which comprises the baseline for the following wave. Reduction waves were also observed well into the anodic region. The first peak observed after poising at 1.0 v corresponded exactly to the oxide desorption wave observed at 680 mv. The initial waves in the other two traces, however, could not be oxide desorptions since the poise potentials lie within the potential range where oxide desorption is occurring.

4.1.5. Discussion

The fact that the Au electrode could be activated by anodic cycling (Figures 4.1.2., 4.1.3., and 4.1.4.), cathodic cycling (Figures 4.1.6. and 4.1.7.), oxidizing acid (Figure

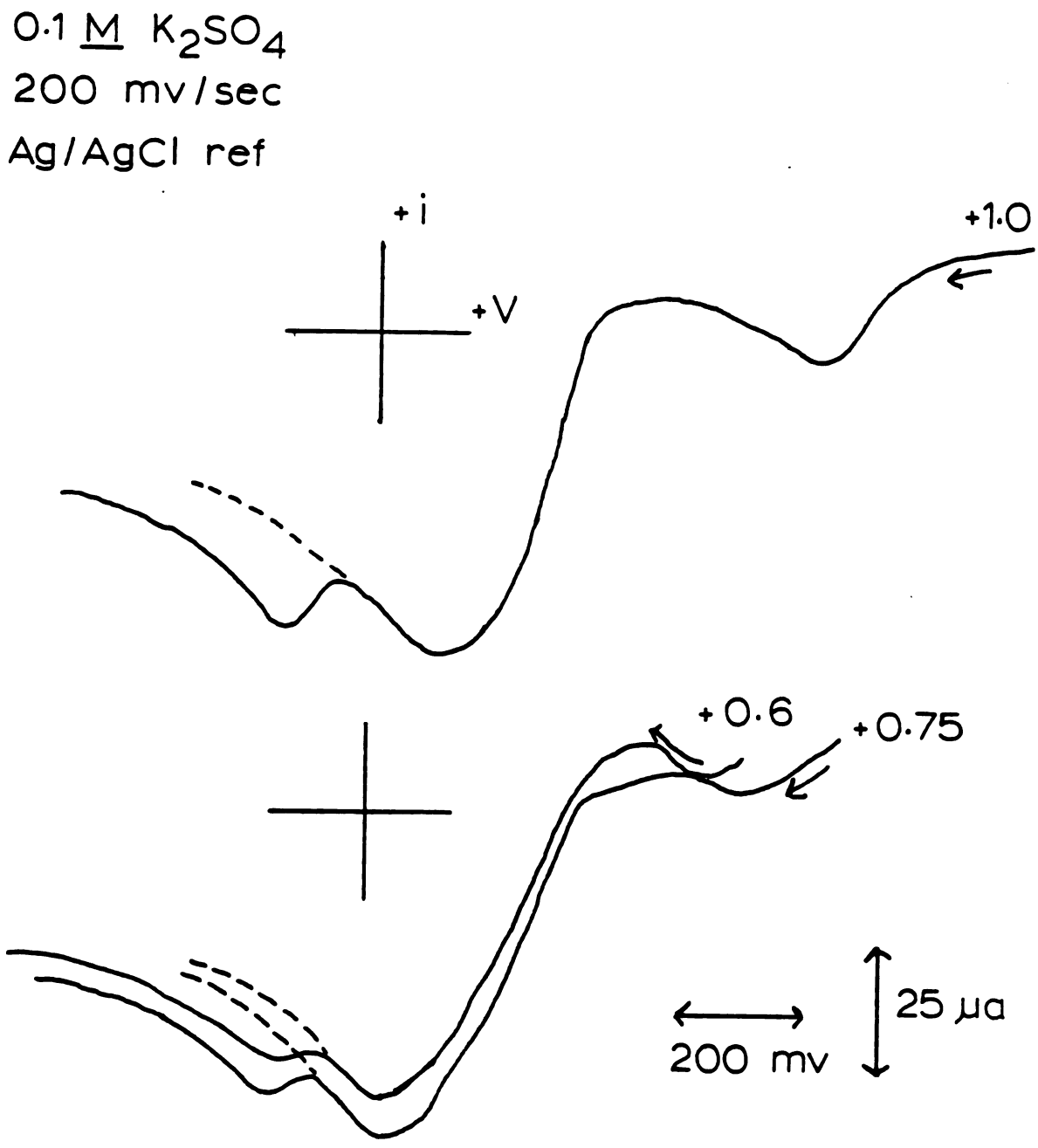

Figure 4.1.20: Fast Cathodic Sweep in Neutral Electrolyte

4.1.13.), and mechanical polishing (Figure 4.1.14.), and deactivated by resting (Figure 4.1.9.) or rotating (Figures 4.1.10. and 4.1.11.) the electrode in solution showed that one or more adsorbates were responsible for the variable activity of H_2Q. The possibility that H_2Q itself was responsible was eliminated when the electrode was successfully activated in the absence of H_2Q (Figure 4.1.5.). Deactivation in supposedly purified water (Figure 4.1.11.) is strong evidence for the presence of a background impurity. Previous tests of the water with UV spectrophotometry and atomic absorption had failed to detect any measurable background contaminant, however. It has long been suspected that the Nalgene vessel used to store the electrochemistry water may be leaching organic substances into the purified water, yet the water sample used in Figure 4.1.11. was collected directly from the glass still.

Alternative explanations for aqueous deactivation of the Au surface could involve some fundamental alteration of the double layer such as the reorientation of water molecule dipoles, or the adsorption of hydroxyl (OH^-) or hydronium (H_3O^+) ion from the surface. None of these arguments, however, can hold up against all of the experiemntal evidence. Since rotating the electrode hastened its rate of deactivation, mass transport of solution species must be involved. The possibility of water molecules activating the electrode through an adsorption interaction can then be eliminated, since at a solvent concentration of 55 M it would

not be influenced by rotation. The hydroxyl ion concentration at pH 4 is 10^{-10} M, too small to have any influence.

Adsorption of hydronium ion, however, was an appealing alternative to the background contaminant theory. Having a concentration in KHP solution of 10^{-4} M, it seemed plausible that some part of the Au surface could be covered with adsorbed H_3O^+. They could serve as a readily available source of protons for the reduction of quinone. A reaction scheme could be envisioned, where

$$H_3O^+ (aq) + H_2O (ads) \rightleftharpoons H_2O + H_3O^+ (ads)$$

$$Q + 2\ H_3O^+ (ads) \underset{-2\ e^-}{\overset{+2\ e^-}{\rightleftharpoons}} H_2Q + 2\ H_2O (ads)$$

Thus the Au surface is activated toward Q when the adsorbed H_2O water is protonated; reduction then deprotonates the adsorbed hydronium ion, leaving adsorbed H_2O on the Au surface that is now receptive toward H_2Q oxidation. The anodic and cathodic cycling treatments could be thought of as preparing the Au surface by removing unwanted neutral and ionic species and depositing a favorably oriented layer of water molecules on the surface. Reduction of H_3O^+ on the Au surface during cathodic cycling would alternately produce H_2 and then oxidize it, leaving adsorbed H_3O^+ on the surface. Anodic cycling would alternately consume H_2O to form Au_2O_3 and H_3O^+ and then desorb the oxide to form $Au(H_2O)_{ads}$. These

procedures would tend to raise or lower, respectively, the adsorbed H_3O^+ coverage on the Au surface with respect to the reequilibration of the double layer, where the concentration of adsorbed H_3O^+ decreased or increased to the equilibrium coverage at pH 4.

However, this mechanism requires H_3O^+ to perform in a way that is not consistent with its known behavior. Proton exchange among water molecules is very fast, so that 80% of the unusually high 36 x 10^{-4} cm^2/v-sec proton mobility in water is due to the tunneling transfer mechanism rather than drift of an H_3O^+ species (160). Despite a steady state concentration of H^+ in aqueous solution, solvated H_3O^+ only has an effective existence, since each ion exists for only a short period of time.

Therefore, the H_3O^+ adsorption theory fails, since it depends on a solution rate of protonation and deprotonation that is much slower than that associated with H_2O electrolysis. Reequilibration of the double layer with respect to H^+ would be expected to occur much faster than the time scale of the cyclic voltammetric experiment. Furthermore, protonation of the O atom in H_2O may eliminate its ability to adsorb strongly. Another issue concerns the point of zero exchange, or pzc. Literature values place the pzc of Au around 0.18 v vs. NHE (161, 162). Therefore, at potentials positive of this value the Au surface contains a net positive charge. In order for the positively charged H_3O^+ to adsorb in the anodic potential region, there would

have to be some sort of H_3O^+ specific adsorption on Au for which there is no precedent.

It is conceivable that the process used by the Sierracin company to vapor deposit the Intrex films forms a crystalline face which has poor kinetics towards the electrolysis of H_2Q. Anodic and cathodic cycling may serve to reorganize the electrode surface, providing a crystalline plane which is more active toward H_2Q. The change from one crystalline plane to another upon electrochemical formation and desorption of the oxide has been demonstrated on Au (164-166). If this were true for a KHP/H_2Q electrolyte, one should be able to substantiate this reorganization by the appearance of new voltammetric waves and the disappearance of others. But, as with bulk Au in Figure 4.1.8., the oxide wave in KHP does not exhibit any new features with successive anodic cycling. Thus a correlation between Au activation toward H_2Q and the crystalline plane exposed cannot be made.

One other very likely source of contamination of the Au surface is chloride ion that originated from the reference electrode. With a reference electrolyte of 3.5 M KCl, any cracks or bad seals in the reference electrode in contact with the electrolyte would rapidly cause a background Cl^- concentration. Even with defect-free construction, there is still the diffusion of Cl^- through the frit separating test and reference electrolyte. Some ion flow must exist in order to maintain electrical contact between reference and working electrodes, so actually it just is a matter of time before

the Cl^- concentration in the test electrolyte begins to rise. For the experiments involving rotating disk electrodes, the frit material was thirsty quartz, a common frit material, sealed onto the electrode by heat-shrink tubing. The reference electrode was 1½ inches from the center of the disk electrode, and the test electrolyte had a volume of 180 ml, ensuring a large solution volume for the escaped reference electrolyte.

The specific adsorption of Cl^- on Au electrodes has been examined by several groups (163, 164). Cadle and Bruckenstein (163) found that a background concentration of Cl^- at 2 x 10^{-6} M in 0.2 M H_2SO_4 could reach its saturation coverage in 5 minutes at 2500 rpm, and remain adsorbed as long as the disk potential remained above -0.2 v and below +1.55 v vs. SCE. While precise quantitation of the degree of surface coverage of Cl^- was not done, it was observed that by integrating the current collcted at a Pt ring electrode due to gold chloride complexes of oxidized Au, an estimated surface coverage of slightly more than one monolayer at 1.0 v was obtained. Lower coverages were inferred at lower potentials. Thus it seems plausible that adsorbed Cl^- could passivate the Au surface toward H_2O electrolysis.

There are some differences between the adsorption experiments performed here and the one done by Cadle and Bruckenstein that point to adsorption of substances other than Cl^-. In their experiment, Cl^- was observed to shift the Au_2O_3 formation wave to more anodic potentials; no shift was

observed here. Also, they found a correlation between potential and degree of coverage; the Au electrode in KHP electrolyte for these experiments could be completely passivated toward H_2Q at 0.0 v or at its rest potential, implying total coverage by the adsorbate. Also, the presence of $SO_4^=$ did offer some degree of protection to Au from adsorption in this series of experiments. Finally, they were able to completely desorb the Cl^- off the Au surface by briefly poising the electrode at -0.3 v vs. SCE, while in this system poising the electrode in the cathodic region only has a moderate effect on Au activity toward H_2Q electrolysis.

Being reasonably certain that Cl^- and other background contaminants in the electrochemistry water were present, an estimate of their concentration was made. By assuming that the rate of adsorption was diffusion controlled, the Levich equation governing mass transport at rotating disk electrodes could be utilized: $i_L = 0.62\ nFAC_oD^{2/3}\nu^{-1/6}\omega^{1/2}$; all variables are defined in the experimental chapter. The rate of molecular flow to the electrode surface can be derived from the current: $\frac{\#\ \text{molecules}}{\text{sec}} = \frac{N_o\ i_L}{nF}$

where N_o is Avogadro's number.

It was also assumed that a single monolayer of coverage was sufficient to deactivate the electrode, and that each adsorbate molecule occupied an area of 25 square Angstroms. The number of molecules requiredto passivate the electrode would then be A/a, where a is the area per molecule. The time t required to deactivate the electrode would then be:

$$t = \frac{\text{\# molecules needed to deactivate}}{\text{rate of molecular flow to electrode}}$$

$$= \frac{A/a}{N_o\ i_L/nF}$$

$$= \frac{(A/a)\ nF}{0.62\ nFAN_oC_oD^{2/3}\ v^{-1/6}\ \omega^{1/2}}$$

$$= (0.62\ aN_oD^{2/3}\ v^{-1/6}\ \omega^{1/2})^{-1}\ (\frac{1}{C_o})$$

Thus there is an inverse relationship between the concentration of the contaminant and the time required to deactivate the electrode. By exchanging t and C_o, the concentration of background contamintion can be found as a function of the time of deactivation. For this system, the minimum time required to deactivate the electrode at 2000 rpm was about 20 minutes, or 1200 seconds. Typical values for D and v in aqueous solution are 5×10^{-6} cm^2/sec and 0.01 cm^2/sec, respectively. The rotation rate must be expressed in radians/sec, so 2000 rpm becomes 209.4 rad/sec. The calculated background concentration is:

$$C = [0.62\ (25\text{Å}^2)(\frac{10^{-16}\ cm^2}{\text{Å}^2})(6.02 \times 10^{23}\ mole^{-1})(\frac{10^{-3}\ l}{cm^3})$$

$$\times\ (5\times10^{-6}\ cm^2/sec)^{2/3}\ (0.01\ cm^2/sec)^{-1/6}\ (209.4\ rad/sec)^{1/2}]^{-1}$$

$$\times\ \frac{1}{1800\ sec} = 9.8\times10^{-8}\ moles/liter$$

We can use Bruckenstein's data (163) to estimate a possible background Cl^- concentration in this system. He observed an equilibrium in 5 minutes at 2500 rpm; in this experiment, complete passivation was established in 20 minutes at 2000 rpm. After correcting for the difference in mass transport rates, a possible background Cl^- concentration of 6×10^{-7} M is obtained. This result is quite comparable to that from the equation above, since the calculation above assumed an irreversible, diffusion controlled adsorption, which would be the fastest rate possible, and yield the lowest possible concentration.

Thus it is possible for an extremely small concentration level of background impurities to eventually contaminate an electrode. This is an important consideration for long-term studies, especially on rotating disk electrodes. Comparing Figure 4.1.9. to 4.1.10., the rate of deactivation on stationary electrodes is fortunately at least an order of magnitude slower than on electrodes rotating at 2000 rpm.

Much of the evidence associated with the new redox wave observed at pH 7 seemed to support the existence of a complexed quinhydrone structure. H_2Q oxidation produced quinone which could then associate with solution H_2Q near the electrode surface to form the quinhydrone charge transfer complex. This does not occur at lower pH, because if either Q or H_2Q is protonated, the complex cannot form. The scan rate dependence studies (Figures 4.1.19. and 4.1.20.) support the idea of an equilibrium being set up between the electrogenerated Q and quinhydrone formation.

However all indications from the literature are that the redox couple could not be quinhydrone. In neutral H_2O, Granger and Nelson (167) determined a dissociation constant of 0.289 with a maximum $Q:H_2Q$ concentration of 9.8×10^{-4} M. In a millimolar H_2Q solution, however, a localized concentration could not exceed $(10^{-3})^2/(0.289) = 3.3 \times 10^{-6}$ M, which is far too small to account for the size of the unidentified wave. As for the pH effect, the quinhydrone electrode has been used since the early 1920s as a pH indicator, and so is known for its uncomplicated acid/base equilibria up to pH 8 (168). In other words, neither QH^+ or QH^- are stable species in acidic aqueous solution.

Results obtained on the bulk Au rotating disk electrode can now be applied toward the Au Intrex. The true Au surface is the active surface toward H_2Q. The inactive surface, which was always initially present on new Au Intrex electrodes, is due to an adsorbed organic layer, which probably forms during the manufacturing process when Au vapor is deposited onto a polyester backing. It may also be true that some parts of the polymer support protrude from the 300 Å Au layer. While in some cases this is an undesirable feature, with regard to chemically modified electrodes it may be posible to use these carbon functionalities to bond redox species to the Au surface (169).

The adsorbate could be easily removed by anodic and cathodic cycling, however, so that the Au Intrex can be expected to behave just as bulk Au. The adsorbate was not

removed by ultrasonication in ethanol or water, so that the Au substrate was in its inactive form when GaPc-Cl was deposited on it. Considering the voltammetric results in subsequent sections of this thesis, however, the adsorbed layer could not have significantly hindered electrical contact between the dye film and the Au substrate. O_2-plasma cleaning has been shown to have a significant effect on the Au Intrex surface (see reference 168 and section 4.4.2. of this thesis). Part of the reason for this is undoubtedly the consumption of adsorbed organic species, but it is doubtful whether the Au Inrex surface could be exposed to the plasma long enough to remove all the carbonaceous material without damaging it.

4.2. Comparison of GaPc-Cl to Other Phthalocyanine Derivatives

4.2.1. Introduction: Comparison to Silicon Phthalocyanine

Both silicon phthalocyanine, SiPc, and chlorogallium phthalocyanine, GaPc-Cl, were brought to the attention of this author and coworkers in his group as part of a set of phthalocyanine derivatives which possessed unusual crystalline order. The dihydroxy $SiPc(OH)_2$, was known to polymerize in a stacked manner with the linkage occurring via an axial bond between Si centers through an oxygen atom (170, 171). Monomer, dimer, and trimer SiPc's could be isolated in reasonable purity. The fluoro-derivatives of the group

III phthalocyanines, Al, Ga, and In, were also reputed to stack axially through the fluoride counterion. These derivatives were thought to be potentially good candidates as multi-layer dye sensitizers, their axial stacking characteristics suggested an enhanced conductivity because of increased π orbital overlap between adjacent phthalocyanine rings, while the high molar absorptivity of phthalocyanines in general was maintained. Samples of each of the derivatives described above were obtained for photoelectrochemical experimentation. Several chloro-derivatives of the group III phthalocyanines were included as well, even though they had shown no unusual crystallographic properties. But since they were readily available, because they were precursors in the synthesis of the fluoro-derivatives, and since they would provide good comparisons as to effect of axial stacking in phthalocyanine films, they were tested along with the others.

Thin films, whose absorbance maxima were less than 0.5 in the wavelength region from 500 to 900 nm, were sublimed upon SnO_2 and scanned in a narrow potential window (-0.2 to +0.5v) in the light and dark in a KHP, pH 4 electrolyte that was 10 mM in H_2Q. Photocurrents were observed in each case, but the most pronounced effects came from the chloro-gallium and chloro-aluminum derivatives (41). Similar tests on the various oligomeric forms of SiPc showed that the monomer form was a better sensitizer than the dimer or trimer (172). Thus the expected correlation between crystalline phase andd photoelectrocatalytic ability was not found.

The two phthalocyanine derivatives that had given the best results, SiPc and GaPc-Cl, were then selected for further study. An initial objective was to compare the ability of phthlocyanine-modified electrodes to oxidize H_2Q compared to a more common electrode material, such as Pt. The voltammetric comparison between GaPc-Cl/SnO_2, SiPc/SnO_2, and Pt for H_2Q electrolysis is shown in Figure 4.2.1. While the Pt electrode showed prominent waves for both oxidation and reduction, the irradiated Pc film electrodes showed fairly good rectification; the positive currents were much larger than the negative ones. Also, the amount of positive charge transferred during the same potential excursion on the same geometrical area electrode was significantly larger for the Pc film electrodes than for Pt. Another observation was the onset of anodic photocurrent on the Pc film electrodes well negative of the dark E° as determined by the position of the Pt waves. Finally, the necessity of light to activate the Pc films was also evident; the response of these electrodes in the dark was negligible as far out as +0.5 v, past the current maxima for these electrodes in the light and for Pt.

There were also clear differences in the light voltammetric response of the two Pc film electrodes. The GaPc-Cl/SnO_2 electrode photocurrent rose on the anodic sweep to a rough plateau upon which two slight maxima lay, and then decayed just slightly to form a new plateau. On the return sweep the current initially ran parallel just below the

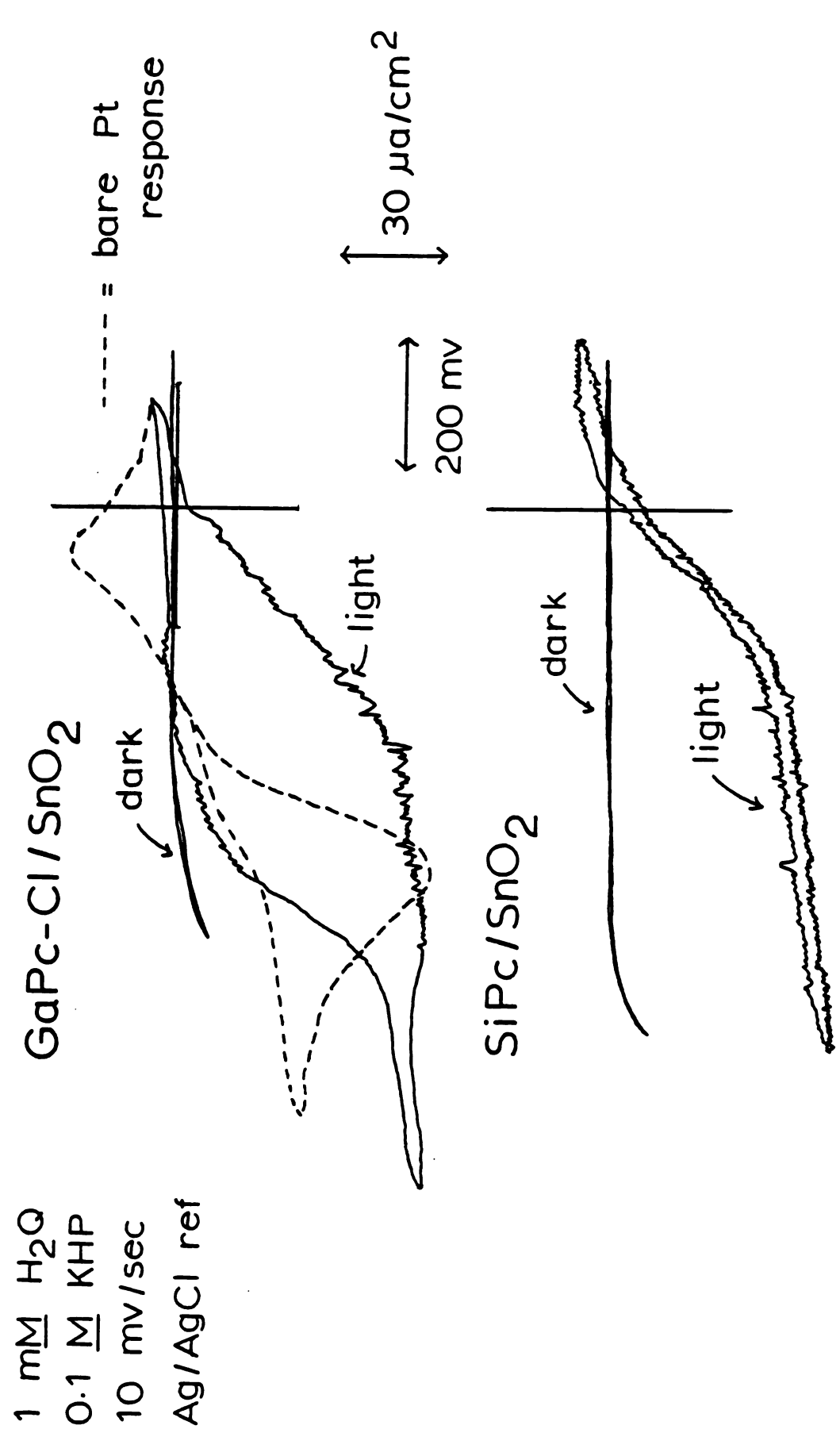

Figure 4.2.1: Comparison of H_2Q Voltammetry for GaPc-Cl and SiPc

outward sweep but as the first plateau region was reached it decayed back to the baseline. For the SiPc/SnO_2 electrode, the photocurrent rose to a single, level plateau. The return sweep virtually traced the outward sweep all the way back to the origin, in contrast to GaPc-Cl/SnO_2. A slightly larger cathodic photocurrent was noticed as well.

Another difference between the two electrodes concerned those regions on the voltammetric curve where the trace is jagged or smooth. The trace is sometimes jagged because the xenon lamp used as a light source for these experiments had a flicker associated with it, so that the light intensity delivered to the electrochemical cell had a small random component on top of a steady output. Most of the time this flickering of the intensity was a nuisance, but it had one virtue in that it revealed whether an electrochemical reaction had some degree of intensity control or not. For the GaPc-Cl/SnO_2 voltammogram, the trace was only slightly jagged on the leading edge of the anodic wave because the reaction was kinetically controlled -- the electrode potential was determining the rate of reaction. As the potential moved more positive, the rate constant for charge transfer increased, so that the intensity eventually became rate limiting. Thus the trace became quite jagged as the photocurrent leveled off into a region of intensity control. As the rate constant for charge transfer continued to increase with potential, a third region was reached where diffusion of reactant to the electrode was rate limiting.

The trace was then quite smooth, since an increased intensity has no effect on a mass transport limited current.

The situation was much simpler for SiPc/SnO_2. The trace appeared to be equally jagged along its entire length. It was somehow possible to scan out to +0.8 v and still maintain some degree of intensity control.

Thus, while the gross features of Pc-film electrode response, such as photoelectrocatalytic ability and contrast between light and dark activity, are quite similar, a closer examination shows that there may be distinct mechanistic differences in how SiPc and GaPc-Cl electrodes operate. In light of this observation, GaPc-Cl was compared to a much broader spectrum of phthalocyanine derivatives.

4.2.2. Comparison of Optical Absorbance Spectra

In Figure 4.2.2., the optical absorbance spectra of various phthalocyanine derivatives between 500 and 900 nm, in solution and as a solid film on glass are shown. For the sake of consistency, pyridine was used as a solvent whenever possible. When solubility problems arose with pyridine, chloronapthalene was used. The wavelengths of the various absorbance maxima are marked in each figure.

The solution phase spectra were very similar in appearance: a strong ($\varepsilon > 10^5$ 1/mole-cm) $\pi \longrightarrow \pi^*$ singlet transition, known as the Q band, occurred in the far red

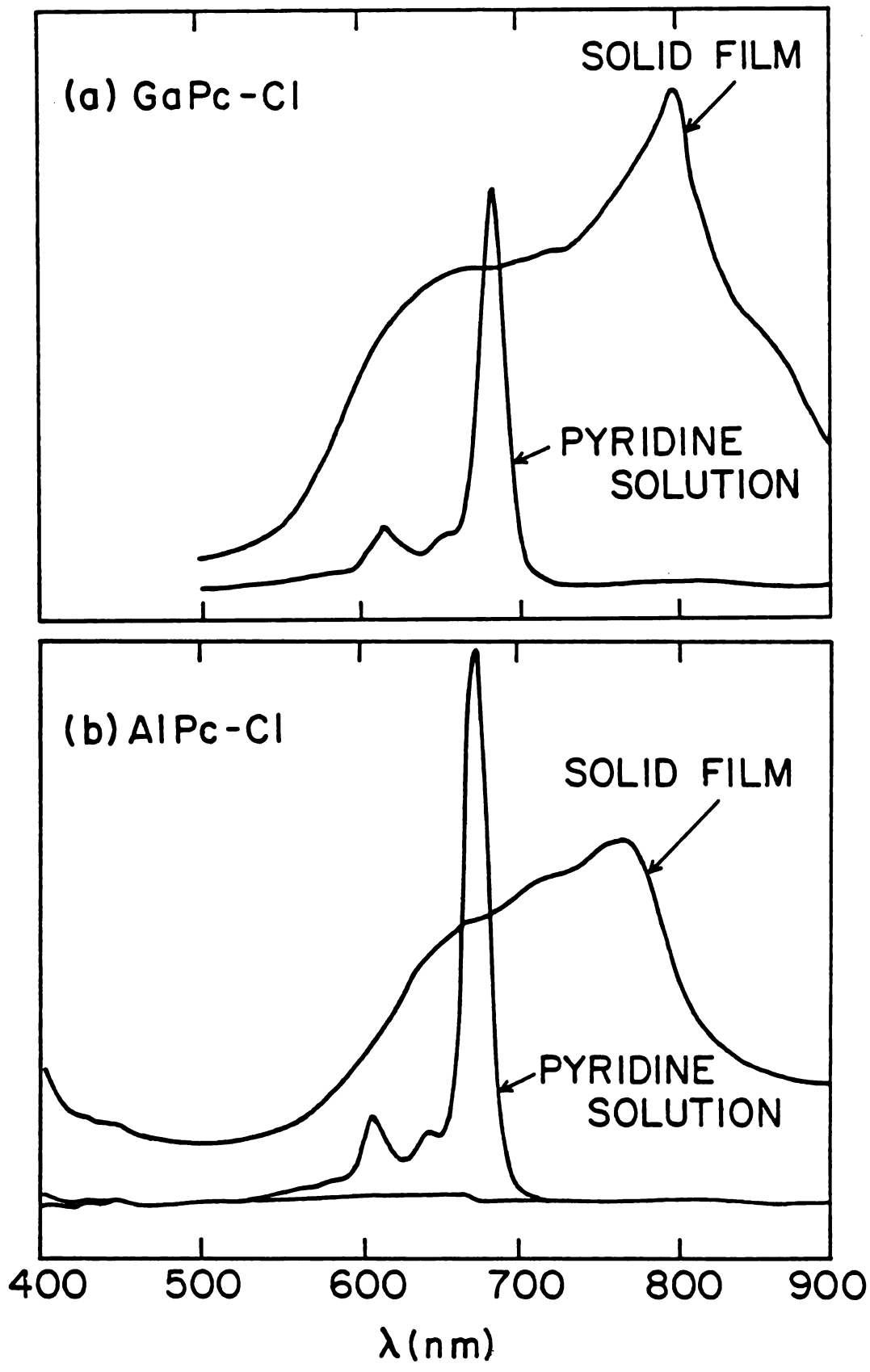

Figure 4.2.2: Absorption Spectra of MPc's: (a) GaPc-Cl and (b) AlPc-Cl

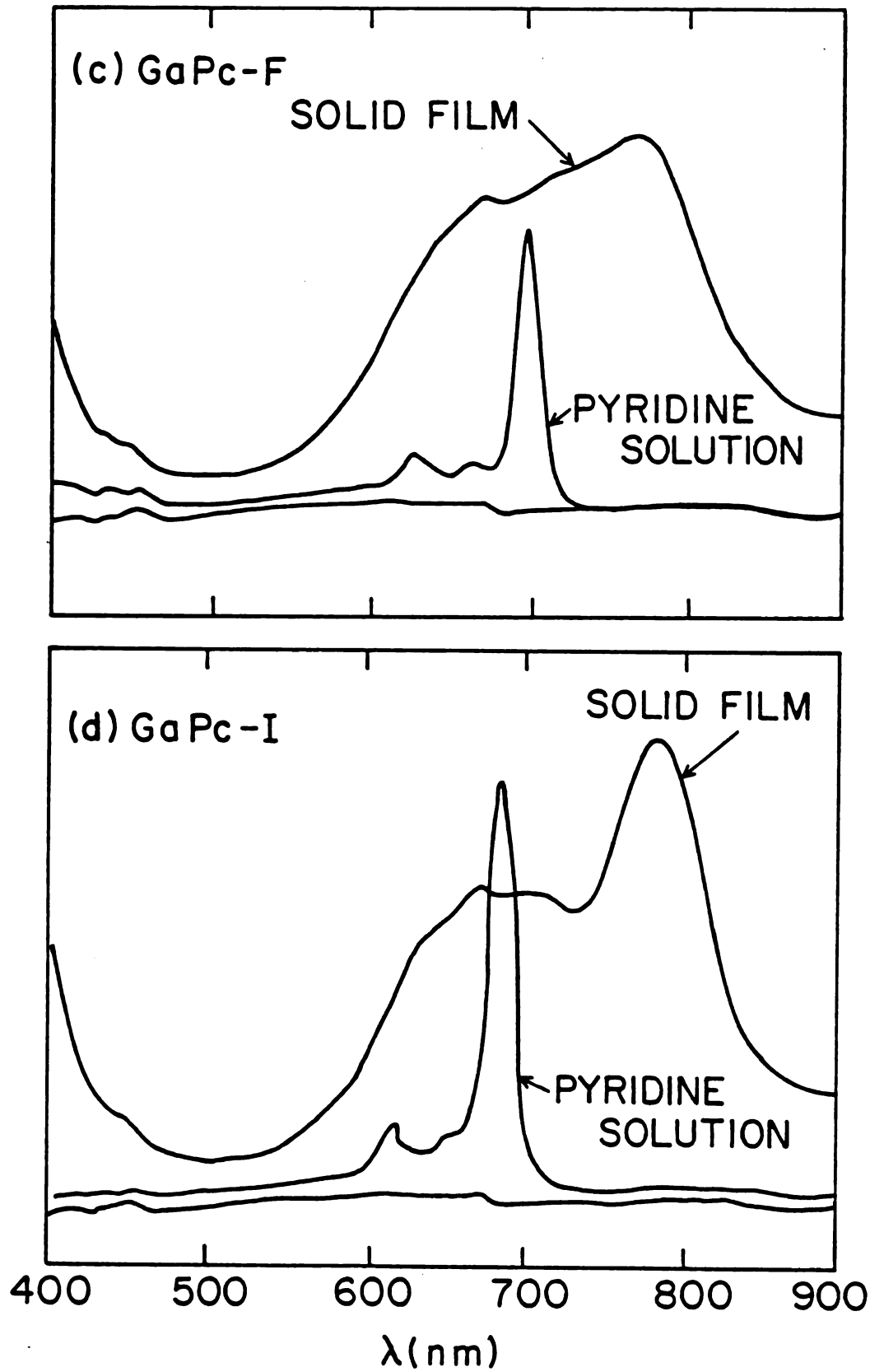

Figure 4.2.2 continued: Optical Absorption Spectrum of MPC's: (c) GaPc-F and (d) GaPc-I

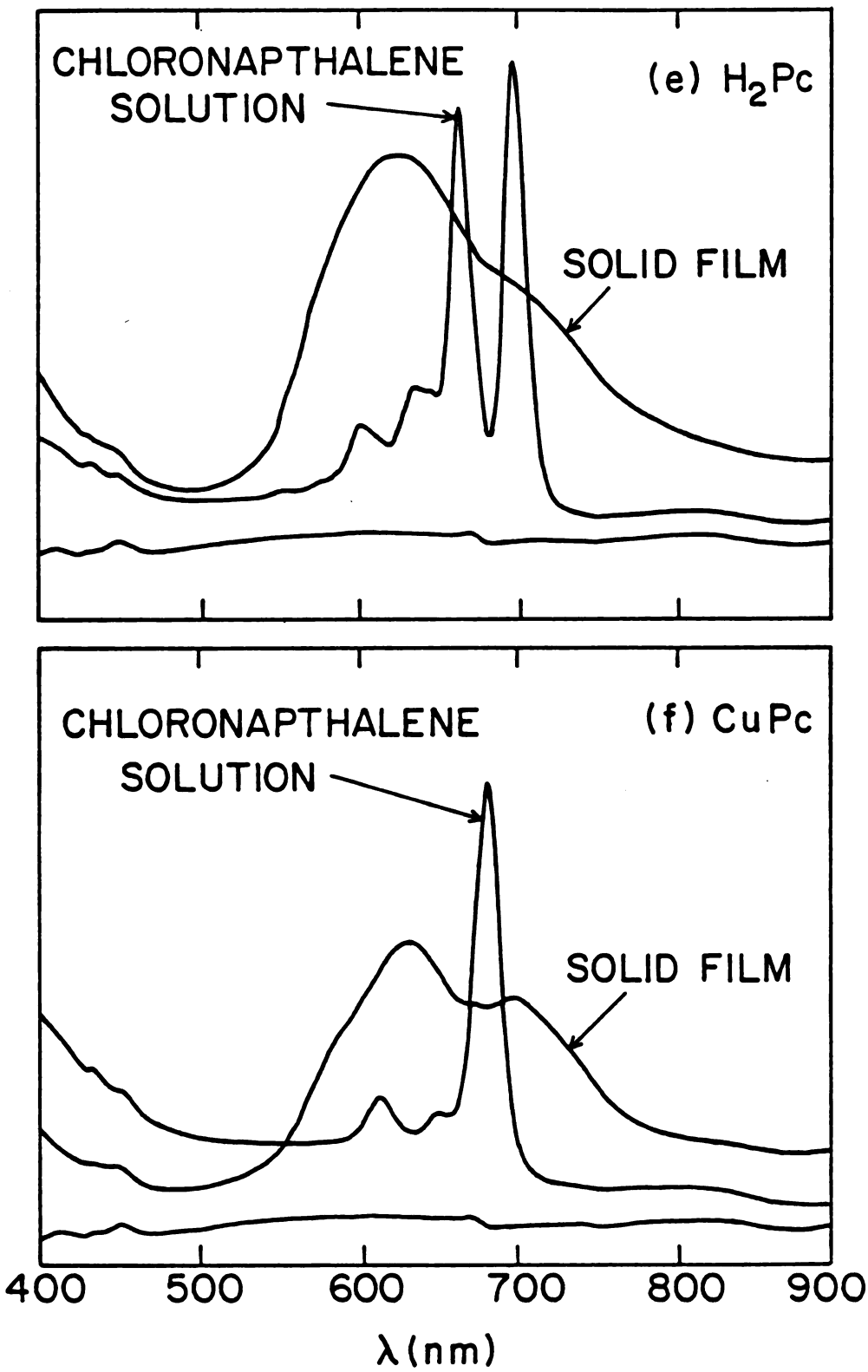

Figure 4.2.2 continued: Optical Absorption Spectrum of MPC's: (e) H_2Pc and (d) CuPc

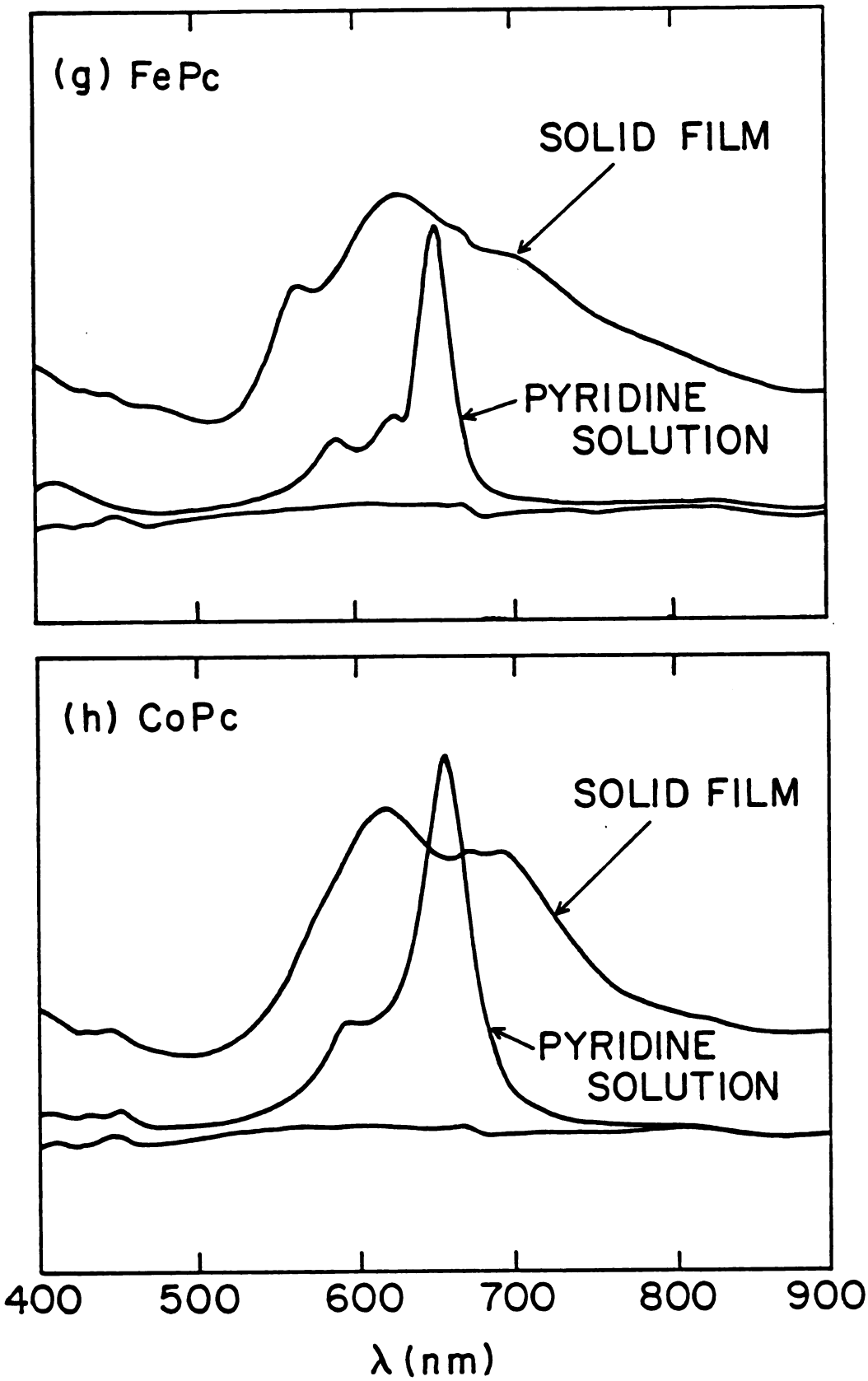

Figure 4.2.2 continued: Optical Absorption Spectrum of MPC's: (g) FePc and (h) CoPc

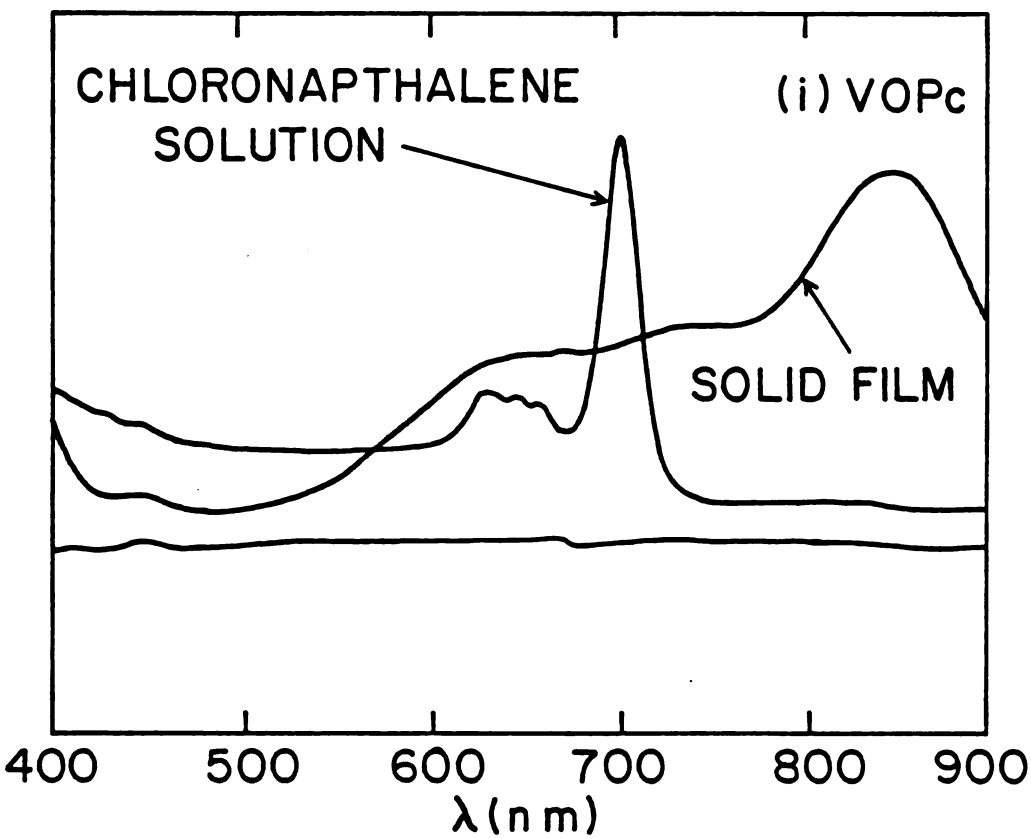

Figure 4.2.2 continued: Optical Absorption Spectrum of MPC's:
(i) VOPc

region of the visible spectrum; another less intense peak occurred on the high energy side of the Q band, separated usually by around 70 nm, and corresponds to the 0 to 1 vibronic transition of the same identity; a third, even less intense transition was commonly found between the two previously mentioned peaks. Its presence has been observed by other researchers (173, 174), but its spectroscopic identity has not been firmly established. The solution spectrum of H_2Pc (Figure 4.2.2.e) had twin peaks, because the presence of two H atoms instead of a single metal center reduced the molecular symmetry from H_{4h} to D_{2h}, splitting the normally degenerate e_g (π^*) orbitals. All solution spectra agreed well with the available literature data (173, 174), except for an anomalous peak observed for VOPc at 646 nm.

Another strong $\pi \longrightarrow \pi^*$ transition, called the B, or Soret band, occurs in the ultraviolet region around 330 nm, but is generally not observed in solution because the few organic solvents in which the phthalocyanines are miscible also absorb strongly in that region. This problem can be circumvented under some circumstances by sulfonating the benzene rings of the macrocycle. This can be neatly done by synthesizing the phthalocyanine with the sodium salt of 4-sulfophthalic acid as a starting material. The resulting tetrasulfonated phthalocyanine is then soluble in polar solvents, such as H_2O and DMSO, which have no absorption in the near UV, so that the Soret band stands alone for observation. Since the emphasis of this dissertation is on

spectral sensitization with visible wavelength light, the Soret band was not of direct interest.

Solid film spectra showed two distinct types of behavior. One group of Pc- derivatives, which included H_2, Cu, Fe, and CoPc (Figures 4.2.2.e-h respectively) gave an absorbance maximum that was blue-shifted with respect to the solution, with a smaller peak on the low energy side. Curve, shape, and maxima agreed well with literature data for the α polymorphs of Pc-derivatives (175). It should be cautioned here that it is incorrect to say that the transition was blue-shifted; the observed transitions may well correspond to new exciton states which arise from the solid state, but their identity cannot be definitely established until the α phase crystal structure has been better defined (165). FePc may well belong in a class of its own, because of the prominent shoulder on the high energy side of the absorbance maximum at 630 nm.

The other group of Pc-derivatives, which included GaPc-Cl, AlPc-Cl, GaPc-F, GaPc-I, and VOPc (Figures 4.2.2.a-d and i respectively) showed a pronounced red-shifting of absorbance maxima. The smallest shift was for GaPc-F, whose λ max shifted 71 nm, while VOPc had the largest shift of 142 nm, out to 843 nm. The crystalline structure of α VOPc is undoubtedly not isomorphous with the first group of α polymorphs. Thus the α designation does not imply anything regarding the structure of the Pc crystal. It applies approximately to a set of conditions under which a Pc crystal

is formed. The α-β designations worked well only as long as each Pc derivative was found to form polymorphs that were isomorphous with the other Pc derivative polymorphs formed under the same conditions.

All four of the group III phthalocyanines examined showed a red shift, with the λ max lying on the low energy side of the collective absorption region.

4.2.3. Comparison of Voltammetric Response to H_2Q

A preliminary investigation into the relative photoelectrocatalytic ability of GaPc-Cl compared to other phthalocyanines showed that it may be one of the more active Pc-derivatives (41). A more extensive test was designed to confirm that conclusion, where films of all the Pc derivatives examined in the previous section were sublimed upon gold substrates and used as electrodes in the light and dark electrolysis of H_2Q. The results are shown in Figure 4.2.3.a-i.

The GaPc-Cl/Au electrode response, along with that of the plain Au-MPOTE substrate, are shown in Figure 4.2.3.a. The electrolysis of H_2Q on plain Au in pH 4, shown by the dotted trace, is only poorly reversible (subject to the qualifications discussed in 4.1) with a peak to peak separation of 500 mv or more. After a nonporous film of GaPc-Cl had been sublimed onto it, two significantly different voltammetric responses were obtained, depending

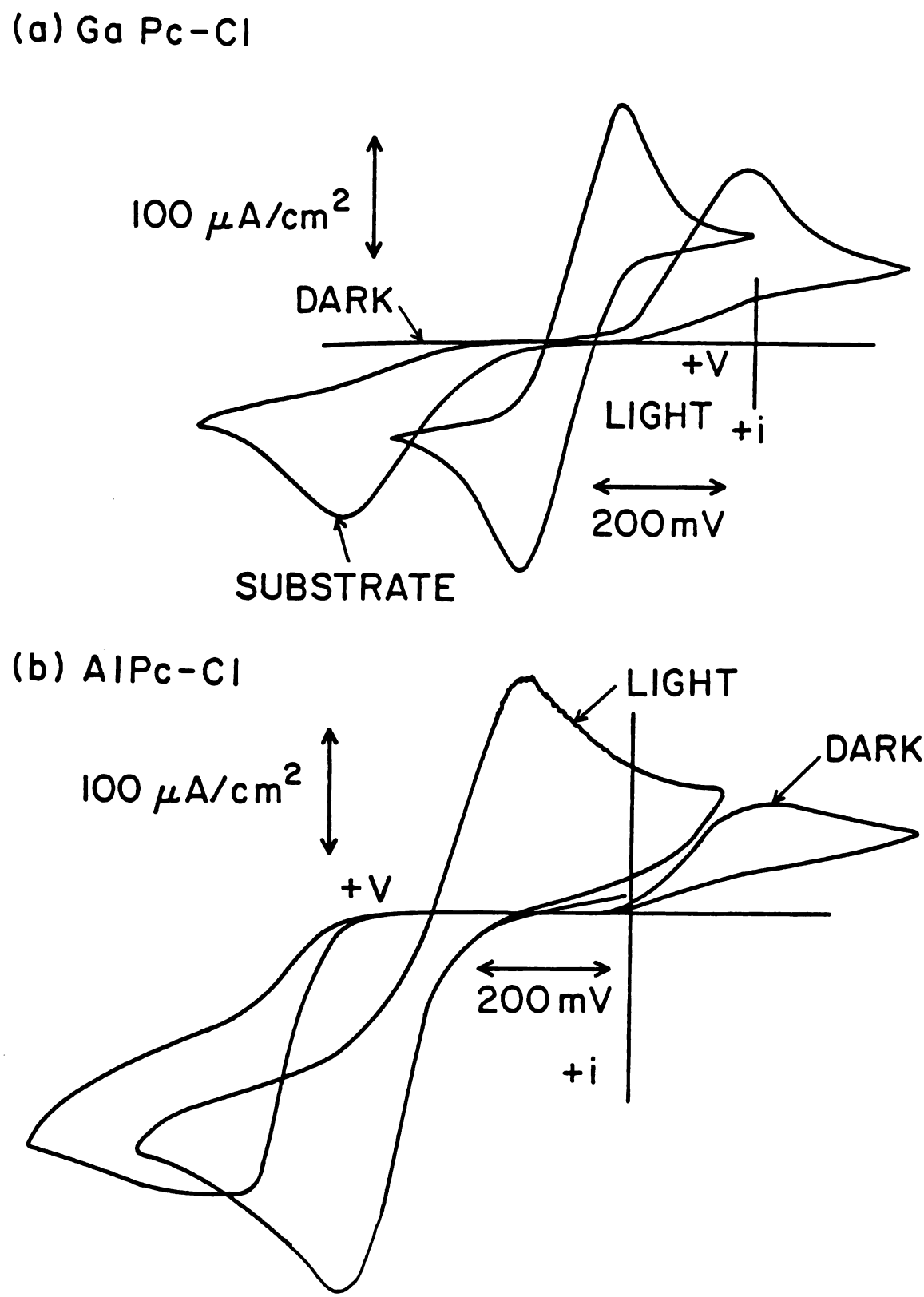

Figure 4.2.3: Voltammetric Response of MPc Film Electrodes: (a) GaPc-Cl and (b) AlPc-Cl

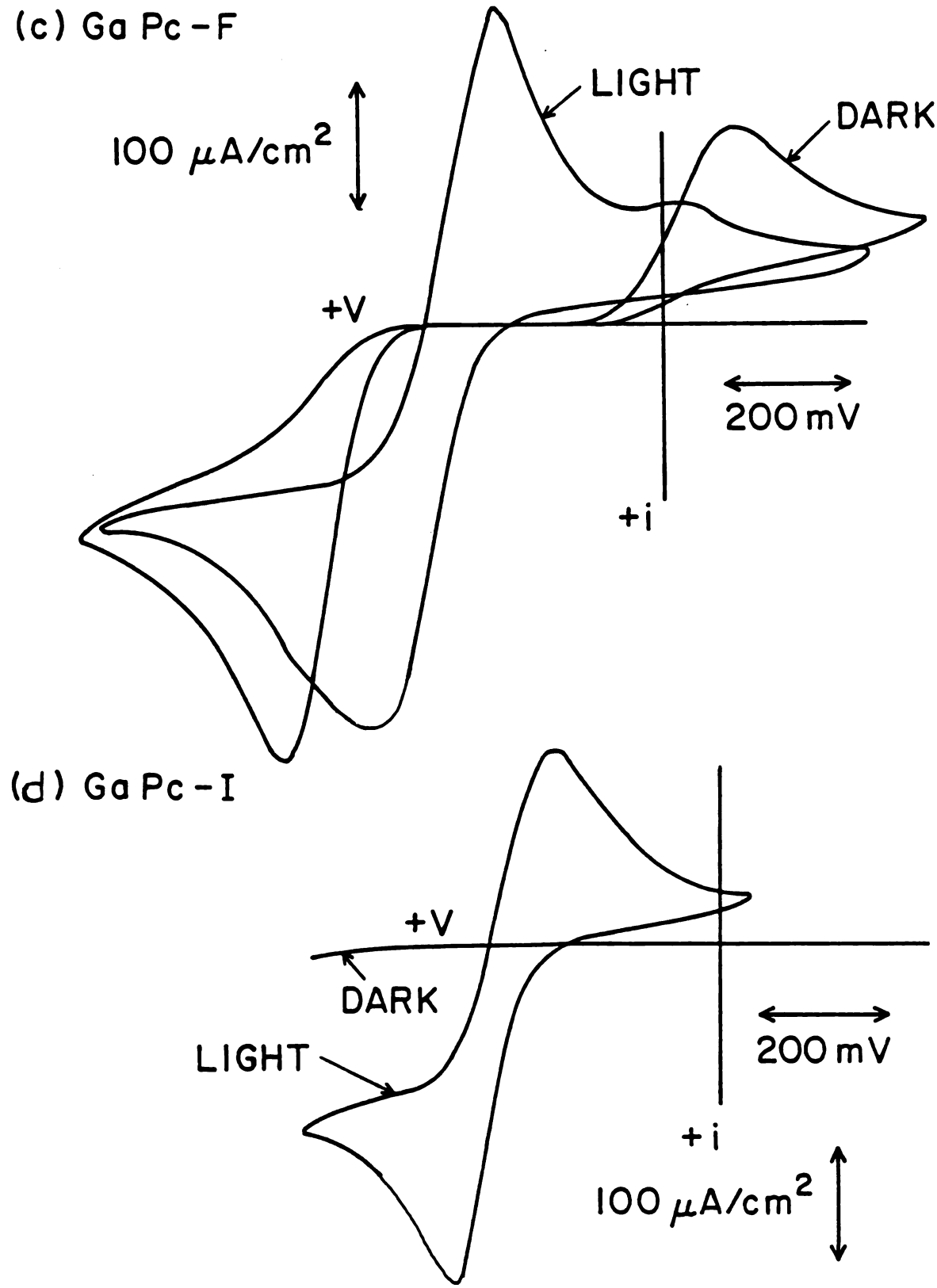

Figure 4.2.3 continued: Voltammetric Response of MPc Film Electrodes: (c) GaPc-F and (d) GaPc-I

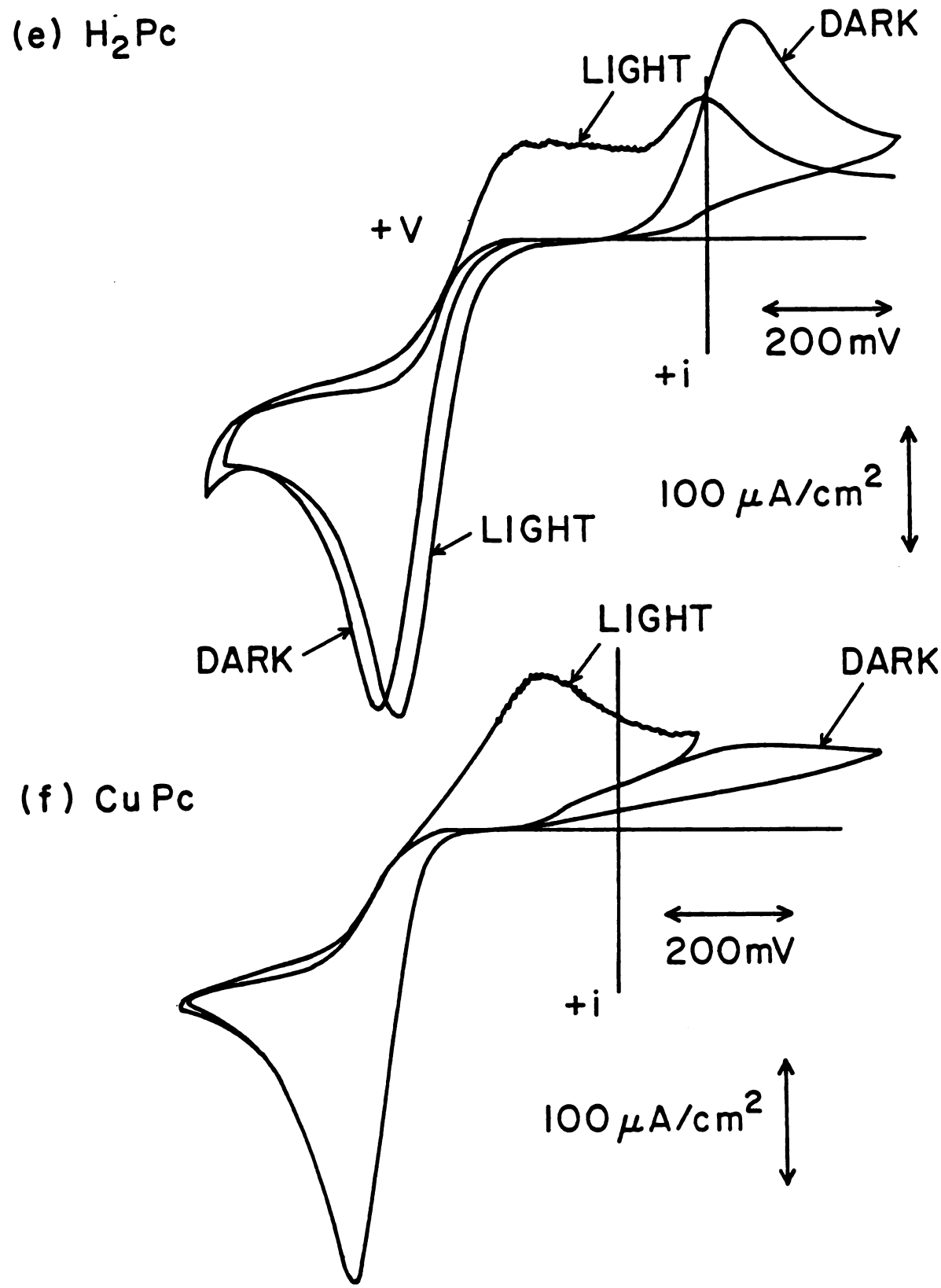

Figure 4.2.3 continued: Voltammetric Response of MPc Film Electrodes: (e) H_2Pc and (f) CuPc

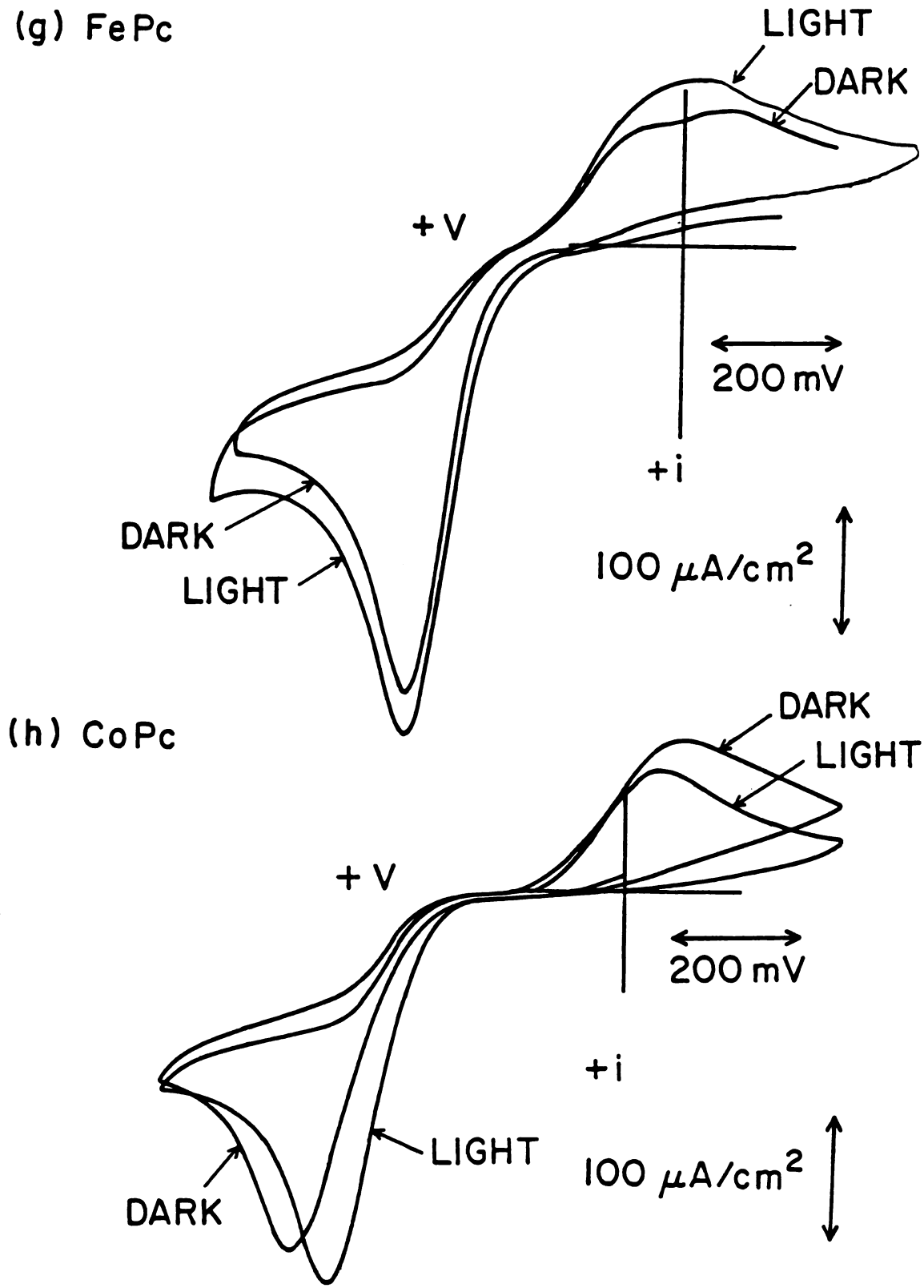

Figure 4.2.3 continued: Voltammetric Response of MPc Film Electrodes: (g) FePc and (h) CoPc

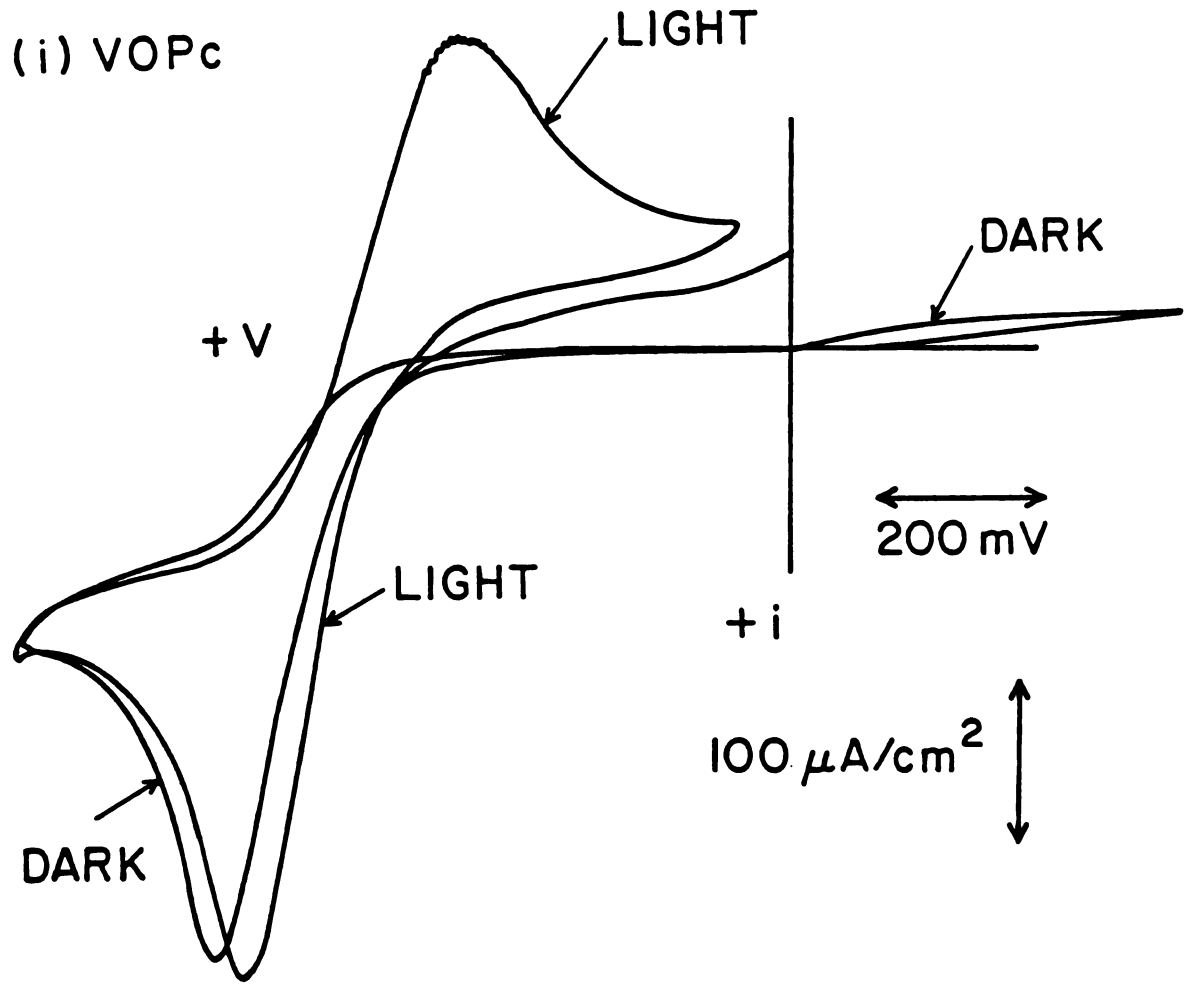

Figure 4.2.3 continued: Voltammetric Response of MPc Film Electrodes: (i) VOPc

on whether the GaPc-Cl/Au electrode was irradiated or not. In the dark, the electrode is essentially an inert surface, with little or no measurable current; in the light, quite reversible charge transfer is observed for both oxidation of the H_2Q and reduction of the electrogenerated quinone. A peak to peak separation of 120 mv was measured. This represents a significant photocatalytic effect with respect to the inactive Au surface, demonstrating an activity nearly equal to the activated Au substrate (Figure 4.1.1.).

Several prominent features of the voltammetric response of the GaPc-Cl/Au electrode are at variance with the expected results predicted by models of dye sensitization and semiconductor photoelectrochemistry. The mere fact that the electrolysis was performed on a metallic substrate is in conflict with the idea that a semiconductor electrode with its space charge layer is a required component for obtaining efficient charge transfer because it prevents the back reaction. Also, the fact that equally large reversible photocurrents were observed for oxidation and reduction is in conflict with the idea of phthalocyanines as p-type semiconductors, in which case one would expect at least some degree of rectification, where the negative reduction current would be larger than that for oxidation. Finally, the current response of a semiconductor photoelectrode involving the majority carrier, which in this case is oxidation, should be nearly the same in light or dark. Instead, the GaPc-Cl/Au electrode gave an extreme contrast between oxidative, or

hole currents, with a vigorous reaction in the light and a negligible reaction in the dark.

When AlPc-Cl was used as a dye sensitizer on Au, the photocurrent was not as reversible, and the dark current was considerably larger, as seen in Figure 4.2.3.b. The degree of reversibility of the photocurrent was still qualitatively the same in both directions, however. The dark current, exhibiting an irreversible response, was also distorted somewhat in that the current maxima appeared flattened and broadened, as if two unresolved redox processes were occurring almost simultaneously. Increasing or lowering the scan rate failed to improve the shape of the curve.

The voltammograms for GaPc-F/Au are shown in Figure 4.2.3.c. In the light, a nearly reversible response is seen just as before with GaPc-Cl, but the dark response resembled that of the bare Au substrate. Whether the dark redox process was occurring at the Pc/electrolyte interface or inside a pore at the substrate/electrolyte interface is difficult to tell.

The voltammograms for GaPc-I/Au are shown in Figure 4.2.3.d. A reversible trace in the light, and a negligible response in the dark made it the only other electrode whose light and dark behavior was the same as GaPc-Cl.

The behavior of H_2Pc/Au electrodes is shown in Figure 4.2.3.e. A large, well shaped oxidation wave was observed in the light and in the dark. For reduction, the light current appeared as two waves, the first forming an intensity-limited

plateau, and the second corresponding to whatever process was occurring in the dark. By lowering the intensity of incident light on the electrode surface, it was possible to decrease the size of the first curve, resulting in an increase in the second. Thus, the two waves represented competitive cathodic processes, one of which required photon excitation. For the CuPc/Au electrode (Figure 4.2.3.f), the anodic behavior is the same as that observed on H_2Pc. The cathodic current, however, showed a single curve, much larger and more reversible in the light than in the dark.

Similar behavior was obtained for FePc and CoPc, as seen in Figures 4.2.3.g and 4.2.3.h, respectively. The peak separation and curve shape were basically identical in the light and the dark, with the light current magnitude being slightly larger. The negative peak current for CoPc, however, was actually larger in the dark than in the light. This may be attributable to an initial nonequilibrium proportion of Q and H_2Q at the electrode surface, however, caused by initiating a scan too soon after the completion of the previous one. Little indication of a photovoltage is observed for these two Pc derivatives. These results are consistent with those obtained by this author for light versus dark O_2 reduction on FePc films (176).

The voltammetry of H_2Q on VOPc/Au, shown in Figure 4.2.3.i, gave the best example of p-type semiconductor behavior of all the derivatives tested: an identical anodic current response for light and dark, and a large cathodic

photocurrent obtained from a reversible wave in the light and virtually no activity in the dark.

From the ideal p-type semiconductor behavior observed for VOPc, one might expect a photovoltage to be present as well. In Table 4.2, the open circuit photovoltages measured against a Pt electrode for a number of the Pc derivatives are shown.

It is worth noting that the photovoltage measurements were obtained by the difference between readings in the dark and in the light. One would expect that two electrodes in the same electrolyte in the dark would have the same potential, but instead a potential difference of several hundred millivolts was typically measured between the Pc/Au electrode and the Pt electrode in the dark. The dark potential was observed decaying toward zero at a rate of about 1 mv/sec. Exposure to light caused the potential to climb within a few seconds to a higher value, which then continued to decay at the same rate. Thus, despite the drifting potential readings, a constant potential difference between light and dark was observed, which was measurable to within ± 3 mv. The matter of potential drift and other transients will be discussed in section 6.3.

The results gave a fair correlation between photovoltage and the difference between light and dark cathodic current. The order of photovoltages was VO > H_2 > Cu > Ga-F > Ga-I > Al-Cl > Ga-Cl, while a qualitative ordering of the difference between light and dark negative current response

TABLE 4.2

Photovoltages Measured for Various

Phthalocyanine Derivatives

Cell: Au/MPc//H_2Q, KHP//Pt

PHTHALOCYANINE DERIVATIVE	PHOTOVOLTAGE (millivolts)
CuPc	-110
H_2Pc	-150
VOPc	-260
GaPc-Cl	- 20
GaPc-I	- 50
GaPc-F	- 70
AlPc-Cl	- 25

would be Ga-Cl, Ga-I > VO > Cu > H_2 > Ga-F, Al-Cl > Co > Fe. Were it not for the chloro- and iodo-GaPc, a nearly direct correlation would have been made.

4.2.4. Comparison of Phthalocyanine/Au Electrodes via Electron Microscopy

There was some question at the outset of whether scanning electron microscopy could yield any structural information on the phthalocyanine films. When studying organic materials with SEM, there are always the problems of charging and beam damage. When a poorly conductive sample is subjected to an electrom beam, a net charge builds up which can distort the trajectory of secondary electrons emitted from the surface, and hence the image. Heat also builds up and can cause physical and chemical changes in the sample if not dissipated quickly enough. These problems limited the useful magnification to around 30,000X. However, it turned out that there were surface features on the phthalocyanine films sufficiently large (tenths of microns) to be discerned at magnifications as low as 10,000X, so that use of the EM technique could be made.

Electron micrographs of each of the Pc derivatives on Au at 10,000X and 30,000X are shown in Figure 4.2.4.a-i. While each Pc film appeared slightly different from the others, they could be generally characterized as having a round convoluted structure, or sometimes globular structures on an

amorphous background. The only exceptions were GaPc-Cl and GaPc-I, which possessed mainly puckered granular structures that had grown together.

Thus, the only two Pc films that showed any crystallinity at these magnifications as evidenced by sharp angles and planar faces, were GaPc-I and GaPc-Cl. These granular structures were typically four-sided and about 0.3 microns across. A few granules appeared to have a square pyramidal geometry. An additional feature observed only for the GaPc-Cl film was a fair density of micron-long, needle-like structures dispersed over the granular background. A large portion of the GaPc-Cl sample surface was examined under the electron microscope to insure that the needles were indeed part of the film surface and not just an artifact. Several other GaPc-Cl/Au samples were checked and found to have both types of structures.

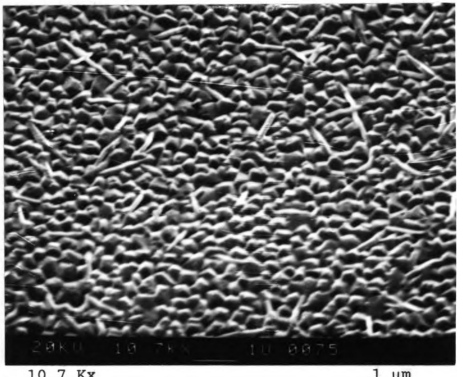

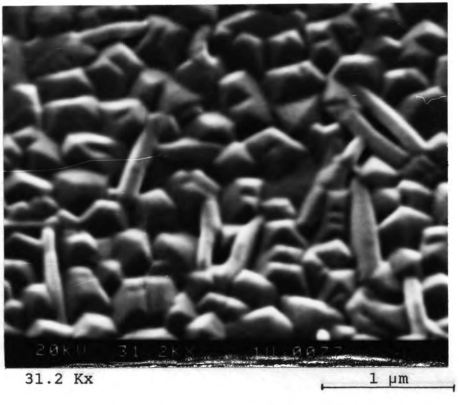

Figure 4.2.4.a: Electron Micrographs of MPc Films on Au: GaPc-Cl

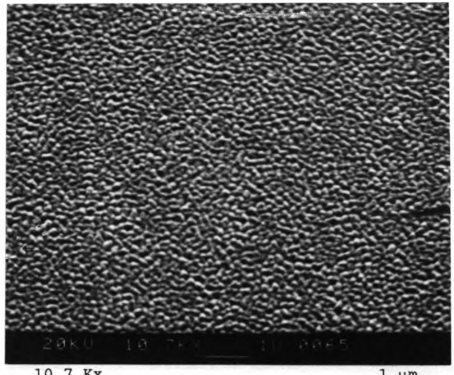

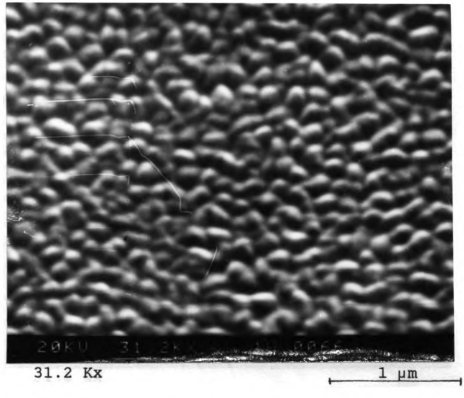

Figure 4.2.4.b: Electron Micrographs of MPc Films on Au: AlPc-Cl

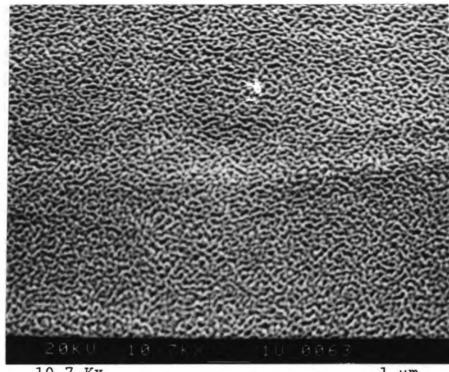

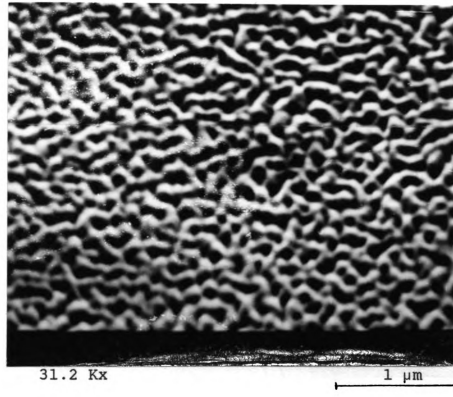

Figure 4.2.4.c: Electron Micrographs of MPc Films on Au: GaPc-F

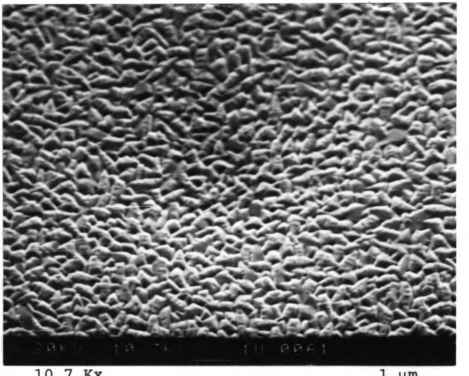

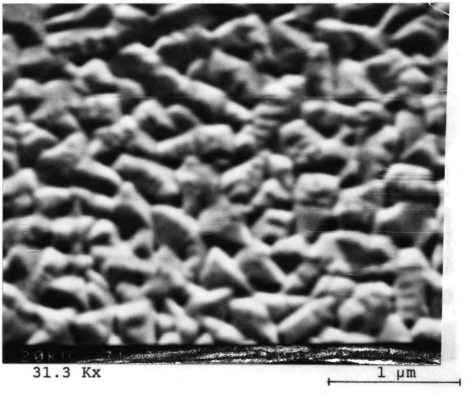

Figure 4.2.4.d: Electron Micrographs of MPc Films on Au: GaPc-I

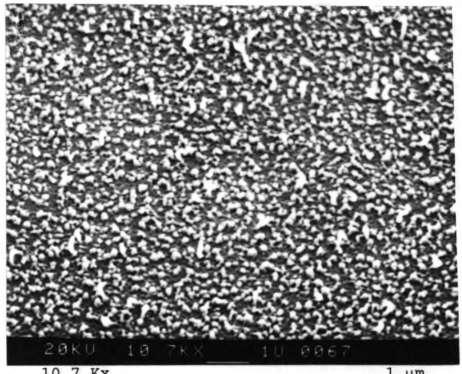

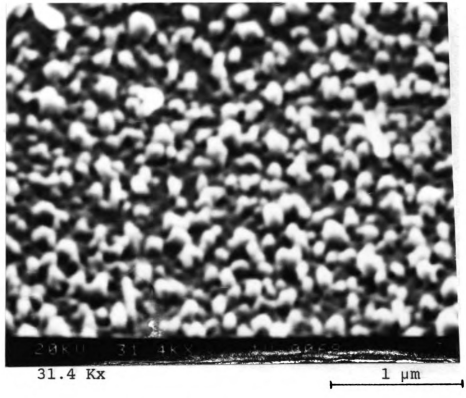

Figure 4.2.4.e: Electron Micrographs of MPc Films on Au: H_2Pc

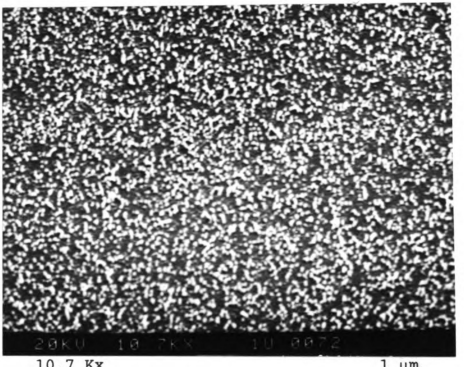

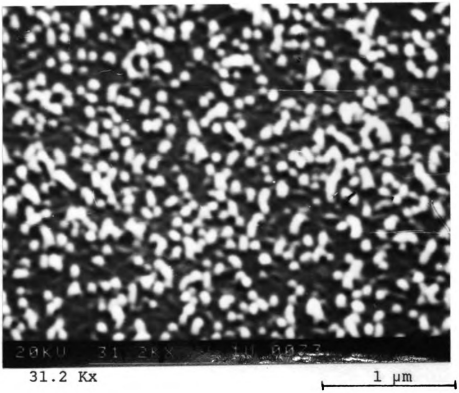

Figure 4.2.4.f: Electron Micrographs of MPc Films on Au: CuPc

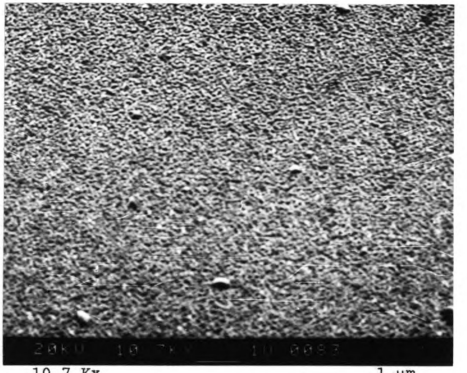

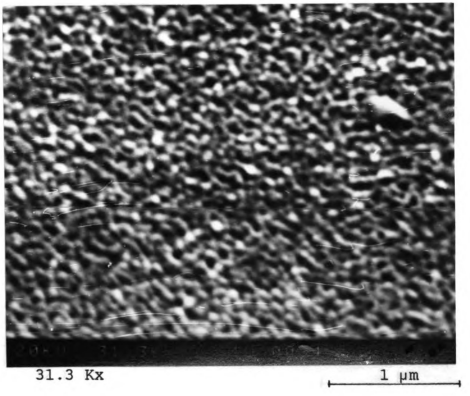

Figure 4.2.4.g: Electron Micrographs of MPc Films on Au: FePc

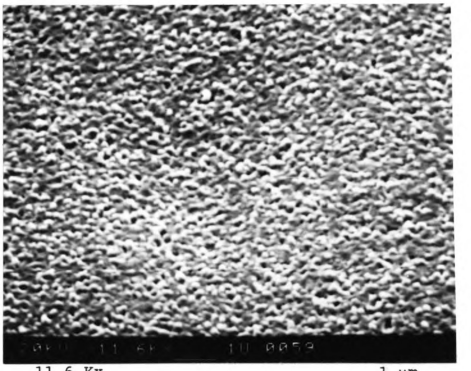

11.6 Kx 1 μm

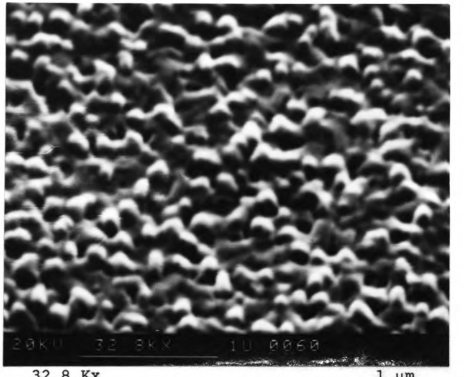

32.8 Kx 1 μm

Figure 4.2.4.h: Electron Micrographs of MPc Films on Au: CoPc

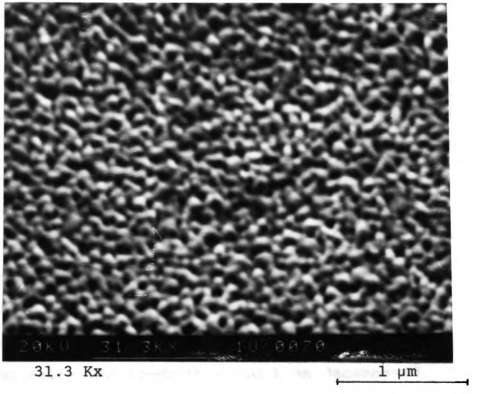

Figure 4.2.4.i: Electron Micrographs of MPc Films on Au: VOPc

4.3 Variation of GaPc-Cl Behavior with Substrate and Electroactive Species

4.3.1. Substrate Effect

The voltammograms presented thus far which have used GaPc-Cl have had Au and SnO_2 as a substrate. Films were also deposited on other substrate materials in order to see what effect the substrate had on the voltammetric response.

The cyclic voltammogram for the electrolysis of H_2Q on a GaPc-Cl/Ag electrode is shown in Figure 4.3.1.a. The light and dark response is basically the same as that observed for GaPc-Cl/Au electrodes. One significant difference between the two electrodes, however, is the voltammetric behavior of the substrates themselves. At pH 4, the $E^{o'}$ for H_2Q is sufficiently positive that the anodic decomposition potential for the Ag-MPOTE was also reached, so that after one or two cycles the Ag electrode had deteriorated. The surface oxidized Ag was apparently much more able to form water soluble complexes than that on the Au-MPOTE. The current response is then represented in Figure 4.3.1.a as a dotted trace rising off scale with the onset of H_2Q electrolysis. The GaPc-Cl film then could be thought of as a photoconductive corrosion inhibitor, since a GaPc-Cl/Ag electrode under irradiation was able to reversibly oxidize H_2Q at a potential where normally the Ag-MPOTE would have decomposed. The use of an Ag substrate was also a rigorous test of the nonporosity of the GaPc-Cl film, since any water reaching

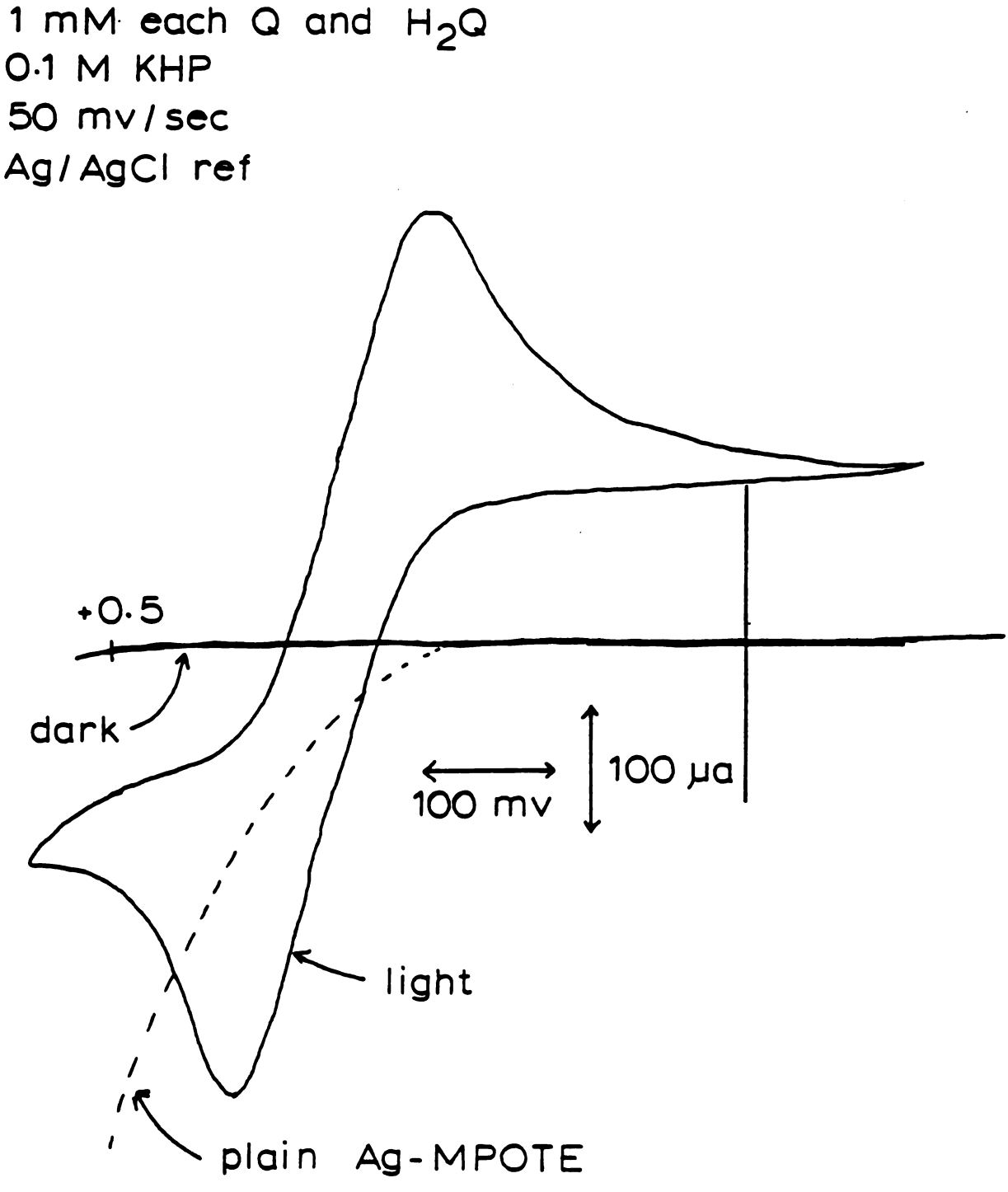

Figure 4.3.1.a: Effect of GaPc-Cl Film Substrate on H_2Q Electrolysis: Ag

the substrate surface under potential scan would have oxidized it.

Continuing with the idea of extending the anodic limit to the substrate material, GaPc-Cl films were deposited on brass. As can be seen in Figure 4.3.1.b, anodic electrochemistry is not possible with a brass electrode versus an Ag/AgCl reference electrode, since the electrode begins to corrode even before the zero of potential. Nevertheless, the diffusion limited oxidation of H_2Q on an irradiated GaPc-Cl/brass electrode was accomplished some 500 mv past the decomposition potential of the substrate. The shape of the voltammogram, however, indicates poor reversibility. Furthermore, the significant dark current suggested a porous film. The GaPc-Cl film apparently mass transport limited the dissolution of brass, but the abnormal current crossover on the return sweep indicated steady erosion of the organic layer. It is not certain whether film porosity on brass compared to Au and Ag was due to unavoidable differences in surface preparation (see Experimental chapter) or to fundamental differences in adsorption and nucleation characteristics during sublimation that cause variability in phthalocyanine film growth. XPS data from this laboratory has indicated a small concentration of organic functionalities on the MPOTE surface which may facilitate good adhesion and crystal growth of the phthalocyanine (149).

Although it was discussed previously in section 4.2.1., the voltammetric response of another GaPc-Cl/SnO_2 electrode

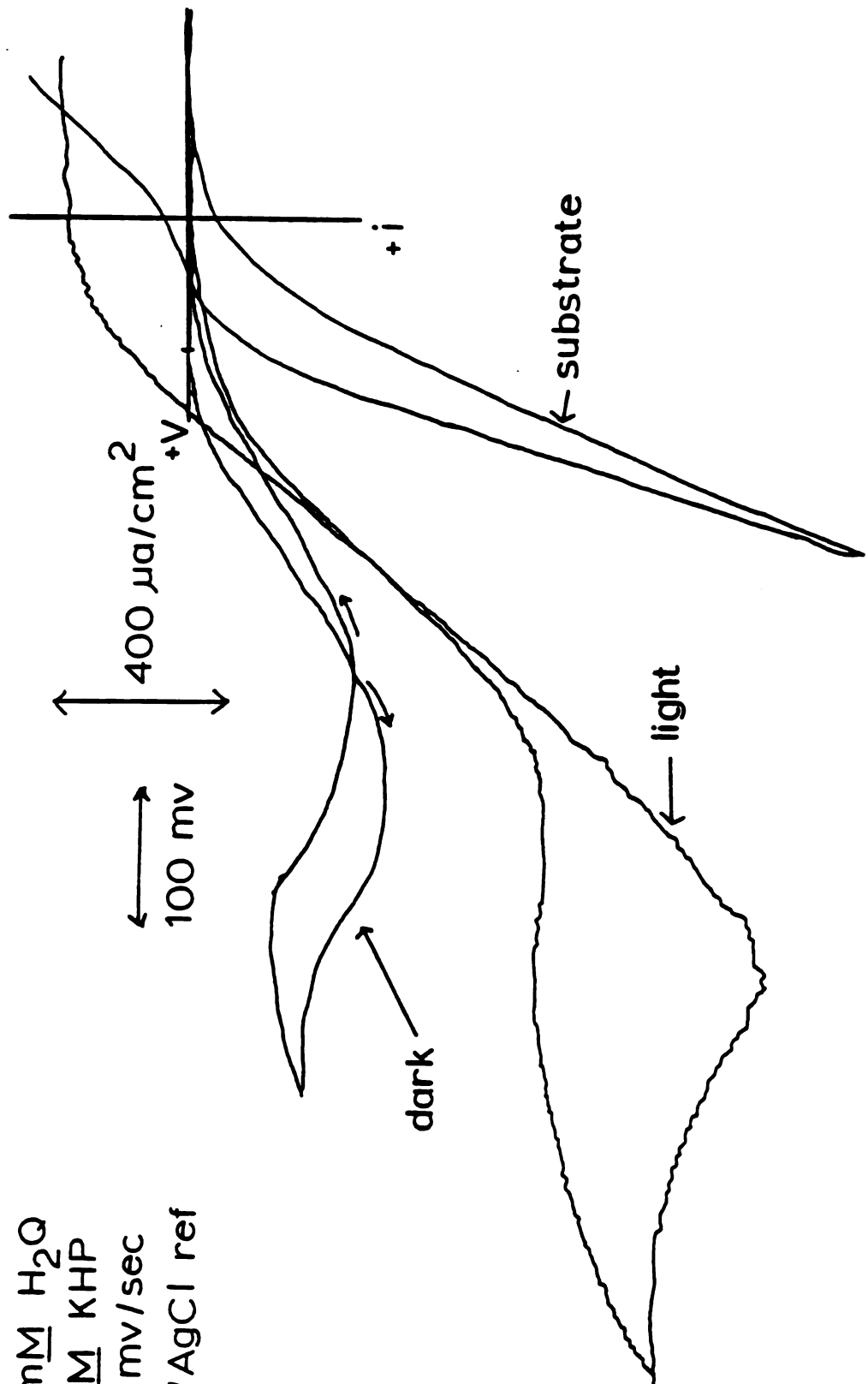

Figure 4.3.1.b: Effect of GaPc-Cl Film Substrate on H_2Q Electrolysis: Brass

is presented here which yields additional information. The bare SnO_2 substrate response is also shown here for the sake of comparison. The main difference between the response shown here in Figure 4.3.1.c and Figure 4.2.1. is the presence of a large cathodic photocurrent. The reason lies in the scan rate used to record the voltammograms: the trace in Figure 4.2.1. was scanned at 10mv/sec while the one in Figure 4.3.1.c was scanned at 50 mv/sec. The increased scan rate also served to eliminate any semblance of a plateau current. While the GaPc-Cl/SnO_2 voltammetric response was not as active as was seen for GaPc-Cl films on Ag and Au, the degree of catalysis is actually much greater, since the electrolysis of H_2Q and SnO_2 is so irreversible to begin with. The dark current was negligible as usual, although some faradaic activity began at +0.6 v. The return sweep gave a larger current just after reversal than on the anodic sweep. This was interpreted as the onset of oxidative desorption of the film, which then exposed the SnO_2 underlayer which was able to react with the H_2Q redox species.

4.3.2. Effect of Various Quinones

It was of interest to determine whether there was any specific chemical interaction between the GaPc molecule and H_2Q or Q. Possibilities included adsorption, charge transfer complex formation, or axial coordination before or during

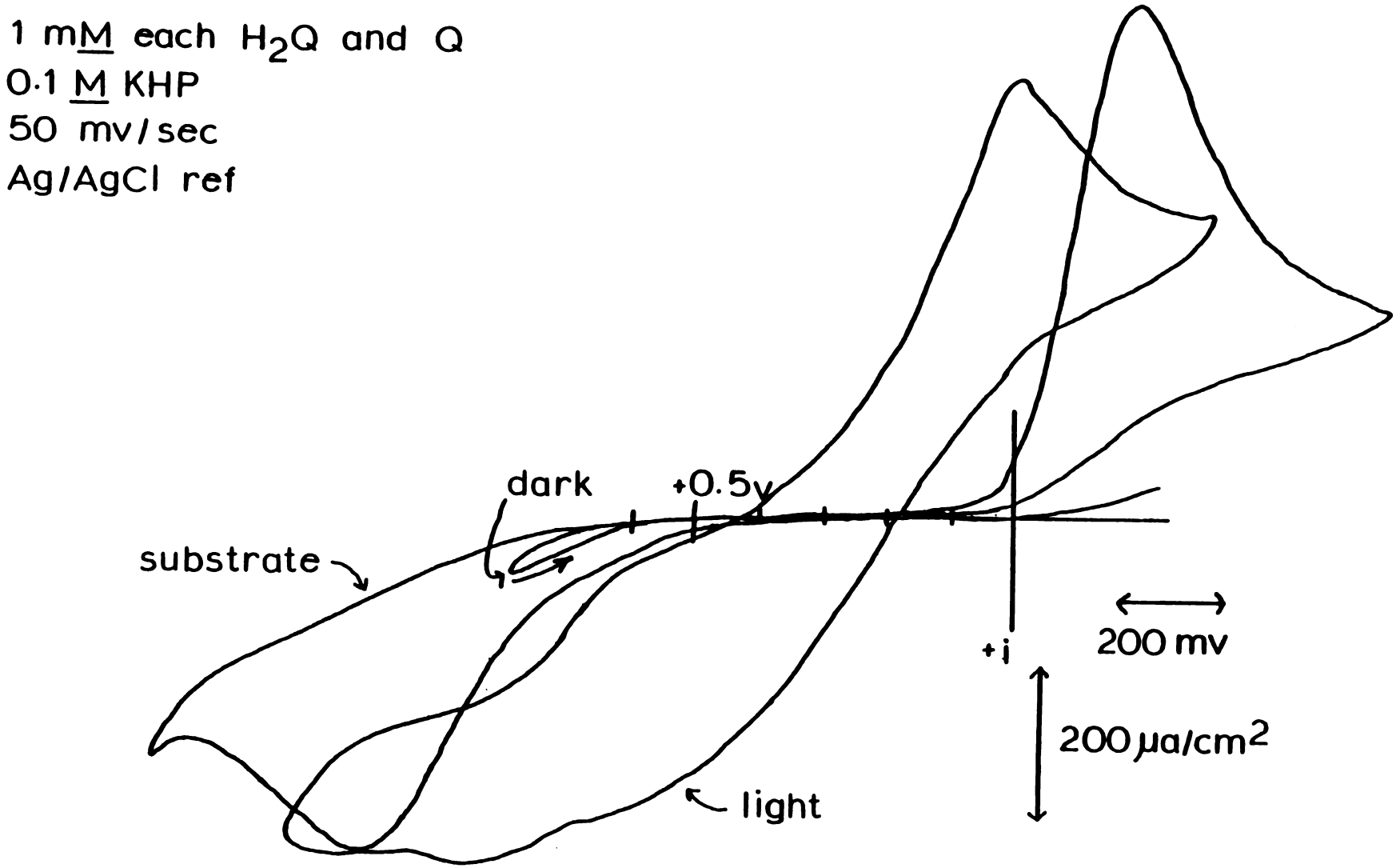

Figure 4.3.1.c: Effect of GaPc-Cl Film Substrate on H_2Q Electrolysis: SnO_2

charge transfer. One method of testing for specific interaction was to examine other quinones which would be expected to have similar kinetics in the absence of steric interference.

The voltammograms for the electrolysis of catechol, 1,4-napthoquinone-2-sulfonate, and 9,10-anthraquinone-2-sulfonate on GaPc-Cl/Au are shown in Figure 4.3.2.a-c, respectively. All three redox species gave a nearly reversible response in the light, and a negligible response in the dark. Thus, adding side substituents to the quinone plane did not reduce the ability of GaPc-Cl to electrolyze it.

Another aspect of these voltammograms was the possible existence of photopotentials. When a reversible trace in the light is shifted away from a reversible trace for the same redox couple in the dark, a photopotential must be present. For catechol (Figure 4.3.2.a), a quasi-reversible trace on Au straddles the more reversible response on GaPc-Cl/Au, and so little, if any, photopotential would be expected from it. For the napthoquinone, nearly identical cathodic waves are observed on Au and GaPc-Cl/Au, but their peak potentials are separated by 300 mv, strongly suggesting a positive photopotential. For the anthraquinone, the trace on GaPc-Cl/Au in the light was shifted well positive with respect to that on Au in the dark. Since the E° for a redox couple must lie somewhere between its peak potentials regardless of reversibility, and since the V_p for reduction on GaPc-Cl/Au in the light was positive for the V_p for

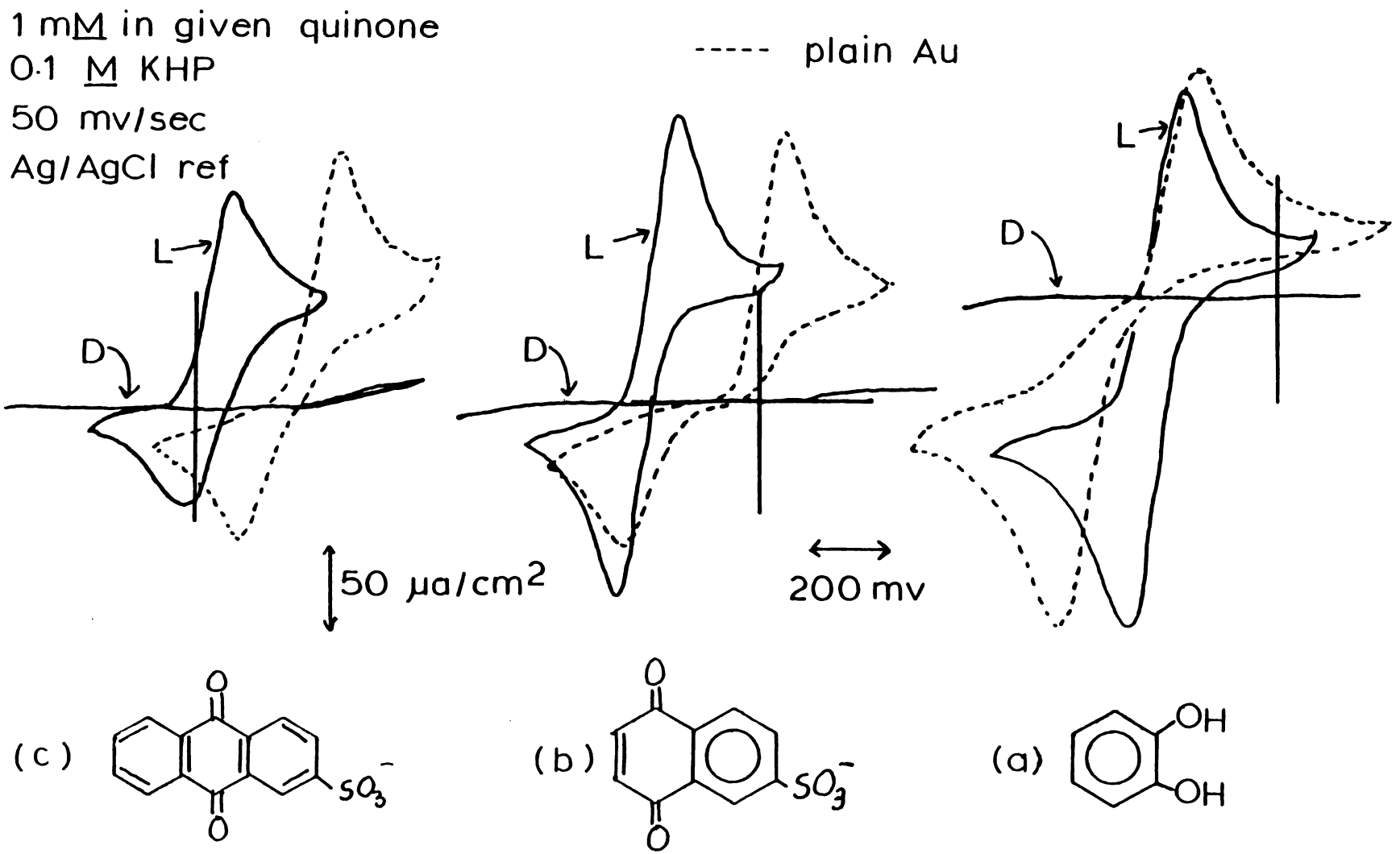

Figure 4.3.2: Electrolysis of Different Quinones on GaPc-Cl/Au Electrodes: (a) catechol; (b) 1,4-napthoquinone-2-sulfonate; and (c) 9,10-anthraquinone-2-sulfonate

oxidation in the dark, a ΔE° between the two cycles must exist. While from the voltammogram a positive photopotential of over 200 mv would be predicted, actual measurement of the open-circuit potential only gave a value of 50 mv. This may be due to the fact that different quantities are being measured. The voltmeter only measures the electric field, whereas the voltammogram is sensitive to the overall thermodynamic change due to illumination.

4.3.3. Effect of Other Redox Species

The original intent in using potassium ferrocyanide, $K_4Fe(CN)_6$, on GaPc-Cl electrodes was to test their porosity, since $Fe(CN)_6^{4-}$ was found to be reversible on all the substrates employed. In order to interpret any results, however, the behavior of $Fe(CN)_6^{4-}$ on a nonporous GaPc-Cl film electrode must first be known. The results are shown for a GaPc-Cl/Au electrode in Figure 4.3.3.a. The behavior was essentially the same as was seen for all the quinones: negligible current in the dark, but a nearly reversible response in the light. A peak-to-peak separation of 145 mv was observed in the light, which may be compared to 80 mv obtained on activated Au under the same conditions.

In Figure 4.3.3.b, the voltammograms for the light and dark reduction of O_2 on a GaPc-Cl/pyrolitic graphite (PG) electrode are shown. The dark current was quite small, scarcely better than what would be obtained on bare PG.

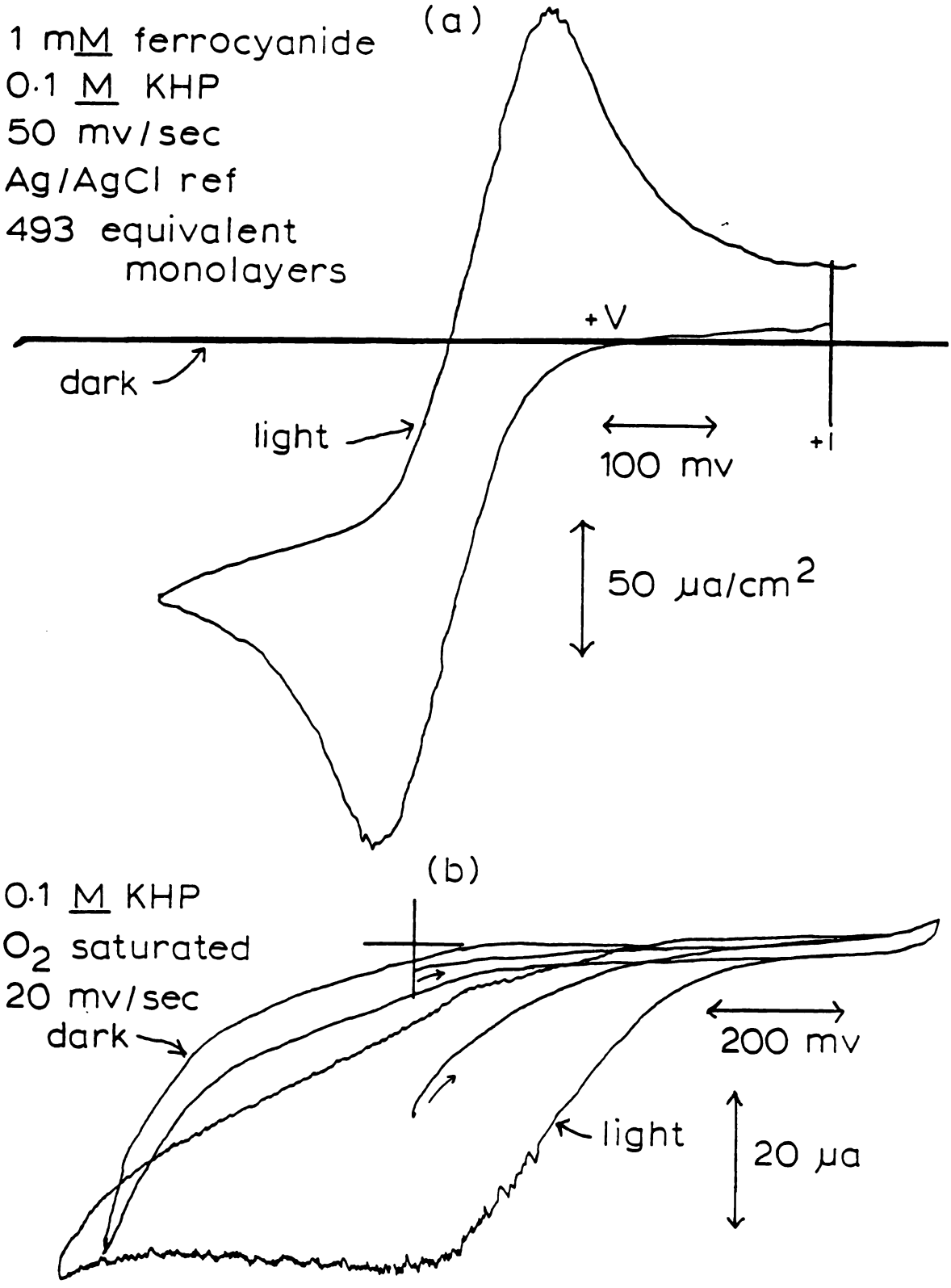

Figure 4.3.3: Electrolysis of Other Redox Species on GaPc-Cl Electrodes:

(a) $Fe(CN)_6^{4-}$; and (b) O_2

Under irradiation, however, a large light intensity-limited wave with an $E_{1/2}$ of +0.25 v was obtained, a considerable reduction in overporential. This behavior was in contrast to that of FePc/PG electrodes, which gave a 500 mv reduction in overpotential over PG in the dark, but showed no further improvement in the light (176). O_2 reduction was also observed for GaPc-Cl films on SnO_2 and Au, and so it would sometimes be an interference if the electrolyte were not thoroughly degassed. One problem that FePc and GaPc-Cl shared on PG was that their activity toward O_2 was short-lived. The initial cathodic sweep would give a fairly well shaped curve, comparable to a noble metal electrode. The second sweep would show the wave reduced by half. Continued cathodic scans would eventually reduce the catalytic activity to a negligible level. Inspection of the electrode after thorough use showed that the film had been decimated. Apparently, a peroxo- or other intermediate in the O_2 reduction process was able to attack and break down the phthalocyanine ring.

4.4. Variability of Film Characteristics

4.4.1. Solid Film Absorbance Maximum

In Figure 4.2.2.a, the λ max for a solid film of GaPc-Cl was given as 795 nm. But actually, the λ max tended to vary from one sublimation trial to the next, so that it has been found as low as 760 nm, or as high as 810 nm. In Figure 4.4.1.,

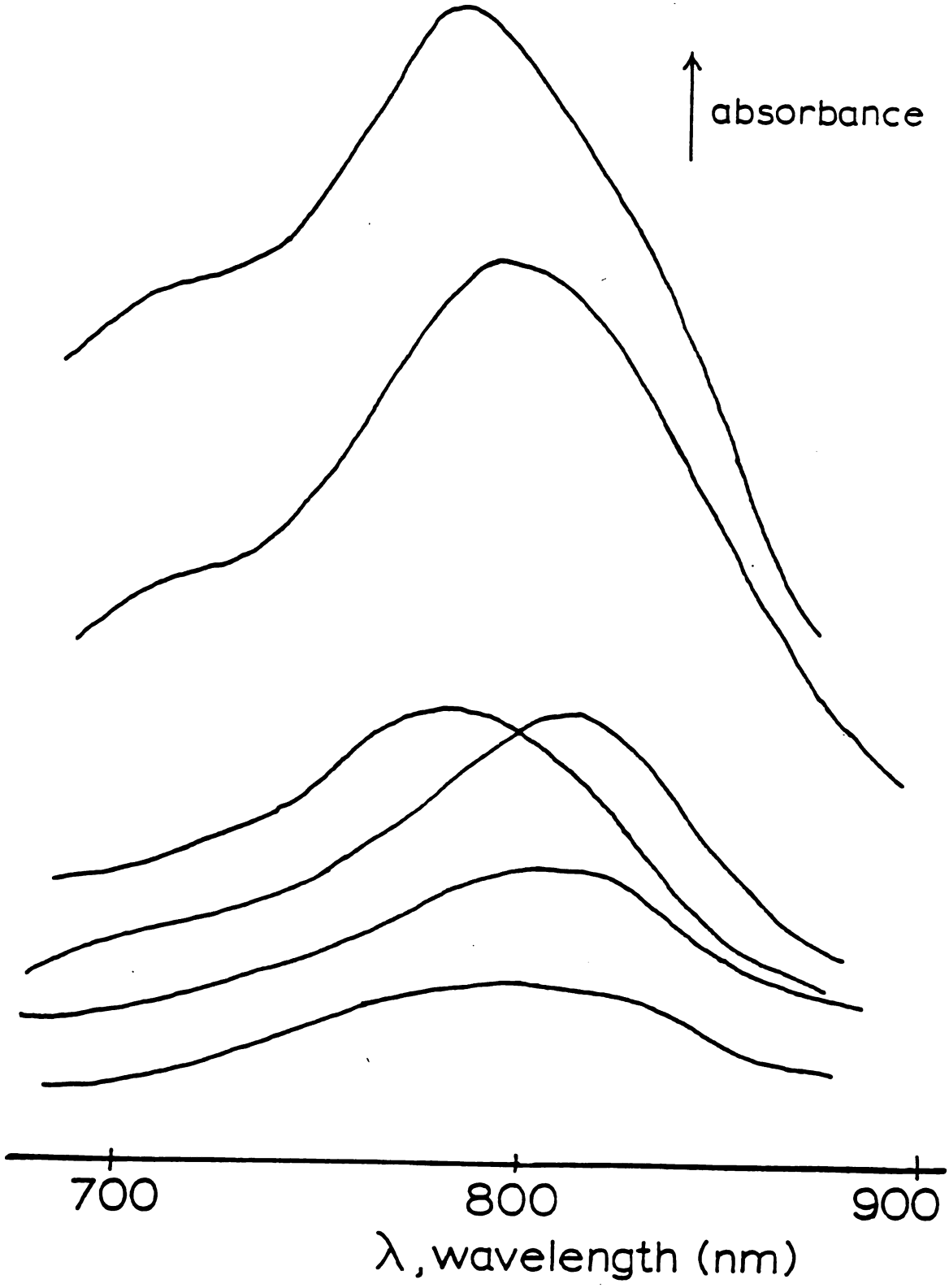

Figure 4.4.1: Variability of GaPc-Cl Film Absorbance Maxima

a set of solid GaPc-Cl absorption spectra are shown in the spectral range from 700 to 900 nm. No trend in λ max as a function of film thickness was observed; likewise, no trend was recognized with respect to substrate temperature, since the thicker films underwent longer sublimation times, and so eventually reached higher temperatures.

The electron micrograph of a GaPc-Cl film on Au in Figure 4.2.4.a showed two distinct crystalline structures. It is possible that these structures represent different phases, whose absorption spectra are slightly different so that a varying proportion of the two phases will cause λ max to shift. Another possible combination would be the absorbance of an amorphous or monomer phase, plus that of an aggregate phase. A number of dyestuffs, such as the simpler cyanine dyes, can form what is called a "J-aggregate", which causes an abrupt red shift in λ max (177-179). A comparison of J-aggregate spectral characteristics to those of the phthalocyanines can be found in the Discussion chapter.

4.4.2. Film Thickness and Porosity

With the film deposition procedure and apparatus employed, it was impossible to maintain strict control over the deposition conditions (background pressure, sublimation temperature, and substrate temperature). As a result, it was very difficult to prepare a film of predetermined thickness in a single trial. Instead, a hit-or-miss approach had to be

adopted, where several sets of films were deposited, the best set used in the experiment, and the rest set aside for use at a later time. While there was, of course, a direct dependence of film thickness on time of sublimation, the variation was so great that the only way to grow a film of a desired thickness was for the operator to directly monitor the growth of the film through the glass walls of the sublimation apparatus. With practice, acceptable GaPc-Cl/ substrate electrodes could be made 80% of the time.

Film thickness was an important parameter in the voltammetric performance of GaPc-Cl electrodes. The light and dark voltammetry of $Fe(CN)_6^{4-}$ on GaPc-Cl of various thicknesses on SnO_2 is shown in Figure 4.4.2. The thinnest film tested was 23 equivalent monolayers. As shown in Figure 4.2.2.a, the light and dark curves for the thin film were nearly the same.

In this situation, there is some question as to whether the dark current is due to pores in the inactive GaPc-Cl film which allow electroactive species to reach the SnO_2 substrate and react, or is due to a dark reaction on the GaPc-Cl/ electrolyte interface. The dotted trace, which represents the voltammogram for $Fe(CN)_6^{4-}$ electrolysis on plain SnO_2, has been placed in the figure for comparison. The electrolysis appeared more reversible than on the GaPc-Cl modified electrode. An electrode that consists of an inert material with a sparse density of pinholes over an active substrate will have a different voltammetric response in

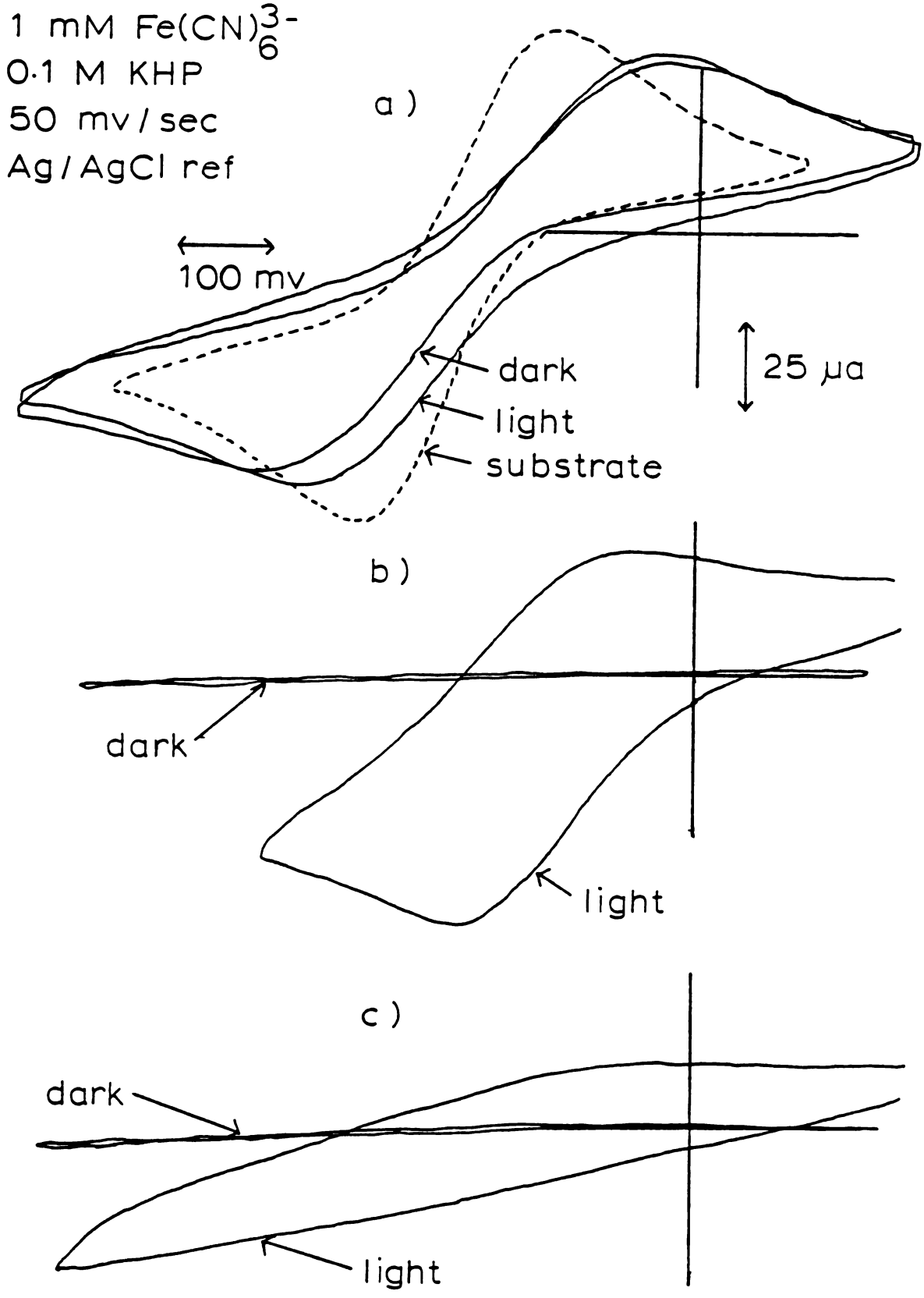

Figure 4.4.2: Effect of Film Thickness on Voltammetric Response of GaPc-Cl/SnO_2 Electrodes: (a) 23; (b) 82; and (c) 400 monolayers

comparison to the bare substrate because of altered mass transport kinetics (180-181).

If one were to plot the photocurrent (light current minus dark current) from the data in Figure 4.4.2.a, a small drawn-out curve of only a few μA would be obtained. This electrode then gave a poorer light response than the thicker film electrodes discussed previously.

When the GaPc-Cl film thickness was increased to 82 equivalent monolayers, a dramatic difference between light and dark behavior arose. As shown in Figure 4.4.2.b, the dark current was completely suppressed, just as in the voltammograms shown previously for GaPc-Cl films on Au and Ag, as well as SnO_2 (Figures 4.2.3.a, 4.3.1.a, and 4.2.1., respectively). Irradiation produced a curve that was quite broad, yet rather reversible, with a peak to peak separation of 140 mv. A plot of the photocurrent in this case would yield a trace identical to the observed light current, since the dark current was effectively zero throughout.

The suppression of the dark current with the concomitant rise of the photocurrent can be interpreted as a transition in film character from a state where the dye film is actually an array of islands or separated grains, each growing from their own nucleation site, to a state where the grains have grown together to form a continuous film. Thus the idea of film porosity should be reintroduced here, since, as will be shown later in more detail, the four-fold increase in film resistance in going from a 23 to an 82 monolayer film is

insufficient to effect such a large difference in dark current response. There is a possibility, however, that crystalline order in the film is much greater near the substrate surface where the first few layers are deposited, thus lowering its electrical resistance, so that the actual resistance increase from one film to the other may be much greater than four-fold. The increase in photoresponse can be explained as an increase in conductivity due to enlarged grain size or, with the islands growing together, the possibility of carrier migration between grains.

As the film thickness is further increased to 400 monolayers, the light response is hindered as well as the dark. The dark current is negligible as before, but even the voltammogram in the light is seriously distorted. This result may be interpreted as a pure resistance effect if the film is nonporous, or as a light attenuation and redox species depletion problem in a porous film.

Further support for the existence of porosity on thin films was obtained by electron microscopy. An ultrathin, GaPc-Cl/Au electrode, and an exceptionally thick GaPc-Cl/Au electrode were studied under approximately equal magnification. In light of the previous film thickness work, SnO_2 was the preferred substrate to perform this study on, but Au was the only substrate examined for which detail on the thinnest films could be resolved. The micrographs, shown in Figure 4.4.3., revealed tiny 0.1 μ sized grains that had not yet grown together. Also, the presence of both needle and

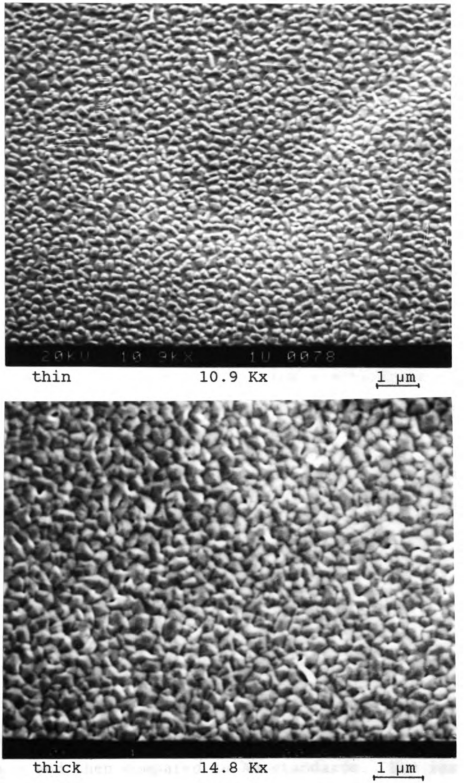

Figure 4.4.3: Electron Micrographs of Thin and Thick GaPc-Cl Films on Au

granule structures was noted. Thus, if the two crystalline structures represent different phases, there exists a well-mixed equilibrium between the two, such that it would be nearly impossible to separate them by sublimation techniques. The thick film showed the solid granular structure observed previously on thinner films (Figure 4.2.4,a), with perhaps a lower proportion of the needle-like structure. Thus it may be inferred a GaPc-Cl film which nucleates and grows initially in a highly ordered manner will maintain that degree of order, at least within the rates of sublimation used in these experiments (10's of Å/min).

Porosity of GaPc-Cl/Au electrodes was observed in thick films as well. In Figure 4.4.4., the electrolysis of $Fe(CN)_6^{4-}$ on two thick GaPc-Cl/Au electrodes in the dark gave quite different results. A 493 monolayer electrode, prepared and tested by the author, gave a baseline current trace indicating a nonporous electrode, while a 503 monolayer electrode, prepared and tested by T. Klofta of this laboratory (182), gave a reversible, although somewhat attenuated, current response consistent with the theory of partially covered electrodes (180, 181).

Identical samples or the electrodes themselves were then examined by X-ray photoelectron spectroscopy. High resolution scans of the Au-4f transition were made on the GaPc-Cl/Au electrode and then compared to Au standards. The results, shown in Figure 4.4.5., corroborated the results of the voltammetric experiment. The voltammetrically porous

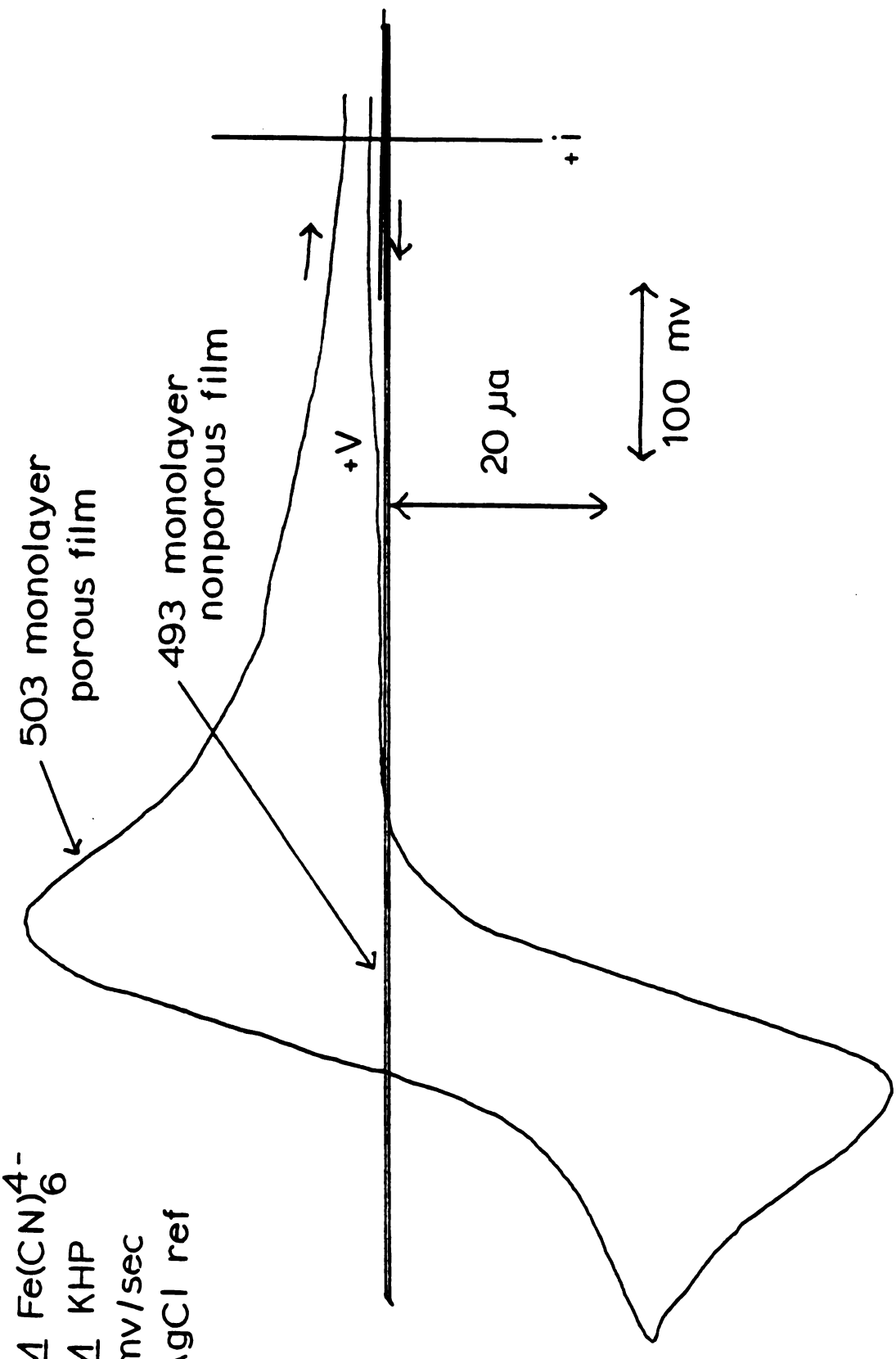

Figure 4.4.4: Variability in Porosity of GaPc-Cl/Au Electrodes: Voltammetric Observation

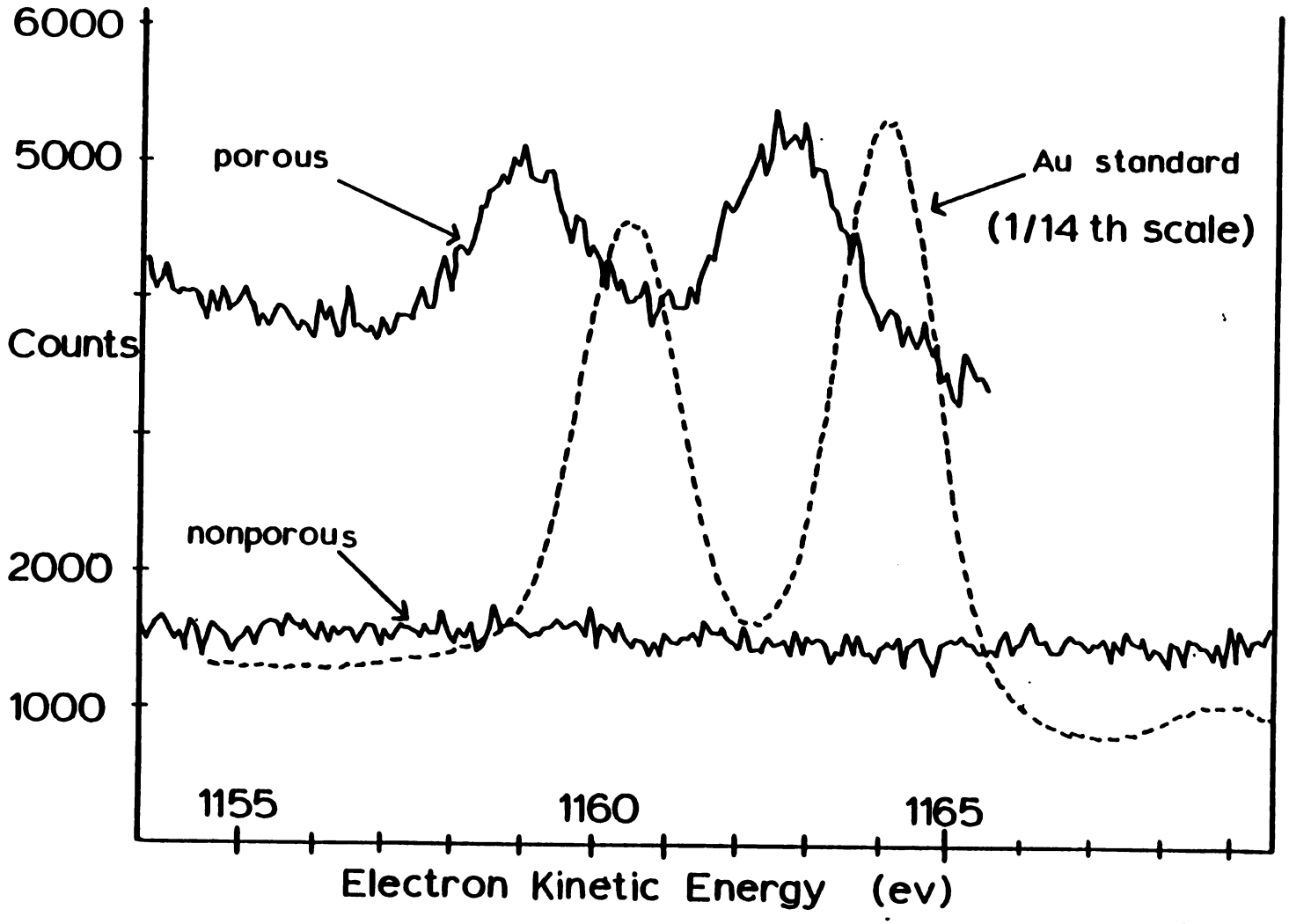

Figure 4.4.5: Variability in Porosity of GaPc-Cl/Au Electrodes: X-Ray Photoelectron Observation

electrode showed two peaks corresponding to the Au($4f_{5/2,7/2}$) transitions, while the voltammetrically nonporous electrode showed no signal above background throughout the Au(4f) region. The Au signal from the porous electrode was shifted +2 eV from the Au standard. A likely explanation is that secondary electron emission from the Au substrate and the dye film caused a slight charge distribution within the organic film, which then acted as a retarding potential for emitted electrons, giving them a lower kinetic energy.

The explanation of how thick GaPc-Cl/Au electrodes could possess extremes of porosity and nonporosity lay in the deposition procedure. A technique developed by P. Rieke (183) in this laboratory involved brief O_2-plasma cleaning of the Au substrate, and then very slow (< 1 Å/min) film sublimation at reduced temperature (about 200°C) in a greaseless vessel. The intent of the plasma cleaning step was to remove adventitious organic species, but also acted to create metastable surface oxides and may have O-functionalized some of the more strongly bound species, such as those that belonged to the polymer backing (169). The use of a Teflon valve and a Viton O-ring seal on the sublimation vessel cost an order of magnitude in attainable pressure, so that the operating vacuum was no higher than 5×10^{-5} Torr. This procedure resulted in a film which consisted of a low density of large, 0.5 micron sized grains, so that many equivalent monolayers of dye could be deposited and still leave gaps between adjacent grains, where the Au

substrate would then be exposed. A GaPc-Cl/Au electrode prepared by P. Rieke over a 24-hour period is shown in Figure 4.4.6., along with a typical nonporous GaPc-Cl/Au electrode prepared as described in the Experimental chapter.

4.4.3. Film Thickness and Impedance

Mainly due to the results of the film thickness experiments in the previous section, it was of interest to know the effect of a series electrical resistance on the kinetics of a reaction at the electrified interface. The more specific case concerning the effect of uncompensated solution resistance on a voltammetric curve had been previously worked out by Nicholson (156). It was noted that in terms of circuit equivalents, a resistive electode and a resistive solution would have the same effect on the current drawn through the system. This is shown in Figure 4.4.7. In other words, uncompensated iR drop or electrode resistance, as in an organic film, could be modelled as a resistor in series with the double layer, and so an external resistor could be inserted into the working electrode connections to simulate their effect.

Using potassium ferricyanide on Au in a pH 4 KHP electrolyte, the effect of a resistance in series between potentiostat and working electrode was studied by cyclic voltammetry. A family of such curves is shown in Figure 4.4.8. The voltammogram for the usual cell with no

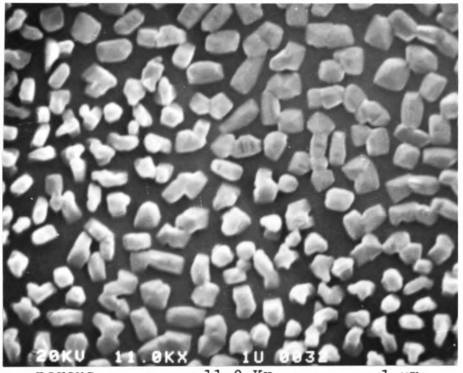

Figure 4.4.6: Variability in Porosity of GaPc-Cl/Au Electrodes: Electron Microscopic Observation

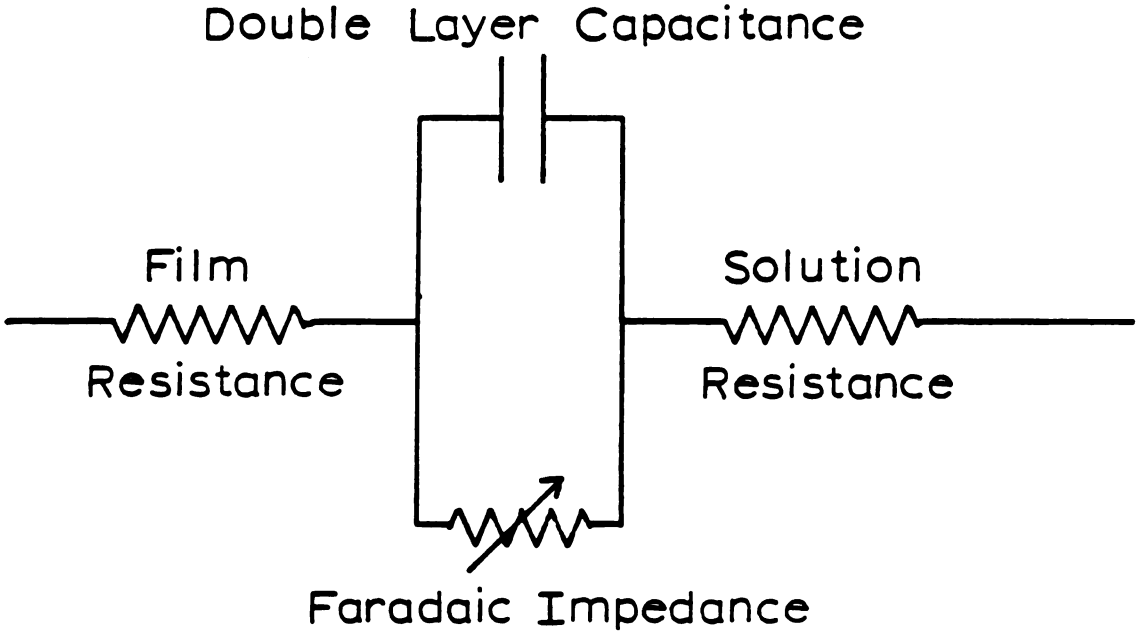

Figure 4.4.7: Electrical Circuit Equivalent of an Electrode System

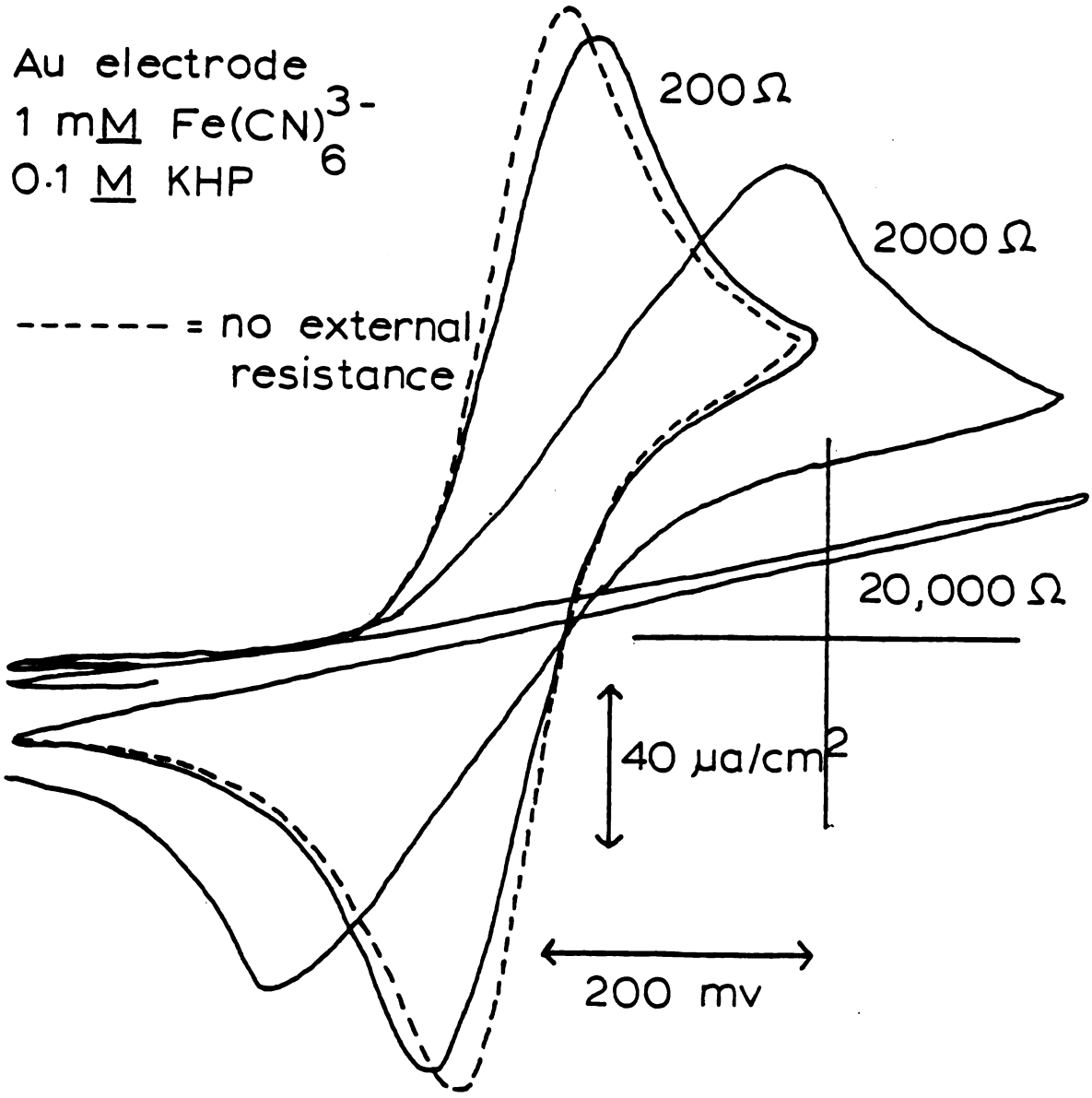

Figure 4.4.8: Effect of Series Resistance on Cyclic Voltammogram

intentionally introduced external resistance is given by the dotted trace. Even a 200 Ω resistor had an observable effect, decreasing i_p and shifting V_p. Increasing the external resistance to 2000 Ω, the voltammogram became quite distorted, with the peak to peak separation increasing to 382 mv. After increasing the external resistance to 20,000 Ω, any semblance of a faradaic process had disappeared; instead, a straight line corresponding to the current/voltage plot for a linear resistor was obtained. By measuring the slope of the return sweep, the resistance (dv/di) was calculated to be 2.1 x 10^4 Ω, in close agreement with the value of the external resistor.

The effect of a series capacitance on electrode kinetics was also of interest. One way of modelling the thick dye film electrode was as two capacitors in series, one corresponding to the substrate/dye interface, the other to the dye/electrolyte interface. For a nonporous electrode, the faradaic process would be occurring only at the dye/ electrolyte inerface, but the kinetics of reaction could be affected by the capacitance associated with the other interface. For resistors in series, the total resistance is the sum of each of the individual resistors:

$$R = \sum_{i=1}^{n} r_i$$

For capacitors, the total capacitance for a number connected in series is calculated by adding the reciprocals of each of the individual capacitors, which is then equal to the reciprocal of the total capacitance:

$$\frac{1}{C} = \sum_{i=1}^{n} \frac{1}{C_i}$$

For a two capacitor system such as the one described above,

$$\frac{1}{C_T} = \frac{1}{C_1} + \frac{1}{C_2}$$

$$C_T = \frac{C_1 C_2}{C_1 + C_2}$$

If, however, one capacitor is much larger than the other, for example $C_1 \gg C_2$,

$$C_T = \frac{C_1 C_2}{C_1 + C_2} = \frac{C_1 C_2}{C_1} = C_2$$

Thus for a set of capacitors in series, the smallest capacitance will tend to dictate the behavior of the circuit.

This effect was observed as shown in Figure 4.4.9., where a two capacitor circuit had been set up by putting various capacitors in series with an Au metal electrode. The trace for a normal wave with no external capacitance is present for comparison. It could be thought of as a two capacitor system where capacitance of a copper wire is

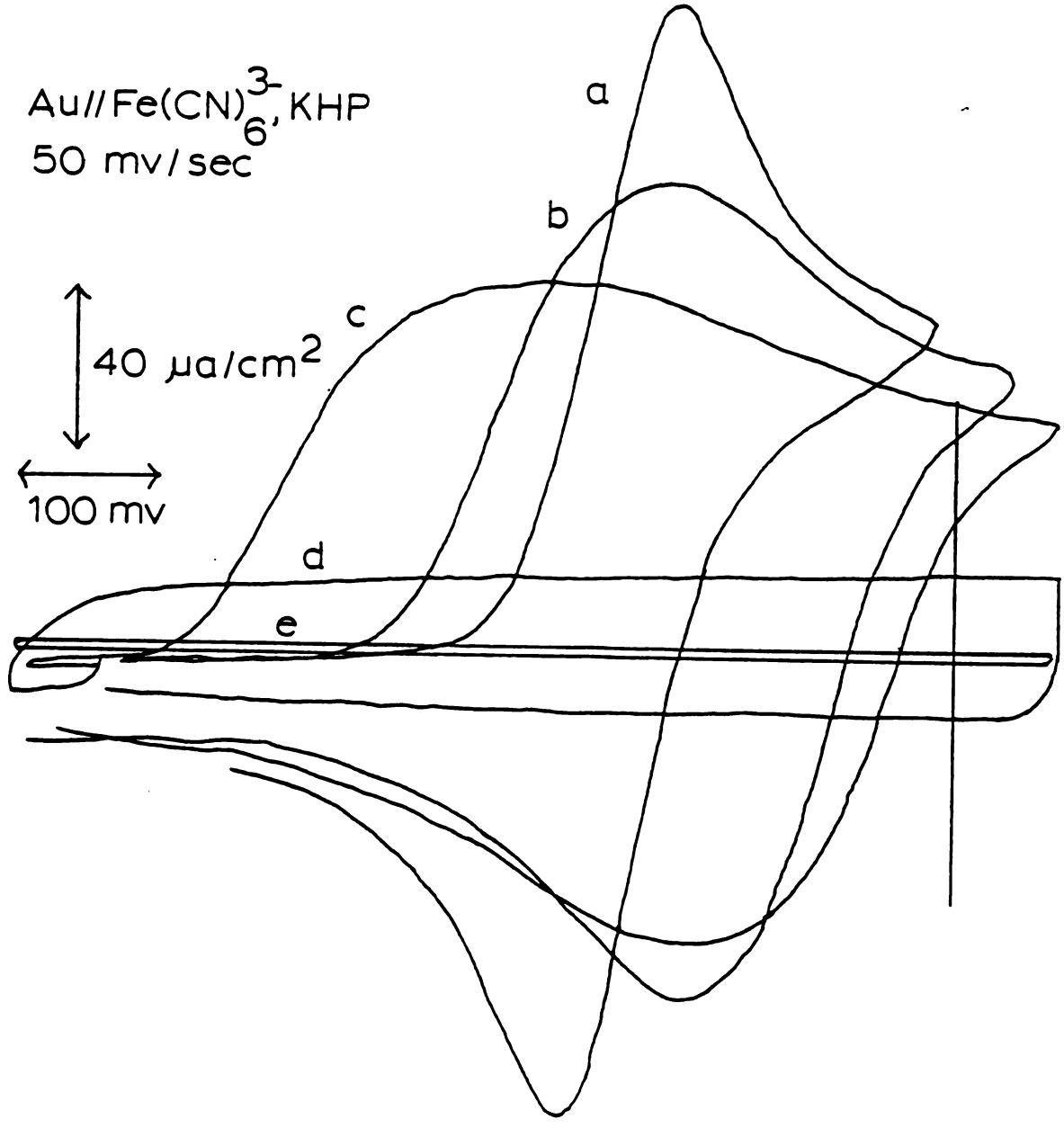

Figure 4.4.9: Effect of Series Capacitance on Cyclic Voltammogram: (a) normal wave; (b) 2000 μf; (c) 1000 μf; (d) 150 μf; (e) 1 μf

essentially infinite; the double layer capacitance being much less, controlled the circuit so that the voltammogram appeared unaltered. When the series capacitance was lowered to 2000 μf, the two capacitance elements were then of comparable value, and the voltammetric response was affected. A large drop in V_p with general broadening of the curve occurred. Lowering the external capacitance to 100 μf, peak suppression and broadening worsened. When the external capacitance had dropped as low at 150 μf, a flat curve given by $C \frac{dv}{dt}$ was obtained. To check this result, the theoretical value may be calculated:

$$i = C \frac{dv}{dt} = (150\ \mu f)(50\ mv/sec)(10^{-6} f/\mu f)(10^{-3}\ v/mv)$$
$$(10^{6}\ \mu A/A) = 7.5\ \mu A,$$

which is close to the 10 μA value measured off the voltammetric curve. A slight faradaic current should still be expected, however, which could easily account for the difference. Finally, the 1 μf capacitor in series reduced the previous current plateau by a factor of 150, and so on the same current scale its curve simply ran along the baseline.

It should not be concluded that the flat curve for the 150 μf capacitor implies a double layer capacitance greater than that value. As the value of the external capacitor decreased, it also began assuming a larger share of the working electrode potential drop, which has the effect of

reducing the field strength across the double layer, thus affecting the electrode kinetics. Impedance measurements on the Au-Intrex gave a double layer capacitance of 10 $\mu f/cm^2$, in agreement with literature values (184).

4.4.4. Crystalline Order vs. Substrate

After testing numerous samples it became clear that GaPc-Cl/Au electrodes performed fundamentally better than GaPc-Cl/SnO_2 electrodes in terms of rate of photoelectrolysis of H_2Q (Figure 4.2.3.a vs. 4.2.1. and 4.3.1.c). One of many possible explanations is that GaPc-Cl films grown on Au substrates tend to possess a higher degree of crystalline order than on other substrates. Electron microscopy was used to examine films grown on several substrates, in order to compare degree of crystallinity as a function of substrate.

Electron micrographs of substrates and GaPc-Cl films grown on them are shown in Figure 4.4.10.a-f. In Figure 4.4.10.a and b, respectively, are micrographs of an Au-MPOTE and GaPc-Cl/Au. The GaPc-Cl micrograph has been shown before in Figure 4.4.6.b, but is inclued here again for the sake of comparison. The bare Au-MPOTE showed some very small features, round bumps or nodules less than 0.1 μ across. Attempts to view them at a higher magnification than 11.1 Kx were futile, since the loss in resolution at higher magnification and higher electrom beam current densities blurred them out, but at any rate the surface features viewed

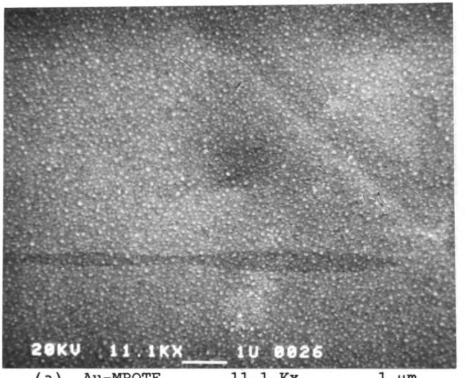

(a) Au-MPOTE 11.1 Kx 1 μm

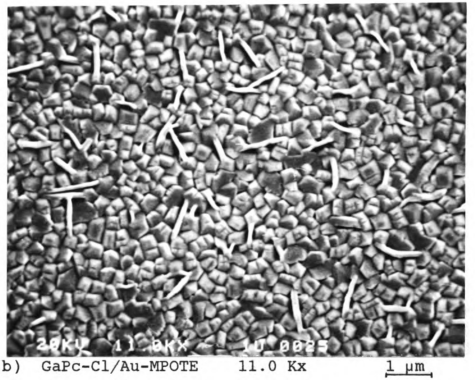

(b) GaPc-Cl/Au-MPOTE 11.0 Kx 1 μm

Figure 4.4.10: Electron Micrographic Comparison of GaPc-Cl Films and Their Substrates: (a) Au-MPOTE and (b) GaPc-Cl/Au-MPOTE

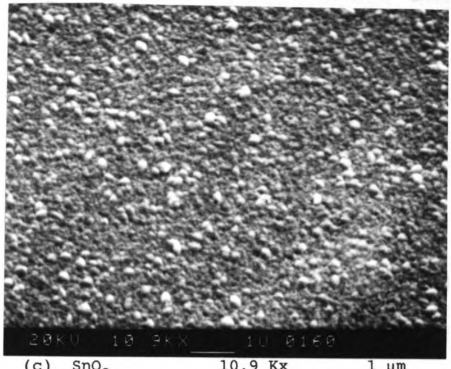

(c) SnO_2 10.9 Kx 1 μm

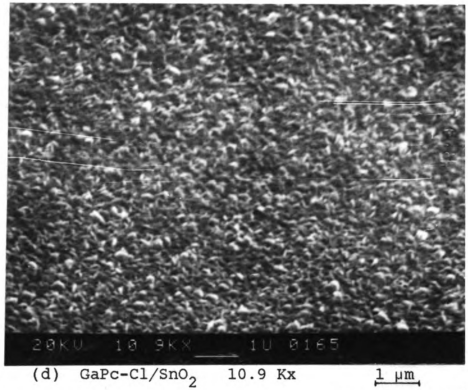

(d) GaPc-Cl/SnO_2 10.9 Kx 1 μm

Figure 4.4.10 continued: Electron Micrographic Comparison of GaPc-Cl Films and Their Substrates: (c) SnO_2 and (d) GaPc-Cl/SnO_2

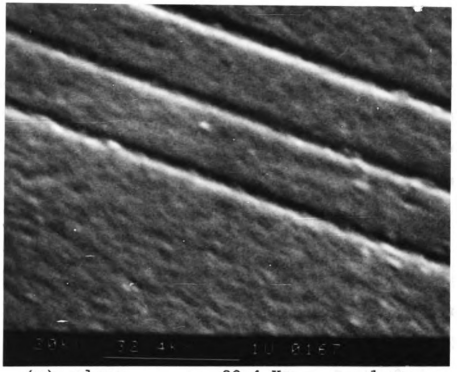

(e) glass 32.4 Kx 1 μm

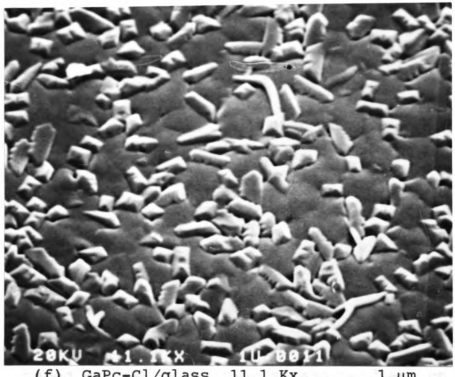

(f) GaPc-Cl/glass 11.1 Kx 1 μm

Figure 4.4.10 continued: Electron Micrographic Comparison of GaPc-Cl Films and Their Substrates: (d) glass and (e) GaPc-Cl/glass

in Figure 4.4.10.b are verified as being GaPc-Cl. Figure 4.4.10.c and d, respectively, show the micrographs for a plain SnO_2-OTE and GaPc-Cl/SnO_2-OTE. The SnO_2 electrode features nodular growth with some of the larger ones several tenths of microns across. A GaPc-Cl film on SnO_2 showed much smaller structures than on Au and showed what appeared to be small, flake-like structures no more than a few tenths of microns in length. Some of the SnO_2 nodules appear to be projecting through the film. It may be that the SnO_2 surface is slightly undulating, so that the dye molecules tend to collect in the concave portions of the surface, leaving the high spots exposed. Comparing higher magnification (31,000X) micrographs of the two surfaces, a great deal of the phthalocyanine was seen deposited as a smooth covering over the SnO_2 surface.

In Figure 4.4.10. e and f, respectively, are electron micrographs of a plain glass flat substrate and a GaPc-Cl film on glass. While certainly an improbably conductive substrate for thin film electrodes, the importance of substrate surface in the ordering of GaPc-Cl films deposited on them is emphasized. The glass flat was essentially featureless, save for the microscopic scratches included as an aid in focusing and to prove that the picture was indeed focussed. The GaPc-Cl film consisted of a sparse population of well shaped grains, both granules and needles, on a smooth background. Apparently there were a few nucleation sites on the glass surface which promoted highly ordered features,

while most of the film deposited as an amorphous coating. The type of glass was important; GaPc-Cl films grown on microscopic slide glass were grown in this laboratory which were just as ordered as those on Au (185). Thus, the choice of substrate and its preparation have a great influence on the degree of crystalline order of GaPc-Cl film deposited on it.

4.5. Effects of Light on Voltammetric Response

4.5.1. Effect of Intensity

In Figure 4.5.1.a, a plot of steady state photocurrent versus the incident intensity of a He-Ne laser for the electrolysis of a 50 mM H_2Q solution on a GaPc-Cl/SnO_2 electrode is shown. Since two orders of magnitude in intensity were covered, the data were split into two sets and used in low intensity and high intensity plots. The vertical and horizontal scales in the high intensity plot were expanded in the same proportion from the low intensity plot, so that if a direct proportionality between photocurrent and intensity existed, the two graphs would not only be linear but also have the same slope. Clearly this was not the case; at lower intensities a linear plot was obtained, while at higher intensities the photocurrent began to level off, or saturate.

The deviation from linearity at high intensity may be due to a change in the rate determining step for current flow.

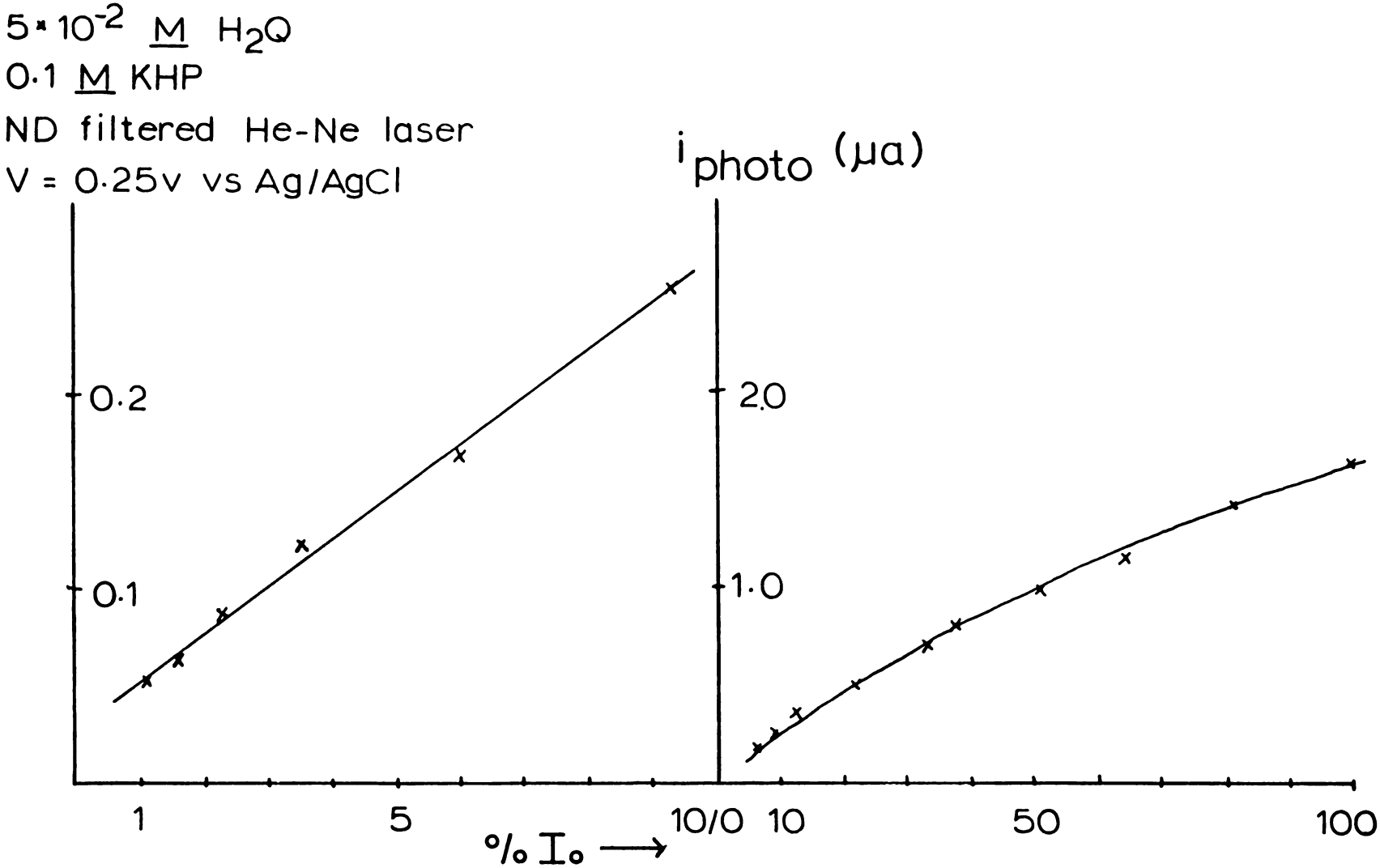

Figure 4.5.1.a: Photocurrent vs. Intensity for H_2Q Electrolysis on a GaPc-$ClSnO_2$ Electrode

same data as in Figure 4.5.1.a

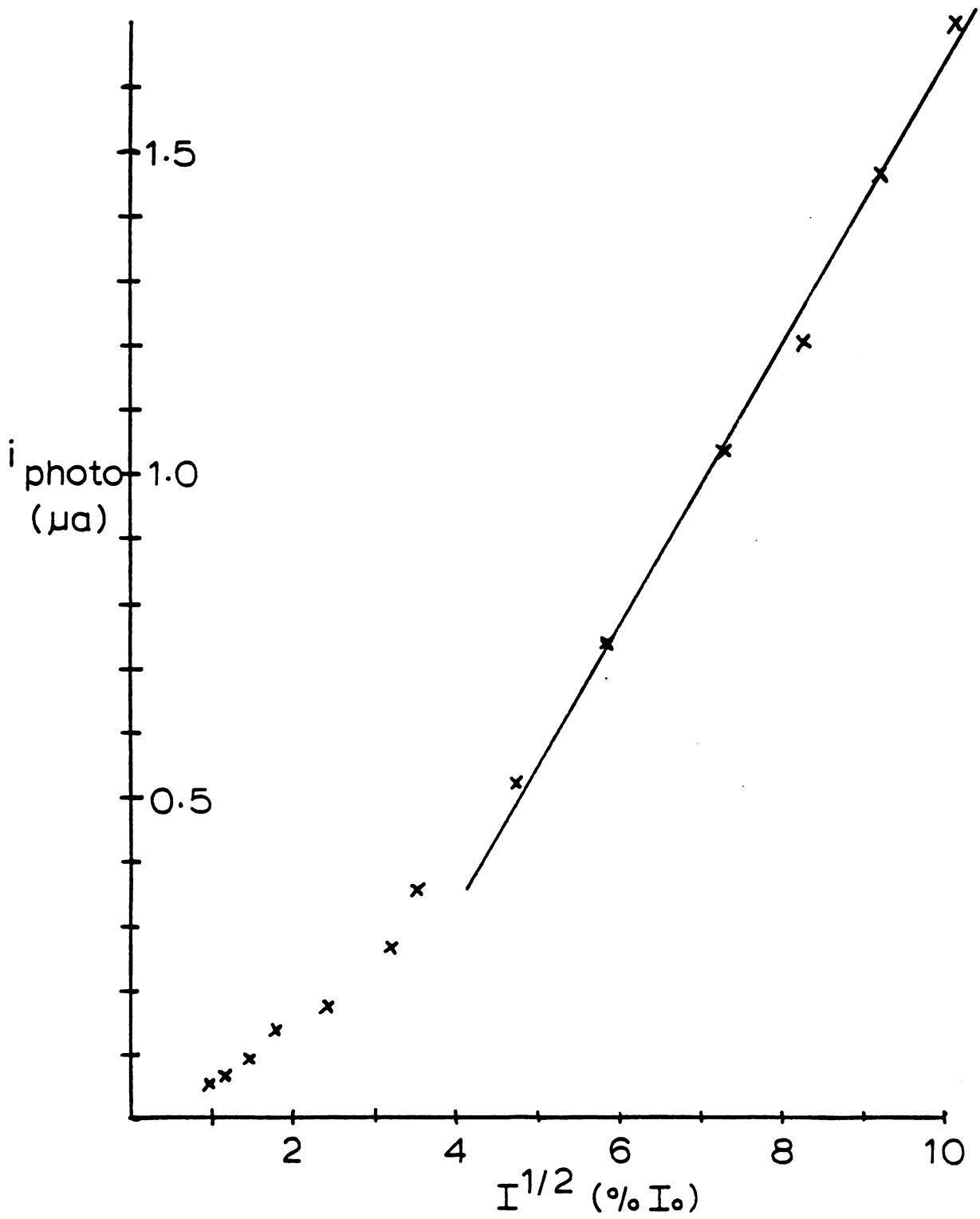

Figure 4.5.1.b: Plot for a Square Root Dependence of Photocurrent on Intensity

The same data are reploted in Figure 4.5.1.b, to see if a square root dependence on intensity was followed. While the low intensity data certainly did not agree, a good fit with the data at high intensity was obtained. Thus within the transition from low to high intensity there is a change in the rate limiting step for charge transfer.

4.5.2. Current Transients Caused by Stepped Voltage and Intensity

By poising a GaPc-Cl/SnO_2 electrode at some potential and suddenly exposing it to a light source, a transient curve would be obtained that was a function of intensity, concentration, poise potential, and other factors discussed below.

In Figure 4.5.2.a, the current/time curves resulting from stepping the potential from 0.0 to +0.5 v in an H_2Q/KHP electrolyte in the light and dark are shown. As would be expected from previous voltammetric results, the steady state light current obtained was several times larger than the dark current. The GaPc-Cl film used in this trial was rather thin, and so the photocurrnt is smaller than expected; also, the dark current may be partly due to the SnO_2 substrate.

This same electrode was poised at a lower overpotential and observed upon exposure to an LP47-filtered Xenon lamp at very low current sensitivity (0.2 μA/in). Even though the electrode potentials were well within the kinetic control

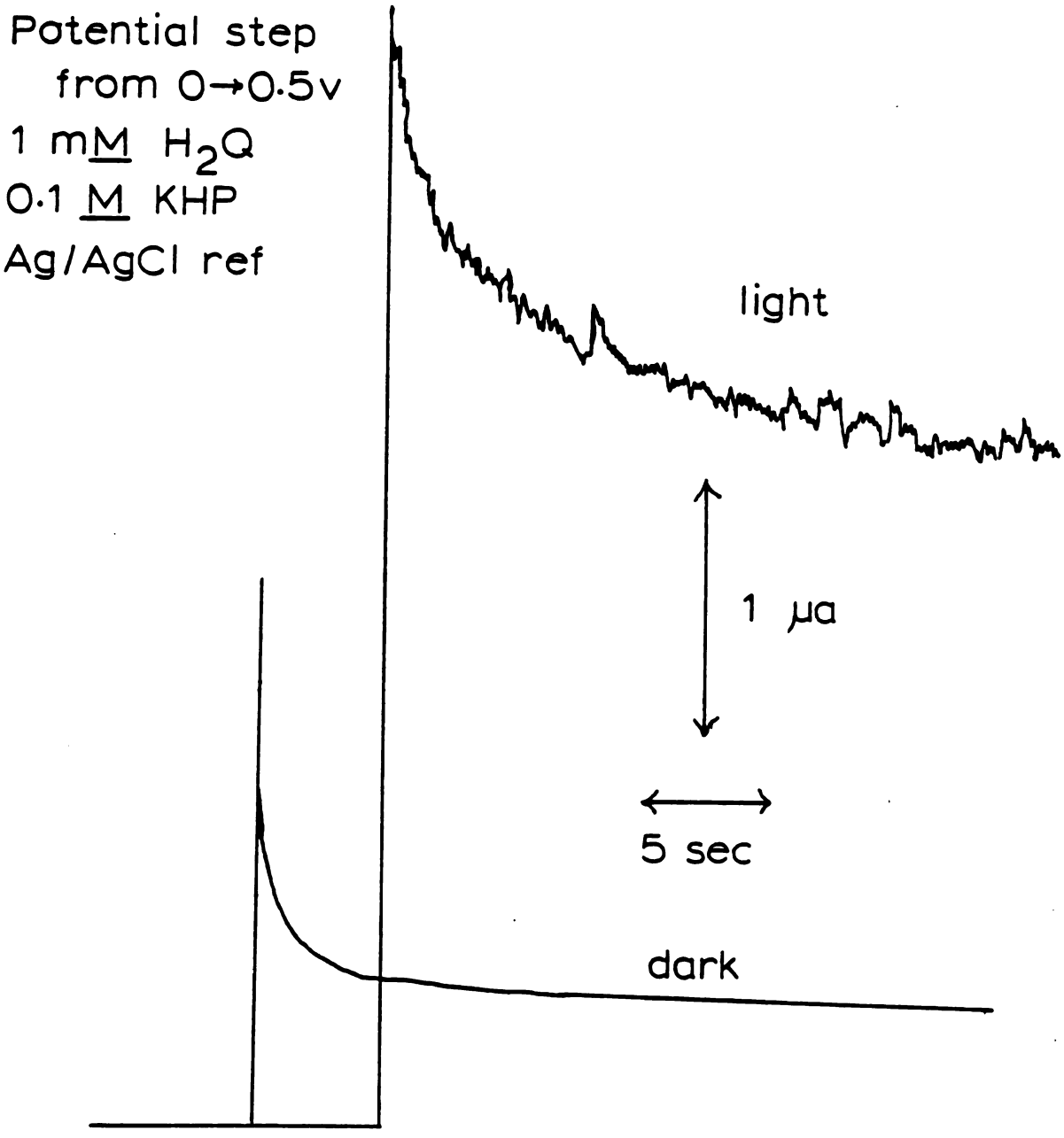

Figure 4.5.2.a: Current Transients Caused by Stepped Intensity and Voltage: Stepped Potential, Light and Dark

region, slowly decaying current transients were observed. At 0.0 v, allowing the current to drift for some 20 seconds, a light current that was initially positive fell to a negative value. Thus an anodic photocurrent had slowly reversed itself so that reduction was the favored reaction. Photocurrents reached a steady state more quickly at higher potentials. When the electrode was poised at +0.1 v, a definite, steady state anodic photocurrent was observed within 15 seconds. At +0.4 v, a steady state was immediately reached, without even an initial charging transient.

Another feature of these intensity-stepped current/time curves was the very short transient, or spike, observed just before the growth of the previously described, drawn-out transient. These can be observed in Figure 4.5.2.b as a negative spike at the foot of each on/off cycle. The current sign of the spike was the same whether the subsequent transient curve was positive or negative, as seen in Figure 4.5.2.c.

The magnitude and direction of the spike may somehow be related to the electrolyte composition. In Figure 4.5.2.d, two on/off cycles are shown from a blank electrolyte; i.e., KHP only. At a potential of -0.2 v, a positive spike with a 0.5 μA magnitude was observed, which was some five times larger than any observed in KHP solutions which contained H_2Q. Some background redox species may have been present, since extended photocurrent signals were also observed. The zero point of photocurrent, or crossover current, was found for

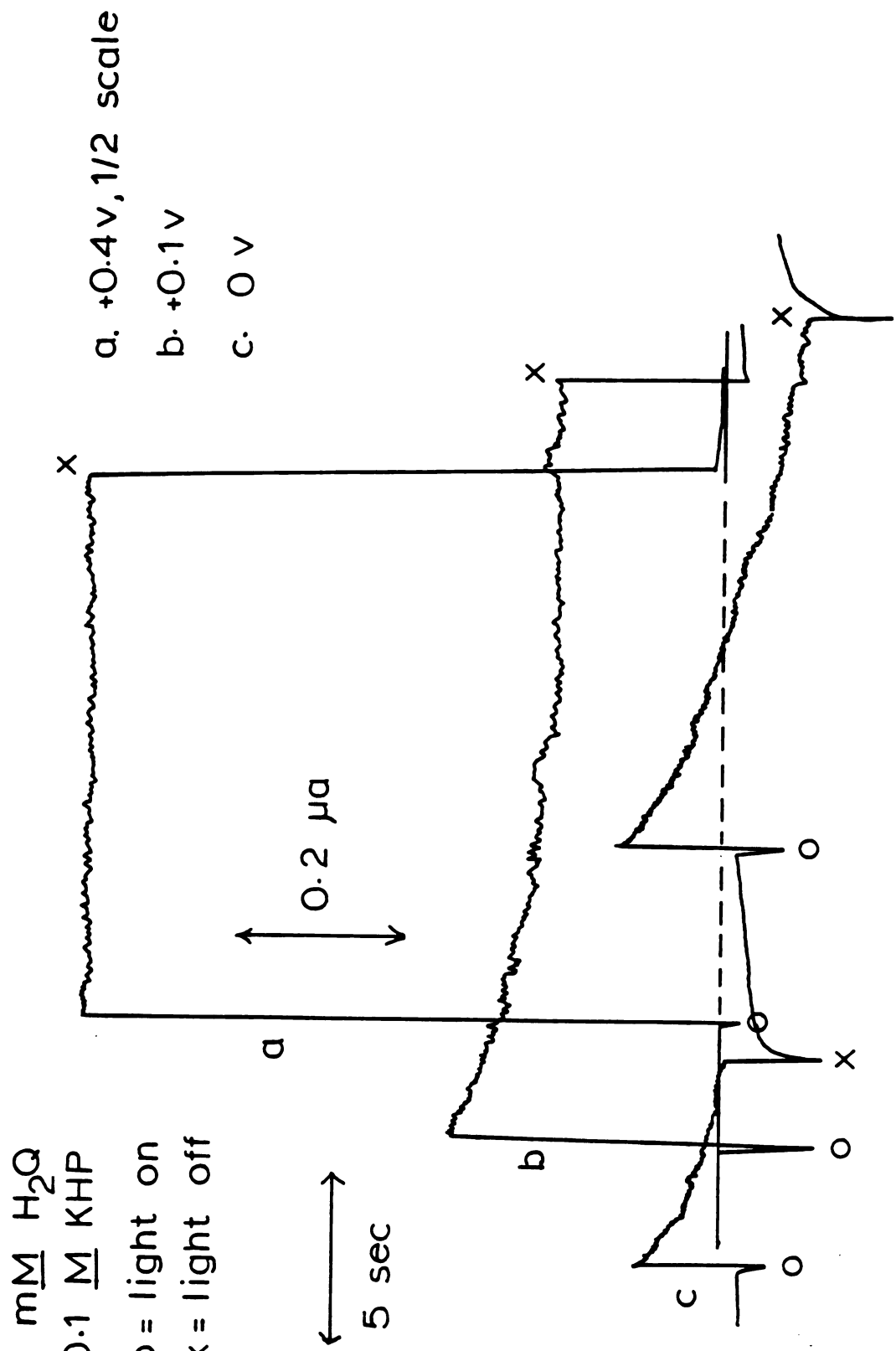

Figure 4.5.2.b: Current Transients Caused by Stepped Intensity and Voltage: Stepped Intensity at Various Potentials

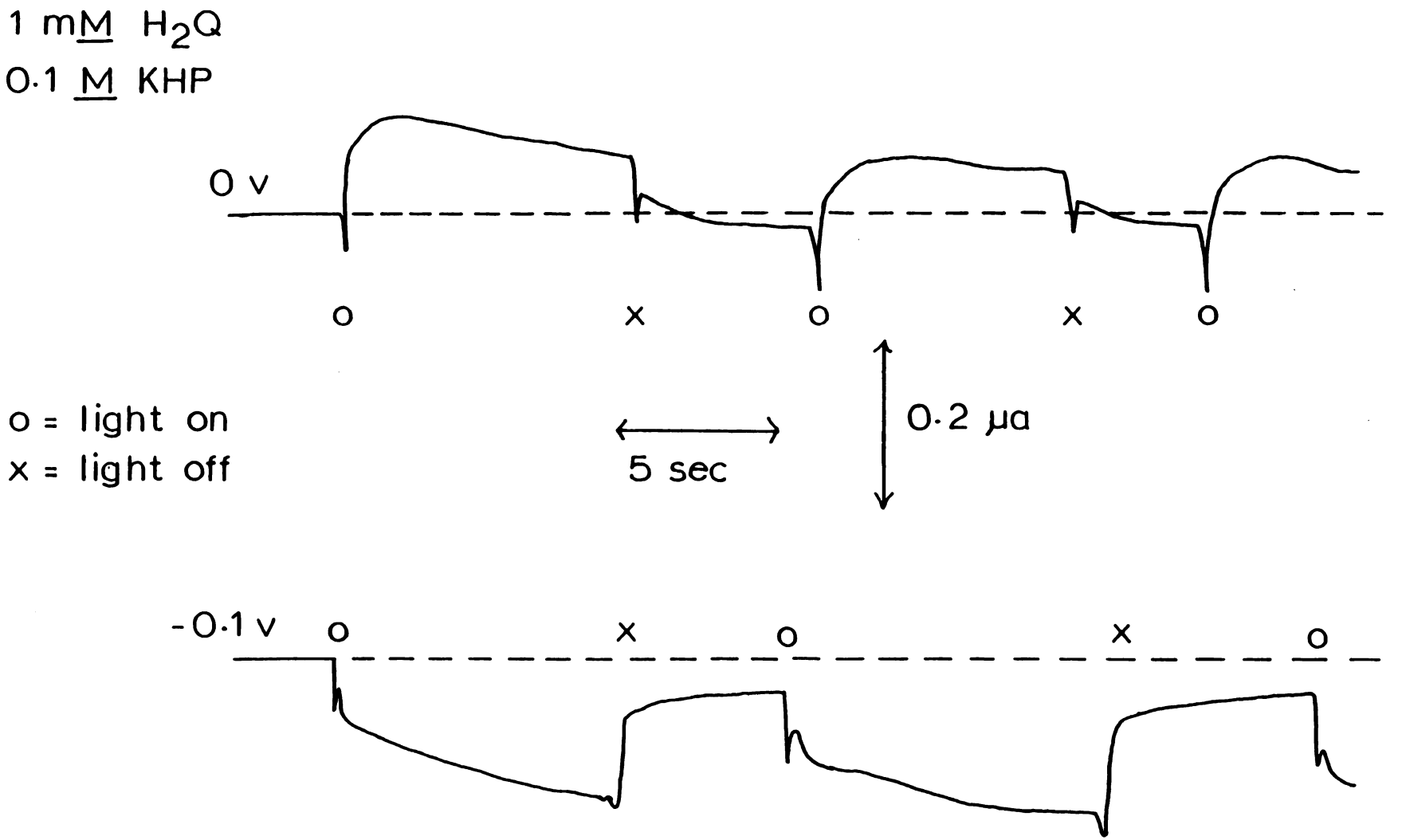

Figure 4.5.2.c: Current Transients Caused by Stepped Intensity and Voltage: Other Aspects of Stepped Intensity

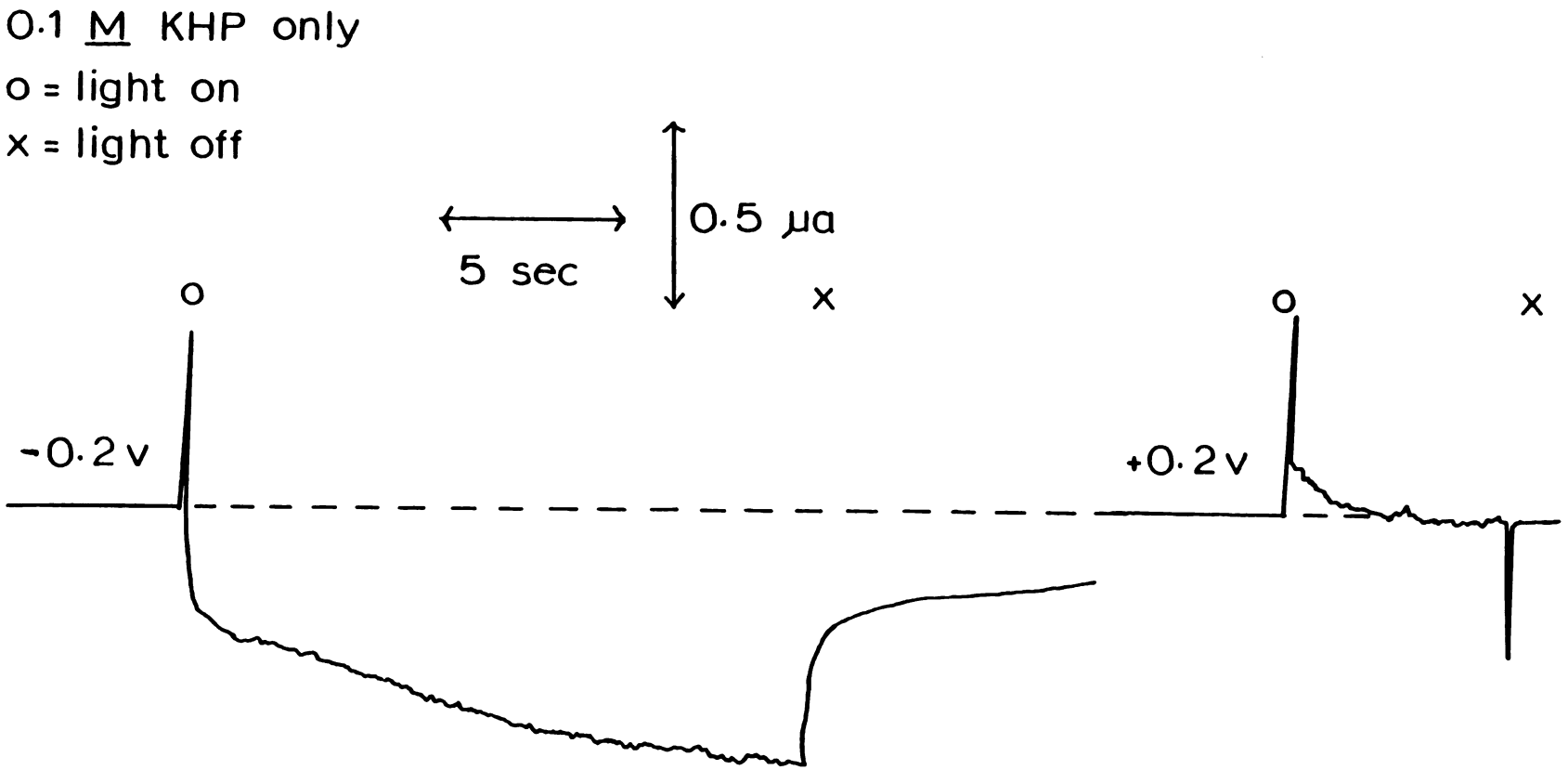

Figure 4.5.2.d: Current Transients Caused by Stepped Intensity and Voltage: Blank Electrolyte

that particular electrode at +0.2 v. Exposure to light at the crossover potential caused the positive spike again, but also a negative spike of similar magnitude was observed when the light was turned off. At that potential, the photocurrent was essentially equal to the dark current, yet removal of light caused the transient spike. The cause of these spikes must involve the charging and discharging of some capacitative element by a mechanism that does not involve faradaic processes. A direct correlation between spike direction and electrolyte could not be made, since a thick film electrode was tested which gave positive transient spikes in a H_2Q electrolyte (Figure 4.5.2.e). The transient spikes were only observed in the low overpotential region; as overpotential increased, the spikes tended to shrink into the baseline.

Sometimes a photocurrent transient would rise suddenly, recede for about one second, and then continue its growth to a steady state value. This initial current lag, or induction period, was found to be a function of delay time between on/off cycles. Frequently, if the next on/off cycle were commenced within 10 seconds of the previous cycle, the transient would show an induction period, as in the on/off cycles at -0.1 v in Figure 4.5.2.e. This was due to the slow rate at which the dark equilibrium reestablished itself. When the light reaction was reinstated, the concentration of H_2Q had not yet returned to its bulk value.

By comparing the approximate crossover points in Figure 4.5.2.b-e, it is evident that the crossover point

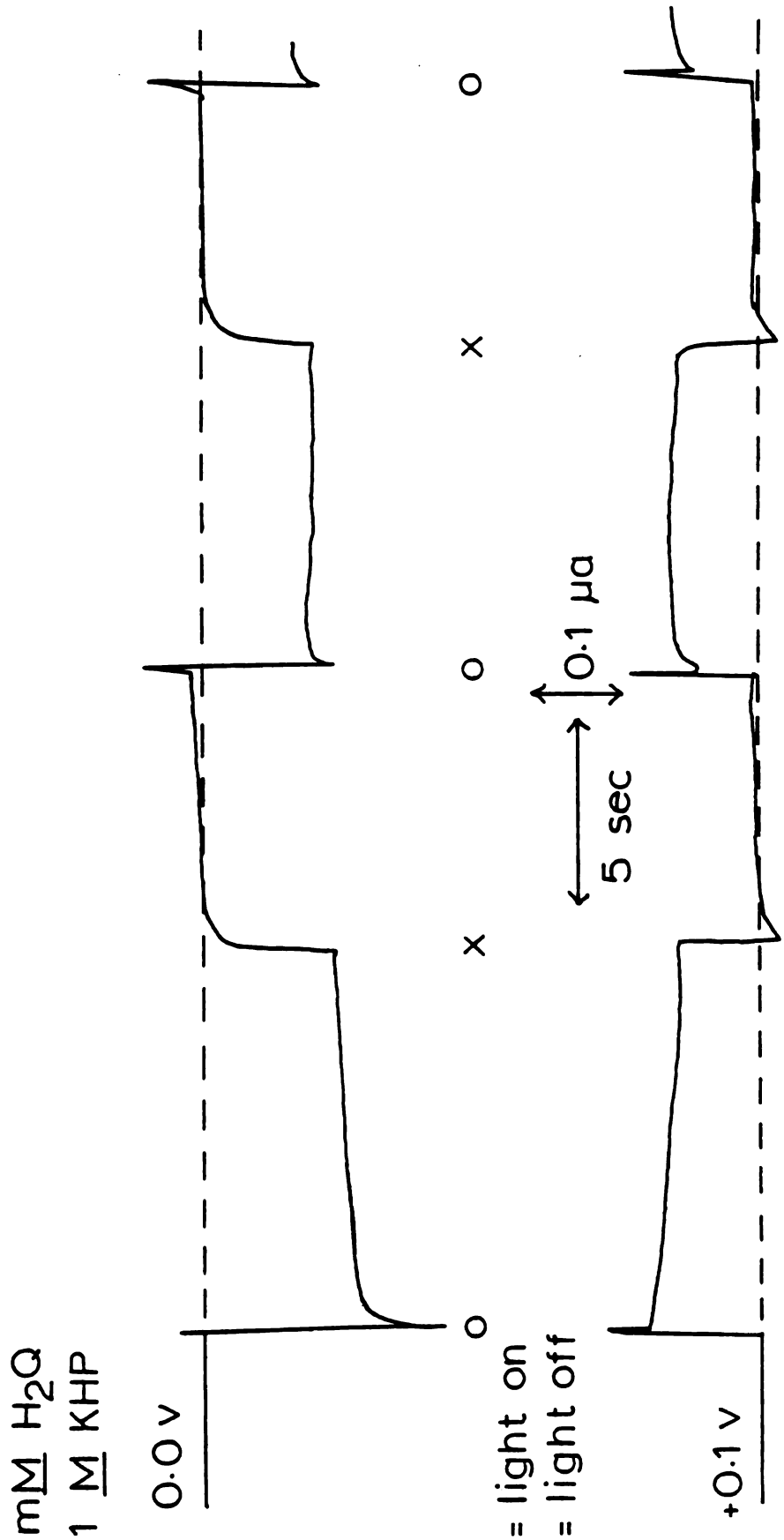

Figure 4.5.2.e: Current Transients Caused by Stepped Intensity and Voltage: Induction Period in Transient Response

varied from one electrode to another. For all the electrodes tested, the crossover point ranged from -0.1 to +0.2 v, too great a difference to be explained by drift in reference electrode potential or other external factors instead of variability in film characteristics, which may have been due to variability of the work function of the GaPc-Cl film. Lack of control over film deposition produces films with different degrees of order. If the semiconductivity of the film is extrinsic, caused by lattice vacancies and other defects, then the position of E_F and hence the crossover point would vary with the degree of crystalline order.

4.5.3. Intensity Effect on Cyclic Voltammetric Curve

In section 4.5.1., the effect of intensity on steady state current was described. At a constant potential, a reduced light flux was seen to reduce the current flow, or rate of electrochemical reaction. The perspective of a reduced rate of electrolysis is enhanced by observing the effect of intensity on a voltammetric curve.

In Figure 4.5.3., the anodic portions of the cyclic voltammograms for the electrolysis of H_2Q on GaPc-Cl/Au at different light intensities are shown. The cathodic portions appeared exactly the same and so were omitted for clarity. The intensity was varied over an order of magnitude, from the full visible output of the Xe lamp to less than one-tenth, through the use of neutral density filters.

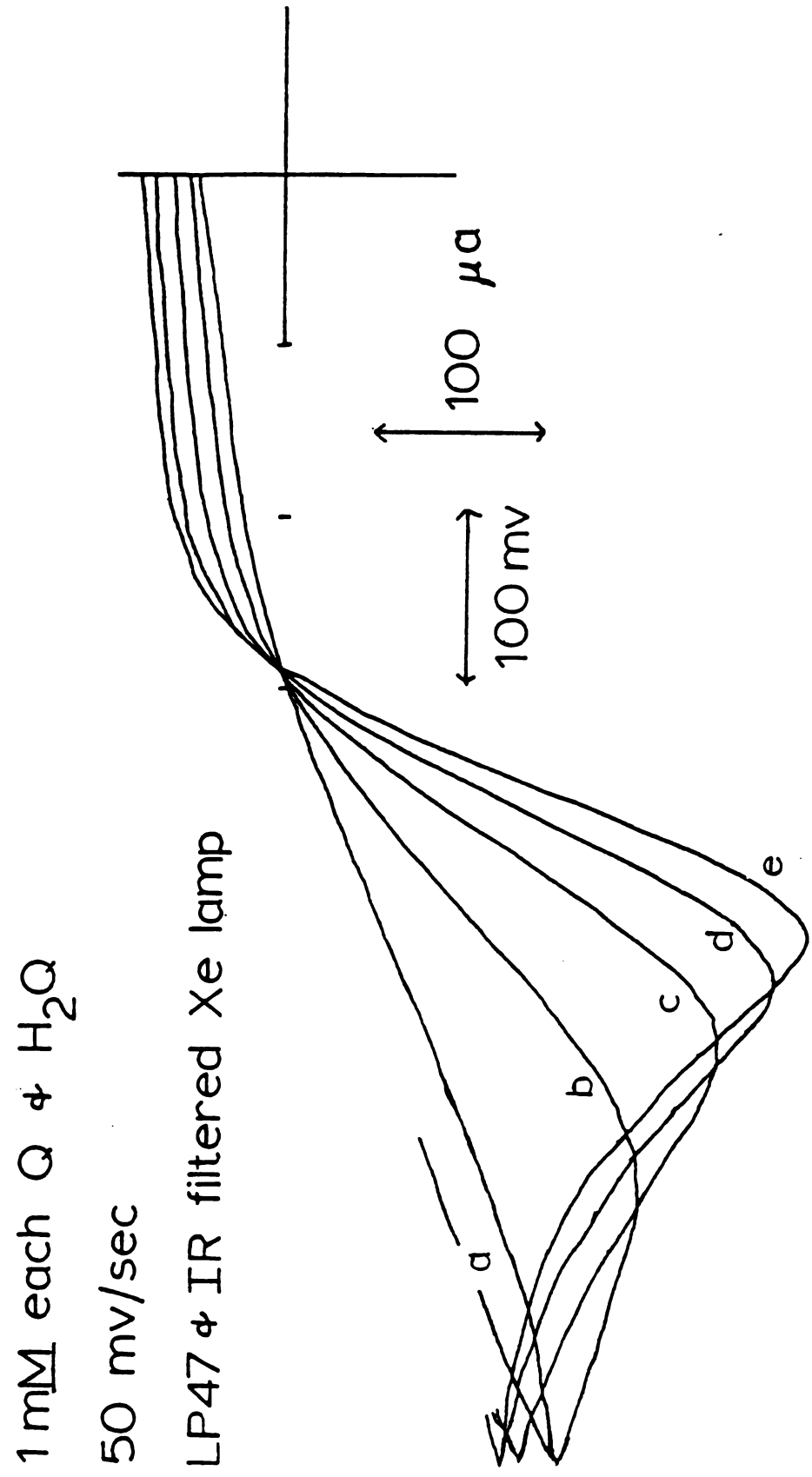

Figure 4.5.3: Effect of Light Intensity on H_2Q//GaPc-Cl/Au Voltammetric Wave: Neutral Density Factor: (a) 1.30; (b) 0.89; (c) 0.49; (d) 0.20; and (e) 0.

The shape of the voltammetric curve appeared less and less reversible as intensity decreased, so that the curve with a neutral density factor of 1.30 was nearly a slanted line, devoid of any features. The current was still greater than the dark current, however, which would simply run along the baseline.

The intensity effect can be incorporated into the kinetic expression for charge transfer in the following way: the normal expression for oxidative charge transfer is

$$i = i_o \exp [(1-\beta)F\eta/RT]$$

i_o can be expressed as $nFAk_sC_o$, where k_s is the fundamental rate constant for charge transfer. Electrode processes are generally thought to be unimolecular, so that only one concentration term is present. However, currents on irradiated GaPc-Cl/Au electrodes also have some dependence on light, which may be interpreted as the surface concentration of excited state GaPc-Cl molecules [GaPc-Cl*]. The i_o term then becomes

$$i_o = nFAk_s'C_o \quad \text{where } k_s' = k_s[\text{GaPc-Cl*}]$$

In other words, k_s' is a pseudo-first order rate constant which includes the true fundamental rate constant and the intensity-dependent excited state GaPc-Cl term. Therefore, the intensity could be thought of as affecting the rate of

reaction by operating on the exchange current density, making it large or small, resulting in reversible or irreversible kinetics.

4.5.4. Tafel Data

In Figures 4.5.4. and 4.5.5., the Tafel plots for the electrolysis of H_2Q on Au and on GaPc-Cl/Au under irradiation in a KHP electrolyte are shown. The calculated exchange current densities for 1 m$\underline{M}$ Q or H_2Q were 0.27 $\mu A/cm^2$ for inactivated Au, and 15.6 $\mu A/cm^2$ for GaPc-Cl/Au, over a 50-fold increase in fundamental reaction rate. As it turned out, the film electrode selected for this experiment performed worse than average in terms of cyclic voltammetry, with a 310 mv peak to peak separation. Using the method of rate constant determination from peak separation in cyclic voltammetry as described by Nicholson (154), an i_o was estimated from Figure 4.2.3.a as 100 to 200 $\mu A/cm^2$, or some 400 to 700 times as great as on inactivated Au.

From the slopes of the Tafel curves, the following table of transfer coefficients was calculated.

TABLE 4.3

Transfer Coefficients for H_2Q/Q Electrolysis on Inactivated Au and GaPc-Cl/Au

ELECTRODE	$\overrightarrow{\alpha}$	$\overleftarrow{\alpha}$
Au	0.97	0.71
GaPc-Cl/Au	0.41	0.51

1 m$\underline{M}$ each Q and H_2Q
0·1 $\underline{M}$ KHP
electrode area 0·55 cm^2

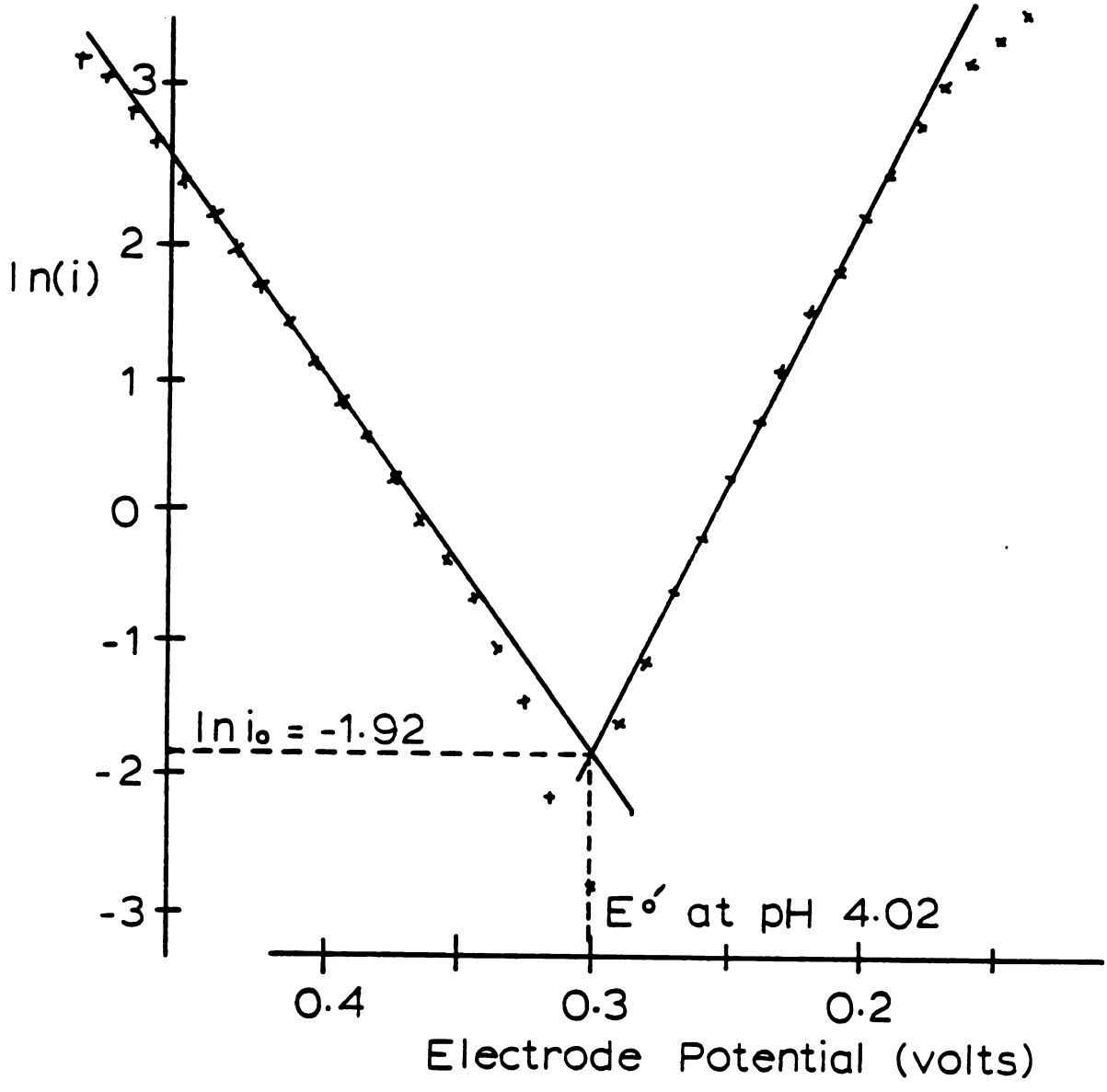

Figure 4.5.4: Tafel Plot for Q/H_2Q Electrolysis on Inactivated Au

1 m<u>M</u> Q and H_2Q
0.1 <u>M</u> KHP
electrode area 0.55 cm^2

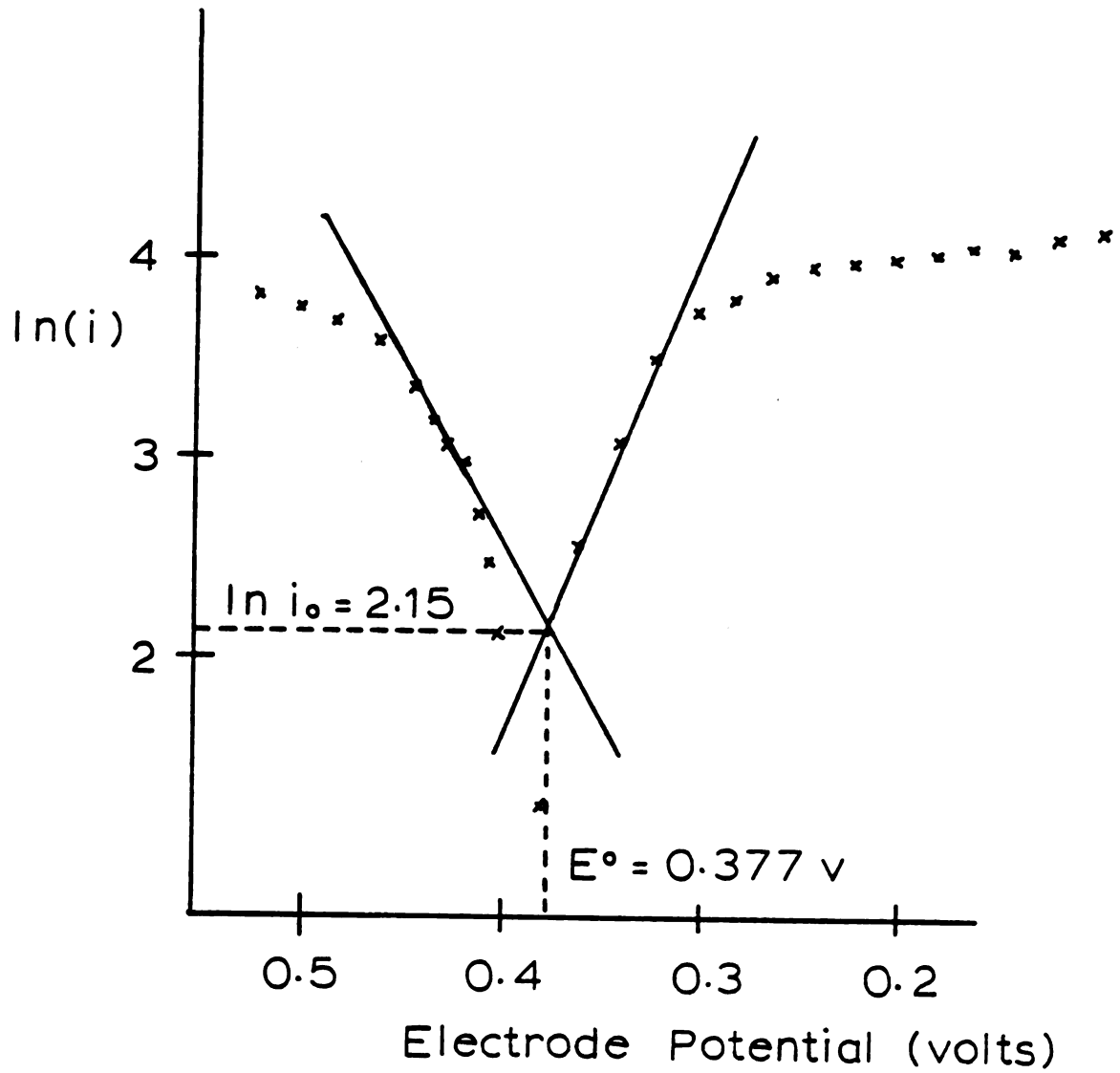

Figure 4.5.5: Tafel Plot for Q/H_2Q Electrolysis on GaPc-Cl/Au

4.5.5. Effect of Frontside vs. Backside Illumination

With the use of the cell design described in the Experimental chapter and optically transparent electrode substrates, it was possible to irradiate the electrode from two directions, either through the electrolyte to reach the dye film, or through the electrode substrate. The convention adopted will be that radiation passing through the electrolyte before reaching the dye film will be called frontside illumination, and radiation passing through the substrate before reaching the dye film will be called backside illumination. With this capability the distribution of photoexcited species could be weighted either toward the substrate interface or the electrolyte interface within the film.

Whenever a solid sample is irradiated, excited state species are created according to Beers Law:

$$A\ (\lambda) \quad = \quad \varepsilon\ (\lambda)\ x$$

where A is the absorbance at some wavelength, λ, ε is the absorptivity coefficient at that wavelength, and x is the thickness of the sample. In terms of intensity:

$$A \quad = \quad \log \frac{Io}{I}$$

where Io is the incident intensity and I is the intensity of light remaining after passing through the same. Rearranging terms and substituting for A,

$$I = Io\ 10^{-A}$$

$$= Io\ 10^{-\varepsilon x}$$

The intensity absorbed, or the number of photons absorbed per second by the sample, is Io - I, or

$$\#\ \text{absorbed photons/sec} = Io\ (1 - 10^{-\varepsilon x})$$

This number is also equal to the number of photoexcited species generated per second. Furthermore, the equation describes the distribution of excited states within the sample. A substance with large ε, such as the phthalocyanines, would effect a steep exponential decay so that samples on order of 100 Å thickness or more would have a very unequal distribution of excited species. In terms of electrochemical reaction, the proximity of excited state species to the double layer may play an important role as to whether those species can participate in the reaction.

A series of GaPc-Cl/SnO_2 electrodes of variable thickness were examined voltammetrically with frontside and backside illumination. All the thin and normal thickness (around 100 equivalent monolayers, absorbance maximum = 1.0

to 1.2) electrodes showed no difference in response between the two modes of illumination. The only electrode which gave a difference between frontside and backside illumination was the thickest one tested, whose voltammetric response is shown in Figure 4.5.6. Its absorbance maximum was too high to measure with the spectrophotometer, which puts its thickness at greater than 300 equivalent monolayers or on order of 1000 Å.

The dark current was flat along the baseline, indicating a nonporous electrode. The light voltammograms were quite distorted, as had been observed before for very thick film electrodes. The backside trace showed larger currents than the frontside trace, implying that photoexcited species near the rear, or substrate/dye interface, are more likely involved in a rate limiting step in the photoelectrochemical reaction. One big source of error in this experiment, however, was the difference in transmission loss through the substrate as opposed to through the cell window and electrolyte. This will cause a difference in intensity delivered to the photoactive film, which, as shown in Figure 4.5.2., has a pronounced effect on the voltammetric response.

4.5.6. Photoaction Spectra

A photoaction spectrum is a plot of the photocurrent drawn from a photoelectrochemical cell as a function of

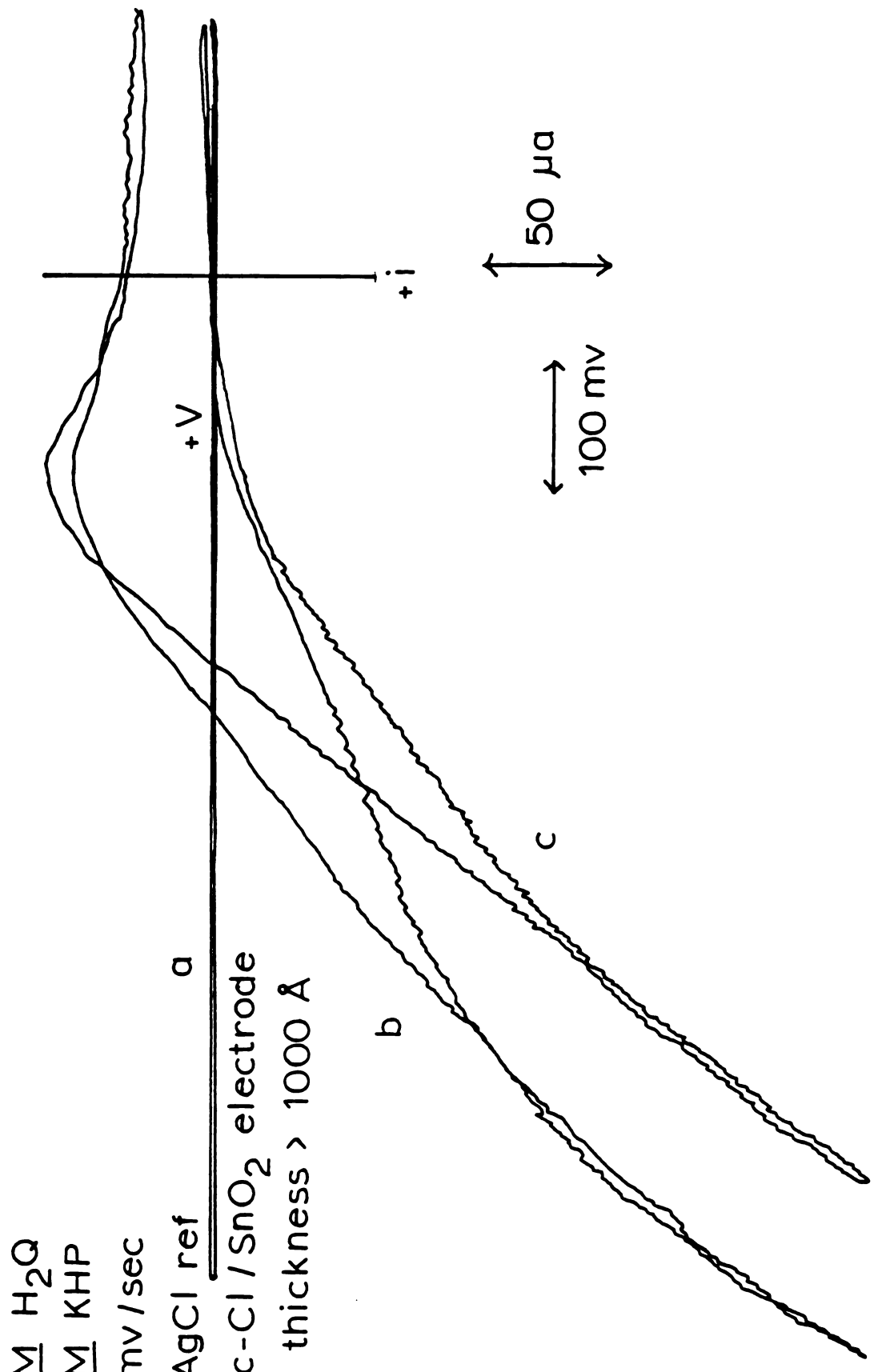

Figure 4.5.6: Effect of Frontside vs. Backside Illumination on Voltammetric Curve: (a) dark; (b) light, frontside; and (c) light, backside

wavelength. Aside from the electrode characteristics themselves, the measured photocurrent will be a function of the spectral output of the lamp, the throughput of the monochromator, the geometry and position of the cell, the potential applied to the electrode, the electrode area, and the concentration of electroactive species. As a result, care must be exercised in the presentation of photoaction spectra, or else it will be difficult to compare intra- or interlaboratory results.

With this in mind, a photoaction spectrum where the current has been normalized to the spectral output of the optical apparatus was made. This was accomplished by measuring the voltage output of a photodiode placed where the cell would be in the optical path as a function of wavelength. With the use of quantum efficiency data supplied by the photodiode manufacturer, the normalized spectrum could be obtained by solving the following equation for each wavelength increment (10 nm):

$$y = \frac{i_e \phi d}{i_d}$$

where y is the normalized vertical coordinate in the photoaction spectrum, i_e is the measured photocurrent from the electrochemical cell, i_d is the measured photocurrent from the photodiode, and ϕ_d is quantum efficiency of the photodiode. The variable y could be called the photon conversion

efficiency, since the ratio on the right hand side describes the number of electrons injected per incident photon. The resulting spectrum will show which photons are most capable of creating a photocurrent.

In Figure 4.5.7., the photon conversion efficiency of a GaPc-Cl/Au electrode poised at +0.4 v in a 1 m$\underline{M}$ H_2Q pH 4 solution versus wavelength is shown. The absorption spectrum of an equivalent film deposited on glass is included as a dotted trace for comparison. The photoaction curve rose above 500 nm to form a broad curve in the red region of the visible region and then fell quickly after 770 nm. The fine structure on top of the wave was found to be reproducible, and so care was taken to intersect all the data points. The curve fairly well tracked the absorption spectrum, except for the maximum at 780 nm, which is right on the edge of the efficiency drop-off in the photoaction spectrum. Thus, the conversion efficiency of a photon appeared to be directly related to its molar absorptivity.

Another useful quantity is the conversion efficiency of an absorbed photon. The resulting spectrum could differ from the previous one if there were electronic states whose relative abilities to create charge carriers did not match their relative absorptivities. Another reason for a different spectrum would be reflectivity. Whenever an interface is irradiated, a certain portion of the light is reflected. If true quantum efficiencies for charge transfer, or electrons injected per photon absorbed, are desired, the

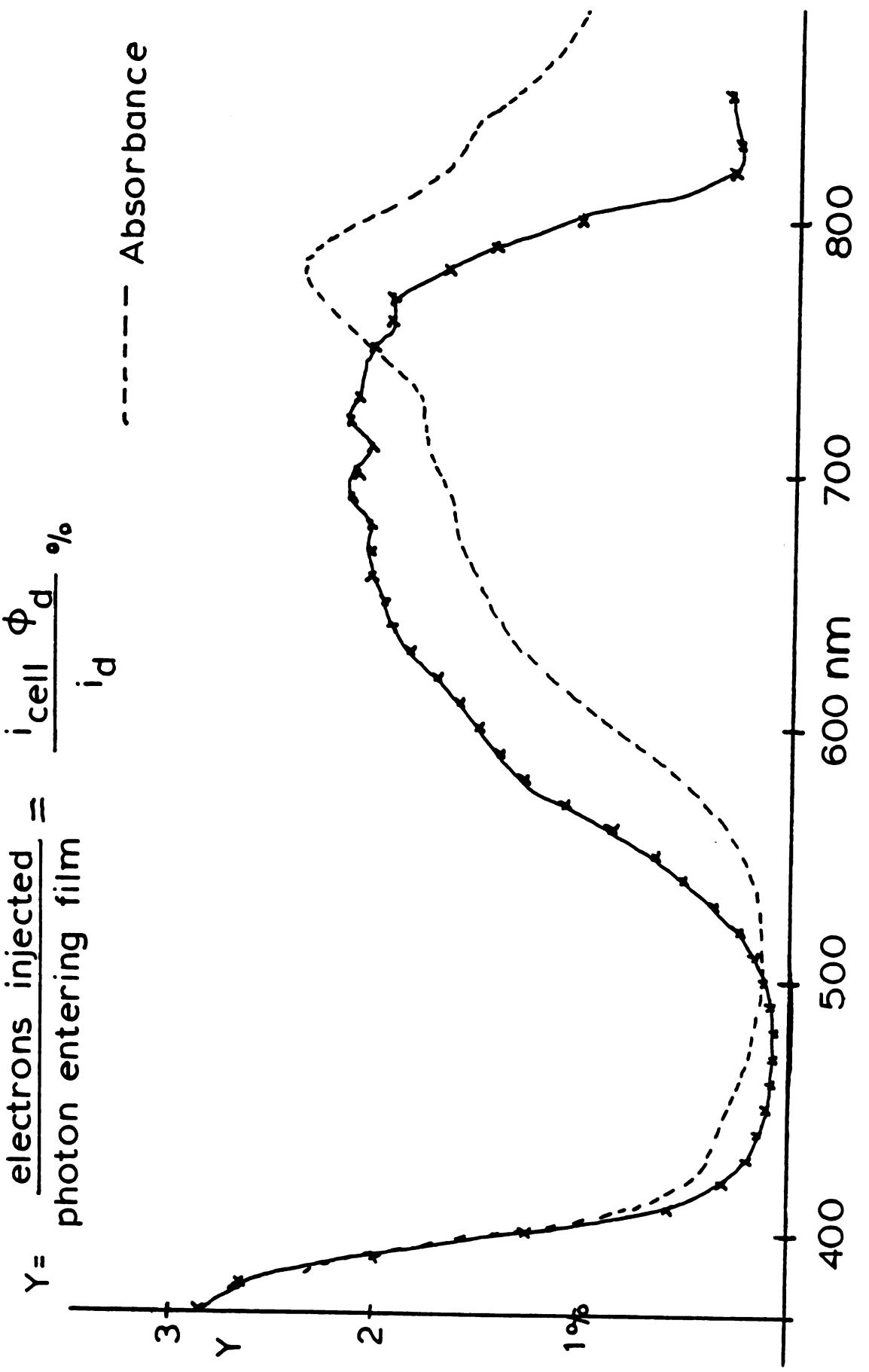

Figure 4.5.7: Photoaction Spectrum for a GaPc-Cl/Au Electrode

wavelength dependent specular reflectance spectrum must be obtained for the electrode. This was done on a Cary 14 spectrophotometer with a specialized attachment. The quantum efficiency can now be calculated for each wavelength increment by

$$\frac{i_e \, \phi_d}{i_d \, (1-R) \, (1-10^{-A})}$$

where R is the reflectance (normalized to 1), A is the absorbance, and the other variables were defined previously.

The plot of quantum efficiency versus wavelength is shown in Figure 4.5.8. The low energy part of the curve appeared much as the previous photoaction curve, but the rising edge on the high energy side displayed a prominent peak. It was uncertain whether the peak should be split by the data points at 550 and 560 nm. It would appear that the lower the molar absorptivity, the higher is the quantum efficiency for charge transfer. Arguments will be presented in the Discussion section to refute this result.

4.5.7. Capacitance Data

The results presented so far have not definitely distinguished GaPc-Cl as a p-type semiconductor. Likewise, the treatment of capacitance data as for an ideal, p-type semiconductor did not yield the predicted result.

$$\Phi = \frac{\text{electrons injected}}{\text{photon absorbed}} = \frac{(i_{cell})\,\Phi_d}{i_d(1-R)(1-10^{-A})}$$

corrected for reflectance

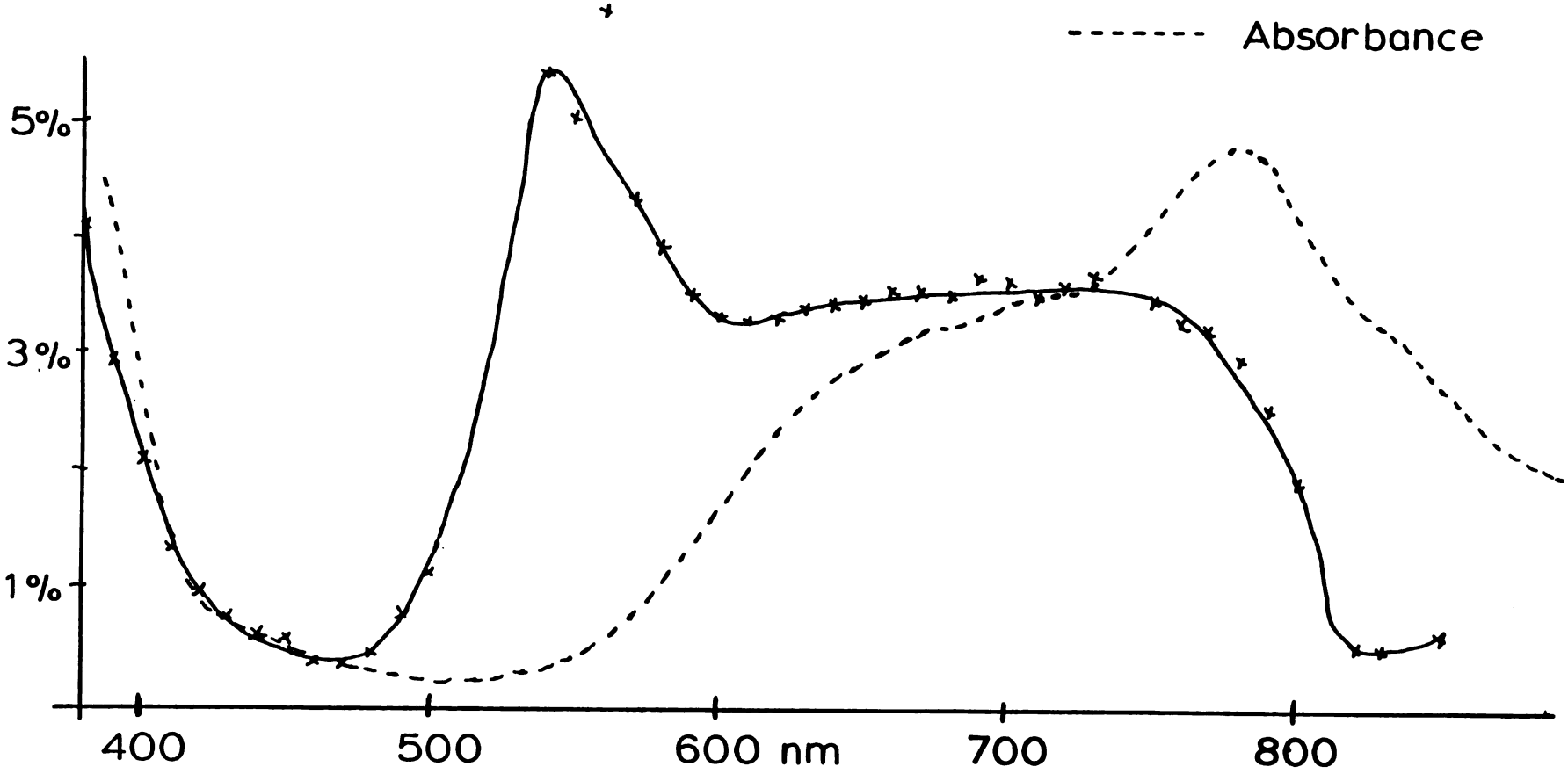

Figure 4.5.8: Quantum Efficiency vs. Wavelength for a GaPc-Cl/Au Electrode

Mott-Schottky plots ($\frac{1}{C}2$ vs V) for semiconductor electrodes will give a straight line, whose slope is inversely proportional to the carrier density and whose horizontal intercept is approximately equal to the flat band potential.

Mott-Schottky plots for GaPc-Cl/Au electrodes in light and dark in an inert electrolyte are shown in Figure 4.5.9. The electrolyte was 0.1 M in KHP only, and the modulation frequency was 1000 Hz. Data were taken from 0 to +0.8 v. Far from yielding a linear plot, the capacitance in the light curved downwards with increasing potential, further perturbed by a peak around +0.35 v, while in the dark the capacitance curved upwards with potential increase, forming a peak again at +0.35 v.

The possibility that GaPc-Cl capacitance as a function of potential varied as if for a metal was also examined. Examples already existed in the literature where phthalocyanines exhibited metallic behavior in terms of its conductivity dependence on temperature, even though the conductivity was in the semiconductor range (51). The capacitance of a metal is somewhat independent of potential, so that plots of capacitance versus potential generally show a flat curve, rising near the point of zero charge (186).

Plots of capacitance versus potential for GaPc-Cl/Au electrodes using the same data as that used for the Mott-Schottky plots are shown in Figure 4.5.10. As could be qualitatively predicted from the previous graphs, capacitance

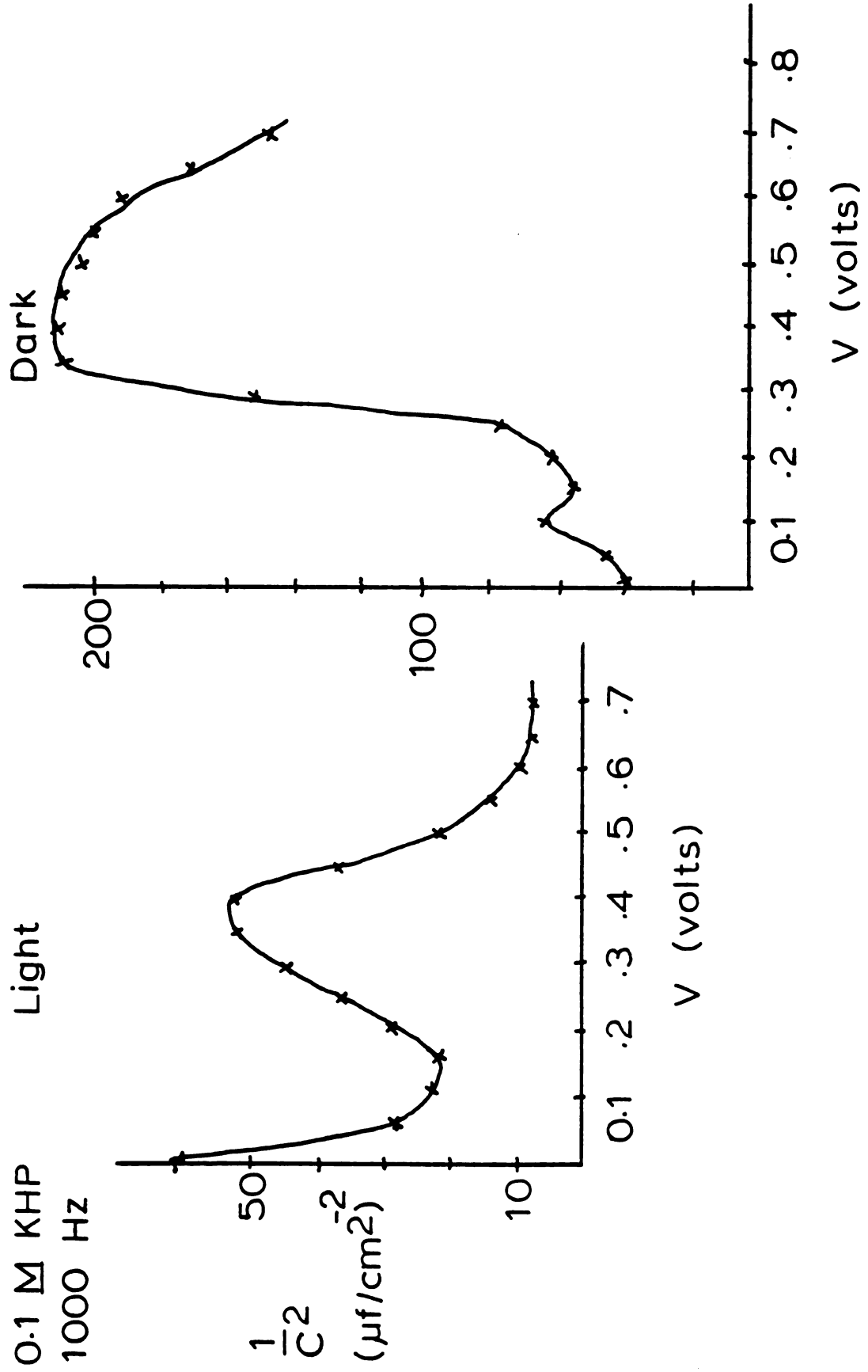

Figure 4.5.9: Mott-Schottky Plot for GaPc-Cl/Au

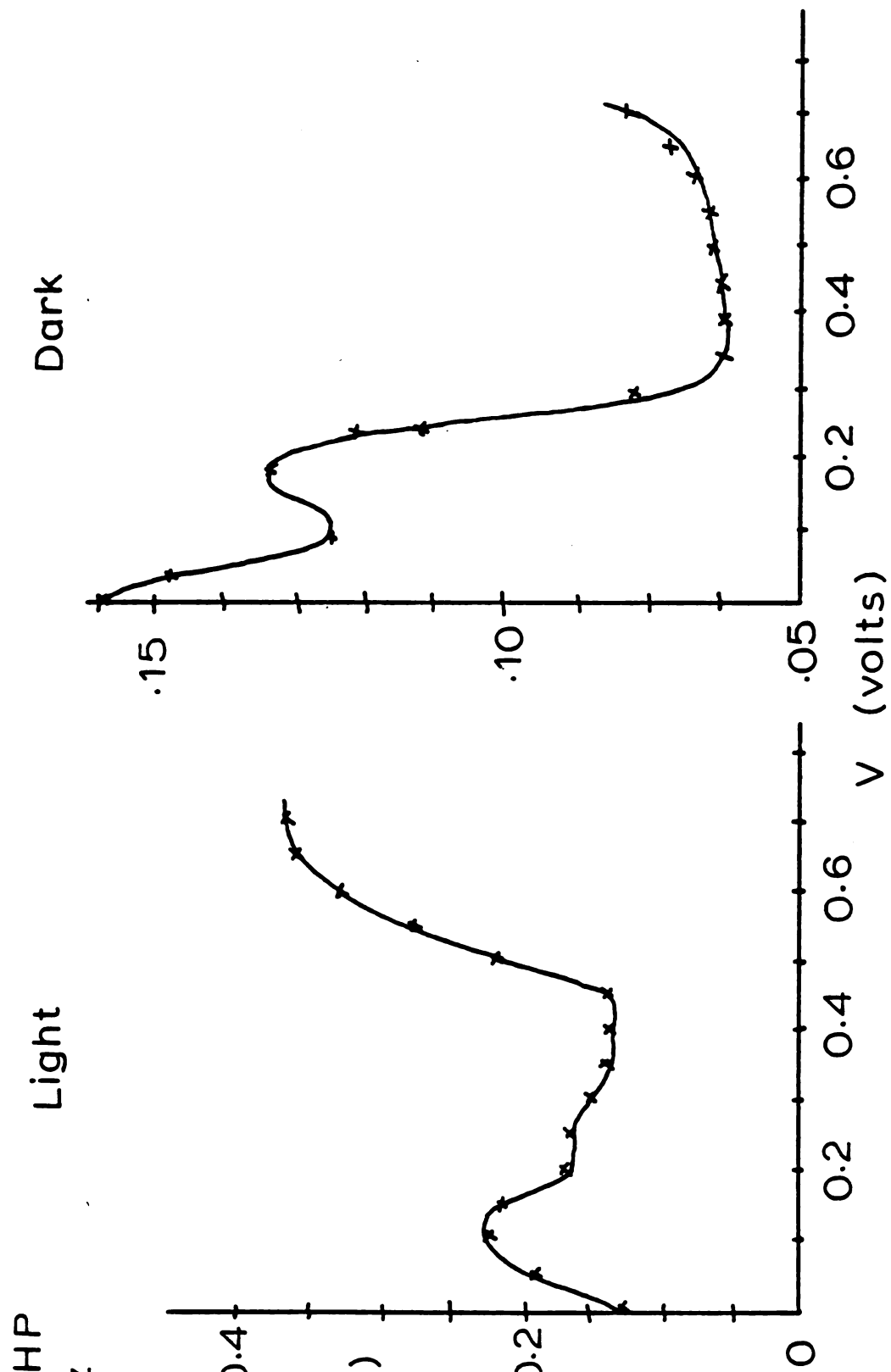

Figure 4.5.10: Capacitance versus Potential Plot for GaPc-Cl/Au

generally increased with potential in the light curve and decreased in the dark. A maximum in the light curve occurred at +0.1 v, while in the dark a maximum occurred at +0.15 v. Thus, the capacitance behavior of GaPc-Cl/Au electrodes varied greatly between light and dark, but could not be easily ascribed to metallic or semiconductor behavior.

4.6. Other Experiments on GaPc-Cl Electrodes

4.6.1. Dependence of Photocurrent on Concentration

The effect on steady state photocurrent when a GaPc-Cl/SnO_2 was poised at +0.4 v in solutions of variable H_2Q concentration is shown in Figure 4.6.1. The H_2Q concentration was varied from 5 x 10^{-5} M to 5 x 10^{-2} M, covering two orders of magnitude. The data were split between two graphs of different scale for study. At the lower concentrations, millimolar and below, a linear plot was obtained. However, it is uncertain whether that fact alone proves that the reaction is first order in H_2Q. In order to increase the photocurrent by a factor of four, the H_2Q concentration increased by an order of magnitude. A significant deviation from linear behavior occurred at higher concentrations. The photocurrent only increased from 0.7 to 10.5 μA through the hundred-fold increase in H_2Q concentration. This behavior may be due to passivating adsorption, which would increase at higher concentrations, or a rate determining process within the GaPc-Cl film.

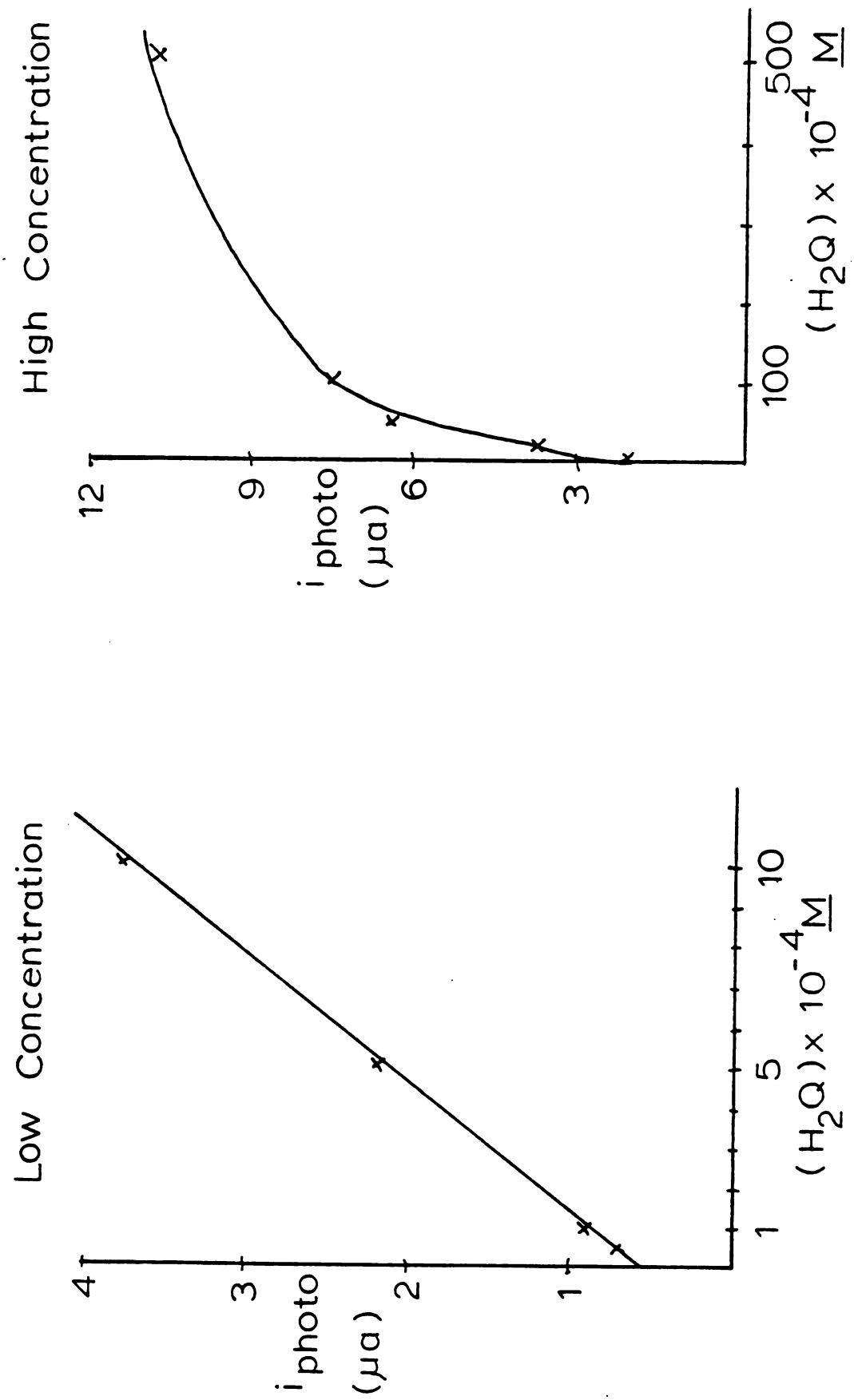

Figure 4.6.1. Photocurrent vs. H_2Q Concentration

4.6.2. Effect of Slow Scan Rate on Voltammetric Curve

The difference in cyclic voltammetric response at 10 mv/sec and 50 mv/sec for GaPc-Cl/SnO_2 electrodes was demonstrated in Figures 4.2.1. and 4.3.1.c. The validity of such a comparison is questionable, however, since the voltammograms were performed on different electrodes of different film thicknesses in different experiments. Furthermore, of all the electrode substrates examined, SnO_2 provided the most variable results. Therefore, the scan rate effect was examined with a single GaPc-Cl/Au electrode in the same electrolyte, over a time scale of a few minutes.

In Figure 4.6.2., the relevant voltammograms are shown. A flat baseline trace in the dark indicated a nonporous electrode. The light current at 10 mv/sec, shown as a solid line, initially rose to form a well shaped peak. The decaying diffusion current, however, quickly leveled off into a plateau which remained steady at potentials well past 1.0 v. Upon the return sweep, the current plateau exactly retraced itself until below +0.5 v, when the trace curved to form a small but well shaped cathodic wave. Several times as much positive charge had been transferred as negative charge.

The light voltammogram at 10 mv/sec precisely duplicated work that P. Rieke had done on porous GaPc-Cl/Au electrodes (185). The dark trace for his electrodes naturally showed a large, poorly reversible dark wave characteristic of inactivated gold substrates. Thus, porosity could not be used to explain the observed voltammetric shape.

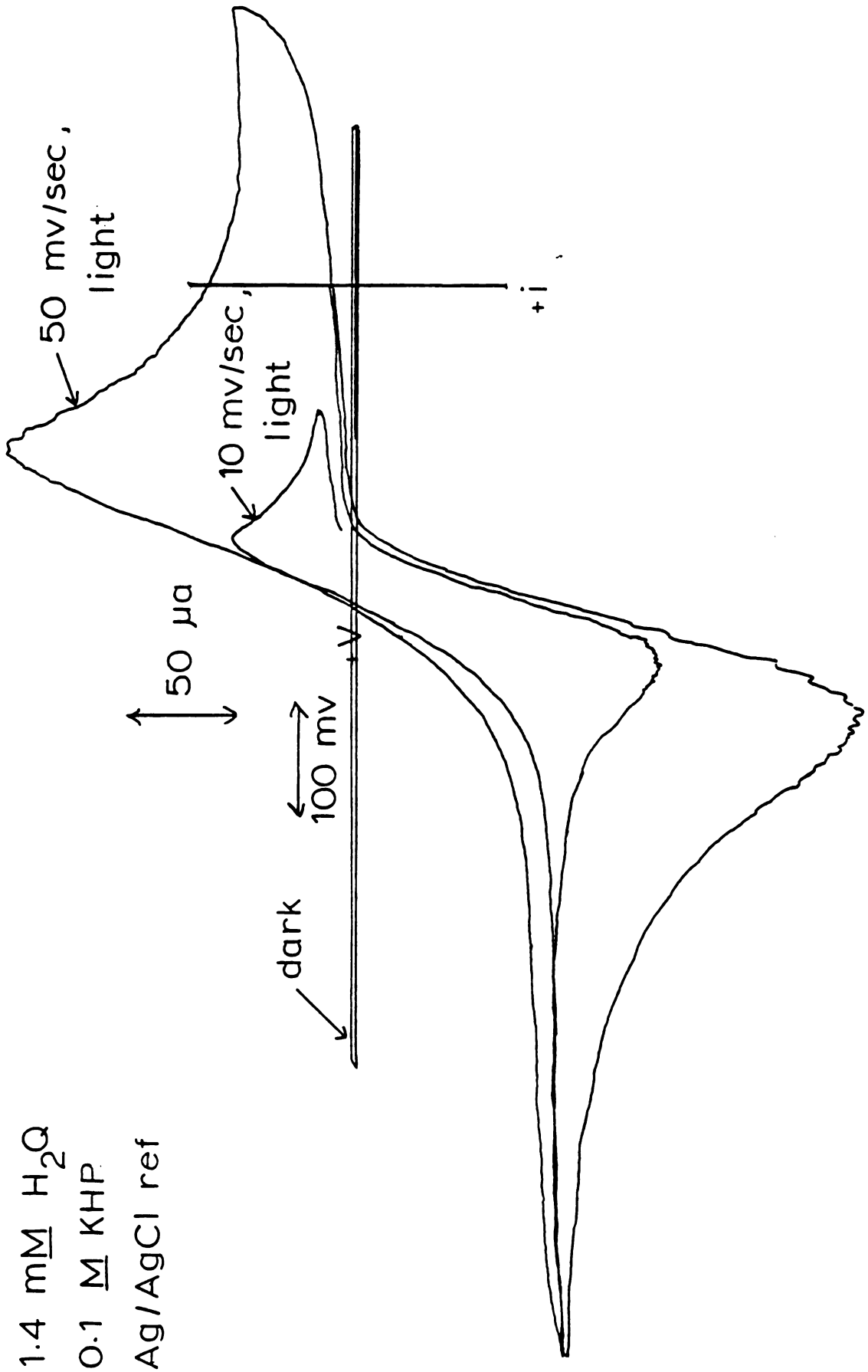

Figure 4.6.2: Cyclic Voltammogram of H_2Q Electrolysis on GaPc-Cl/Au at a Slow Scan Rate

The voltammogram obtained at 50 mv/sec is shown as a dotted trace in Figure 4.6.2. Scanning well into the anodic region, the diffusion current continued to decay without leveling off. Upon the return sweep, a much larger portion of the electrogenerated quinone was reacted.

These results can be explained in terms of the time required to make each cycle. At 10 mv/sec, the electrode must spend five times as much time in the diffusion control region as at 50 mv/sec. Thus the electrode at slow scan rate is more likely to reach a situation of convective control. Convective control on a stationary electrode usually occurs after the electrode has been poised in the mass transport control region for long periods of time, typically hundreds of seconds. In this case, however, the full visible wavelength output of the 450W Xe lamp is brought to bear upon the highly absorptive GaPc-Cl film. The result is heat generation which prematurely caused convective currents to take control. Thus the plateau current is limited by convection, a conclusion corroborated by P. Rieke (185), who saw the same plateau effect for different redox couples and supporting electrolytes, in both cathodic and anodic regions. He also observed that the plateau current level could be sustained as long as 10 minutes at a poised potential in the plateau region, demonstrating that diffusion control could not be in effect.

4.6.3. X-Ray Photoelectron Studies on GaPc-Cl/Au

The full range XPS spectrum for a GaPc-Cl/Au electrode is shown in Figure 4.6.3.a and b. The data are presented in digital form, just as they were collected from the analyzer. The full range spectrum was obtained in two 500 ev windows, one point per ev, with three signal-averaged scans. The plotting routine automatically adjusted the vertical scale so that the spectrum would appear nicely balanced within its borders; in this case, one inch approximately equals 1000 counts per second.

Photoelectron transitions from GaPc-Cl/Au samples can be expected for Ga, C, N, Cl, and Au. Some background carbon and oxygen will also be detected as surface contamination at the operating pressure employed, typically 2.5×10^{-6} torr. Because of the large Brehmstrahlung background beneath the XPS signal, and the low cross section for core electron emission, most of the elemental peaks are scarcely detectable about noise level. The most prominent transitions that were usually observable on the full range spectra are labelled above where they appear in the spectra.

The peak of a given photoelectron transition could be studied in greater detail by means of high resolution spectra. These were made by signal averaging from 10 to 30 scans over a 15 to 30 ev window approximately centered around the peak of interest. High resolution spectra for the C 1s, Ga 3d, Cl 2p and Ga Auger, N 1s, and O 1s transitions are shown in Figure 4.6.3.c through g, respectively.

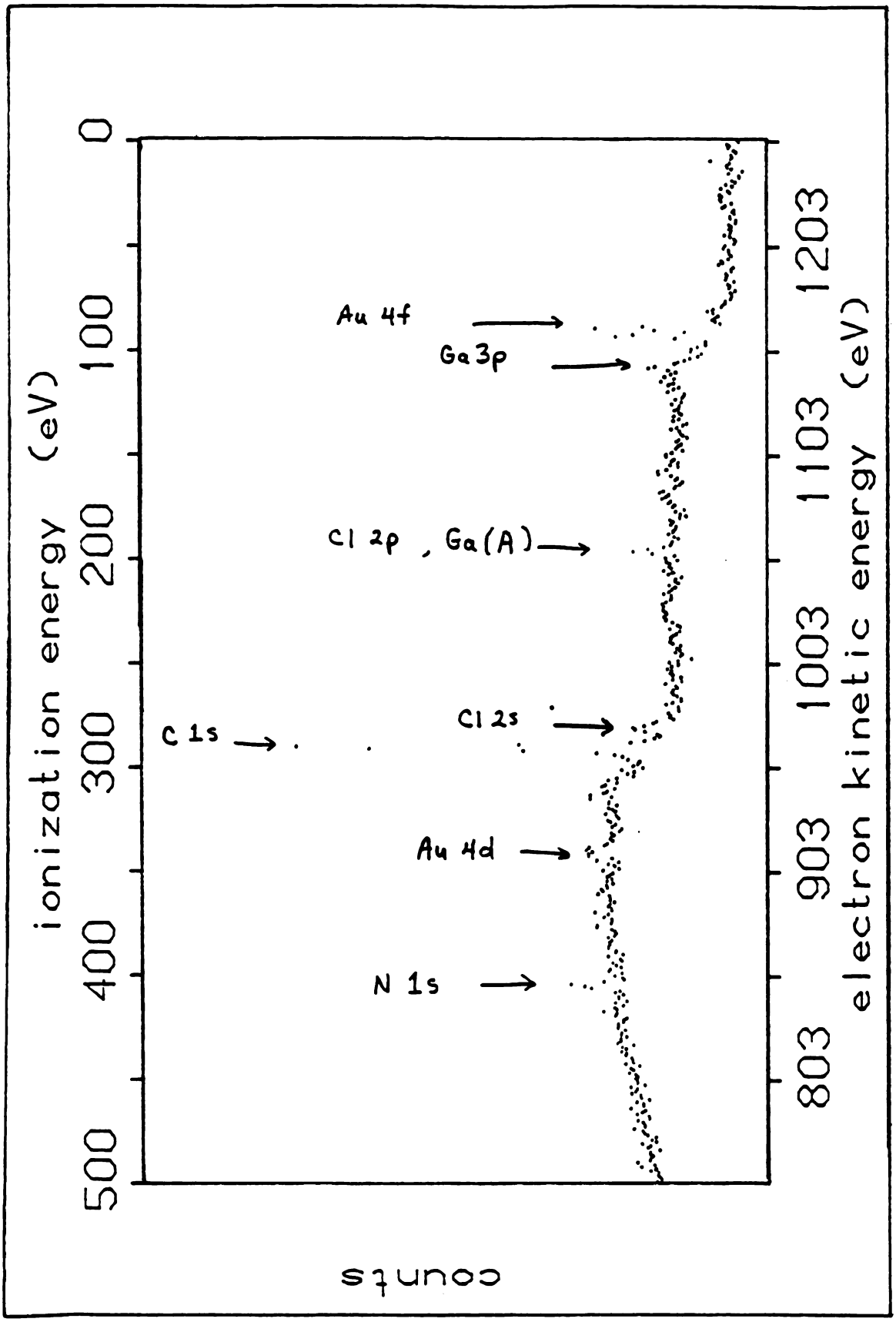

Figure 4.6.3.a: XPS Spectrum of GaPc-Cl/Au-MPOTE: Full Range Spectrum, Low Binding Energy Scale

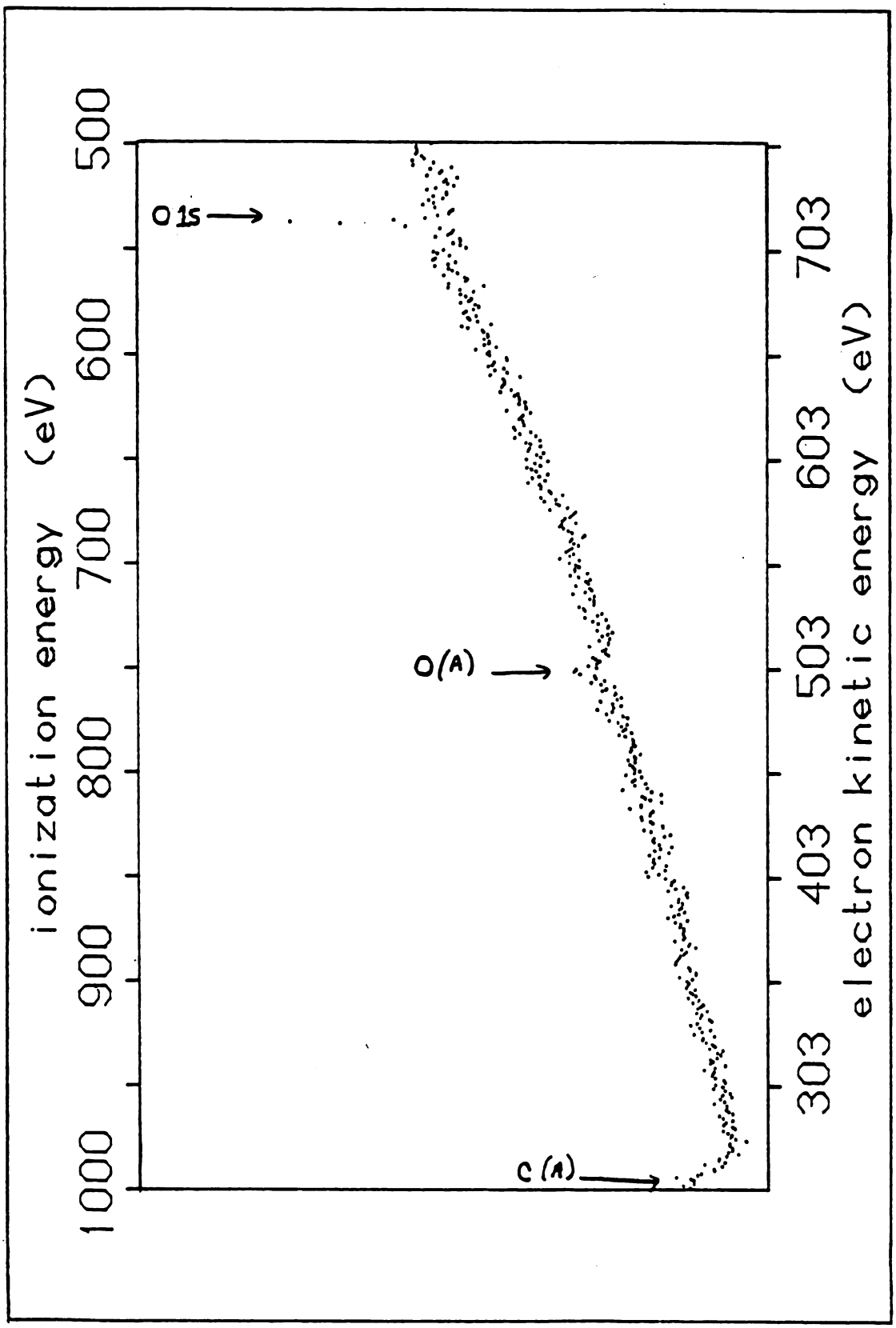

Figure 4.6.3.b: XPS Spectrum of GaPc-Cl/Au-MPOTE: Full Range Spectrum, High Binding Energy Scale

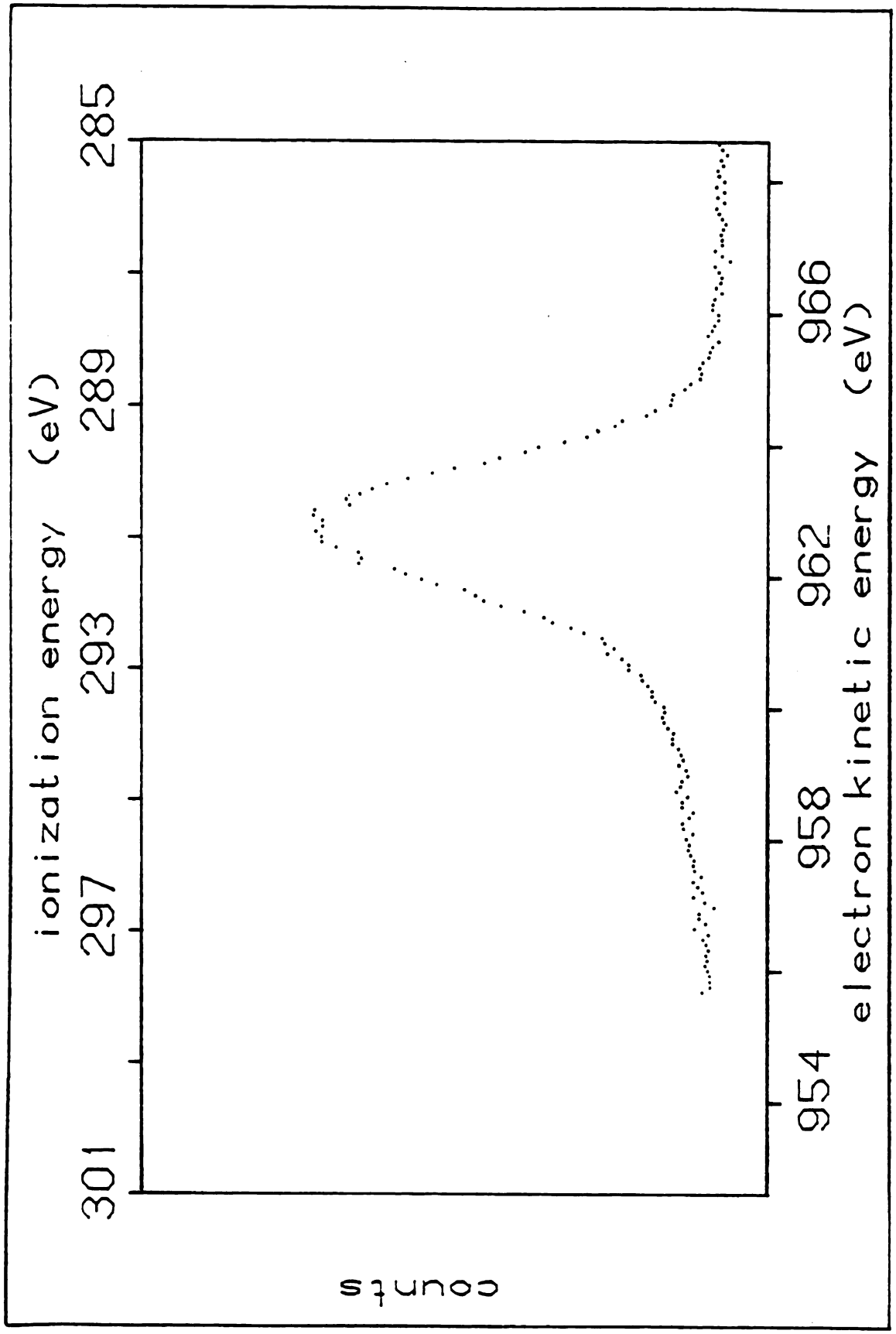

Figure 4.6.3.c: XPS Spectrum of GaPc-Cl/Au-MPOTE: C 1s Transition

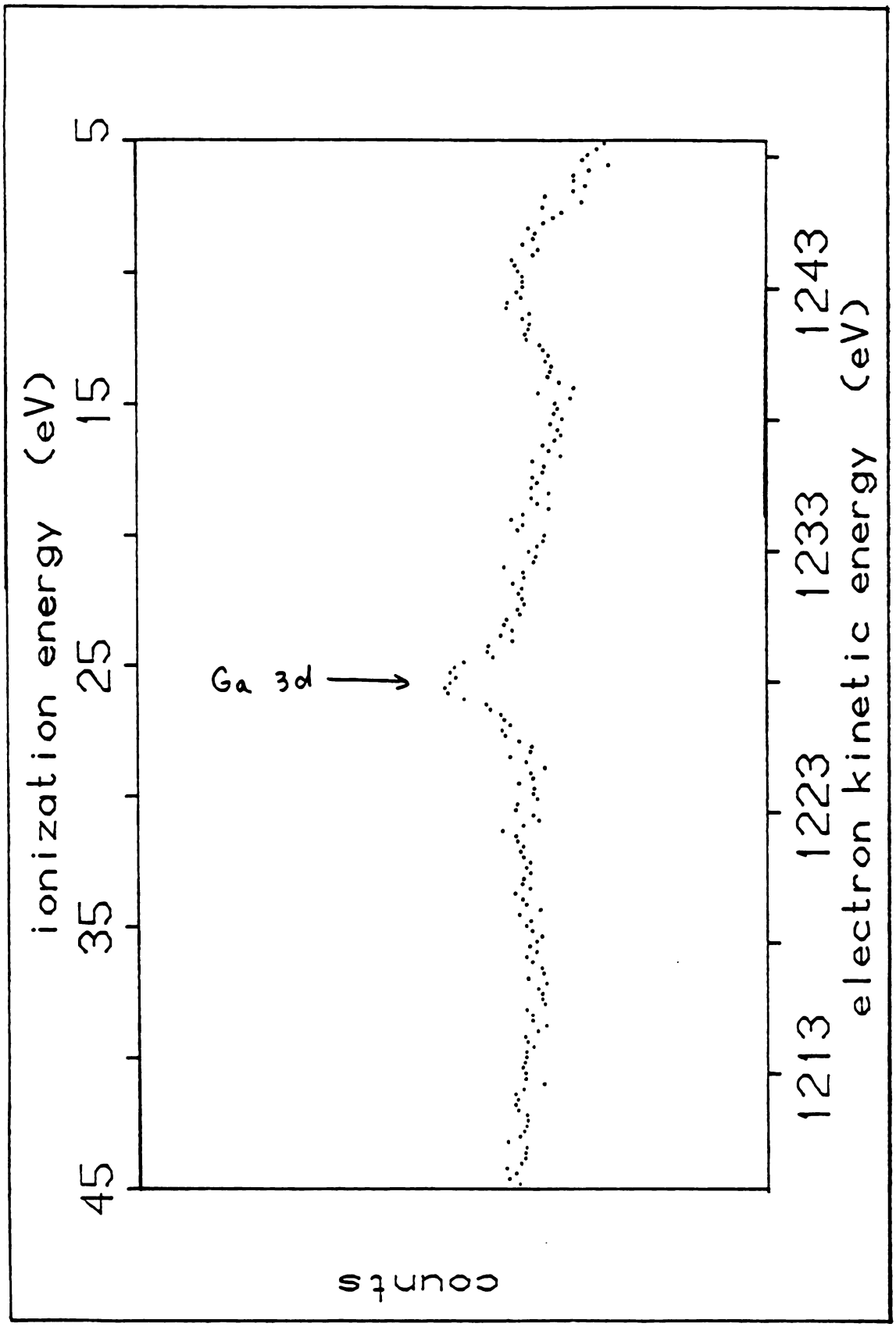

Figure 4.6.3.d: XPS Spectrum of GaPc-Cl/Au-MPOTE: Ga 3d Transition

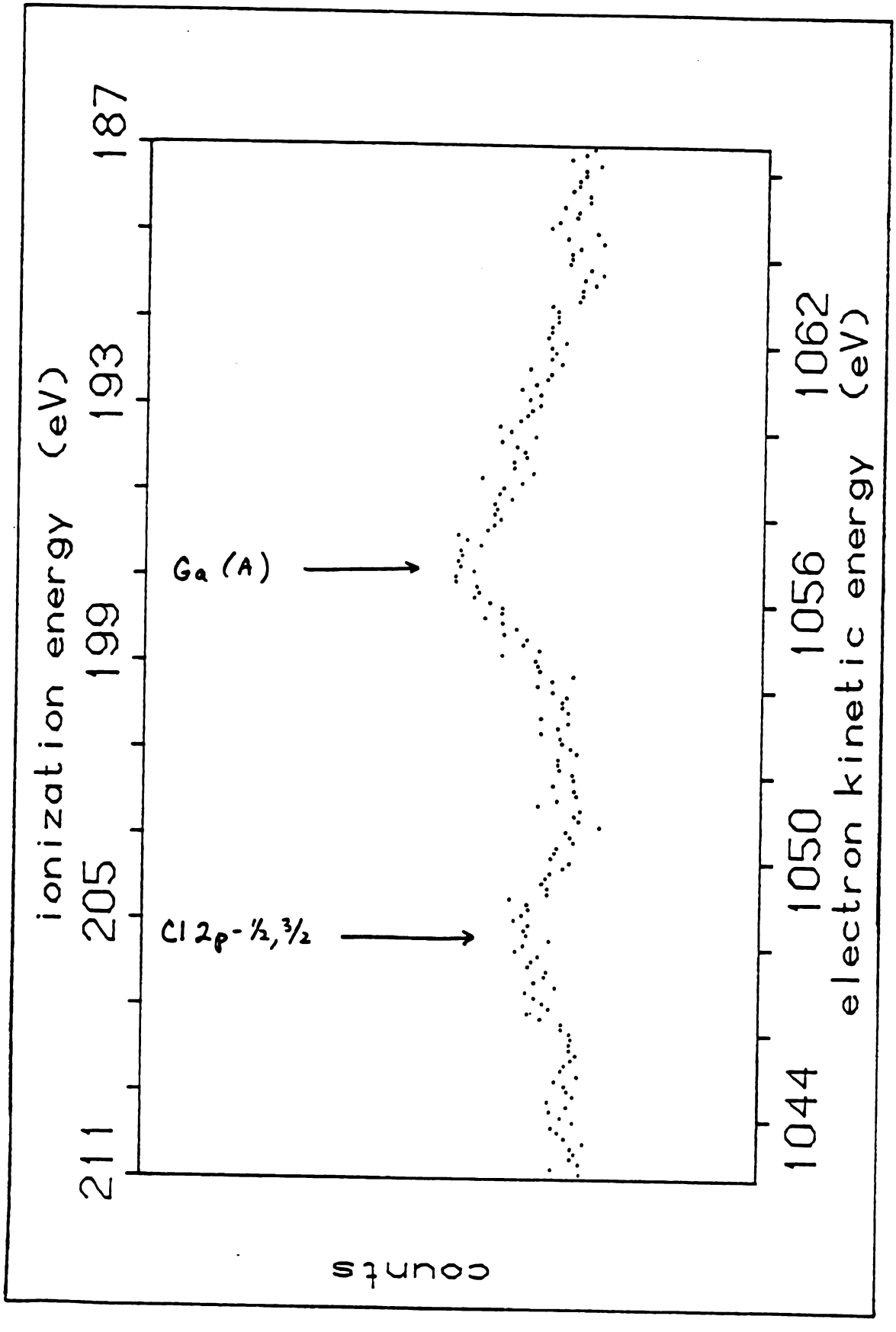

Figure 4.6.3.e: XPS Spectrum of GaPc-Cl/Au-MPOTE: Cl 2p and Ga (A) Transition

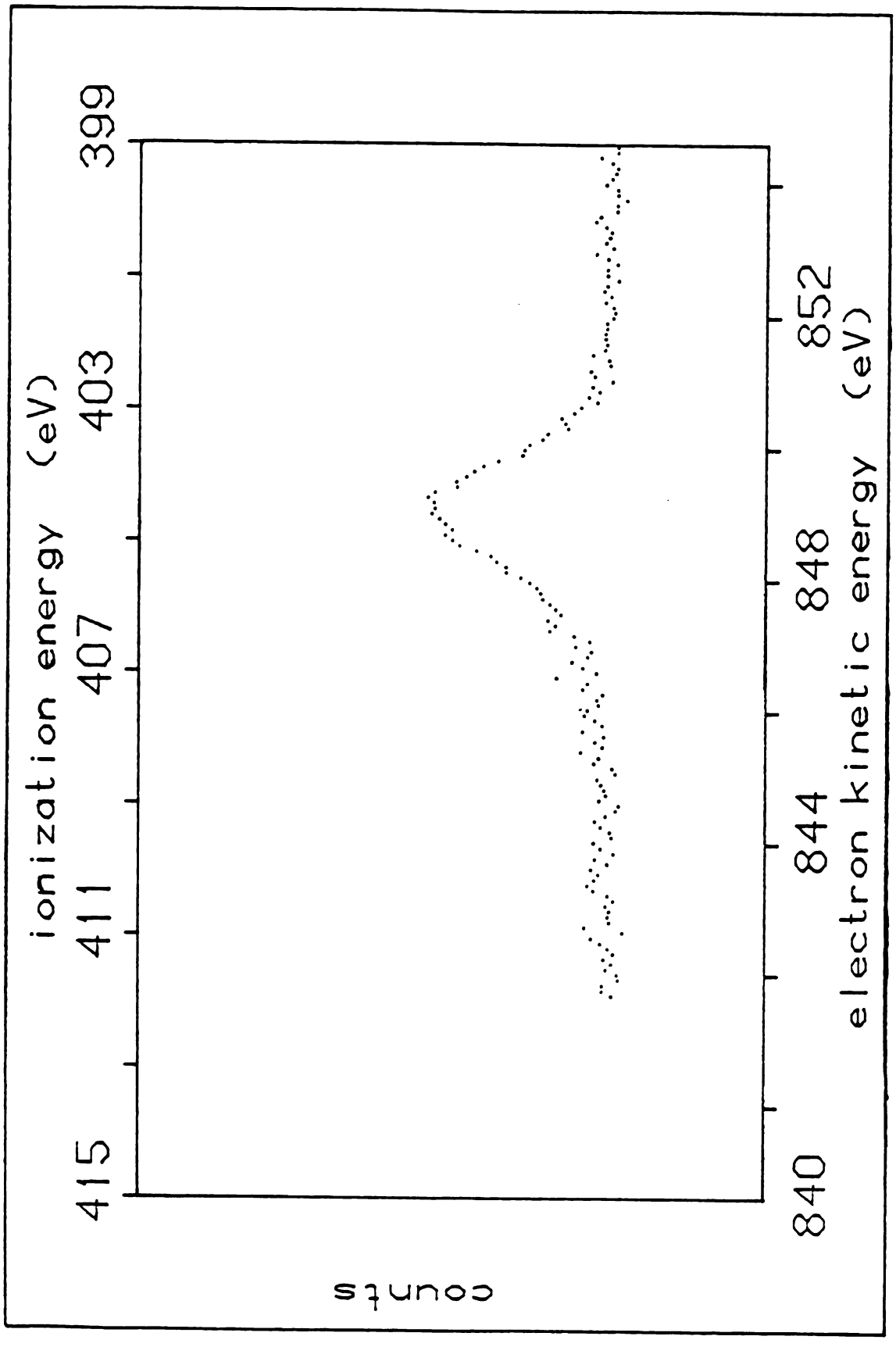

Figure 4.6.3.f: XPS Spectrum of GaPc-Cl/Au-MPOTE: N 1s Transition

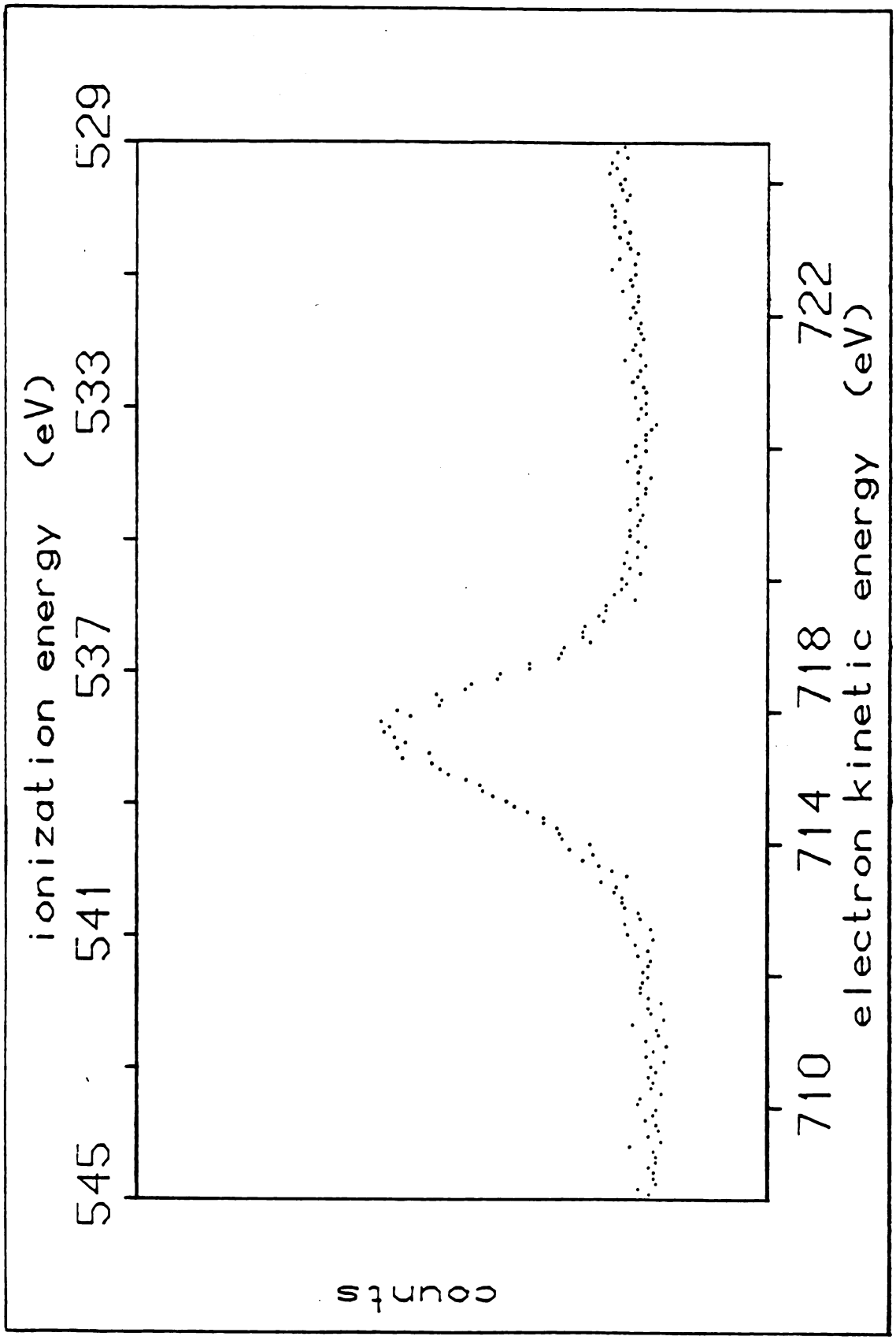

Figure 4.6.3.g: XPS Spectrum of GaPc-Cl/Au-MPOTE: O 1s Transition

In Figure 4.6.3.c, the high resolution XPS spectrum for the C 1s peak of a GaPc-Cl/Au electrode is shown. The literature value for this peak on the binding energy scale (ionization energy) is 285 ev, while in the spectrum the maximum was just under 291 ev, nearly a 6 ev shift. Since C 1s is usually the strongest transition obtained, and since at least a part of it is due to background contaminants, its position is commonly used as an instrumental calibration. While other procedures would have to be adopted if the carbon signal was expected to exhibit chemical shifts, in this case it was considered reliable, especially since the peak maxima in all the other high resolution spectra were from 5 to 7 ev greater than literature values. Therefore, the instrumental calibration factor was taken as -6 ev.

In Figure 4.6.3.d, the high resolution XPS spectrum for the Ga 3d transition is shown. While other, more intense Ga transitions could have been examined by the high resolution treatment, this one was selected because it is a valence band transition, hence any contact of the Ga center with electron-donating or withdrawing groups that would case shifting of the XPS peak would most probably be observed with this transition. The Ga peak was observed at 25 ev, which is 5 ev higher than reference values. Taking the -6 ev calibration factor into account, a possible chemical shift of -1 ev on the binding energy scale was noted. Some additional structure was observed at very low binding energy, but the identity of the broadened peak was not obvious.

The high resolution XPS spectrum for the Cl 2p peak and a Ga Auger peak are shown in Figure 4.6.3.e. The Cl peak is barely noticeable above background as a doublet corresponding to the 2p - 3/2 and 1/2 transitions, normally occurring at 198 and 199 ev, respectively. A Ga Auger transition is observed 8 ev lower at 197 ev, with a literature value of 191 ev. The Ga Auger peak tailed off more slowly on the low binding energy side than on the high energy side, suggesting a small negative chemical shift by a portion of the Ga centers.

The N 1s peak probably exhibits the largest range of chemical shifts of all the elements, covering 11 ev in the solid state (178). With equimolar amounts of bridging and Ga-coordinating nitrogen present, it seemed worthwhile to do a high resolution XPS spectrum of the N 1s signal. The result, however, shown in Figure 4.6.3.g, consisted of a single symmetrical peak with a half-width of about 1.5 ev, centered between 404 and 405 ev, nearly 6 ev positive of its literature value of 399 ev.

One general observation about the high resolution spectra was that they scarcely showed a higher signal-to-noise ratio than the full range spectra. The reason was due to the steady loss of signal due to contamination of the samples and the metal foil window proecting the anode. As shown in Figure 4.6.4.a and b, high resolution spectra of the Au(4f) peaks on the same gold standard taken before and after the GaPc-Cl scans were run show a clear loss in peak height

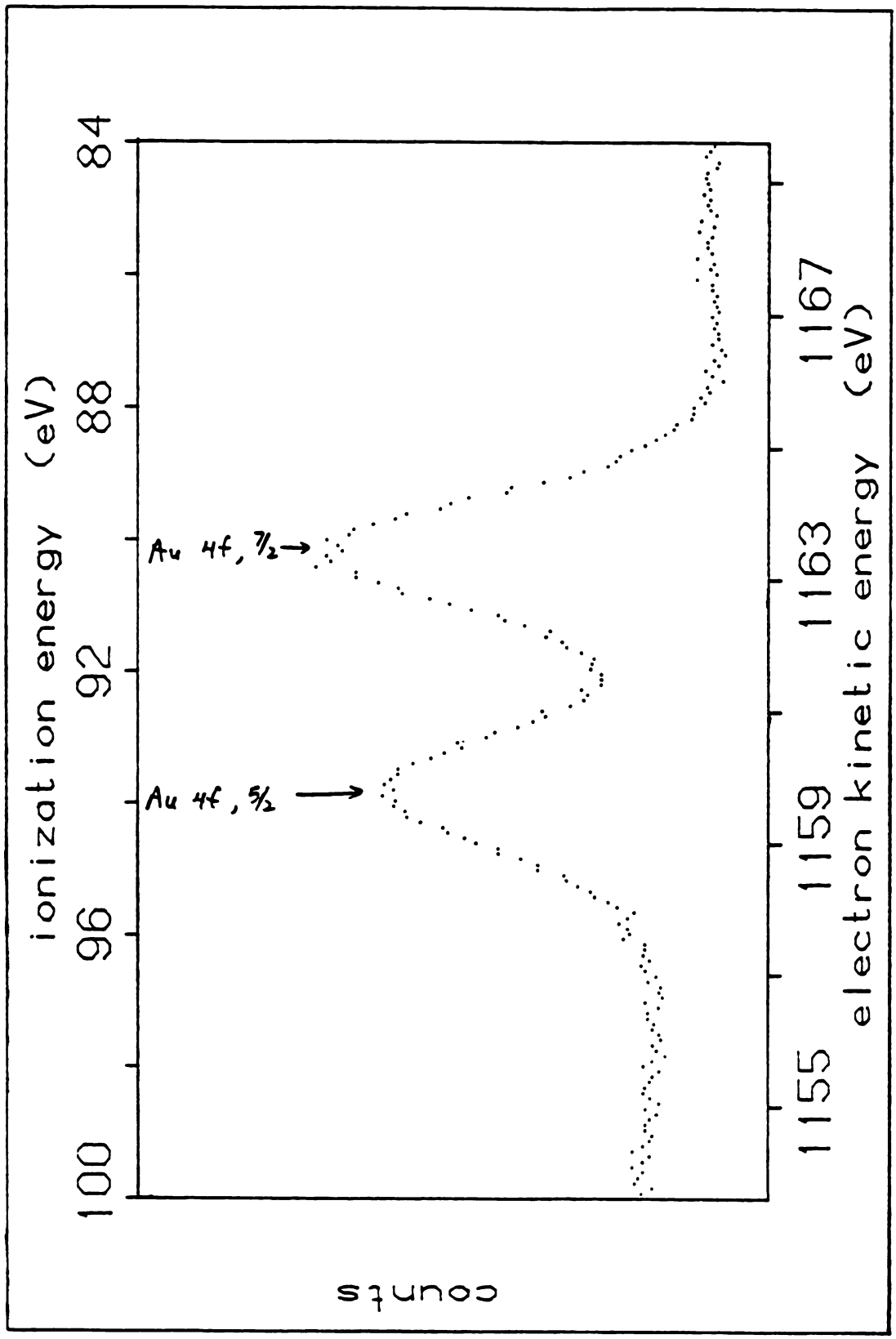

Figure 4.6.4.a: XPS Spectrum of Au 4f Standard: Before GaPc-Cl Scans

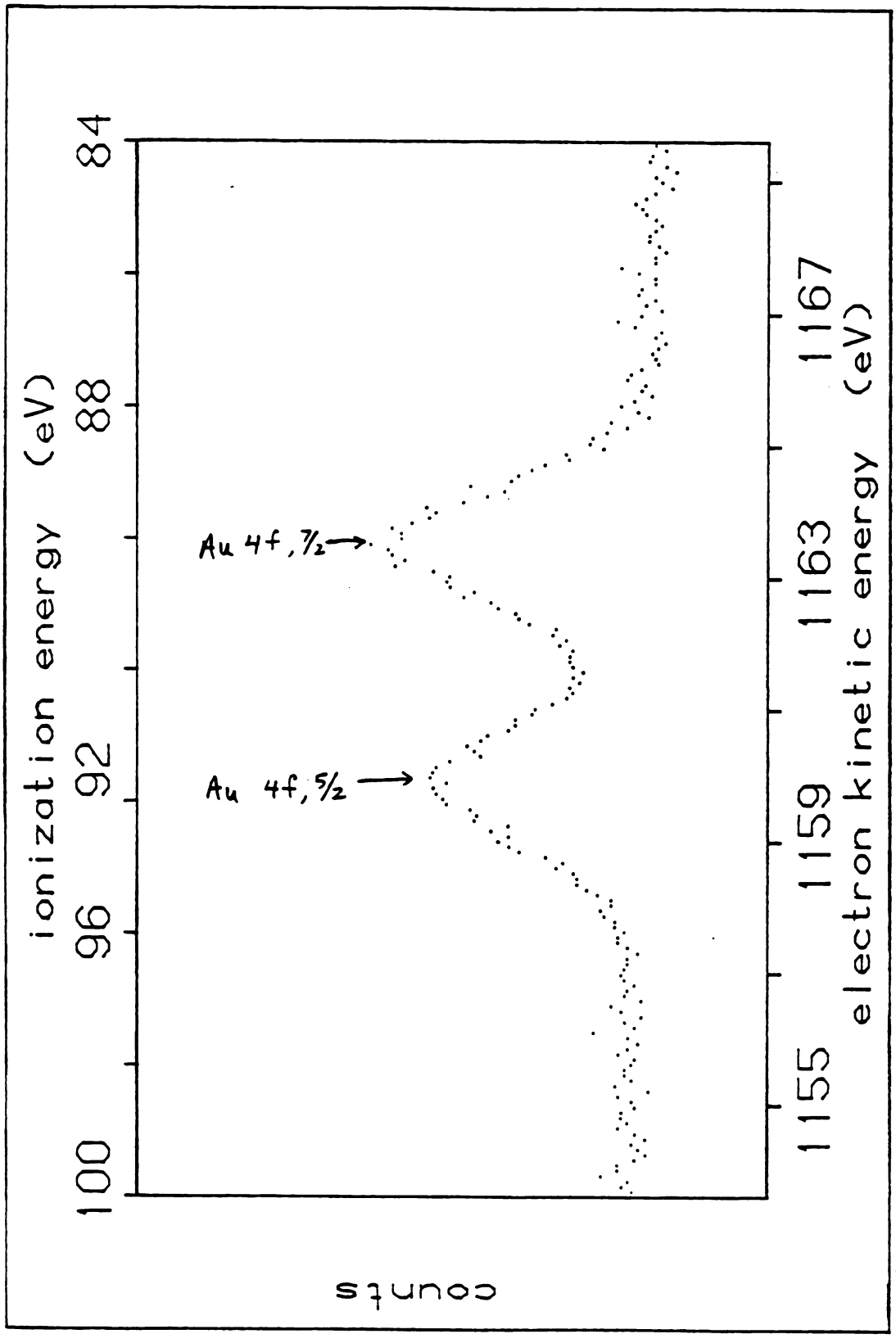

Figure 4.6.4.b: XPS Spectrum of Au 4f Standard: After GaPc-Cl Scans

and resolution. After running several samples, it was noticed that each successive GaPc-Cl/Au sample showed a lower overall signal than the previous one. Examination of the sample chamber revealed the cause: a powdery, gray film had covered the foil window over the anode. Removal of the film with a dry, mildly abrasive cloth restored signal output to original levels. It subsequently became standard practice to clean the anode after every two or three samples.

While the phthalocyanine samples appeared undamaged, they were undoubtedly the souce of material for the gray attenuating film. This could have been effected by emissive heating of the sample by the anode. X-ray production by the Mg anode occurs when the anode is bombarded by a stream of electrons accelerated through high voltage field. The X-ray emission is accompanied by production of large amounts of heat. The excess heat is supposedly carried off by a circulating water line, but unless the system is well designed much of the heat will still be delivered to the sample through emissivity. It is worth noting that the particular anode design employed in this system is not used in any of the commercial XPS equipment currently being sold (187). With an operating vacuum in the 10^{-6} torr range, a localized heating over 200°C would cause resublimation of the GaPc-Cl film. Another associate has observed coatings on the sample carousel and the chamber walls after phthalocyanine samples had been run in this particular spectrometer (188).

The high resolution XPS spectrum of the O 1s transition for GaPc-Cl/Au electrodes is shown in Figure 4.6.3.g. While in principle there should be no signal at all, a relatively large peak was observed inall GaPc-Cl/Au spectra. The signal is mostly attributable to background species, but it is possible that some of it is due to hydroxide ion that has replaced chloride as the axial counterion for the trivalent Ga center. Trace H_2O in the reaction vessel or the $GaCl_3$ ampule itself may have produced some GaPc-OH synthesis. The transition appeared as a single, symmetrical peak 7 ev above the literature value of 531 ev.

The presence of hydroxide ion on the Ga center and the lability of chloride ion were potentially important factors in the electrolysis of H_2O. An experiment was designed to test the ability of one to substitute for the other on the GaPc film surface. Freshly prepared GaPc-Cl films on Au were soaked in 1 m KCl or 1 mM KOH for an hour. A more highly alkaline solution was found to break up the Au-polymer support interface, destroying the electrode. Each sample was thoroughly rinsed with water, dried, and then had an XPS spectrum run on it. High resolution spectra of the Cl 2p signal was obtained for each of the two types of samples. These spectra, shown in Figure 4.6.5., were taken at approximately the same amount of beam time after the anode had been cleaned. A small yet unmistakable Cl peak was observed for the Cl^- soaked sample that was larger than that found for untreated GaPc-Cl samples. A potassium signal was

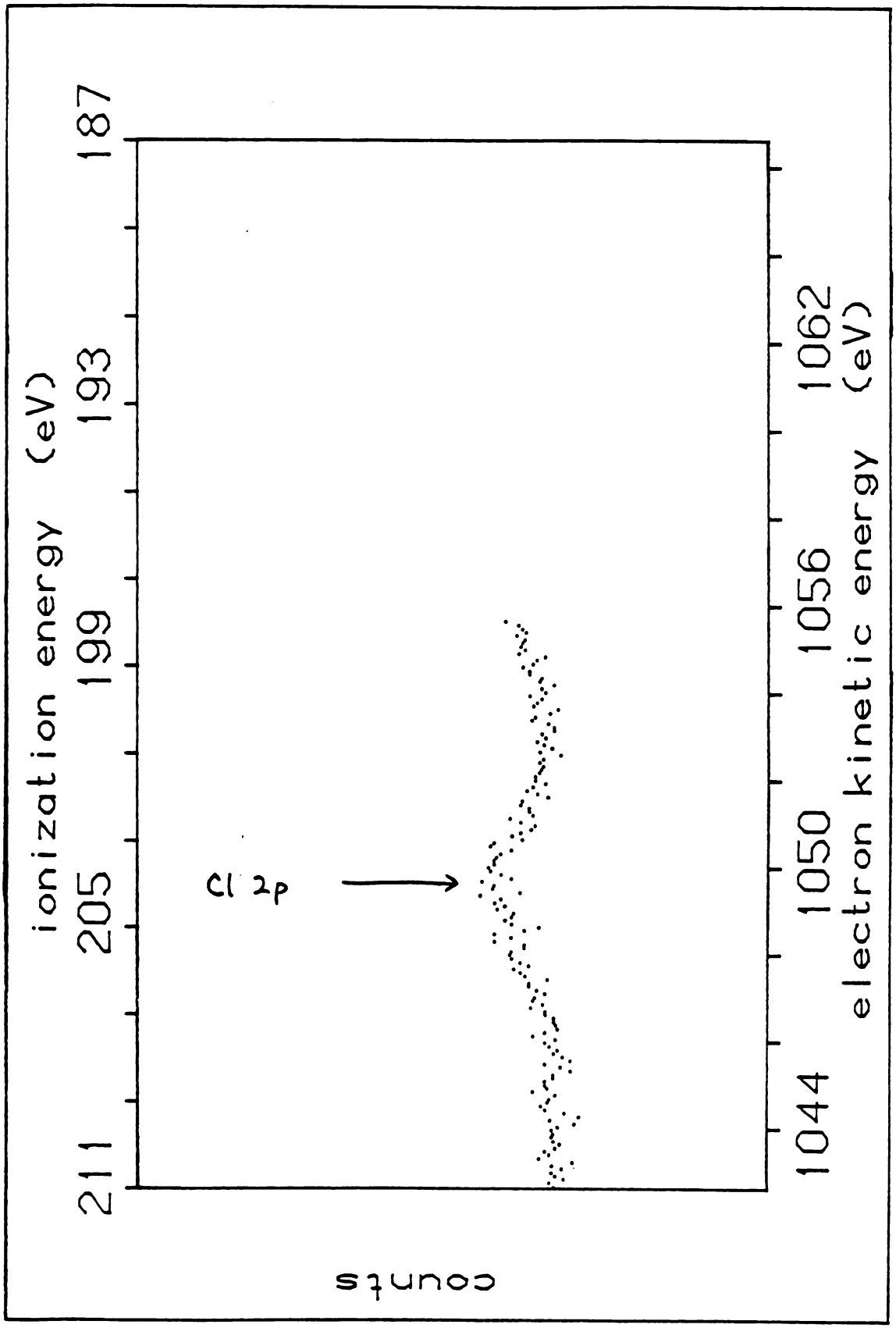

Figure 4.6.5.a: XPS Spectrum of the Cl 2p Transition for GaPc-Cl/Au-MPOTE: After Soaking in KCl Solution

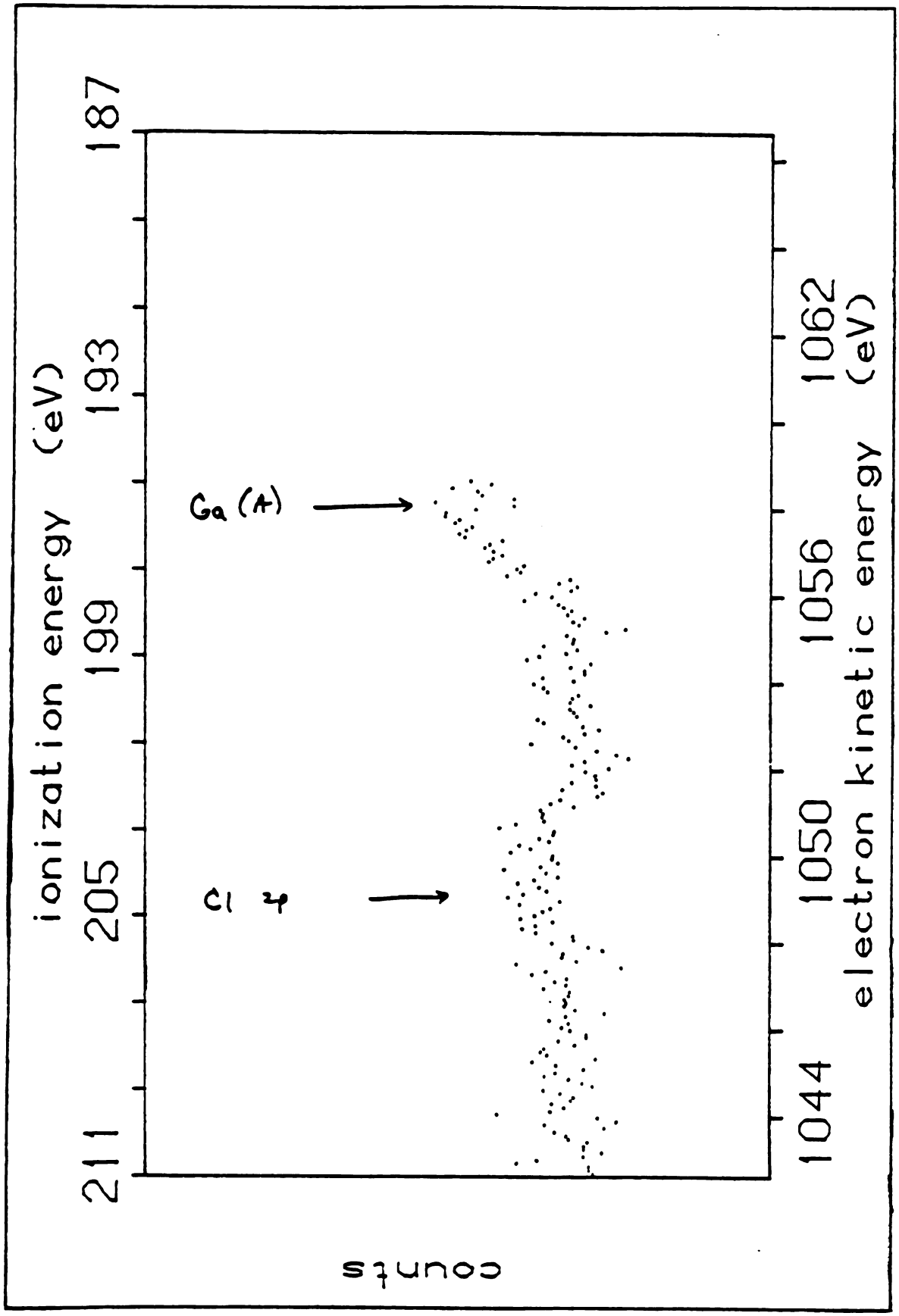

Figure 4.6.5.b: XPS Spectrum of the Cl 2p Transition for GaPc-Cl/Au-MPOTE: After Soaking in KOH Solution

also observed elsewhere in the full range spectrum, however, so whether the films were partly GaPc-OH to begin with is uncertain. The OH^- soaked sample showed virtually no Cl signal above background, indicating substitution of OH^- for Cl^- in the axial counterion position.

An attempt at corroborating this substitution was made by taking high resolution spectra of the O 1s peak for the two samples. These results are shown in Figure 4.6.6. Both spectra consist of single peaks with the same peak position at 537 ev, but the peak for the OH^- soaked sample was decidedly shorter and broader, suggestive of two closly spaced peaks corresponding to O in different chemical environments.

4.6.4. Longevity of GaPc-Cl/Au Electrodes

For device and synthetic applications, it is important to know how long the photoelectrocatalytic properties of GaPc-Cl will hold up under continuous use. This was tested by continuously cycling an irradiated GaPc-Cl/Au electrode around the Q/H_2Q redox couple at 50 mv/sec. The results are shown in Figure 4.6.7. Having set the scan rate and voltage range with a continuous wave signal generator, it was possible to calculate how many cycles had been completed at any given time; however, the rate of reaction became progressively slower, thus requiring adjustment of the cycle limits to include the entire voltammogram. Excluding the

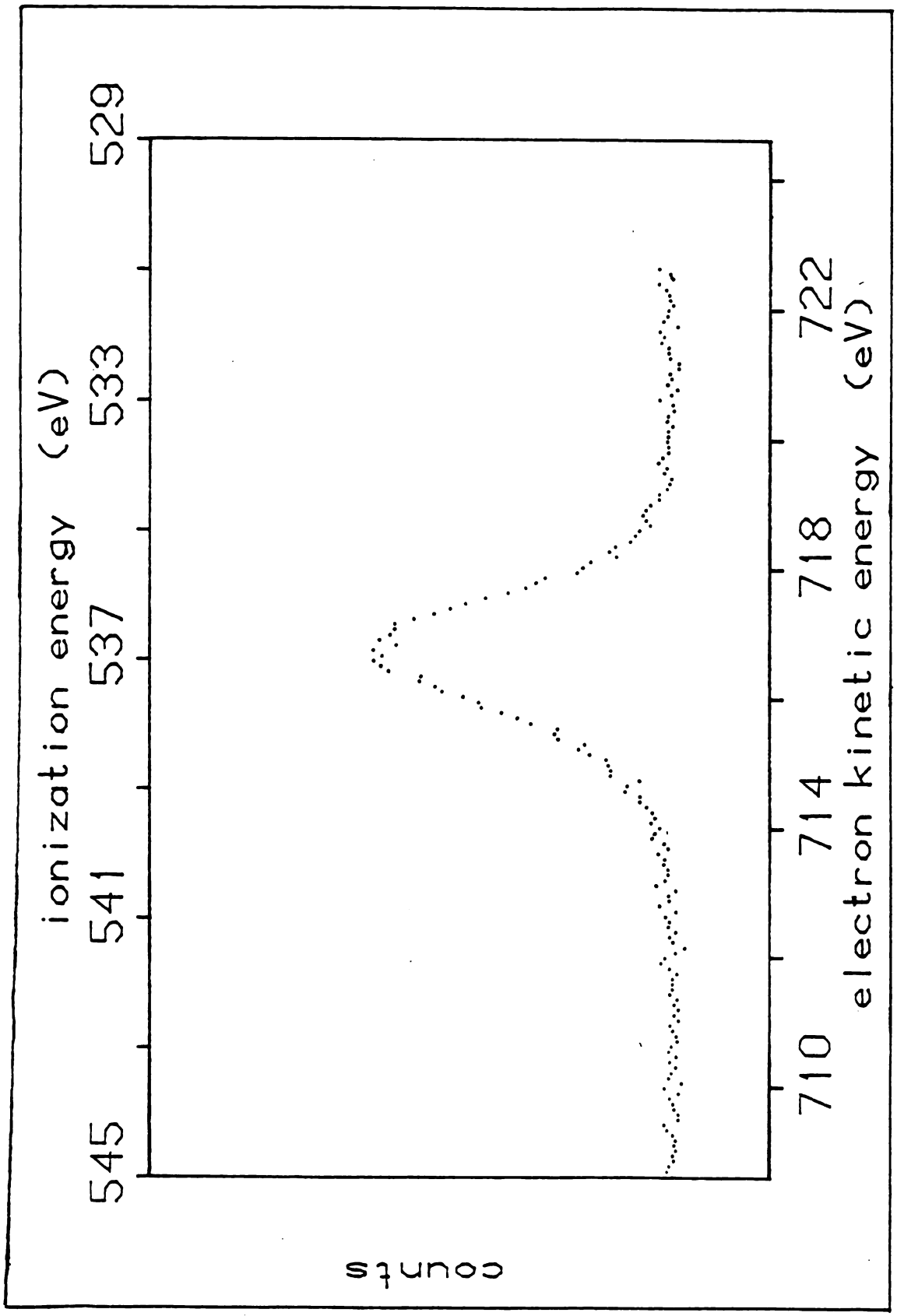

Figure 4.6.6.a: XPS Spectrum of the O 1s Transition for GaPc-Cl/Au-MPOTE: After Soaking in KCl Solution

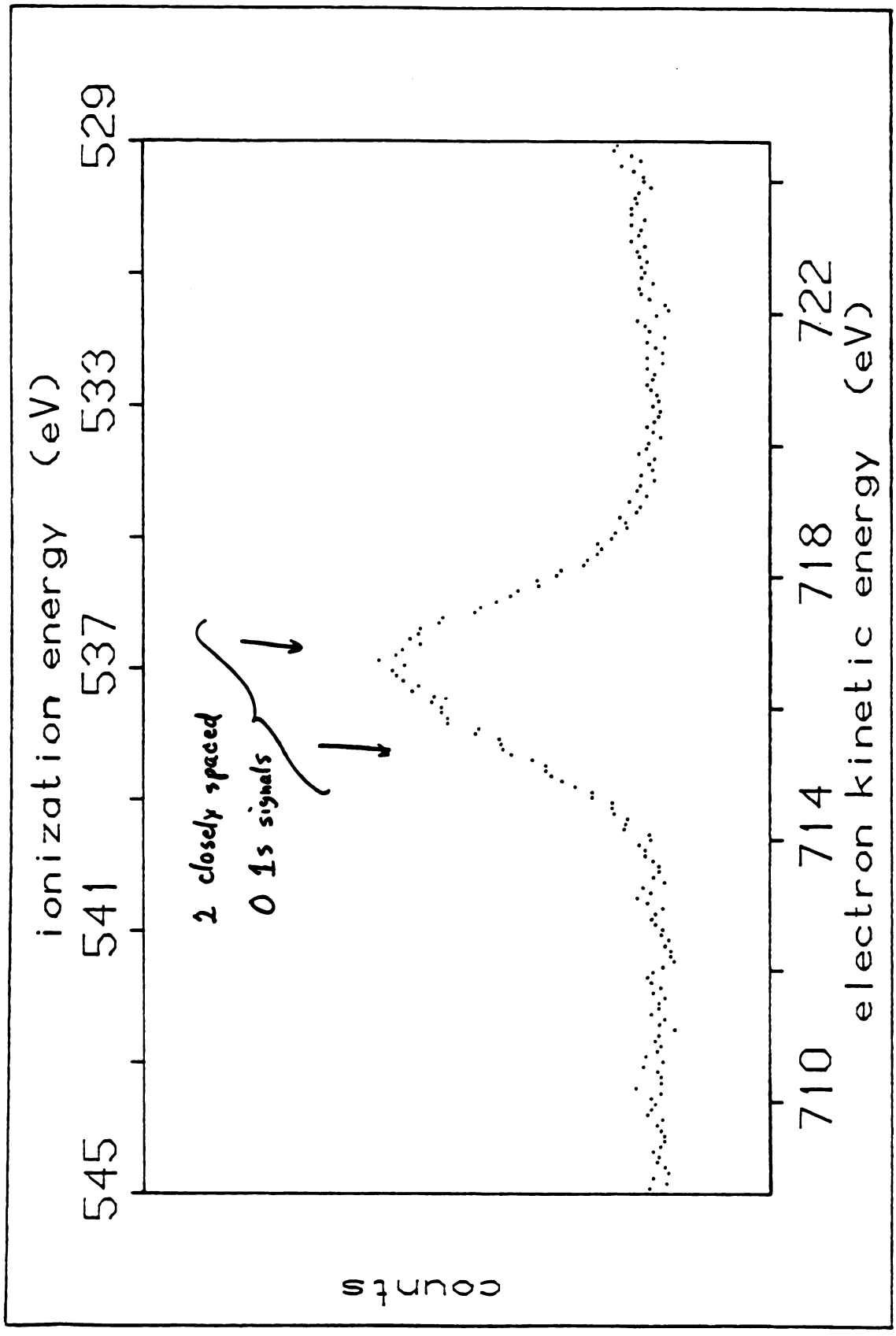

Figure 4.6.6.b: XPS Spectrum of the O 1s Transition for GaPc-Cl/Au-MPOTE: After Soaking in KOH Solution

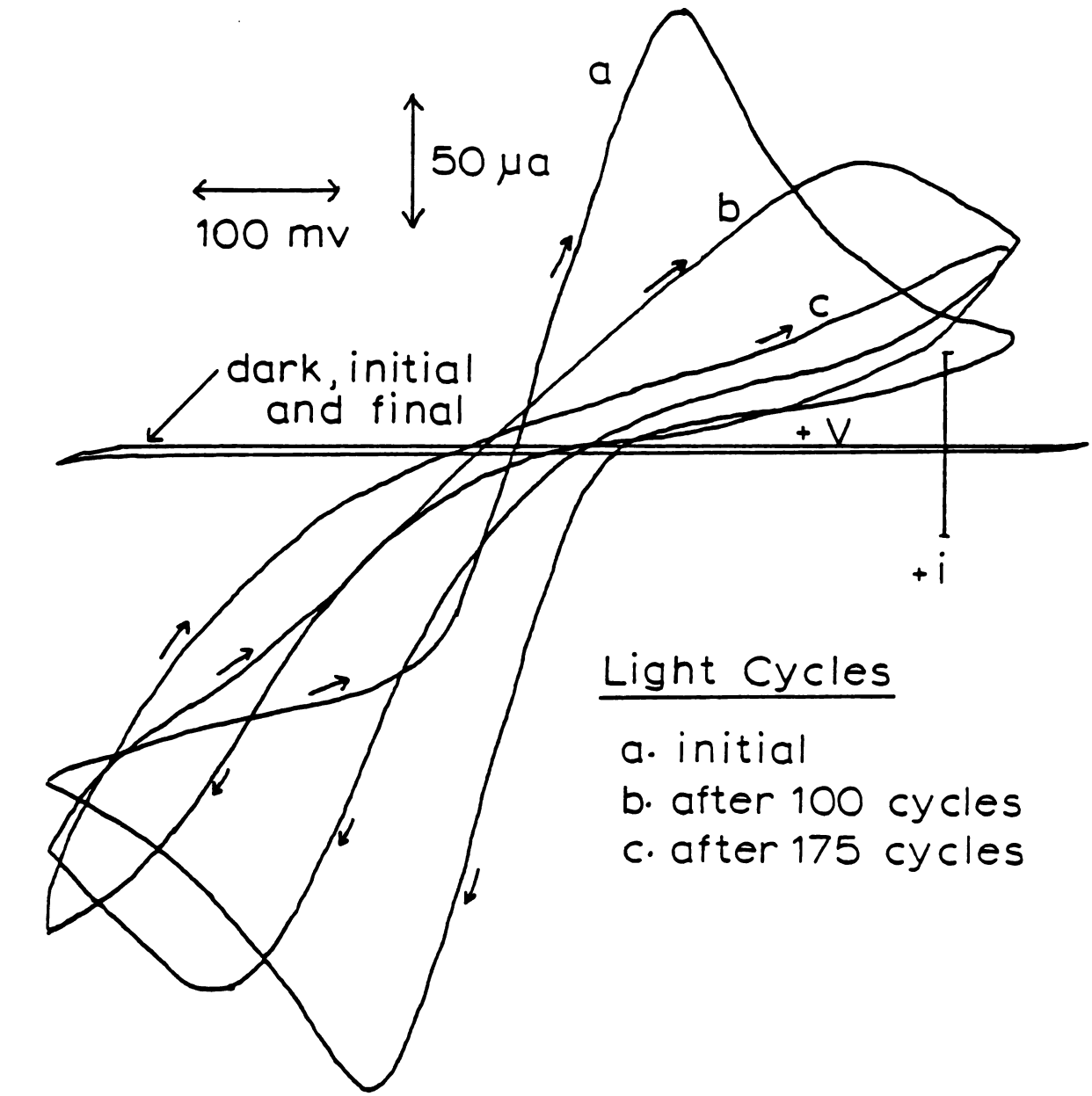

Figure 4.6.7: Degradation of GaPc-Cl Surface Under Continuous Cycling

delays for signal generator readjustment, during which the electrode was still irradiated, the electrode was cycled 200 times over a 1.5 hour period. The peak to peak separation had increased with each successive cycle from an initial 200 mv to 750 mv for the 200th cycle.

Upon removal the electrode did not appear any different from its initial state, indicating no significant loss of phthalocyanine material. The passivating process then may have been due to an adsorbed overlayer. Soaking in water for days, however, did not change the passivated state of the cycled electrode. Solvent extraction in acetone may have removed an overlayer, but this also desorbed or solvated most of the GaPc-Cl film material. Ultrasonication was not attempted since it had previously been shown to disintegrate GaPc-Cl films.

The indication was that the faradaic process itself had altered the GaPc-Cl surface structure. It was thought that perhaps an adverse chemical reaction had been operating briefly at the far anodic end of each cycle, which had a cumulative effect after 200 cycles. Therefore, a different kind of longevity experimnt was run in which the steady state photocurrent at low overpotential was observed with respect to time on a strip chart recorder. A GaPc-Cl/Au electrode was selected whose absorbance maximum was small enough to be measured on the spectrophotometer.

Cyclic voltammograms taken in a H_2Q solution before and after 2 hours continuous electrolysis are shown in Figure

4.6.8. Dark traces made before and after showed that the electrode maintained its nonporosity. A decrease in rate of H_2Q electrolysis, although not as severe as for the cycled electrode, was observed. Before and after spectrophotometry on the electrode showed no more than a 5% loss of material, which could be explained by mechanical damage caused by compression of the rubber O-ring against it in the electrochemical cell. The steady state photocurrent was examined for any kind of first order decay process by a ln i vs t plot, but only a poor fit with the data was obtained. A second order dependence also gave a poor fit. The entire cell felt quite warm at the end of the 2-hour period, so a gradual heating of the electrochemical reaction may have perturbed any obvious decay characteristics. A final possibility was that there was a slow depletion of H_2Q in the cell, perhaps due to solution oxidation by trace O_2.

A turnover number (number of electrons injected/number of reacting dye molecules) was calculated. Based upon the total number of dye molecules in the film, the turnover number was 24; however, based upon the number of dye molecules on the outermost monolayer in contact with the solution, the turnover number was 2373.

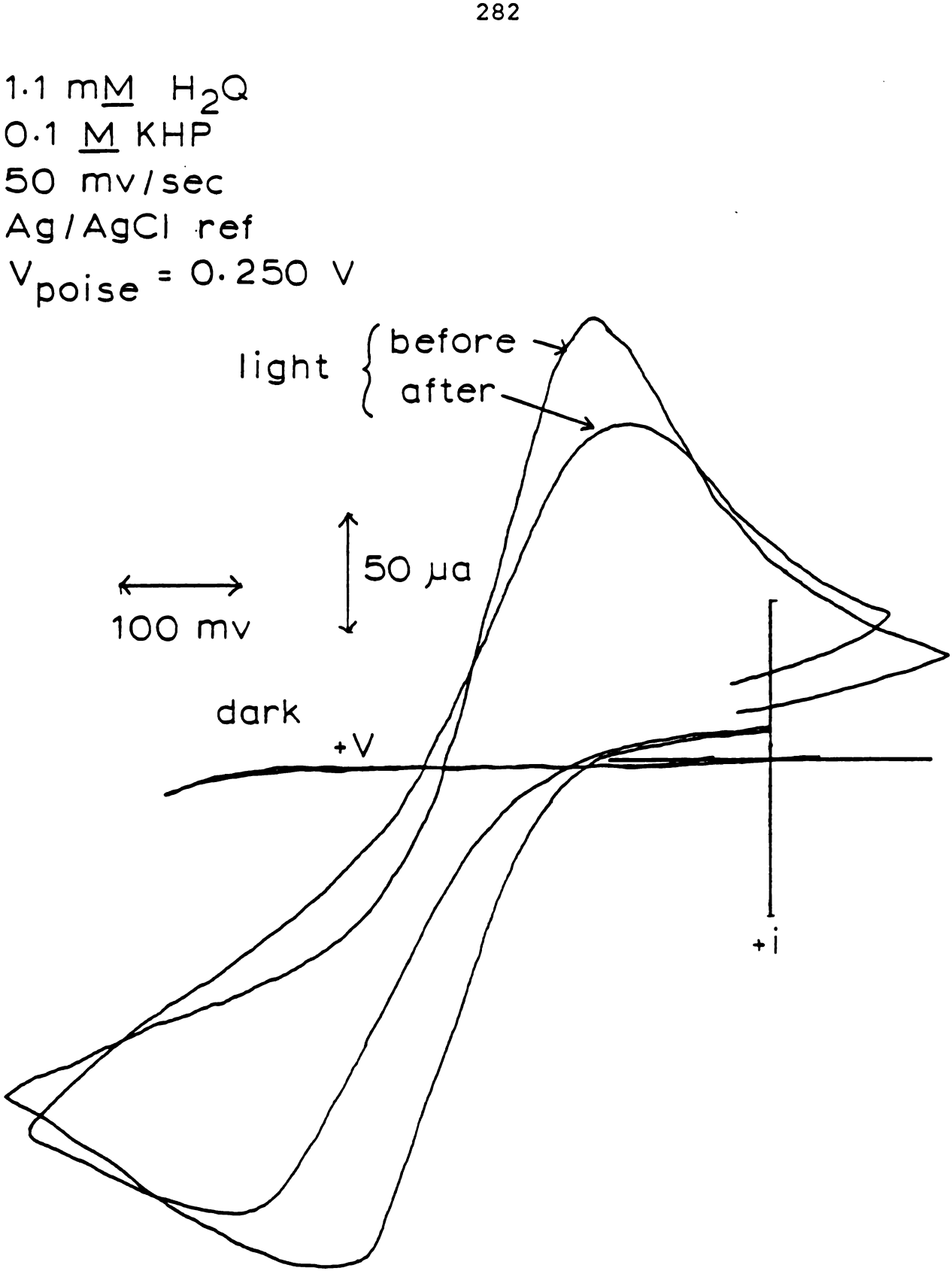

Figure 4.6.8: Cyclic Voltammograms of GaPc-Cl/Au Before and After 2 Hours Electrolysis Time

5. DISCUSSION

5.1 Correlations Between Spectroscopic, Voltammetric, and SEM Results

When it was first observed that SiPc and GaPc-Cl differed in their photoelectrocatalytic ability (Figure 4.2.1.), a question arose about whether either one represented a trend in the voltammetric behavior of phthalocyanines. To answer that question, eight other phthalocyanine derivatives were tested. It is clear that GaPc-Cl is not representative of phthalocyanine voltammetric behavior (Figure 4.2.3.a); in fact, only one other derivative, GaPc-I (Figure 4.2.3.d) exhibited the same voltammetric behavior as GaPc-Cl. This behavior consisted of fast, equally reversible electrolysis in the light, and negligible activity in both cathodic and anodic regions in the dark.

A general trend in phthalocyanine voltammetry was hard to find. The best that can be concluded from the nine derivatives tested is that four general categories can be described:

(1) Light-activated, reversible electrochemistry, no dark activity: GaPc-Cl and GaPc-I.

(2) Reversible or nearly reversible electrochemistry in the light, with less reversible electrochemistry in the dark: GaPc-F and AlPc-Cl.

(3) Light and dark redox reactions equally reversible for oxidation, but a large difference in reversibility for reduction: H_2Pc, CuPc, and VOPc.

(4) Little difference between light and dark voltammetry: FePc and CoPc.

The voltammetric response for SiPc/Au electrodes in H_2Q electrolysis is negligible in the dark, but in the light can be thought of as being the same as the anodic SiPc/SnO_2 response (shown in Figure 4.2.1.) in both cathodic and anodic regions, with the crossover point occurring near the dark E°' for H_2Q (189). Thus putting SiPc on Au resulted in a great increase in cathodic activity with respect to SnO_2. Except for the unusual current trace on the return sweep (Figure 4.2.1.) which follows the outward sweep, the voltammetric behavior of SiPc on Au resembles most clearly those Pc's in category (1).

The determination of whether the dark currents observed on some of the Pc derivatives are due to electrolysis on the phthalocyanine electrode or on the Au substrate via pores in the Pc film is difficult in some cases. Comparing the plain Au oxidative response to that of some of the phthalocyanine electrodes in the dark, such as H_2Pc (Figure 4.2.3.e), yielded no appreciable difference in voltammetric shape and position. In the specific case of H_2Pc, however, the fact that the first light wave of the cathodic sweep grew at the expense of the second wave, which appeared also in the dark,

is a strong indication of a redox reaction occurring in parallel at two interfaces on the porous electrode. In other words, under high illumination, the H_2Pc layer is activated, reducing Q at such a rate that the reaction becomes mass transport limited. Under those conditions, most of the quinone that reaches the front electrode surface, or the Pc/ electrolyte interface, has reacted, leaving little or none fo the Au/electrolyte interface, or rear surface. In the dark, the phthalocyanine front surface is inactive, and so Q may approach the rear Au surface and react at a rate corresponding to the dark voltammetric wave in Figure 4.2.3.e. A schematic diagram which depicts the dual interface effect is shown in Figure 5.1.

For electrodes in category (3), the dark current must be due to the Pc film itself, because the reaction of H_2Q proceeded faster than the reduction of Q. If an area of the Au substrate were exposed, it would react with Q and H_2Q at basically the same rate, as shown in Figure 4.1.1. These electroddes also must justify the characterization of phthalocyanines as p-type semiconductors, since they exhibit large negative photocurrents with little difference between light and dark in the positive region.

Dark currents for AlPc-Cl are probably a mixture of processes occurring at both front and rear interfaces at nearly the same rate. That would explain why both the cathodic and anodic waves in the dark appear broadened and flattened.

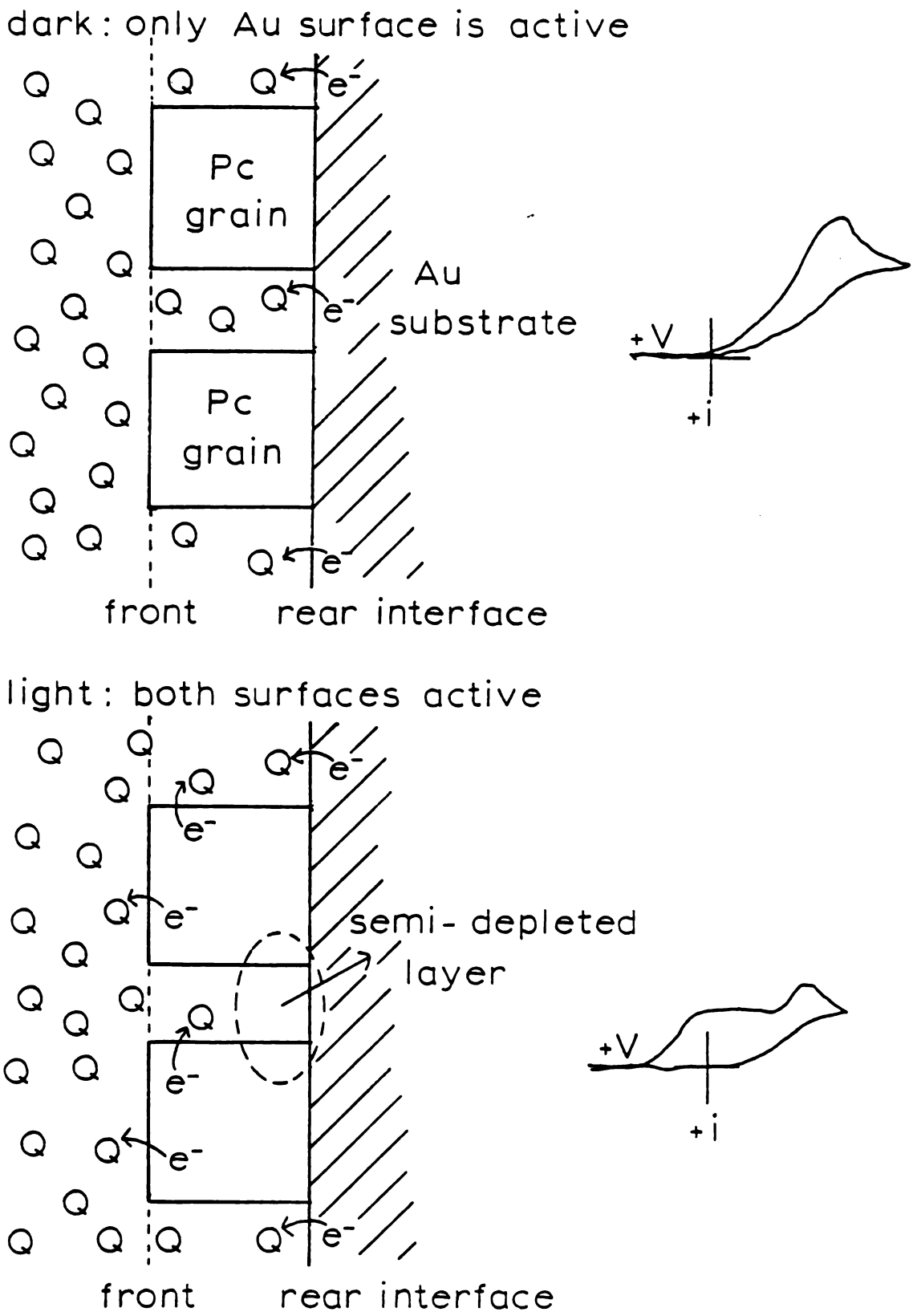

Figure 5.1: Dual Interface Effect on Voltammetric Waves

The two most difficult cases to explain are CoPc and FePc of category (4). Both light and dark voltammetric waves appear poorly reversible, so that the contributions of either surface to the current cannot be separated. The most reasonable interpretation, however, is that the dark trace is due to a reaction on Au alone, and the light trace is the sum of the dark reaction on Au plus a small photocurrent on the Pc surface under illumination. This explanation is preferable to one which assumes that the light reaction on the Pc surface proceeds at the same rate as the dark reaction on Au; in that case, some degree of flattening and broadening in the light voltammogram similar to that seen in the dark voltammogram of AlPc-Cl should be expected, since the light activated Pc surface would not be reactive enough to keep redox species away from the Au surface. The scanning electron micrographs gave no help in determining which films were porous. While the degree of crystalline order and size and shape of observable features varied greatly from one Pc derivative to another, they all appeared to be continuous films. The 31,000x micrographs could resolve details down to the 0.05 μm, or 500Å level in some cases, with no indication of film discontinuity.

The solution phase electronic absorption spectra are basically the same in appearance, with the metal center shifting the Q band maximum to a characteristic λ between 650 and 700 nm. The solid phase spectra, however, could be easily categorized into two separate groups, those which were

red-shifted with respect to their solution spectra, and those which were not. The Pc derivative which possess axial groups (GaPc-Cl, GaPc-I, GaPc-F, Al-Pc-Cl, and VOPc) were in the red shifted group, and the rest which did not possess axial groups or counterions were in the other group. The correlation between red-shifting and axial groups is potentially informative, but many more Pc derivatives need to be tested to be certain of this effect. A red-shifted spectrum gave little indication as to whether the film would be porous or highly ordered, but could be associated with reversible light-activated electrochemistry. However, reasonably reversible light response was observed in six out of the nine Pc derivatives in three out of four voltammetric categories, so this is not an exclusive correlation.

Although the SEM pictures only proved GaPc-Cl and GaPc-I to be crystalline in nature, it would be incorrect to conclude that the other films were amorphous. In reference 175, X-ray crystallographic and optical absorption data were presented side by side for, among others, α phase Cu, Co, H_2, and VOPc. The spectroscopic data for those phthalocyanines agreed well with this work, as did the means of preparation. We can conclude then that all the phthalocyanines examined were α phase. Thus, the lack of crystalline structure in the SEM pictures means only that the grains are too small to be resolved at the usable magnifications. Judging from the voltammetric results, grain size does not appear to be much of a determinant in light voltammetric response.

The lack of correlation between film surface morphology and light voltammetric response was found not only for different phthalocyanines on the same substrate, but also for the same Pc on different substrates. Comparing Figures 4.4.10.b and d, a great difference in film morphology and grain size is observed for GaPc-Cl films on Au and SnO_2, yet their photoelectrocatalytic ability is quite comparable. Electron micrographs taken of SiPc/SnO_2 electrodes which gave results as in Figure 4.2.1. were featureless -- the micrographs of the SnO_2 substrate and the SiPc/SnO_2 electrode appeared identical (190).

By far the most outstanding correlation in the voltammetric and SEM results is the similarity between GaPc-Cl and GaPc-I, and the dissimilarity between GaPc-Cl, GaPc-F, and AlPc-Cl. In terms of crystalline structure, one would expect AlPc-Cl to be most likely to imitate GaPc-Cl, since they have the same axial counterion, thus eliminating any kind of lattice spacing effect. Any type of chemical behavior that could be related to Pc crystal structure such as coordination of H_2O, ability to form halides, hydroxides, or nitrides, or form organometallic compounds is virtually the same for Al and Ga (191).

The fact that GaPc-F is unlike GaPc-Cl or GaPc-I in structure or at least in degree of order implies the existence of a size effect in axial counterion in determining crystalline structure. Indeed, GaPc-F supposedly forms a stacked polymer with F^- ions as bridging groups between metal

centers, while GaPc-Cl and GaPc-I do not (55). However, nothing in the spectroscopic, voltammetric, or SEM results would suggest higher order or unique crystalline structure for GaPc-F in comparison to other related Pc derivatives.

One difference of potential importance is that the group III metals differ in their preference for four-coordinate or six-coordinate solid state structures for the trihalides. Al prefers a coordination number of six for Cl, while Ga prefers four (191). $AlCl_3$ forms a monoclinic crystal of space group c2/m, and could be described as a slightly distorted NaCl crystal with two-thirds of the metal atoms omitted (192). The trichloride of In, which is one period below Ga in column III of the Periodic Table, also forms the six-coordinate, monoclinic crystal, although the lattice parameters are slightly larger than for $AlCl_3$. $GaCl_3$, on the other hand, crystallizes in a four-coordinate bridged dimer structure of D_2h symmetry (193), where each Ga center has a distorted tetrahedral geometry:

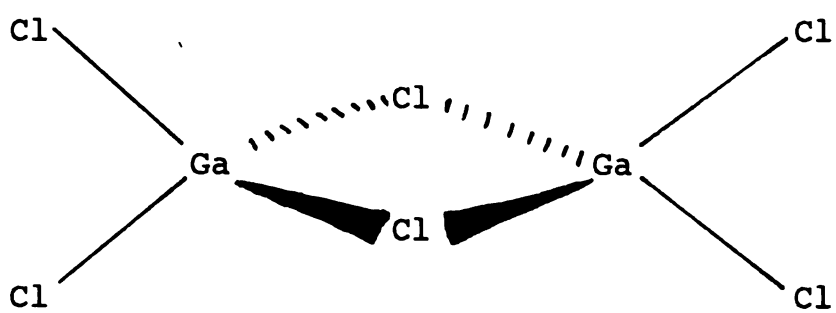

All the Group III fluorides are 6-coordinate, while all Group III iodides are four-coordinate (191). Thus there is a correlation between size of the halide and the coordination state of the metal. Ga demonstrates a distinct preference for the four-coordinate scheme, breaking the periodic trend in six-coordinate trichloride structure.

This effect could be transferred over to the stability of Group III phthalocyanine halides. Al and Ga may fit comfortably into the phthalocyanine macrocyclic ligand when paired with Cl^- and F^-, respectively, but when the F^- counterion on GaPc is replaced by Cl^- or I^-, an instability results for which a different crystalline structure is more stable. This effect is in accord with the X-ray crystallographic observation that the fluoro forms of AlPc and GaPc stack in a cofacial, F-bridged structure, while the other halides do not (55). This may also explain why incorporation of nonstoichiometric amounts of I_2 into a Group III phthalocyanine and other group phthalocyanine lattices tends to form an anisotropic conductor with segregated stacks of Pc molecules and I_3^- ions (51).

The spectroscopic, voltammetric, and electron microscopic results point to a unique crystalline structure for GaPc-Cl and GaPc-I, whose electronic band structure and/or surface morphology prevents the dark electrolysis of H_2Q and Q. There is little precedent for this conclusion, however. M.E. Kenney(55), in articles concerning studies on Group III phthalocyanines, described the structure of AlPc-Cl

and GaPc-Cl as "ordinary, square-pyramidal phthalocyanine complexes," with no published structural data. He found the triiodide of AlPc to be likewise. No comment has been made about the structure of stoichiometric GaPc-I. Also, ionization potential data suggests that conduction and valence band edges are basically insensitive to changes in metal center, so that all phthalocyanines have basically the same band structure (194).

5.2 Mechanism of Photoelectrolysis

The original intent in preparing GaPc-Cl electrodes from metallic substrates was to show the importance of a semiconductor substrate; in other words, GaPc-Cl/Au and GaPc-Cl/Ag electrodes were supposed to perform poorly by exhibiting very low photocurrents, as opposed to GaPc-Cl films on semiconductor substrates which could effectively separate injected charge with a space charge layer (Figure 2.3.8.). The results (Figures 4.2.3.a and 4.3.1.a) showed nearly the opposite effect: a metallic substrate showed slightly better light voltammetric response than the semiconductor substrate (Figure 4.3.1.c).

The observation of reversible photocurrents in the light had several implications. One implicaton was that both the dye film/electrolyte and substrate/dye film interfaces made ohmic contacts, which means that the contact resistance is a constant, independent of potential. Ohmic contacts in

general do not exist as junctions where one or both phases contain space charge layers. Changing the applied potential to an interface under depletion layer conditions will increase or decrease the amount of band bending (Figure 2.3.5.). This in turn changes the electrical resistance of the space charge layer so that rectification of current results. In order to have an ohmic contact, either the space charge layer band bending must be fixed, or there is no space charge layer to begin with. For GaPc-Cl this result means that either its band edges were negligibly bent at both front and rear surfaces during electrolysis, or that a band structure model is inappropriate.

From the voltammetric work on the various quinone redox couples, two types of information were obtained, one kinetic, the other thermodynamic. The kinetic information concerned possible steric effects on coordination of quinone to GaPc-Cl and hence its rate of reaction. By adding benzene rings to the sides of the quinone base and shifting the position of the OH-functionalities with respect to each other, certain orientations with respect to the electrode surface would be eliminated or at least hindered, which may reflect itself by a decrease in the rate of charge transfer. As it turned out, the three additional redox species, catechol, 1,4-napthoquinone-2-sulfonate, and 9,10-anthraquinone-2-sulfonate, reacted on the GaPc-Cl surface comparably well, with peak to peak separations of 150, 180, and 90 mv, respectively. These values are within the range typically

observed for H_2Q electrolysis on GaPc-Cl.

Thus the structural alterations on the quinone base did nothing to affect its reactivity on irradiated GaPc-Cl. This would tend to support an outer sphere electron transfer mechanism as the rate limiting step with no specific interaction with the metal center. This is corroborated by the Pc derivative results, where even H_2Pc, with no metal center at all, was quite reactive toward H_2Q (Figure 4.2.3.e). The only example found in the literature where a quinone was found to adsorb to a phthalocyanine surface was a report by Loutfy and Sharp (195), who adsorbed a napthoquinone derivative to manganese phthalocyanine, MnPc. The adsorbate derivative, however, was 1,3-dioxadinaptha-(2,1-3',3') furan-6-(2"-pyridyl) carboxamide, which could have adsorbed via the pyridyl appendage independently of any quinone functionality.

Thermodynamic information could be obtained from the position of the voltammetric wave of a given redox couple on GaPc-Cl in the light to that of the same couple on Au in the dark. The shift in E° between light and dark, according to theory, equals the open circuit photopotential observed for the reaction between the two electrodes. For catechol, whose E° is nearly equal to H_2Q, very little shift of the light voltammogram with respect to the dark is observed. For the NQ and AQ sulfonates, whose formal potentials were found to be +0.02 and -0.12 v, respectively, substantial shifts between the apparent light and dark voltammograms were

observed. Using the potential difference between the cathodic peak potential in the light and the dark as an estimate of the photopotential, -50, -285, and -200 mv were measured for catechol, NQ, and AQ, respectively. A qualitative model explaining these results is shown in Figure 5.2.

The electrolysis of $Fe(CN)_6^{3-,4-}$ is the classical, one electron, outer sphere charge transfer reaction for aqueous solutions. The fact that its behavior on GaPc-Cl (Figure 4.3.3.a) is similar to H_2Q is another indication that outer sphere reactions proceed quickly on GaPc-Cl electrodes. The reduction of O_2, however, is undoubtedly not an outer sphere reaction, and so the coordinative nature of the Ga center should again be considered. It is difficult to imagine how O_2 would interact with a phthalocyanine without a metal center, yet there are references include H_2Pc as a catalyst for O_2 reduction (200-202). At any rate, Ga compounds are not well known for their O_2-binding abilities.

Another issue concerning steric and coordinative properties of GaPc-Cl is the lability of the axial chloride ion. Certainly no electroactive species can coordinate with the Ga center if the Cl^- counterion is immobile. XPS data in Figures 4.6.5.a and b, and 4.6.6.a and b suggest that OH^- can at least substitute for Cl^- in the electrode double layer. This result is not surprising since the halides of Ga are known to readily react with H_2O to form hydroxides (191). Furthermore, GaPc-Cl is a synthetic precursor for the other GaPc-halides (55), so that its lability must be quite high.

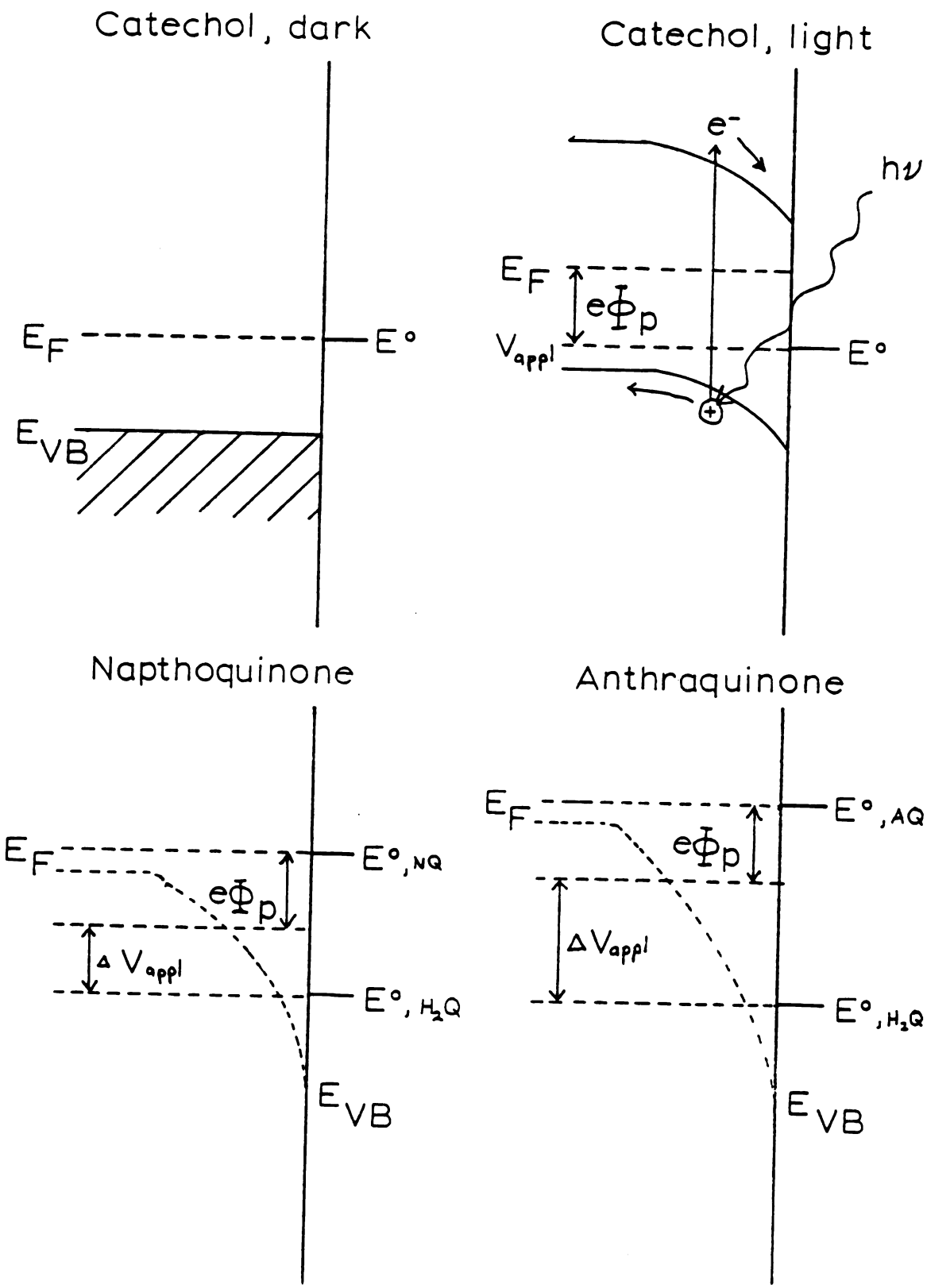

Figure 5.2: Photocurrents on Quinones of Different E°

Consider GaPc-Cl to be a p-type semiconductor, whose E_F as an isolated component is close to the E° for catechol or H_2Q when referenced to the energy of an electron in vacuum. Thus, when the electrode/electrolyte junction is formed, only a very slight depletion layer is formed. Upon irradiation, a photopotential is developed, raising E_F by about 200 mv, or 0.2 ev. This electron energy increase in the dye layer is more than enough to drive the reduction of catechol, and so it is reduced at potentials very near the dark E°'. For NQ, however, the E°' is more negative than E_F under illumination when the electrode is held at initial potential of 0.5 v. Thus the electrode must be scanned an additional 100 mv before E_F is raised to the point where NQ can be reduced. For AQ, the E°' is even more negative, so in this case the electrode must be swept negative some 300 mv before reduction can occur.

In order to explain the experimental results, it must be assumed that upon immersion in the electrolyte, the Fermi level of the dye film is near the E° of H_2Q, regardless of whether H_2Q is in the solution or not. When immersed in a solution containing another redox couple of different E°, the Fermi level is still initially around the 0.25 v potential. This explains why a nonzero potential between the film electrode and the Pt electrode could be measured in the dark. It also explains why a steady drift in the potential difference was observed. There is apparently no fast mechanism by which the film electrode can come to rest or thermodynamic equilibrium with the solution. An identical

rate of potential drift was also observed in the light, however. Since the rates of charge transfer were so fast in the light, irradiation should have hastened the rate of equilibration.

The explanation for the slow potential drift in the light and the dark is diagrammed in Figure 5.3. An energy level diagram is shown where the H_2Q redox species has equilibrated with the Pt electrode, corresponding to difference between E_{redox} of the solution and the intrinsic E_F of the dye. In order for the film to equilibrate with the electrolyte, electrons must cross from the dye phase into the solution phase by reductiion of electroactive species. However, the predominant species in solution, H_2Q, is already in its reduced form, and so equilibration must occur via trace anounts of Q and impurities. Irradiation raises E_F to an even more negative potential, but unless there are new oxidized species whose redox levels now become positive of E_F, the addition of light will not hasten electrode equilibration.

This slow rate of equilibration was also observed for the steady state photocurrent vs time plots in Figure 4.5.2. Specifically, in Figures 4.5.2.b, c, and d, photocurrents required up to 15 seconds and more to reach a steady state. The poised potentials are well within the activation control region, so a steady state current in the light should be immediately reached after exposure to illumination. The steady state was reached more quickly at higher potential;

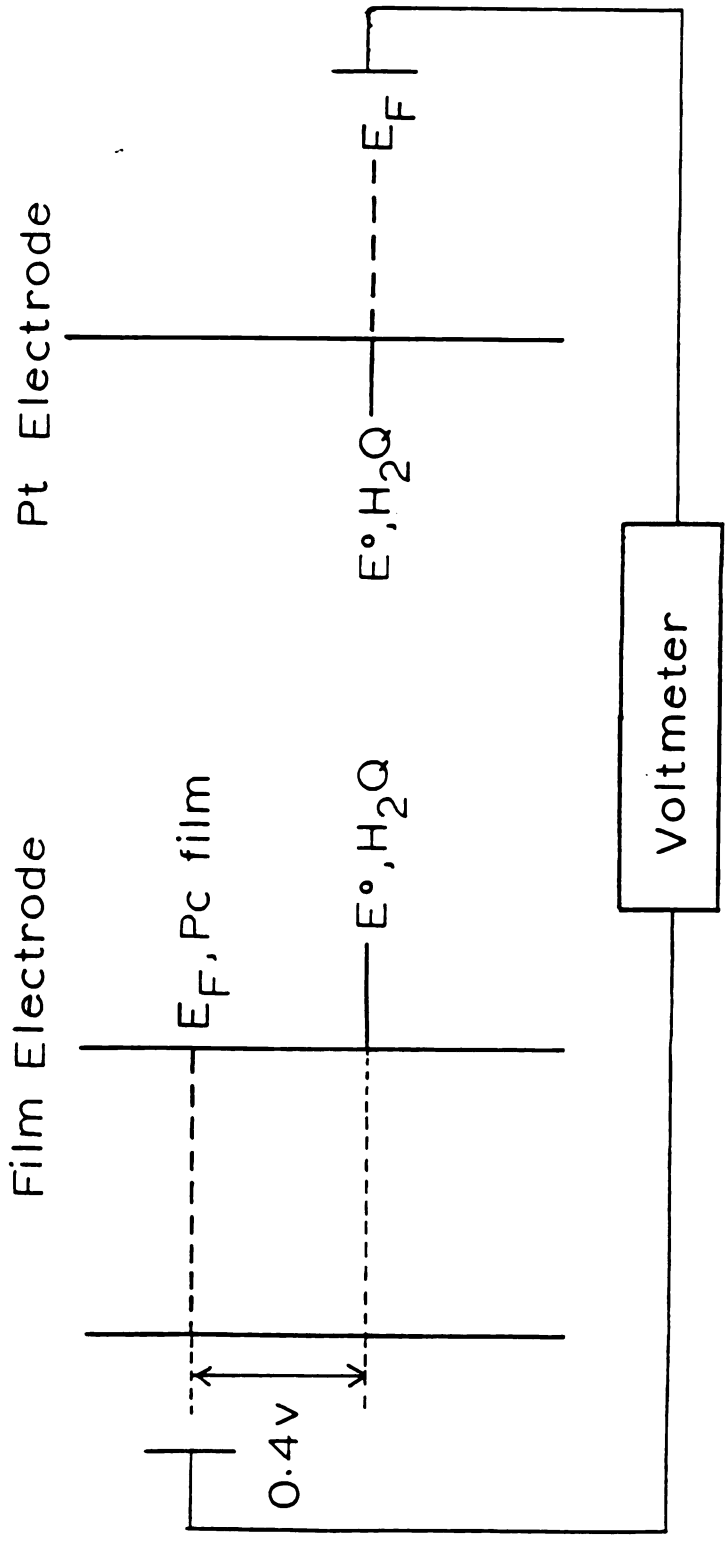

Figure 5.3: Nonequilibrated Film Electrode Under Open Circuit Conditions

apparently, the presence of a higher electric field gradient within the film helps achieve a steady state more quickly since photoconductivity is field dependent. If the rate determining step in the achievement of a steady state in the light was the adjustment of the concentration profile of redox species in solution near the electrode surface, the opposite effect would be observed; namely, that at low overpotential the steady state would be reached quickly, and at higher overpotential the onset of mass transport would slow the equilibration. Therefore, the slowly decaying light transients must involve a potential drift within the film.

A schematic diagram showing how transients such as the one seen crossing the voltage axis at 0.0 v in Figure 4.5.3.b can occur is shown in Figure 5.4. An unequilibrated electrode sits at zero volts in the dark. Most of the potential drop between the working electrode contact and the solution is across the dye film. The Fermi level is slanted across the dye layer to represent the nonequilibrium situation. H_2Q is injecting electrons into the dye layer but at a negligible rate. Upon irradiation, E_F is raised by an amount e ϕ_p, where ϕ_p is the photopotential. If E_F is raised above (negative) of E_{redox}, then a negative photocurrent will result. For the transient of interest, however, the photovoltage increase was apparently not enough to raise E_F above E_{redox}, and so oxidation may occur much more quickly, and so a measurable oxidative photocurrent is obtained. Light also promotes faster equilibration within

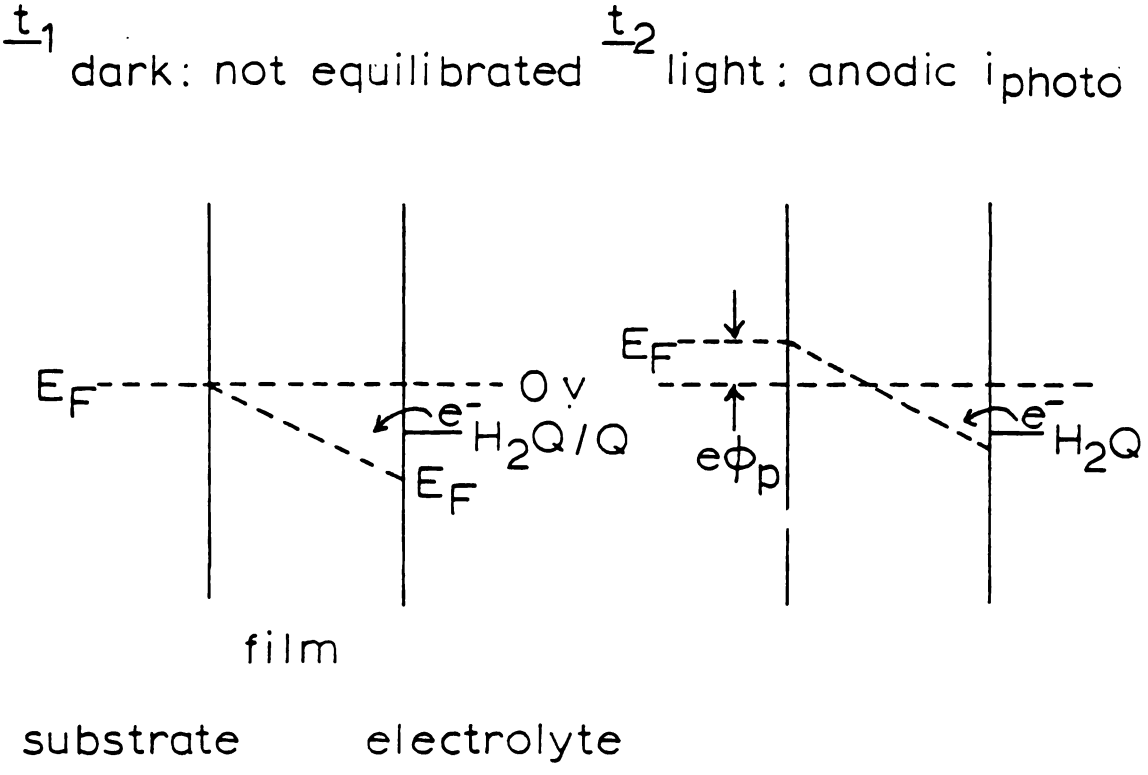

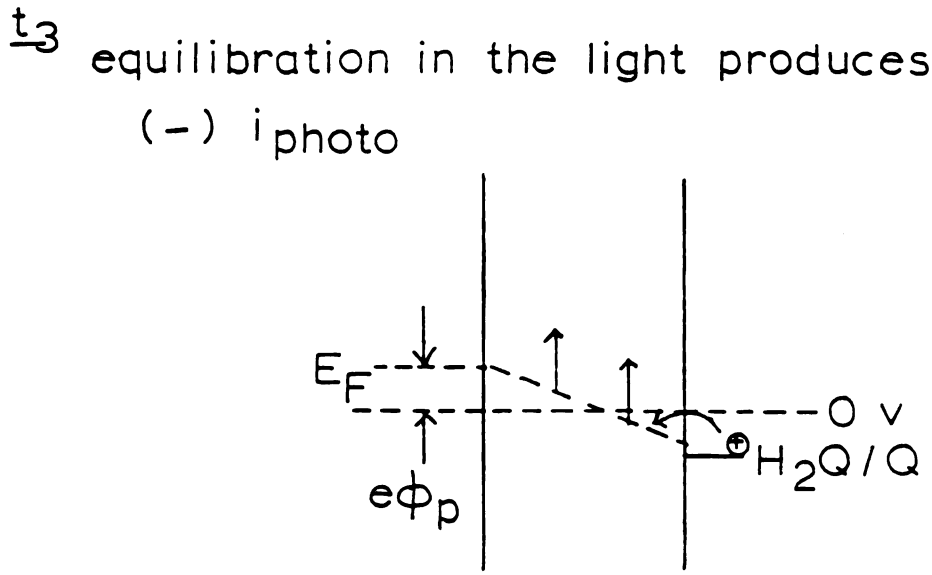

Figure 5.4: Slow Transient Crossing Zero of Current

the film, however, and so the Fermi level begins to level off. During the leveling off process, E_F at the electrolyte interface passes through E_{redox}, and so the electrode reaction now becomes a reduction.

The short current-time transients, or spikes, were too fast to be observed on the time scale used to study photocurrents, but a few qualitative remarks about them will still add to the total picture. When the sign of the photocurrent was the same as that of the spike, it was difficult or impossible to observe, but it was easily observable when the two transients had opposite signs. The sign and magnitude of the spike was determined by the direction and amount of band bending at the electrode interface when the light was flashed, which in turn is affected by the electrolyte compositon and applied potential. When the band edges curled upwards going into the bulk of the film, light exposure caused a negative transient as electrons were drawn toward the electrolyte interface by the internal field of the space charge layer. Band edges curling downward would cause a positive spike. There was little consistency observed between poise potential and sign of the spike transient, however, because of the variable degree of thermodynamic equilibration from one electrode to another when tested. The current spikes were largest for the blank electrolyte, because the dye/electrolyte capacitor could not "leak" by means of a faradaic reaction.

The transfer coefficients for oxidation and reduction, $\overleftarrow{\alpha}$ and $\vec{\alpha}$, respectively, were derived from the slopes of the Tafel plots in Figures 4.5.4. and 4.5.5. Using the theory developed for treatment of multi-step electron transfer mechanisms (203), the equations of interest are:

$$\overleftarrow{\alpha} + \vec{\alpha} = \frac{n}{\upsilon}$$

$$\overleftarrow{\alpha} = \frac{n - \vec{\gamma}}{\upsilon} - r\beta$$

$$\vec{\alpha} = \frac{\vec{\gamma}}{\upsilon} + r\beta,$$

where n is the total number of electrons transferred per mole of product formed, υ is the number of times the rate determining step occurs per mole of product formed, $\vec{\gamma}$ is the number of electron transfer steps before the rate determining step, r is the number of electrons transferred during each occurrence of the rate determining step, and β is the symmetry factor of the rate determining step.

By considering all the work that has been reported in the literature on the aqueous electrochemistry of quinones, plus Au rotation ring-disk (196) and thin layer cell (197) work done in this laboratory, n can be assumed to be 2. Then, for the unmodified Au electrode in a solution which is 1 mM each in Q and H_2Q,

$$\overleftarrow{\alpha} + \vec{\alpha} = 0.97 + 0.71 = 1.68$$

$$1.68 = \frac{n}{\upsilon} = \frac{2}{\upsilon} \qquad \upsilon = 1.19$$

If the Tafel data were taken from a system where a single reaction mechanism was predominant, then υ should be equal to a whole number; deviations from integer values would indicate two or more competitive mechanisms. Indeed, Vetter (110) saw a transition in H_2Q kinetics from one mechanism to another at pH 4 on Pt. On the other hand, mixed mechanisms would give a curved Tafel plot, since they would most likely have different transfer coefficients. The experimental Tafel plot definitely had a linear portion in the mid-potential region, and so a single mechanism must operate here. Rounding υ off to the nearest whole number, which is equivalent to rounding $\overleftarrow{\alpha}$ and $\vec{\alpha}$ off similarly, we have

$$\underset{\alpha}{\overleftarrow{\ }} = 1 = \frac{2 - \vec{\gamma}}{1} - \frac{r}{2}$$

$$\vec{\alpha} = 1 = \underset{1}{\vec{\gamma}} + \frac{r}{2}$$

where β has to be approximated as 1/2. The only combinations of $\vec{\gamma}$ and r which fulfill the two equations are:

(1) $\vec{\gamma} = 1;\ r = 0$
(2) $\vec{\gamma} = 0;\ r = 2$

However, if r = 0, then β = 0, since a chemical step must be rate determining. For β = 0, the equation becomes

$$\overleftarrow{\alpha} = 1 = \frac{2 - \vec{\gamma}}{1} = 2 - \vec{\gamma}$$

$$(3)\quad \vec{\alpha} = \frac{\vec{\gamma}}{1} = \vec{\gamma} = 1$$

Thus one electron transfer step may precede the rate determining protonation. For $\vec{\gamma}$ = 0, and r = 2, a simultaneous two electron, or two rapidly successive one electron transfer steps are rate determining, with the order of protonation steps unspecified. The possible mechanisms derived from pairing #2 are CEEC, EECC, or CCEE. For #2 there are two possibilities: E<u>C</u>EC, and CE<u>C</u>E, where the underlined step is rate determining. Out of the six possible mechanisms, five were found to possibly possess the observed Tafel slope. Thus the results of this single determination accomplished little in terms of mechanistic elucidation.

Table 4.3 also has the transfer coefficients for GaPc-Cl/Au electrolysis for Q/H_2Q under irradiation, as calculated from the Tafel slopes. Since both transfer coefficients are close to 1/2, a mechanism derived for $\overleftarrow{\alpha} = \vec{\alpha} = 1/2$ will be considered.

$$\overleftarrow{\alpha} = \vec{\alpha} = 0.51 = 0.41 = 0.92 = 1$$

$$1 = \frac{n}{\upsilon} = \frac{2}{\upsilon}$$

$$\upsilon = 2$$

Thus the rate determining step occurs twice for each product molecule formed. Assuming $\beta = 1/2$,

$$\overleftarrow{\alpha} = 1/2 = \frac{2 - \vec{\gamma}}{2} - \frac{r}{2};$$

$$\vec{\alpha} = 1/2 = \frac{\vec{\gamma}}{2} + \frac{r}{2}.$$

The $\overleftarrow{\alpha}$ equation holds for $\vec{\gamma} = 0$ and $r = 1$, and also for $\vec{\gamma} = 1$ and $r = 0$. The $\vec{\alpha}$ equation also holds for the same two sets of values.

Once again, the pairing $\vec{\gamma} = 1$, $r = 0$ must be thrown out because β was assumed to be 1/2 for a mechanism in which the rds passes zero electrons. For the $\beta = 0$ case, $\vec{\gamma} = 0$.

Since $\upsilon = 2$, which means that the rds must occur twice for each H_2Q formed, the only mechanisms that explain the Tafel slope data are the reduction of quinone before or after protonation to form the semiquinone radical, which then disproportionates to form Q and product H_2Q. The two possible sequences of steps are shown below:

Scheme a

(1) $Q + e^- \rightleftharpoons Q^{\cdot-}$

(2) $Q^{\cdot-} + H^{+} \rightleftharpoons QH^{\cdot}$

(3) $QH^{\cdot} + QH^{\cdot} \rightleftharpoons Q + H_2Q$

Scheme b

(1) $Q + H^{+} \rightleftharpoons QH^{+}$

(2) $QH^{+} + e^{-} \rightleftharpoons QH^{\cdot}$

(3) $QH^{\cdot} + QH^{\cdot} \rightleftharpoons Q + H_2Q$

If the correct pairing is $\vec{\gamma} = 0$, $r = 1$, then Scheme b is the correct one. The possibility $\vec{\gamma} = 0$ when a chemical step is rate determining also implies Scheme b.

Thus we can conclude that benzoquinone electrolysis proceeds via a CE mechanism followed by disproportionation at pH 4 on an irradiated GaPc-Cl electrode. The mechanism on plain, inactivated Au at that pH is well defined, and different from GaPc-Cl, but could not be determined from this experiment alone.

5.4 Light and Dark Conductivity of GaPc-Cl

In the comparison of cyclic voltammograms for different series resistors (Figure 4.4.8.), it was observed that resistors of 20 KΩ magnitude and higher reduced the voltammetric response from quite reversible to a straight line, whose slope was equal to the external resistance. Thus

if the difference in GaPc-Cl activity between the light and the dark were solely due to conductivity differences in the film, the GaPc-Cl film resistance in the dark can be calculated from the slope of the dark voltammetric curve. While the dark traces basically coincided with the baseline at 50 μA/in sensitivity, it would be reasonable to allow up to a 2.5 μA dark current after sweeping out 500 mv and still be consistent with experimental observation. The minimum dark film resistance then would be 200 KΩ. Referring to Figure 4.4.8., the typical GPc-Cl light response implies a maximum 200 Ω film resistance. Therefore, the light source would have to raise the film conductivity by at least a factor of 10^3 to explain the difference between light and dark response.

Conductivity is directly proportional to carrier density, so another way of making the previous statement is that the photon flux must be great enough to raise the free carrier density by a factor of 10^3. The question is, can the 100 mW/cm^2 intensity output of the LP47 filtered Xe lamp produce the required carrier density increase? The main determinant in answering the question is the magnitude of the dark conductivity to begin with. The bulk conductivity of GaPc-Cl in the dark has not been reported, but if the photoconductivity argument is valid we should be able to calculate the light and dark carrier densities from linear voltammogram traces which have been dominated by the series film resistance, as in Figure 4.4.8. The relationship

between the resistance of some electrical element and its conductivity is $R = \frac{1}{\sigma A}$, where 1 is the depth of the element and A is the cross sectional area. Rearranging factors, $\sigma = \frac{1}{RA}$. For the typical 100-equivalent monolayer GaPc-Cl film electrode, then, we have for the dark conductivity,

$$\sigma = \frac{(3.0 \times 10^2 \text{ Å})(10^{-8} \text{ cm/Å})}{(2 \times 10^5 \ \Omega)(0.55 \text{ cm}^2)}$$

$$= 2.72 \times 10^{-11} \ \Omega^{-1} \text{ cm}^{-1}$$

This value is very low, but indicative of an organic semiconductor (198). It is also in basic agreement with some of the experimental values given in the literature for pure, undoped phthalocyanine σ values in the dark. The uncertainty is quite large when measuring such small σ values, and the presence of trace impurities may cause a σ change of many orders of magnitude (55).

The dark carrier density can now be calculated from the conductivity equation: $\sigma = n e \mu$, where μ is the mobility of the charge carrier. Experimentally determined hole and electron mobilities in phthalocyanines have usually varied between 0.1 and 2.0 cm^2/v-sec (199),so we will assume an intermediate value of 1.0. The free carrier density in the dark is then

$$n = \frac{\sigma}{e\mu}$$

$$= \frac{2.72 \times 10^{-11}\ \Omega^{-1}\ cm^{-1}}{(1.6 \times 10^{-19}\ coul)(1\ cm^2/V\text{-}sec)}$$

$$= 1.7 \times 10^{8}\ cm^{-3}$$

A 10^3-fold increase in conductivity in the light would raise n to $1.7 \times 10^{11}\ cm^{-3}$, just into the range indicative of semiconductor materials. The absolute number of carriers inside the volume of the film electrode is

$n \cdot V = n \cdot l \cdot A = (1.7 \times 10^{11}\ cm^{-3})(3 \times 10^{-6}\ cm)(0.55\ cm^2)$

$= 2.8 \times 10^{5}$ charge carriers.

The Xe lamp output must then be able to maintain an excited state population of that magnitude.

The steady state carrier density increase due to irradiation will of course be directly proportional to the light intensity, but will also be determined by the lifetime τ, of free carriers in a given substance, and its absorptivity toward the spectral output of the light source. The absolute carrier density increase, Δn, can be approximated by

$$\Delta n = I_o (1 - 10^{-A})\ \tau$$

The calculation of I_o in terms of photons per second for a polychromatic light source, as well as a representative absorbance of the sample for the entire absorption spectrum are difficult to determine. However, since the radiation source was filtered at 470 nm, the Soret band of the GaPc-Cl

absorption spectrum in the ultraviolet can be neglected, leaving only the broad wave of absorption between 550 and 800 nm. The absorbance throughout that region is fairly constant, so that choosing the midpoint wavelength, 675 nm, will fairly well represent the Pc absorptive behavior. Then, the photon flux is

$$I_o \text{ (photon units)} = \frac{A\ I_o \text{ (energy units)}}{hc/\lambda} = \frac{A\ I_o\ \lambda}{h\ c}$$

$$= \frac{(0.55\ cm^2)(100\ mw/cm^2)(10^{-3}\ w/mw)(675 \times 10^{-9}\ m)}{(6.63 \times 10^{-34}\ J\text{-}sec)(3 \times 10^{9}\ m/sec)}$$

$$= 1.9 \times 10^{17} \text{ photons/sec}$$

Assuming a typical GaPc-Cl film of 100 equivalent monolayers which would have a plateau absorbance of 0.8, and an intermediate carrier lifetime of one nanosecond, the carrier increase would be

$$\Delta n = I_o\ (1 - 10^{-A})\ \tau$$

$$= (1.9 \times 10^{17}\ \text{photon/sec})(1 - 10^{-0.8})(1 \times 10^{-9})\ \text{sec})$$

$$= 1.6 \times 10^{8} \text{ charge carriers}$$

Thus the available photon flux is easily capable of effecting a 10^3 increase in GaPc-Cl film conductivity.

One coarse assumption implicitly used was that each absorbed photon produces a charge carrier. In organic semiconductors, however, direct band gap transitions may be a small or insignificant means of electron/hole pair creations; instead, sub-band gap transition to exciton states can be the dominant mechanism of charge carrier formation (198). Also the determination is directly dependent on τ, whose chosen value was at best an intelligent guess. Flash photolysis work in this laboratory has put an upper limit on carrier lifetime in GaPc-Cl films at 350 ns (198). If the carrier lifetime were as low as one picosecond, then the photogenerated charge carrier increase would not be sufficient to explain the difference between light and dark response on the basis of photoconductivity. The photoconductivity theory just developed depended on the assumption that the dark response was negligible because of high film resistivity in the dark. However, when dealing with semiconductor electrodes, the lack of availability of electronic levels can also be an impediment to reaction. Another objection to the photoconductivity argument is that recently acquired impedance measurements in this laboratory on nonporous GaPc-Cl films on Au in the light and the dark gave the same value of the film resistance at 400 ± 50 Ω (184). This implies that the suppression of activity in the dark cannot be explained by a purely conductive effect.

5.5 Reflectance Effects on Solid GaPc-Cl Spectra

The two types of photoaction spectra are, to some degree, at odds with each other. The photon conversion efficiency, or electrons injected per incident photon (Figure 4.5.6.), basically follows the absorption spectrum, or in other words, the higher the probability of absorption, the more likely a photon will contribute to charge exchange across the electrified interface. This is a reasonable proposition, and would be expected to hold as long as the quantum efficiency for charge transfer (electrons injected per photon absorbed) is a constant, independent of wavelength. However, the quantum efficiency spectrum was not constant (Figure 4.5.8.) and appeared to increase with decreased absorptivity.

The answer lies in the error introduced into the absorption spectrum by reflectance. Reflectance has long been recognized as a souce of error, but had not been actively compensated for. Glass was used as a substrate for a solid film spectra because the reflectance error introduced appeared to be the least of all available substrates. Absorbance data for the various Pc films was obtained by letting the absorption spectrum of the glass substrate act as the baseline and obtaining the absorption of the film by difference.

Because of the reduced reflectance effect, the GaPcCl/glass spectra looked the most reasonable compared to other substrates. Moderately thin GaPc-Cl/Au samples sometimes

showed unmeasurably high absorbance values, while the same thickness films on glass could easily be recorded on scale. GaPc-Cl/Au electrodes prepared by P. Rieke were especially noted for this effect (185). GaPc-Cl/SnO_2 spectra had believable absorbance values, but the approximately 5000 Å thick SnO_2 films exhibited interference fringes in the visible range, which complicated quantitation of solid phase absorbance measurements of the GaPc-Cl films sublimed onto them. A reflectance error was also apparent when absorbance readings for a GaPc-Cl/SnO_2 electrode in the 500 nm range where Pc absorptivity is low would occasionally dip below the spectral curve previously obtained for the bare SnO_2 substrate, implying a spurious negative absorption by the GaPc-Cl film.

The points used to make the quantum efficiency plot in Figure 4.5.8. do not have the same relative error. The quantum efficiency was inversely proportional to $(1-10^{-A})$, so that for small values of A, a small measurement error due to reflectance may cause a large relative error in the absorbance term, thus transferring its uncertainty to ϕ. For example, a negative absorbance measurement error due to reflectance of 0.05 would cause the calculated quantum efficiencies to be high by 90% when A = 0.1 but only 6% high when A = 0.5. Therefore, the peak obtained in the quantum efficiency versus wavelength graph should be discounted due to the extremely high relative errors possibly attached to the low absorbance values in that region.

The SEM data may provide a clue as to why identical thickness films on different substrates gave absorption spectra that were similar in shape, but whose magnitude of absorption varied greatly. Reflection would be a greater factor on films with large, flat faces and prominent features which increased the surface area, than on films with small, rounded features. Therefore, GaPc-Cl films on glass and SnO_2, which mainly contained particle sizes on the order of 0.1 μ or less, gave somewhat more reasonable absorption spectra, while the large crystalline granules and needles on GaPc-Cl/Au electrodes caused large reflectance errors. The largest reflectance errors occurred with the most porous GaPc-Cl/Au electrodes, which also had the largest grain sizes (Figure 4.4.6.)

One feature of the GaPc-Cl film absorption spectrum that neither of the photoaction spectra contained was the absorbance maximum at 780 nm. The reason is that when the specular reflectance of GaPc-Cl is taken into account, the maximum is found to occur not through absorption, but through reflection. In Figure 5.5, the frontside specular reflectance spectrum of a GaPc-Cl/Au electrode prepared as described in the Experimental chapter is shown. The dotted trace for a GaPc-Cl/glass electrode is included for comparison. Except for a peak in the low Pc-absorptivity range around 500 nm, which is probably due to the substrate, the reflectance spectrum largely follows the absorption, with an even more prominent peak at 800 nm. This will have an

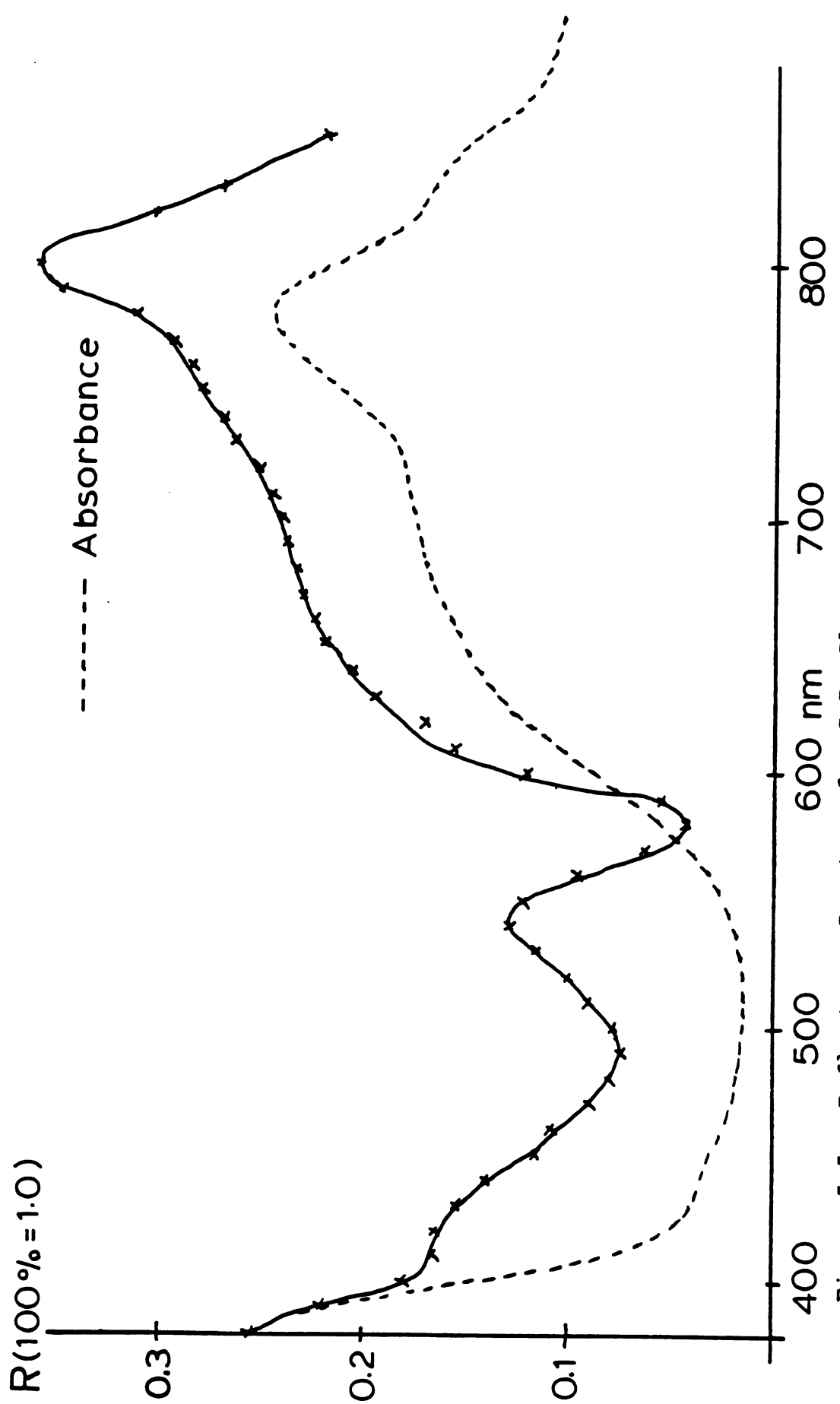

Figure 5.5: Reflectance Spectrum for GaPc-Cl

effect of damping out the spectral features previously attributed to absorption only.

Increased reflection means that less pure absorption is occurring. Mathematically, the effect of reflection can be shown as follows: The apparent absorbance, A_o, is calculated from the incident intensity, I_o, and the transmitted intensity, I, by the relation $A_o = \log \frac{I_o}{I}$. The true absorbance, A, can be calculated from the reflection-attenuated intensity entering the film, I_o', which is calculated from I_o with

$$I_o' = I_o (1-R).$$

Then, $$A = \log \frac{I_o'}{I}$$

$$= \log \frac{I_o (1-R)}{I}$$

$$= \log \frac{I_o}{I} + \log (1-R)$$

$$= A_o + \log (1-R)$$

Thus the true absorbance can be calculated from the apparent absorbance with the reflectance at that wavelength. Using the GaPcCl/glass absorption spectrum as an example, elimination of the absorbance maximum would require an 0.2 absorbance unit difference between apparent and true absorption. Then,

$$10^{(A-A_o)} = 1-R$$

$$R = 1 - 10^{-0.2} = 37\%$$

which is only one percent higher than the reflectance value for GaPc-Cl/Au at 800 nm. Thus an adjustment of the absorption spectrum for reflection can effectively eliminate the maximum observed near 800 nm.

It is no coincidence then that of the red-shifted solid phase Pc absorption spectra, the sharpest and most distinct peak maxima belonged to GaPc-Cl and GaPc-I, whose rough angular surface brought on a higher reflectance effect. VOPc is exceptional in this regard, since its distorted square pyramidal geometry causes a crystalline structure that is unusual for phthalocyanines (150). In a very real sense, the photoaction spectra were better indicators of true light absorption than the absorption spectra, since reflected light did not contribute to the measured observable, i.e., photocurrent.

5.6 Conclusion

The idea of solar energy conversion with semiconductor photoelectrodes is only ten years old. The idea of using dye-sensitized semiconductor photoelectrodes is even younger. Quantum efficiencies on the first dye sensitized electrode systems were quite low, on order of several tenths of a

percent. Since for these original systems the dye was either solvated or formed an adsorbed monolayer, the useful absorbance of incident radiation was 1% or less, so that the power conversion efficiency was an additional two orders of magnitude less. With a solar power conversion efficiency of 10% generally accepted as the break point for practical device application, an improvement in efficiency of over 10^3 was needed.

Early attempts in this laboratory at improving the quantum efficiency of dye-sensitized metal oxide electrodes involved covalent attachment of chromophores to the electrode surface via silane linkages. Cobalt and copper phthalocyanine, as well as erythrosin, were attached to n-SnO_2 electrodes and tested in solutions of oxalate and ascorbate ions. The quantum efficiency of each covalently attached dye molecule was improved in comparison to the adsorbed state, but loadings of no more than one or two equivalent monolayers could be obtained.

More recent experiments in this laboratory have sought to improve the power conversion efficiency by subliming multilayer depositions of dye sensitizer on the semiconductor surface. By using phthalocyanines which crystallized in a cofacial, axially stacked manner, it was hoped that the increased film absorption would not be offset by a drop in quantum efficiency. The cofacial arrangement of phthalocyanine molecules was thought to enable strong interaction between the π electron clouds on adjacent

macrocyclic rings, which would reduce ohmic losses that in turn affect the quantum efficiency. GaPc-F and AlPc-F,in which a fluoride ion is shared equally between the metal centers of successive MPc units, were tested along with other group III phthalocyanine halides. Another type of axially stacked phthalocyanine was SiPc, which could be polymerized by means of an O-linkage between the Si centers. Monomer, dimer, and trimer forms could be isolated and evaporated onto electrode substrates for voltammetric examination.

As it turned out,the cofacially stacked phthalocyanines did not distinguish themselves from the others tested. Of the SiPc oligomers, the monomer form gave the greatest light activated response. While GaPc-F and AlPc-F also gave light activated currents, it was GaPc-Cl and AlPc-Cl that showed the greatest contrast in terms of current onset for H_2Q oxidation in the light and the dark.

A closer examination of GaPc-Cl was then undertaken by this author, the results of which have been detailed in this dissertation. GaPc-Cl was found to be a highly efficient dye sensitizer, with quantum efficiencies under a 400 mv bias vs Ag/AgCl on order of 3.5% over much of the visible spectrum, from 550 nm to the near infrared. This efficiency represents an order of magnitude improvement over the original dye systems and ranks among the highest obtained to date for dye sensitization. Furthermore, this was accomplished with film thicknesses on order of 100 equivalent monolayers, or several hundred Ångstroms, so that with its high molar absorptivity

in the red region of the visible spectrum, GaPc-Cl was able to capture up to 90% of the incident radiation at certain wavelengths and maintain a high quantum efficiency. The combination of increased absorbance and quantum efficiency in GaPc-Cl has enabled an improvement of between 10^2 and 10^3 in power conversion efficiency for dye sensitizers over initial experiments in this area, leaving one final order of magnitude to be achieved before commercial energy conversion devices involving dye sensitized electrodes can become competitive with other technologies. Once that point is reached, attention can be directed toward the lifetime of the electrodes, which loses half of its photoelectrocatalytic ability after 2400 charge transfers per surface molecule.

The contrast between the voltammetric activity of GaPc-Cl and GaPc-I in the light and in the dark was found to be unequalled by any other dye or organic semiconductor, much less the other Pc derivatives examined in this dissertation. In the dark, the GaPc-Cl surface was essentially inert, with no faradaic activity observed throughout most of the normal operating potential range in aqueous electrolytes. However, under exposure to visible and near-infrared light, the GaPc-Cl surface would become activated, performing electrochemical reactions reversibly at a rate comparable to a noble metal electrode. The reversible photoelectrochemical response was observed for $Fe(CN)_6^{3-,4-}$ and four quinones, whose range of $E^{\circ\prime}$s spanned over 500 mv. The reduction of O_2 was also found to be catalyzed on irradiated GaPc-Cl,

reacting at a rate which rivaled FePc, the best known phthalocyanine catalyst and one of the best known overall catalysts for O_2 reduction.

The reason for this extreme contrast lies in two effects, both of which can be related to a unique crystalline structure for GaPc-Cl. The first effect is porosity. The α phase films of all the Pc derivatives were observed to be continuous and nonporous by electron microscopy down to 0.05 μm, yet the voltammetric results showed that for most of the samples the Au surface was contacting the electrolyte. The typical α phase film had a tendency to form a microporous structure, while GaPc-Cl films did not show this effect -- as soon as enough GaPc-Cl material was deposited on an electrode for the grains to grow together, the dark voltammetric response was shut off. The general red shifting of the solid phase electronic absorption spectrum of GaPc-Cl with respect to its solution spectrum was an immediate indication that the film was not typical α phase.

Another indication that GaPc-Cl and GaPc-I possessed unusual crystalline properties was that only electron micrographs of film samples of those two derivatives showed sharp angles and flat faces, evidence of crystalline morphology. Granular crystal structures up to 5000 Å across were observed, while features on the other Pc derivatives were an order of magnitude smaller or less. All films sublimed on Au Intrex were prepared under as nearly identical conditions as possible so that any differences in film

morphology were due to the crystal growth characteristics of the species themselves.

The second effect in causing the extreme voltammetric contrast in GaPc-Cl behavior between the light and the dark is conductivity. Because of the unusually high degree of crystalline order in GaPc-Cl films, the density of lattice vacancies and other crystalline imperfections, which are thought to be responsible for p-type semiconductivity in phthalocyanines, is greatly reduced. The result then is a dark free-carrier density that is low even for phthalocyanines. When used as an electrode material in the dark, the applied potential difference is completely lost across the film, eliminating the electrical driving force for reaction at the double layer.

The other effect of high crystalline order, however, is increased carrier mobility, which is reflected in an increased carrier lifetime. Under a given photon flux, the steady state density of free carriers will be higher than if the crystal were less ordered. Thus the photoconductive effect on GaPc-Cl is much greater than on other Pc derivatives.

The nature of GaPc-Cl crystalline structure is speculated to involve dimeric units which stagger themselves at an angle, as shown in Figure 5.6. In this way both the tendency for Ga to bond in a 4-coordinate tetrahedral geometry and the need for orbital overlap to achieve a reasonably wide conduction band are satisfied.

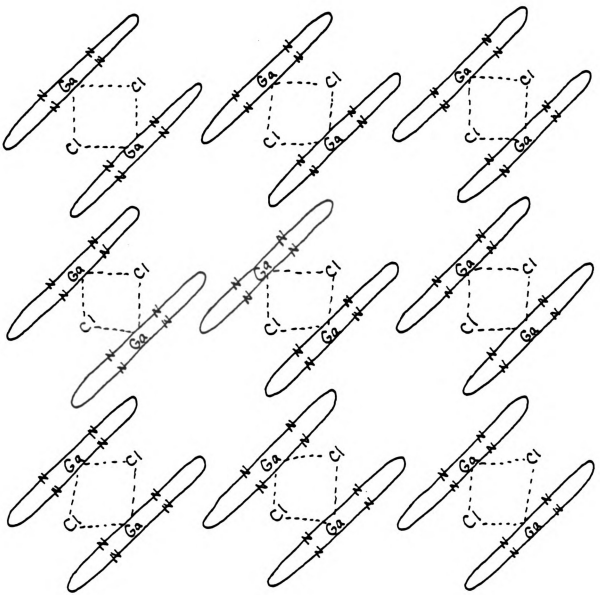

Figure 5.6: Hypothetical Dimer Structure of GaPc-Cl

GaPc-Cl can be characterized as a slightly doped p-type semiconductor, with a band gap of 1.6 ev and a flat band potential of +0.5 v vs NHE. Capacitance and estimated photovoltage measurements indicated a high density of surface states centered aroung +0.1 v vs the Ag/AgCl reference electrode. These surface states are thought to mediate the electron transfer reactions, so as to explain the equal rates of charge transfer in both directions.

This concludes the present investigation on GaPc-Cl. This author sincerely hopes that the results described in this work will aid in the elucidation of the photoconductive and photoelectrochemical properties of phthalocyanines and other organic semiconducting dye sensitizers.

5.7 Future Work

Many of the experiments detailed in this thesis generated new questions and directions of research. Some suggestions for future experimentation are listed below:

(1) Some basic solid state measurements on GaPc-Cl such as a function of temperature and the Hall coefficient may go a long way in explaining its behavior as an electrode.

(2) Obtaining reproducible experimental results was often limited by the ability to produce equivalent Pc films. A controllable sublimation apparatus that could make Pc films according to the

specifications required (thickness, substrate pretreatment, sublimation and substrate temperature, and background pressure) would save much time and effort, and make some experiments, such as a voltammetric comparison of equal thickness electrodes as a function of substrate temperature worth doing.

(3) The two techniques of film preparation described in this thesis had three differing conditions; namely, O_2-plasma cleaning, substrate temperature, and deposition rate. By varying each parameter independently of the others a detailed understanding of Pc film growth characteristics could be made. A good start: prepare GaPc-Cl electrodes by fast sublimation on an O_2-plasma cleaned substrate and by slow sublimation on a substrate that is not plasma treated; see whether porous (Rieke-type) or nonporous (Linkous-type) electrodes result in each case.

(4) Of the nine Pc derivatives examined, all those and only those derivatives with axial groups or counterions showed spectral red shifting. To see if this is a fundamental trend, the list of Pc's examined should be expanded, including species such as FePc-Cl, the chloroferric derivative, whose ferrous counterpart does not red shift, but with the Cl^- counterion may well show some spectral shifting.

(5) X-ray diffraction spectra of Pc's could provide very useful information if acceptable samples could be prepared. Unfortunately, crystals at least 0.1 mm in thickness are required. At 10 Å/min, it would take 2½ months to make the minimum allowed thickness. But once the film deposition parameters are well understood, it may turn out that films can be deposited at a much faster rate without loss of structural integrity. Using an inert entrainer gas could hasten the deposition rate without sublimation temperature increase. Another alternative technique would be utilization of new transmission electron microscopy imaging techniques to obtain structural data.

(6) CoPc and FePc have been heavily studied as O_2 reduction catalysis in the dark. Since GaPc-Cl performed just as well in the light, a kinetic study of O_2 reduction on irradiated GaPc-Cl is in order.

(7) Photopotential measurements on GaPc-Cl electrodes with as many redox couples covering as wide a range of E°'s as possible may more vigorously define the band and surface electronic structure of GaPc-Cl.

LIST OF REFERENCES

6. LIST OF REFERENCES

1 E. Becquerel, C.R. Acad. Sci., 9 (1839) 561.

2 H. Gerischer, z. Phys. Chem. N.F., 26 (1960) 223; 27 (1961) 48.

3 H. Gerischer, Surf. Sci., 13 (1969) 265; 18 (1969) 97.

4 P.J. Boddy, J. Electrochem. Soc., 115 (1968) 199.

5 F. Mollers and R. Memming, Ber. Bunsenges. Phys. Chem., 76 (1972) 469.

6 A. Fujishima and K. Honda, Nature, 238 (1972) 37.

7 K.L. Hardee and A.J. Bard, J. Electrochem. Soc., 124 (1977) 225.

8 Y. Nakato, K. Abe, and H. Tsubomura, Ber. Bunsenges. Phys. Chem., 80 (1976) 1002.

9 Y. Nakato, S. Tonomura, and H. Tsubomura, Ber. Bunsnges. Phys. Chem. 80 (1976) 1289.

10 Y. Nakato, M. Shioji, and H. Tsubomura, J. Phys. Chem., 85 (1981) 1670.

11 A.B. Bocarsly, E.G. Walton, and M.S. Wrighton, J. Am. Chem. Soc., 102 (1980) 3390.

12 A. Fuhishima, E. Sugiyama, and K. Honda, Bull. Chem. Soc. Japan, 44 (1971) 304.

13 F. Sitabkhan, Ber. Bunsenges. Phys. Chem., 76 (1972) 389.

14 B. Miller and A. Heller, Nature (London), 262 (1976) 680.

15 A.B. Ellis, S.W. Kaiser, and M.S. Wrighton, J. Am. Chem. Soc., 98 (1976) 1637.

16 T. Inoue, T. Watanabe, A. Fujishima, and K. Honda, J. Electrochem. Soc., 124 (1977) 719.

17 A. Fujishima, T. Inoue, and K. Honda, J. Am. Chem. Soc., 101 (1979) 5582.

18 S.R. Morrison, Electrochemistry at Semiconductor and Oxidized Metal Electrodes, Plenum Press, New York, 1980, p. 345.

19 H. Gerischer, M.E. Michel-Beyerle, F. Rebentrost, and H. Tributsch, Electrochem. Acta., 13 (1968) 1509.

20 H. Gerischer and H. Tributsch, Ber. Bunsenges. Phys. Chem., 72 (1968) 437; 73 (1969) 251.

21 K. Hauffe, H.J. Danymann, H. Pusch, J. Range, and H. Valy, J. Electrochem. Soc., 117 (1970) 993.

22 A. Fujishima, E. Hayashitani, and K. Honda, Seisan Henkyu, 23 (1971) 363.

23 R. Memming, Photochem. Photobiol., 16 (1972) 325.

24 T. Watanabe and K. Honda, J. Am. Chem. Soc., 97 (1975) 4134.

25 A. Fujishima, J. Watanabe, O. Tatsuoki, and K. Honda, Chemistry Letters (1975) 13.

26 T. Osa and M. Fujihira, Nature, 264 (1976) 349.

27 T. Takiyawa, T. Watanabe, and K. Honda, J. Phys. Chem., 84 (1980) 51.

28 R. Memming and H. Tributsch, J. Phys. Chem., 75 (1971) 562.

29 T. Yamase, H. Gerischer, M. Lübke, and B. Pettinga, Ber. Bunsenges. Phys. Chem., 83 (1979) 658.

30 M.T. Spitler and M. Calvin, J. Chem. Phys., 66 (1977) 4294.

31 M.T. Spitler and M. Calvin, J. Chem. Phys., 67 (1977) 5193.

32 H. Tsubomura, M. Matsumura, K. Nakatoni, K. Yamamoto, and K. Maeda, Solar Energy, 21 (1978) 93.

33 O.A. Ushakov, Yu. B. Vasil'ev, and I.V. Shelepin, Elektrokhimiya, 12 (1976) 976.

34 R. Memming, Faraday Dis., 58 (1974) 261.

35 H. Tributsch, Photochem. Photobiol., 16 (1972) 261.

36 M. Calvin, Science, 184 (1974) 375.

37 T. Miyasaka, T. Watanabe, A. Fujishima, and K. Honda, J. Am. Chem. Soc., 100 (1978) 6657.

38 D.D. Hawn and N.R. Armstrong, J. Phys. Chem., 82 (1978) 1288.

39 R. Memming and F. Schröppel, Chem. Phys. Lett., 62 (1979) 207.

40 V.R. Shepard and N.R. Armstrong, J. Phys. Chem., 83 (1979) 1268.

41 T.M. Mezza, C.A. Linkous, V.R. Shepard, N.R. Armstrong, R. Nohr, and M. Kenney, J. Electroanal. Chem., 124 (1981) 311.

42 R.P. Linstead, J. Chem. Soc., (1934) 1016.

43 A.M. Schaffer, M. Gouterman, and E.R. Davidson, Theoret. Chim. Acta. (Berlin), 30 (1973) 9.

44 A. Kozawa, J. Electrochem. Soc., 117 (1970) 1470; 118 (1970) 1705.

45 V.L. Rapoport and N.N. Zhadin, Dokl. Akad. Nauk. SSSR, 212 (1973) 1155.

46 M.E. Kenney, et al., J. Macromol. Sci., Chem., A16 (1981) 299-312.

47 J.L. Petersen, C.S. Schramm, D.R. Stojakovic, B.M. Hoffman, and T.J. Marks, J. Am. Chem. Soc., 99 (1977) 286.

48 C.J. Schramm, D.R. Stojakovic, B.M. Hoffman, and T.J. Marks, Science, 200 (1978) 47.

49 B.M. Hoffman, T.E. Phillips, C.J. Schramm, and S.K. Wright, "Conductive Molecular Crystals: Metallic Behavior in Partially Oxidized Porphyrin, Tetrabenzporphyrin, and Phthalocyanine," Molecular Metals, NATO Conf. Series VI: Materials Science, W.E. Hatfield, ed., 1979, Plenum Press, New York, p. 393.

50 W.A. Orr and S.C. Dahlberg, J. Am. Chem. Soc., 101 (1979) 2875.

51 C.J. Schramm, R.P. Scaringe, D.R. Stojakovic, B.M. Hoffman, J.A. Ibers, and T.J. Marks, J. Am. Chem. Soc., 102 (1980) 6702.

52 K.F. Schoch, Jr., B.R. Kundalkar, and T.J. Marks, J. Am. Chem. Soc., 101 (1979) 7071.

53 J.P. Linsky, T.R. Paul, R.S. Nohr, and M.E. Kenney, Inorg. Chem., 19 (1980) 3131.

54 P.M. Kuznesof, K.J. Wynne, R.S. Nohr, and M.E. Kenney, J. Chem. Soc., Chem. Comm., (1980) 121.

55 R.S. Nohr, P.M. Kuznesof, K.J. Wynne, M.E. Kenney, and P.G. Siebenman, J. Am. Chem. Soc., 103 (1981) 4371.

56 Y. Yamamoto, K. Yoshino, and Y. Inuishi, J. Phys. Soc. Japan, 47 (1979) 1887.

57 M.K. Nosov, Khim. Teknol. Topl. Masel, 17 (1972) 47.

58 C.R. Cook, Lubric. Eng., 28 (1972) 199.

59 Yu. D. Simkin, E. Stepanova, and G.A. Kuznetsova, Khim. Neft. Mashinostr., 4 (1972) 38.

60 J.W. Reynolds and C.H. Sloan, US Patent #3,724,469, April 3, 1973.

61 F.H. Moser and A.L. Thomas, Phthalocyanine Compounds, 1963, Reinhold Publishing Corp., New York, p. 300.

62 M. Ichikawa, S. Naito, S. Saito, and K. Tamaru, J. Chem. Soc. FT1, 69 (1973) 685.

63 K. Kropf and B. Kasper, Justus Liebigs Ann. Chem., 12 (1975) 2232.

64 P. Robinson and C.C. Reid, U.S. Patent #2,585,037.

65 S.E. Harrison, J. Chem. Phys., 50 (1969) 4739.

66 S.E. Harrison and K.H. Ludewig, J. Chem. Phys., 45 (1966) 347.

67 E.R. Menzel and R.O. Loutfy, Chem. Phys. Lett., 72 (1980) 522.

68 J.Y.C. Chu, R.L. Schank, and S. Tutihasi, U.S. Patent #4,181,772, received 1979.

69 P.P. Sorokin, J.J. Kuzzi, G.D. Petit, and J.R. Lankard, IBM J. Res. Dev., 8 (1964) 82.

70 D.A. Phillips and J.L. Milliet, U.S. Patent #3,531,407, September 29, 1970.

71 A. Shansky and A.G. Shuster, U.S. Patent #3,592,581, July 13, 1971.

72 F.H. Moser and A.L. Thomas, Phthalocyanine Compounds, 1963, Reinhold Pub. Co., New York, p. 23.

73 P.E. Fielding, "Growth and Purification of Phthalocyanine Polymorphs", Energy and Charge Transfer in Organic Semiconductors, M. Silver, ed., Plenum Press, New York, 1974, p. 91.

74 J.F. Byrne and P.F. Kurz, U.S. Patent #3,357,989, December 12, 1967.

75 J.F. Byrne and P.F. Kurz, U.S. Re-Issue 27,177, April 20, 1971.

76 J.N. Sharp and M. Abkowitz, J. Phys. Chem., 77 (1973) 477.

77 E. Jasinski, Nature (London), 201 (1964) 1212.

78 J.P. Randin, Electrochim. Acta., 19 (1974) 83.

79 A.J. Appleby and M. Savy, NBS Special Publ. 455, "Electrocatalysis on Non-Metallic Surfaces", Proc. of Workshop held at NBS, Gaithersburg, Md., December 9-12, 1975 (issued November 1976), p. 241.

80 R.J. Brodd, V.J. Leger, R.F. Scarr, and A. Kozawa, "Electrocatalytic Activity of Phthalocyanines for O_2 Reduction" (same location as reference 79).

81 F. Beck, J. Appl. Electrochem., 7 (1977) 239.

82 S.I. Andruseva, K.A. Radyushkina, and M.R. Tarasevich, Soviet Electrochemistry, 13 (1977) 412.

83 J.H. Zagal, P. Bindra, and E. Yeager, Electrochemical Society Proceedings, Seattle, Wa., 1978.

84 H. Behret, H. Binder, G. Sandstede, and G.G. Scherer, J. Electroanal. Chem., 117 (1981) 29.

85 Yu. S. Shumov, Russ. J. Phys. Chem., 47 (1973) 405.

86 S. Meshitsuka and K. Tamaru, J. Chem. Soc., F II., 73 (1977) 236; 760.

87 T. Tachikawa and L.R. Faulkner, J. Am. Chem. Soc., 100 (1978) 4379.

88 N. Minami, T. Watanabe, A. Fujishima, and K. Honda, Ber. Bunsenges. Phys. Chem., 83 (1979) 476.

89 W.M. Ayers, Faraday Disc., no. 70 (1980) 247.

90 N. Minami, J. Chem. Phys., 72 (1980) 6317.

91 Yu. S. Shumov, V.I. Sevast'yanov, and G.G. Komissarov, Biofizika, 18 (1973) 47.

92 L.R. Faulkner and F.F. Fan, J. Am. Chem. Soc., 10 (1979) 4779.

93 F.F. Fan and A.J. Bard, J. Am. Chem. Soc., 101 (1979) 6139.

94 C.D. Jaeger, F.F. Fan, and A.J. Bard, J. Am. Chem. Soc., 102 (1980) 2592.

95 A. Giraudeau, F.F. Fan, and A.J. Bard, J. Am. Chem. Soc., 102 (1980) 5138.

96 H. Meier, W. Albrecht, U. Tschirwitz, E. Zimmerhackel, and N. Geheeb, Ber. Bunsenges. Phys. Chem., 81 (1977) 592.

97 R.D. Joyner and M.E. Kenney, Inorg. Chem., 1 (1962) 717.

98 T.R. Janson, A.R. Kane, J.F. Sullivan, K. Knox, and M.E. Kenney, J. Am. Chem. Soc., 91 (1969) 5210.

99 I.M. Kolthoff and J.J. Lingane, Polarography, vol. 2, Interscience, New York, 1952, chapter XL.

100 M. Brezina and P. Zuman, Polarography in Medicine, Biochemistry, and Pharmacy, Interscience, New York, 1958, chapter XIV.

101 J.Q. Chambers,"Electrochemistry of Quinones", chapter 14 in Chemistry of Quinonoid Compounds, vol. 2, S. Patai, ed., John Wiley and Sons, Ltd., New York, 1974.

102 P. Zuman, Substituent Effects in Organic Polarography, Plenum Press, New York, 1967, chapter VIII.

103 W. Flaig, et al., Liebigs Ann. Chem., 719 (1968) 96.

104 O. Ryba, et al., Coll. Czech. Chem. Comm., 30 (1965) 843.

105 R. Bentley and I.M. Campbell, "Biological Reactions of Quinones", chapter 13 in Chemistry of Quinonoid Compounds, vol. 2, S. Patai, ed., John Wiley and Sons, Ltd., New York, 1974.

106 R.N. Thompson, Naturally Occurring Quinones, 2nd ed., Academic Press, New York, 1971.

107 Govindjee, Bioenergetics of Photosynthesis, Academic Press, New York, 1975.

108 A. Capon and R. Parsons, J. Electroanal. Chem., 46 (1973) 215.

109 F. Haber and R. Russ, Z. Physik, Chem., 47 (1904) 257.

110 K.J. Vetter, Z. Elektrochem., 56 (1952) 797.

111 J.K. Dohrmann and K.J. Vetter, Ber. Bunsenges. Phys. Chem., 73 (1969) 1068.

112 J.M. Hale and R.Parsons, Trans. Far. Soc., 59 (1963) 1429.

113 Y. Lu-An, Yu. V. Vasil'ev, and V.S. Bagotzkii, Soviet Electrochem., 1 (1965) 141.

114 M.P. Soriaga and A.T. Hubbard, J. Am. Chem. Soc., 104 (1982) 2735.

115 R.F. Lane and A.T. Hubbard, J. Phys. Chem., 77 (1973) 1401.

116 C.A. Bishop and L.K.J. Tong, J. Am. Chem. Soc., 87 (1965) 501.

117 L. Michaelis and S. Granick, J. Am. Chem. Soc., 66 (1944) 1023.

118 T. Sakurai and M. Okunuki, Acta Cryst., B27 (1971) 445.

119 R. Rosenthal, A.E. Lorch, and L.P. Hammett, J. Am. Chem. Soc., 59 (1937) 1795.

120 F. Lohmann, Z. Naturforsch., 22a (1967) 843.

121 N.F. Mott, Proc. Roy. Soc. (London), A171 (1939) 27.

122 J.O'M. Bockris and A.K.N. Reddy, Modern Electrochemistry, vol. 2, 1970, Plenum Press, New York, chapter 7.

123 R.A. Marcus, J. Chem. Phys., 43 (1965) 679.

124 D. Elliot, D.L. Zellmer, and H.A. Laitinen, J. Electrochem. Soc., 117 (1970) 1343.

125 M. Fujihira, N. Ohishi, and T. Osa, Nature (London), 268 (1977) 226.

126 M. Fujihira, T. Kubota, and T. Osa, J. Electroanal. Chem., 119 (1981) 379.

127 S.R. Morrison, Electrochemistry at Semiconductor and Oxidized Metal Electrodes, 1980, Plenum Press, New York, p.7.

128 J.T. Law, "Semiconductor Surfaces", chapter 16 in Semiconductors, N.B. Hannay, ed., 1959, Reinhold Publishing Corp., New York, p. 678.

129 H. Gerischer and F. Willig, Topics in Cur. Chem., 31 (1976) 61.

130 K.M. Hornsby, Basic Photographic Chemistry, 1956, Fountain Press, London.

131 C.E. Mees, The Theory of the Photographic Process, 1954, The MacMillan Company, New York.

132 H. Baines, The Science of Photography, 1970, Model and Allied Publ., Ltd., New York.

133 T.H. James, The Theory of the Phhotographic Process, 4th edn., 1977, The MacMillan Company, New York.

134 H. Vogel, Berichte, 6 (1873) 1302.

135 O. Bloch and F.F. Renwick, Phot. J., 60 (1920) 145.

136 W. West and P.B. Gilman, "Mechanism of Spectral Sensitization", chapter 10 in The Theory of the Photographic Process, 4th edn., 1977, T.H. James, ed., The MacMillan Company, New York, p. 260.

137 S. Faria and V. Chiola, J. Electrochem. Soc., 124 (1977) 623.

138 G.S. Young and H.G. Grieg, RCA Rev., 15 (1954) 469.

139 Y.L. Meltzer, "Phthalocyanine Technology", Chemical Process Rev. No. 42, Noyes Data Corp., Park Ridge, N.J., 1970.

140 D.O. Hall, Educ. Chem., 15 (1980) 8.

141 W. Menke, Ann. Rev. Plant. Physiol., 13 (1962) 27.

142 T.E. Weier, et al., Am. J. Botany, 52 (1962) 339.

143 M. Calvin and J.A. Bassham, The Photosynthesis of Carbon Compounds, 1962, W.A. Benjamin, Inc., New York.

144 R.K. Clayton, Photosynthesis: Physical Mechanisms and Chemical Patterns, 1980, Cambridge University Press, New York, p. 38.

145 R.K. Clayton, Photosynthesis: Physical Mechanisms and Chemical Patterns, 1980, Cambridge University Press, New York, p. 39.

146 R. Hill and F. Bendall, Nature (London), 186 (1960) 136.

147 D.T. Sawyer and J.L. Roberts, Jr., Experimental Electrochemistry for Chemists, 1974, John Wiley and Sons, Inc., New York, p. 160.

148 D.T. Sawyer and J.L. Roberts, Jr., Experimental Electrochemistry for Chemists, 1974, John Wiley and Sons, Inc., New York, p. 137.

149 R. Cieslinski and N.R. Armstrong, Anal. Chem., 51 (1979) 565.

150 R.F. Ziolo, C.H. Griffiths, and J. Troup, J. Chem. Soc., Dalton Trans., 11 (1980) 2300.

151 J.H. Weber and D.H. Busch, Inorg. Chem., 4 (1965) 469.

152 F.A. Cotton and G. Wilkinson, Advanced Inorganic Chemistry, 3rd edn., 1972, John Wiley and Sons, Inc., New York, p. 264.

153 R.S. Nicholson and I. Shain, Anal. Chem., 36 (164) 706.

154 R.S. Nicholson, Anal. Chem., 37 (1965) 1351.

155 A.J. Bard and L.R. Faulkner, Electrochemical Methods: Fundamentals and Applications, 1980, John Wiley and Sons, Inc., New York, p. 143.

156 R.S. Nicholson, Anal. Chem., 37 (1965) 667.

157 D.E. Smith, Crit. Rev. Anal. Chem., 2 (1971) 247.

158 V.G. Levich, Physicochemical Hydrodynamics, 1962, Prentice-Hall, Englewood Cliffs, N.J.

159 R.N. Adams, Electrochemistry at Solid Electrodes, 1969, Marcel Dekker, Inc., New York, p. 206.

160 J.O'M. Bockris and A.K.N. Reddy, Modern Electrochemistry, vol. I, 1970, Plenum Press, New York, p. 487.

161 A. Hamelin and J. Lecouer, Collect. Czech. Chem. Commun., 36 (1971) 714.

162 J. Clavilier and N.V. Huong, J. Electroanal. Chem., 41 (1973) 193.

163 S.H. Cadle and S. Bruckenstein, J. Electroanal. Chem., 48 (1973) 325.

164 P. Stonehart, H.A. Kozlowska, and B.E. Conway, Proc. Royal Soc. London, A310 (1969) 541.

165 K.J. Vetter, D. Dickertmann, and J.W. Schultze, J. Electroanal. Chem., 55 (1974) 429.

166 M.M. Lohrengel and J.W. Schultze, Ber. Bunsenges. Phys. Chem., 80 (1976) 552.

167 F.S. Granger and J.M. Nelson, J. Am. Chem. Soc., 43 (1921) 1401.

168 A.I. Vogel, A Textbook of Quantitative Inorganic Analysis, 3rd edn., 1961, John Wiley and Sons, Inc., New York, p. 918.

169 J.R. White and N.R. Armstrong, J. Electroanal. Chem., to be published.

170 J.N. Esposito, L.E. Sutton, and M.E. Kenney, 6 (1967) 1116-1120.

171 J.B. Davison and K.J. Wynne, Macromolecules, 11 (1978) 186-191.

172 T.M. Mezza and N.R. Armstrong, submitted for publication.

173 R.P. Linstead, et al., J. Chem. Soc., (1938) 1511.

174 M. Whalley, J. Chem. Soc., (1961) 866.

175 E.A. Lucia and F.D. Verderame, J. Chem. Phys., 48 (1968) 2674.

176 C.A. Linkous and N.R. Armstrong, "Investigation of Photoelectrochemical Oxygen Reduction on Iron Phthalocyanine Thin Film Electrodes" The Electrochemical Society, Los Angeles, Ca. Meeting, October 14-19, 1979.

177 T.H. James, loc. cit., ch. 8.

178 E.E. Jelley, Nature, 138 (1936) 1009.

179 J. Frand and E. Teller, J. Chem. Phys., 6 (1938) 861.

180 P.J. Peerce and A.J. Bard, J. Electroanal. Chem., 112 (1980) 97.

181 H. Matsuda, T. Gueshi, and K. Tokuda, J. Electroanal. Chem., 101 (1979) 29.

182 C.A. Linkous, T. Klofta, and N.R. Armstrong, submitted to J. Electrochem. Soc.

183 P. Rieke, under N.R. Armstrong, unpublished work.

184 K. Chan, under N.R. Armstrong, unpublished work.

185 P. Rieke, under N.R. Armstrong, unpublished work.

186 J.O'M. Bockris and A.K.N. Reddy, loc. cit., Vol. II, p. 760.

187 N.R. Armstrong, personal communication.

188 K. Nebesny, under N.R. Armstrong, personal communication.

189 T.M. Mezza, Ph.D. Thesis, University of Arizona, 1982.

190 T.M. Mezza and C.A. Linkous, under N.R. Armstrong, unpublished work.

191 F.A. Cotton and G. Wilkinson, loc. cit., p. 264.

192 D.H. Templeton and G.F. Carter, J. Phys. Chem., 58 (1954) 940.

193 N.N. Greenwood, A. Balls, A.J. Downs, and B.P. Straughan, Trans. Far. Soc., 62 (1966) 521.

194 G.R. Kearns and M.J. Calvin, J. Chem. Phys., 34 (1961) 2026.

195 R.O. Loutfy and J.H. Sharp, J. Phy. Chem., 82 (1978) 2787.

196 C.A. Linkous, under N.R. Armstrong, unpublished work.

197 B. Thacker, under N.R. Armstrong, unpublished work.

198 T. Gutmann and L.E. Lyons, loc. cit., p. 286.

199 T. Gutmann and L.E. Lyons, loc. cit., p. 66.

200 Alferov and Sevast'yanov, Soviet Electrochemistry, 11(5), (1975) 827.

201 Alferov and Sevast'yanov, Russian Journal of Physical Chemistry, 50(1), (1976) 214.

202 Yu.S. Shumov and M. Heyrovsky, J. Electroanal. Chem., 65 (1975) 469.

203 J.O'M. Bockris and A.K.N. Reddy, loc. cit., Vol. II, p. 1000.